INFORMATION TO USERS

This manuscript has been reproduced from the microfilm master. UMI films the text directly from the original or copy submitted. Thus, some thesis and dissertation copies are in typewriter face, while others may be from any type of computer printer.

The quality of this reproduction is dependent upon the quality of the copy submitted. Broken or indistinct print, colored or poor quality illustrations and photographs, print bleedthrough, substandard margins, and improper alignment can adversely affect reproduction.

In the unlikely event that the author did not send UMI a complete manuscript and there are missing pages, these will be noted. Also, if unauthorized copyright material had to be removed, a note will indicate the deletion.

Oversize materials (e.g., maps, drawings, charts) are reproduced by sectioning the original, beginning at the upper left-hand corner and continuing from left to right in equal sections with small overlaps.

Photographs included in the original manuscript have been reproduced xerographically in this copy. Higher quality 6" x 9" black and white photographic prints are available for any photographs or illustrations appearing in this copy for an additional charge. Contact UMI directly to order.

ProQuest Information and Learning
300 North Zeeb Road, Ann Arbor, MI 48106-1346 USA
800-521-0600

UMI®

NOTE TO USERS

This reproduction is the best copy available.

UMI®

A Theoretical and Solid-State NMR Investigation of the Alkenyl and Alkynyl Carbon Chemical Shift Tensors for Some η^2-Unsaturated Carbon Ligands in Metal Complexes

by

Guy M. Bernard

Submitted in partial fulfillment of the requirements

for the degree of Doctor of Philosophy

at

Dalhousie University
Halifax, NS Canada
August, 2000

© Copyright by Guy M. Bernard, 2000

National Library of Canada
Acquisitions and Bibliographic Services
395 Wellington Street
Ottawa ON K1A 0N4
Canada

Bibliothèque nationale du Canada
Acquisitions et services bibliographiques
395, rue Wellington
Ottawa ON K1A 0N4
Canada

Your file Votre référence

Our file Notre référence

The author has granted a non-exclusive licence allowing the National Library of Canada to reproduce, loan, distribute or sell copies of this thesis in microform, paper or electronic formats.

The author retains ownership of the copyright in this thesis. Neither the thesis nor substantial extracts from it may be printed or otherwise reproduced without the author's permission.

L'auteur a accordé une licence non exclusive permettant à la Bibliothèque nationale du Canada de reproduire, prêter, distribuer ou vendre des copies de cette thèse sous la forme de microfiche/film, de reproduction sur papier ou sur format électronique.

L'auteur conserve la propriété du droit d'auteur qui protège cette thèse. Ni la thèse ni des extraits substantiels de celle-ci ne doivent être imprimés ou autrement reproduits sans son autorisation.

0-612-62357-2

Canadä

DALHOUSIE UNIVERSITY

FACULTY OF GRADUATE STUDIES

The undersigned hereby certify that they have read and recommend to the Faculty of Graduate Studies for acceptance a thesis entitled "A Theoretical and Solid-State NMR Investigation of the Alkenyl and Alkynyl Carbon Chemical Shift Tensors for Some η^2-Unsaturated Carbon Ligands in Metal Complexes"

by Guy M. Bernard

in partial fulfillment of the requirements for the degree of Doctor of Philosophy.

Dated: August 16, 2000

External Examiner

Research Supervisor

Examining Committee

[redacted]

DALHOUSIE UNIVERSITY

DATE: August 24, 2000

AUTHOR: Guy M. Bernard

TITLE: A Theoretical and Solid-State NMR Investigation of the Alkenyl and Alkynyl Carbon Chemical Shift Tensors for Some η^2-Unsaturated Carbon Ligands in Metal Complexes

DEPARTMENT OR SCHOOL: Chemistry

DEGREE: Ph.D. CONVOCATION: October YEAR: 2000

Permission is herewith granted to Dalhousie University to circulate and to have copied for non-commercial purposes, at its discretion, the above title upon the request of individuals or institutions.

[redacted]

Signature of Author

The author reserves other publication rights, and neither the thesis nor extensive extracts from it may be printed or otherwise reproduced without the author's written permission.

The author attests that permission has been obtained for the use of any copyrighted material appearing in this thesis (other than brief excerpts requiring only proper acknowledgement in scholarly writing), and that all such use is clearly acknowledged.

To Al, Alice and Doris

"*Whether or not it is clear to you, no doubt*
the universe is unfolding as it should"

—Anonymous

Table of Contents

Dedication iv
Table of Contents v
List of Figures viii
List of Tables xi
Abstract xiii
List of Abbreviations and Symbols xiv
Acknowledgments xix

1 **Introduction** 1
- 1.1 Background 1
- 1.2 Structure of Platinum-Alkene and Platinum-Alkyne Complexes . . 3
- 1.3 Solution NMR Studies 7
- 1.4 Insights From Solid-State NMR 13
- 1.5 Previous Solid-State NMR Investigations of Alkenyl and Alkynyl Carbon CS Tensors 14
  - 1.5.1 Solid-State Carbon-13 NMR Investigations of Ethylene and Acetylene 14
  - 1.5.2 Solid-State Carbon-13 NMR Investigations of Platinum-Alkene Complexes 16
  - 1.5.3 Solid-State Carbon-13 NMR Investigations of Some Copper-Alkene Complexes 20
  - 1.5.4 Solid-State Carbon-13 NMR Investigations of Some Metal-Alkene and Metal-Alkyne Complexes 22
  - 1.5.5 Solid-State Carbon-13 NMR Investigations of η^5- and η^6-Coordinated Metal Complexes. 27
- 1.6 Outline of the Thesis 31

2 **Solid-State NMR—Background** 34
- 2.1 Interactions in the Solid State 34
  - 2.1.1 The Zeeman Interaction 35
  - 2.1.2 Nuclear Magnetic Shielding 36
  - 2.1.3 Indirect Spin-Spin Coupling 37
  - 2.1.4 Direct Dipolar Coupling 39
  - 2.1.5 Nuclear Quadrupolar Coupling 41
- 2.2 Nuclear Magnetic Shielding and Chemical Shifts 43
- 2.3 NMR Spectra of an Isolated Spin-½ Nucleus 46
- 2.4 NMR Spectra of an Isolated Spin Pair 48
  - 2.4.1 The Dipolar-Chemical Shift Method 48
  - 2.4.2 Line Shapes of *AB* Spin Systems Under Conditions of Magic-Angle Spinning. 52
- 2.5 Two-Dimensional NMR—Spin Echo Techniques 54

2.6 Deuterium NMR 56
2.7 Experimental Procedure 61

3 **Calculation of Magnetic Shielding From First Principles** 63
3.1 Introduction 63
3.2 Background 64
3.3 Computational Techniques 68
3.4 Computational Details 72
3.5 Results and Discussion 76
3.5.1 Convergence 76
3.5.2 Calculations on Metal-Alkene Complexes 84
3.5.3 Calculations on Metal-Alkyne Complexes 88
3.6 Summary 90

4 **A Solid-State NMR Investigation of Platinum-Ethylene Complexes: $Pt(C_2H_4)(PPh_3)_2$ and Zeise's Salt, $K[Pt(C_2H_4)Cl_3]$** 93
4.1 Introduction 93
4.2 Experimental 96
4.3 Results and Discussion 99
4.3.1 Carbon-13 NMR Spectra of $Pt(\eta^2\text{-}C_2H_4)(PPh_3)_2$ 99
4.3.2 Carbon-13 NMR Spectra of $K[Pt(\eta^2\text{-}C_2H_4)Cl_3]$, Zeise's Salt 105
4.3.3 Comparison of the Alkenyl Carbon Chemical Shift Tensors for $Pt(\eta^2\text{-}C_2H_4)(PPh_3)_2$ and Zeise's Salt 115
4.3.4 The Internal Dynamics of the Ethylene Moiety in $Pt(\eta^2\text{-}C_2H_4)(PPh_3)_2$ and Zeise's Salt 117
4.4 Summary 122

5 **An Experimental and Theoretical Solid-State Carbon-13 NMR Investigation of *trans*-Stilbene and $Pt(\eta^2$-*trans*-stilbene$)(PPh_3)_2$** 124
5.1 Introduction 124
5.2 Experimental 124
5.3 Results and Discussion 126
5.3.1 Solid-State Carbon-13 NMR Spectra of *trans*-Stilbene 126
5.3.2 Carbon-13 NMR Spectra of MAS Samples of $Pt(\eta^2$-*trans*-Stilbene$)(PPh_3)_2$ 131
5.3.3 Carbon-13 NMR Spectra of Stationary Samples of $Pt(\eta^2$-*trans*-stilbene$)(PPh_3)_2$. 135
5.3.4 Comparison of the Chemical Shift Tensors for *trans*-Stilbene and $Pt($*trans*-Stilbene$)(PPh_3)_2$ 138
5.4 Summary 139

6 **An Investigation of the Carbon Chemical Shift Tensors for Diphenylacetylene and Pt(η^2-Diphenylacetylene)(PPh_3)$_2$** 140
6.1 Introduction 140
6.2 Experimental 142
6.3 Results and Discussion 145
6.3.1 Carbon-13 NMR Spectra of Diphenylacetylene 145
6.3.2 Solid-State ^{31}P and Solution ^{13}C NMR of Pt(η^2-diphenylacetylene)(PPh_3)$_2$ 148
6.3.3 Carbon-13 NMR of MAS Samples of Pt(η^2-Diphenylacetylene-1,2-$^{13}C_2$)(PPh_3)$_2$ 151
6.3.4 Carbon-13 NMR Spectra of Stationary Samples of Pt(η^2-diphenylacetylene-1,2-$^{13}C_2$)(PPh_3)$_2$. 155
6.3.5 A Comparison of the Chemical Shift Tensors for Diphenylacetylene and Pt(η^2-diphenylacetylene)(PPh_3)$_2$. .. 158
6.3.6 A Comparison of the Chemical Shift Tensors for *trans*-Stilbene and Pt(η^2-Diphenylacetylene)(PPh_3)$_2$. 159
6.4 Summary 160

7 **Proposed Future Studies** 162
7.1 Further Studies of Platinum Complexes. 162
7.2 Solid-State NMR Studies of Other Metal-Alkene and Metal-Alkyne Complexes. 163
7.3 Further Computational Studies 165

8 **Concluding Remarks** 166

Appendix 168
A.1 Stationary Powder NMR Line Shapes For an A_2 Spin System: Diphenylacetylene-1,2-$^{13}C_2$. 168

References 171

List of Figures

Fig. 1.1 Molecular structures of Zeise's salt and Zeise's dimer. 2

Fig. 1.2 Molecular structure of Pt(C_2H_4)(PPh_3)$_2$. 4

Fig. 1.3 The Dewar Chatt and Duncanson model and the metallacyclopropane structure describing coordination of alkenes with metals. . 5

Fig. 1.4 Possible orientations for the ethylene ligands in the series Pt(C_2H_4)$_2$($PMe_{3-n}Ph_n$). 10

Fig. 1.5 Structure of Pt(η^2-tricyclo[3.3.1.0]non-3(7)-ene)(PPh_3)$_2$ 11

Fig. 1.6 Orientation of the carbon chemical shift tensor for ethylene. 16

Fig. 1.7 Structures of Pt(nbd) and Pt(cod) complexes.. 18

Fig. 1.8 Orientation of the alkenyl C,C bond and of the oxygen atoms about the copper atom in a typical Cu-OTf complex. 20

Fig. 1.9 Portion of the periodic table encompassing the metal centres discussed in Section 1.5.4. 24

Fig. 1.10 Structures of [Cu(cod)Cl]$_2$ and of the Ag[(cod)$_2$]$^+$ cation. 25

Fig. 1.11 Orientation of the carbon CS tensors for ferrocene. 30

Fig. 1.12 Orientation of the carbon CS tensors for benzene. 32

Fig. 2.1 Orientation of the applied magnetic field, $\mathbf{B}_0$, relative to the PAS of the magnetic shielding tensor. 38

Fig. 2.2 The Pake doublet powder pattern. 42

Fig. 2.3 The shielding, σ, and chemical shift, δ, scales for ^{13}C. 45

Fig. 2.4 The ^{13}C NMR spectra expected for stationary powder samples of ethylene and acetylene at natural abundance. 47

Fig. 2.5 Possible orientations of a CS tensor component about a dipolar vector. 51

Fig. 2.6 Pulse sequence for the 2D spin-echo NMR experiment. 55

Fig. 2.7 Line shape of ^{2}H NMR spectrum as defined by η and C_Q.. 58

Fig. 2.8 Quadrupolar echo pulse sequence and the evolution of the magnetization 60

Fig. 3.1 Examples of magnetic-dipole allowed and forbidden mixing of molecular orbitals. 66

Fig. 3.2 Calculated carbon CS tensor components for ethylene as a function of basis set. 79

Fig. 3.3 Calculated CS tensor components for the alkynyl carbon nuclei of diphenylacetylene as a function of basis set. 81

Fig. 3.4 Calculated carbon CS tensor components for $Pt(C_2H_4)(PPh_3)_2$ and Zeise's salt as a function of the basis set. 82

Fig. 4.1 Carbon-13 NMR spectra of MAS samples of $Pt(C_2H_4)(PPh_3)_2$. . . . 100

Fig. 4.2 Two-dimensional ^{13}C spin-echo NMR spectrum of $Pt(^{13}C_2H_4)(PPh_3)_2$ 102

Fig. 4.3 Calculated and experimental ^{13}C NMR spectra of stationary samples of $Pt(^{13}C_2H_4)(PPh_3)$ 104

Fig. 4.4 Orientation of the alkenyl carbon CS tensors for $Pt(C_2H_4)(PPh_3)_2$. . 106

Fig. 4.5 Carbon-13 NMR spectra of MAS samples of Zeise's salt 107

Fig. 4.6 Calculated and experimental ^{13}C NMR spectra of a stationary sample of Zeise's salt at natural abundance. 110

Fig. 4.7 Two-dimensional ^{13}C spin-echo NMR spectrum of Zeise's salt-$^{13}C_2$. 111

Fig. 4.8 Calculated and experimental ^{13}C NMR spectra of a stationary sample of Zeise's salt. 113

Fig. 4.9 Orientation of the carbon CS tensor for Zeise's salt. 114

Fig. 4.10 Comparison of the principal components of the carbon CS tensors for ethylene, ethane and the platinum-ethylene complexes. 116

Fig. 4.11 Calculated and experimental ^2H NMR spectra of stationary samples of $Pt(C_2{}^2H_4)(PPh_3)_2$ and Zeise's salt-$^2H_4$. 118

Fig. 4.12 Calculated barrier to internal rotation of the ethylene ligand in Zeise's salt. 120

Fig. 4.13 Possible librational motion of the ethylene ligand of Zeise's salt. . 122

Fig. 5.1 Structures of *trans*-stilbene and Pt(η^2-*trans*-stilbene)$(PPh_3)_2$. 125

Fig. 5.2 Carbon-13 NMR spectra of MAS samples of *trans*-stilbene. 127

Fig. 5.3 Orientation disorder at one of the sites in the reported crystal structure of *trans*-stilbene. 127

Fig. 5.4 Calculated and experimental ^{13}C NMR spectra of a stationary sample of *trans*-stilbene-α,β-$^{13}C_2$. 128

Fig. 5.5 Orientation of the carbon CS tensors for *trans*-stilbene. 130

Fig. 5.6 Carbon-13 NMR spectra of MAS samples of Pt(η^2-*trans*-stilbene)$(PPh_3)_2$ 132

Fig. 5.7 Calculated and experimental spectra of MAS samples of Pt(η^2-*trans*-stilbene)$(PPh_3)_2$. 134

Fig. 5.8 Calculated and experimental ^{13}C NMR spectra of a stationary sample of Pt(*trans*-stilbene-α,β-$^{13}C_2$)$(PPh_3)_2$. 135

Fig. 5.9 Orientation of the alkenyl carbon CS tensor for Pt(*trans*-stilbene)$(PPh_3)_2$. 137

Fig. 6.1 Structures of diphenylacetylene and Pt(η^2-diphenylacetylene)$(PPh_3)_2$. 141

Fig. 6.2 Carbon-13 NMR spectra of a stationary samples of diphenylacetylene-1,2-$^{13}C_2$. 145

Fig. 6.3 Orientation of the alkynyl carbon CS tensors for diphenylacetylene. 148

Fig. 6.4 Calculated and experimental ^{13}C NMR spectra for Pt(η^2-diphenylacetylene-1,2-$^{13}C_2$)(PPh_3)$_2$ in CD_2Cl_2. 149

Fig. 6.5 Phosphorus-31 NMR spectra of Pt(η^2-diphenylacetylene)(PPh_3)$_2$. 152

Fig. 6.6 Isotropic region of the ^{13}C NMR spectrum of an MAS sample of Pt(η^2-diphenylacetylene-1,2-$^{13}C_2$)(PPh_3)$_2$ 154

Fig. 6.7 Calculated and experimental ^{13}C NMR spectra of stationary samples of Pt(η^2-diphenylacetylene-1,2-$^{13}C_2$)(PPh_3)$_2$. 156

Fig. 6.8 Orientations for the alkynyl carbon CS tensors for Pt(η^2-diphenylacetylene)(PPh_3)$_2$. 158

Fig. 7.1 Molecular structure of Pt(η^2-C_{60})(PPh_3)$_2$. 163

Fig. A.1 Calculated transitions for the ^{13}C NMR spectrum of solid diphenylacetylene at 4.7 T. 170

List of Tables

Table 1.1 Alkenyl or Alkynyl ^{13}C NMR Data for Some Metal Complexes in Isotropic Liquids. 8

Table 1.2 Principal Components of the Alkenyl Carbon Chemical Shift Tensors for Some Platinum-Alkene Complexes. 17

Table 1.3 Principal Components of the Alkenyl Carbon Chemical Shift Tensors for Some η^2-Coordinated Copper(OTf)-Alkene Complexes. 21

Table 1.4 Principal Components of the Alkenyl Carbon Chemical Shift Tensors for Some Metal-Alkene Complexes. 23

Table 1.5 Isotropic Carbon Chemical Shifts for Some Solid Alkynes and Copper-Alkyne Complexes. 27

Table 1.6 Principal Components of the Carbon Chemical Shift Tensors for Some η^5- and η^6-Coordinated Metal Complexes. 29

Table 3.1 Diamagnetic and Paramagnetic Contributions to the Principal Components of the Magnetic Shielding Tensors for Ethane, Ethylene and Acetylene. 67

Table 3.2 Basis Sets Used for the *Ab Initio* Calculations. 73

Table 3.3 Structural Parameters for the Compounds Investigated by *Ab Initio* Methods 74

Table 3.4 Calculated Carbon Magnetic Shielding Tensor Components for Ethylene. 77

Table 3.5 Calculated Carbon Magnetic Shielding Tensor Components for $Pt(C_2H_4)(PPh_3)_2$ and $[Pt(C_2H_4)Cl_3]^-$. 83

Table 3.6 Calculated Carbon Magnetic Shielding Tensor Components for Some Metal-Alkene Complexes 85

Table 3.7 Calculated Carbon Magnetic Shielding Tensor Components for Some Metal-Alkyne Complexes. 89

Table 4.1 Experimental and Calculated Principal Components of the Carbon Chemical Shift Tensors for Ethylene, $Pt(C_2H_4)(PPh_3)_2$ and Zeise's Salt. 103

Table 4.2 Deuterium NMR Parameters for Ethane, Ethylene, $Pt(C_2H_4)(PPh_3)_2$ and Zeise's Salt. 119

Table 5.1 Calculated and Experimental Alkenyl Carbon Chemical Shift Tensor Principal Components for *trans*-Stilbene and Pt(η^2-*trans*-Stilbene)$(PPh_3)_2$.. 129

Table 6.1 Experimental and Calculated Chemical Shift Tensors for Diphenylacetylene and Pt(Diphenylacetylene)$(PPh_3)_2$. 146

Table 6.2 Parameters Derived From the ^{13}C and ^{31}P NMR Spectra of Pt(η^2-Diphenylacetylene)$(PPh_3)_2$ in CD_2Cl_2. 150

Table A.1 Transition Frequencies in the Directions of the Principal Tensor Components for Diphenylacetylene. 169

Abstract

The carbon chemical shift (CS) tensors for several unsaturated-carbon ligands and their platinum complexes have been investigated by solid-state ^{13}C NMR spectroscopy. The magnitudes of the principal components and their orientations relative to the $^{13}C,^{13}C$ dipolar vector were determined using the dipolar-chemical shift NMR method. Orientations for the CS tensors in the molecular framework are proposed, based on the results from first principles calculations of the magnetic shielding tensors, using restricted Hartree-Fock theory with gauge-independent atomic orbitals (GIAO). The isotropic shielding of the alkenyl carbon nuclei increases significantly upon coordination with Pt(0). For example, the ethylene carbon nuclei of $Pt(C_2H_4)(PPh_3)_2$ are shielded by approximately 85 ppm compared to those for uncoordinated ethylene. The increased isotropic shielding is a consequence of increased shielding in the directions of δ_{11} and δ_{22}; the shielding in the direction of δ_{33} is relatively insensitive to coordination with platinum. In contrast, the alkynyl carbon shielding for diphenylacetylene decreases following coordination with Pt(0). The alkynyl carbon CS tensors for Pt(η^2-diphenylacetylene)$(PPh_3)_2$ are similar to those for uncoordinated *trans*-stilbene. Deuterium NMR studies of $Pt(C_2{}^2H_4)(PPh_3)_2$ and Zeise's salt-$^2H_4$ indicate that motion of the ethylene ligand is not significant for these samples in the solid state at room temperature. *Ab initio* calculation of the carbon magnetic shielding for some nickel and palladium complexes suggest that the effect on the carbon CS tensors of coordination with these metals is comparable to that observed experimentally for platinum.

List of Abbreviations and Symbols

A_2	spin-system consisting of two magnetically and crystallographically equivalent nuclei
AB	spin-system consisting of two nuclei with similar, but not identical chemical shifts
AX	spin-system in which the magnetic shielding of two nuclei is significantly different
B_0	the applied magnetic field
B3LYP	Becke's three-parameter hybrid functional, with the correlation functional of Lee, Yang and Parr.
btsa	*bis*-(trimethylsilyl) acetylene
cod	1,5-cyclooctadiene
cot	1,3,5,7-cyclooctatetraene
Cp	cyclopentadienyl
CP	cross-polarization
CS	chemical shift
CSGT	continuous set of gauge transformations
C_Q	quadrupole coupling constant
$\mathbf{D}$	dipolar tensor
D_{ii}	principal components of the dipolar tensor
DFT	density functional theory
dmb	2,3-dimethyl-2-butene
DPA	diphenylacetylene
e	elementary electron charge

EFG	electric field gradient
Et	ethyl
ESMS	electro-spray mass spectrometry
FID	free induction decay
GIAO	gauge-independent atomic orbitals
$\mathcal{H}_Z$	Hamiltonian describing the Zeeman interaction
$\mathcal{H}_S$	Hamiltonian describing magnetic shielding
$\mathcal{H}_J$	Hamiltonian describing the indirect coupling interaction
$\mathcal{H}_{DD}$	Hamiltonian describing the direct dipolar coupling interaction
$\mathcal{H}_Q$	Hamiltonian describing the quadrupolar interaction
$\hbar$	Planck constant divided by 2π
hmdb	hexamethyl dewar benzene
IGLO	individual gauge for localized orbitals
IGAIM	individual gauge atoms in molecules
$\langle k\|$	the kth excited electronic state
$\mathbf{J}$	indirect spin-spin coupling tensor
J_{ii}	principal components of the $\mathbf{J}$ tensor
J_{iso}	isotropic indirect spin-spin coupling
l_{ki}	a component of the electronic angular momentum
L_k	total electronic angular momentum
m	electron rest mass
MAS	magic angle spinning

MCSCF	multi configuration self-consistent field
Me	methyl
MO	molecular orbital
nbd	norbornadiene
NMR	nuclear magnetic resonance
OTf	trifluoromethanesulfonate
P_i	relative intensity of the ith NMR transition
PAS	principal axis system
Ph	phenyl
ppm	parts per million
PtDPA	(diphenylacetylene)[*bis*(triphenylphosphine)]platinum(0)
PtTSB	(*trans*-stilbene)[*bis*(triphenylphosphine)]platinum(0)
Q	nuclear quadrupole moment
r_{AB}	internuclear separation between atoms A and B
$\mathbf{r}_{AB}$	internuclear vector
R_{DD}	direct dipolar spin-spin coupling
$r_{diffrac}$	value of r_{AB} measured by diffraction techniques
r_{eff}	value of r_{AB} predicted from R_{eff}
R_{eff}	effective dipolar spin-spin coupling
rf	radio frequency
RHF	restricted Hartree-Fock
s	sample standard variance

SCF	self-consistent field
TMS	tetramethylsilane
TPPM	two-pulse phase modulation
TSB	*trans*-stilbene
$\mathbf{V}$	electric field gradient tensor
V_{ii}	component of the electric field gradient tensor
VACP	variable-amplitude cross polarization
α	Euler angle defining the rotation about the original z axis
β	Euler angle defining the orientation of δ_{33} with respect to the dipolar vector
γ	Euler angle defining the rotation of the chemical shift tensor about δ_{33}
γ_A	magnetogyric ratio for nucleus A
ΔJ	anisotropy in the indirect spin-spin coupling tensor
Δ_n	ratio between the observed quadrupolar splitting and that expected in the absence of motion
δ_{ii}	chemical shift of the principal tensor component *ii*, in ppm
δ_{iso}	isotropic chemical shift
η	asymmetry in the electric field gradient
η^i	coordination number for ligands of organometallic complexes
θ_{ii}	orientation of the CS tensor component *ii* relative to the dipolar axis
θ_Q	angle between the rotation axis and the direction of the largest component of the EFG
κ	skew in a chemical shift or magnetic shielding tensor
μ_0	permeability constant

$\nu_{1/2}$	full width at half height of isotropic NMR peaks
ν_{ii}	chemical shift, in Hz, of the tensor component *ii*
ν_{ref}	chemical shift, in Hz, of a reference nucleus
ν_{rot}	MAS frequency, in Hz
$\boldsymbol{\sigma}$	magnetic shielding tensor
σ_{ii}	principal component of the magnetic shielding tensor
$\boldsymbol{\sigma}^{anti}$	antisymmetric magnetic shielding tensor
$\boldsymbol{\sigma}^{symm}$	symmetric magnetic shielding tensor
σ^{d}	diamagnetic contribution to the magnetic shielding
σ^{p}	paramagnetic contribution to the magnetic shielding
φ	angle defining the orientation of the C,C bond for Zeise's salt relative to the plane containing the platinum and chlorine atoms
ϕ	polar angle defining the orientation of B_0 relative to δ_{33}
Ω	span of a chemical shift tensor: $\Omega = \delta_{11} - \delta_{33} = \sigma_{33} - \sigma_{11}$
$\langle 0 \vert$	the ground electronic state wave function

Acknowledgments

I would like to thank my supervisor, Professor Wasylishen, for his help over past four years. His encouragement as I struggle through the intricacies of nuclear magnetic resonance has been invaluable.

Several people assisted with the preparation of the compounds studied in this work. I am very grateful to: Mr. Devon Latimer for preparing Pt(*trans*-stilbene)$(PPh_3)_2$; Mr. Andrew D. Phillips for his assistance in the preparation of Zeise's salt; Mr. Chris McDonald for help in the preparation of diphenylacetylene and the corresponding platinum complex; and Dr. Roland Roesler for his advice, and for translations of German-language papers. I also want to thank Dr. Gang Wu for some of the preliminary work on the analysis of *trans*-stilbene and Dr. Beata Kolakowski for obtaining some mass spectra.

The work presented here entails the use of several computer programs. I thank Professor Ted Schaefer for allowing the use of his computer for some of the calculations reported herein; Dr. Boquin Sun, Professor Malcolm H. Levitt and Professor Aatto Laaksonen, for providing the MAS simulation program, and Dr. Kirk Marat for providing the simulation program XSIM. I also thank Eric Wasylishen for his advice on the use of some computer software.

I am very grateful to my colleagues in the lab, David Bryce, Shelley Forgeron, Kirk Feindel, Myrlene Gee and Mike Lumsden for their help and encouragement, and especially for providing a pleasant working environment. Klaus Eichele was a member of our group when I arrived; despite being far away now, he continues to provide invaluable advice on my various projects.

The financial assistance of the Natural Sciences and Engineering Research Council (NSERC), the Izaak Walton Killam Trust, the Walter C. Sumner Foundation and Dalhousie University is gratefully acknowledged.

The support and encouragement of my family has been invaluable. Thanks to Alice, Doris and Al. I acknowledge the many friends at Dalhousie who have made my stay in Halifax pleasurable. In no particular order I thank Myrlene, Nelaine, Liyan, Roland, Andrew, Cormac and Chris for their friendship and encouragement. Although we will be far apart, I hope our friendship will continue. Finally, I thank my long-time friends, Gérald, Sandra, Louis, Joan and Darrell for their continuing friendship and encouragement.

Chapter 1

Introduction

1.1 Background

Virtually every tool available to chemists has been used to characterize organometallic compounds.[1-4] Since the advent of Fourier transform multinuclear magnetic resonance spectrometers in the 1970s, nuclear magnetic resonance (NMR) has been particularly useful, and would be regarded as indispensable by most researchers. Although many NMR studies of organometallic compounds have focused on the metal nuclei,[5-10] the NMR properties of the ligands in organometallic complexes provide insight into fundamental molecular properties, such as internal dynamics and ligand to metal bonding.[11-13] NMR experiments are usually undertaken with the samples dissolved in isotropic liquids (Section 1.3). However, much more information is available to the chemist if the NMR parameters are determined for solid samples.[14-17] A proper understanding of nuclear magnetic shielding requires a thorough characterization of the nuclear magnetic properties of some model compounds. In this thesis, properties of alkenyl and alkynyl[18] ligands coordinated with platinum are investigated by solid-state NMR spectroscopy. In particular, the carbon chemical shift (CS) tensors for several η^2-coordinated unsaturated-carbon ligands are characterized as fully as is possible at this time.

The field of organometallic chemistry is generally thought to have originated with the preparation of $K[Pt(C_2H_4)Cl_3]$ (Figure 1.1 A) by William Christoffer Zeise in 1827.[19]

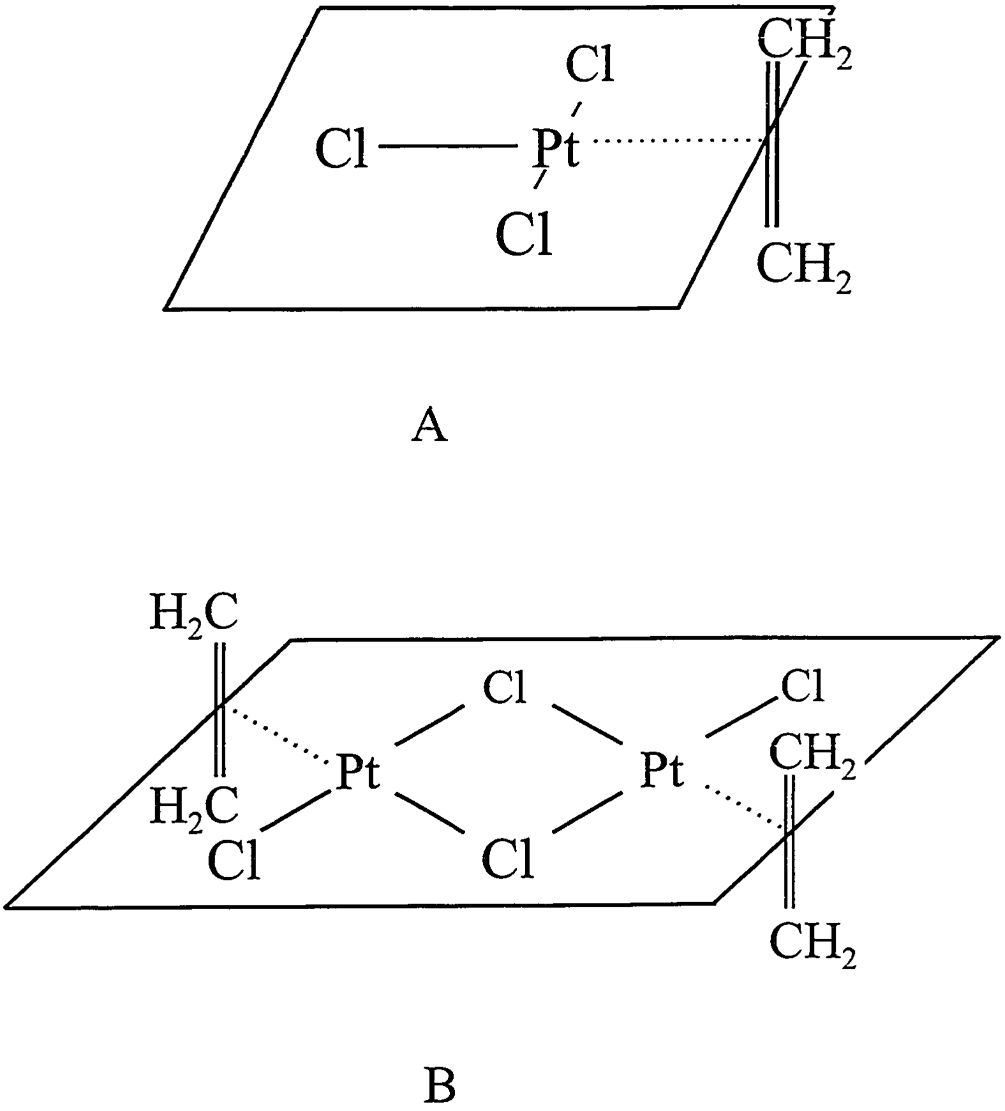
Cl
Cl
Pt
Cl
CH2
CH2
A
H2C
Cl
Cl
Pt
Pt
CH2
H2C
Cl
Cl
CH2
B

Figure 1.1 Structures of the anion of Zeise's salt (A) and of Zeise's dimer (B).

Because Zeise prepared this compound, commonly known as Zeise's salt, from ethanol, his claim that the compound consisted of ethylene coordinated with platinum was contentious,[19c] but was accepted by 1837 after he repeated the preparation.[20] In the latter paper, Zeise also reported the synthesis of $[Pt(C_2H_4)Cl_2]_2$, referred to as Zeise's dimer

(Figure 1.1 B). During the twentieth century, organometallic chemistry has grown into one of the major branches of chemistry, and remains an area of intensive research.[1,4]

1.2 Structure of Platinum-Alkene and Platinum-Alkyne Complexes

In the ensuing discussion on molecular structures, the general structures of Pt(0)- and Pt(II)-alkene complexes are presented, followed by an overview of the accepted concepts regarding the bonding in these and other metal-alkene complexes. Dedieu,[21] as well as Frenking and Fröhlich[22] recently have reviewed the extensive literature on computational studies of the molecular properties of metal-alkene and metal-alkyne complexes.

Most Pt(0) and Pt(II)-alkene complexes, with d^{10} and d^8 electronic configurations, respectively, are diamagnetic.[2] The structures of many of these complexes have been determined by diffraction techniques:[23] the Pt(0)- and Pt(II)-alkene complexes exhibit characteristic structural features which differ significantly. Most Pt(0)-alkene complexes are of the type Pt(alkene)L_2 where L is a substituted phosphine ligand such as triphenylphosphine (PPh_3);[4] only these structures are considered here. Figure 1.2 illustrates the structure of a typical Pt(0) complex, $Pt(C_2H_4)(PPh_3)_2$. In these complexes, the C,C bond lies in the plane defined by the platinum and phosphorus atoms and is lengthened significantly compared to that of the free ligand. The alkenyl C,C bond length in $Pt(C_2H_4)(PPh_3)_2$, 1.434 ± 0.039 Å,[24] is intermediate between that of uncoordinated ethylene, 1.3384 ±0.0010 Å,[25] and that of ethane, 1.5351 ±0.0001 Å.[26] In contrast, the corresponding C,C bond in Pt(II)-alkene complexes is oriented approximately perpendicular to the plane containing the remaining ligands[1-3] and usually is not lengthened significantly compared to that of the free ligand. Zeise's salt (Figure 1.1 A), is a typical Pt(II)-alkene complex. The C,C bond length, 1.375 ± 0.012 Å,[27] is only 0.037 Å greater than that for uncoordinated ethylene. Substituents on the alkene of both the Pt(0) and Pt(II) complexes are bent away from the metal centre.[1,2]

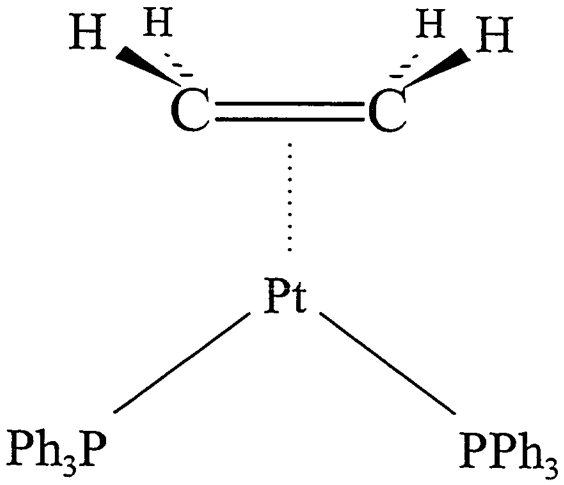

Figure 1.2 Molecular structure of $Pt(C_2H_4)(PPh_3)_2$.[24]

The coordination of alkenes with metals is generally discussed[1,2,22] in terms of a model developed in the 1950s by Dewar, Chatt and Duncanson.[28] The model assumes that metal-alkene bonding is comprised of two components: a σ-type bond formed by the overlap of an occupied π orbital of the alkene with a metal d_{z^2} orbital (Figure 1.3 A) and a π-type "back bond" arising from back-donation of electron density from occupied d_{xz} orbitals of the metal to an unoccupied π^* orbital of the alkene (Figure 1.3 B). Both

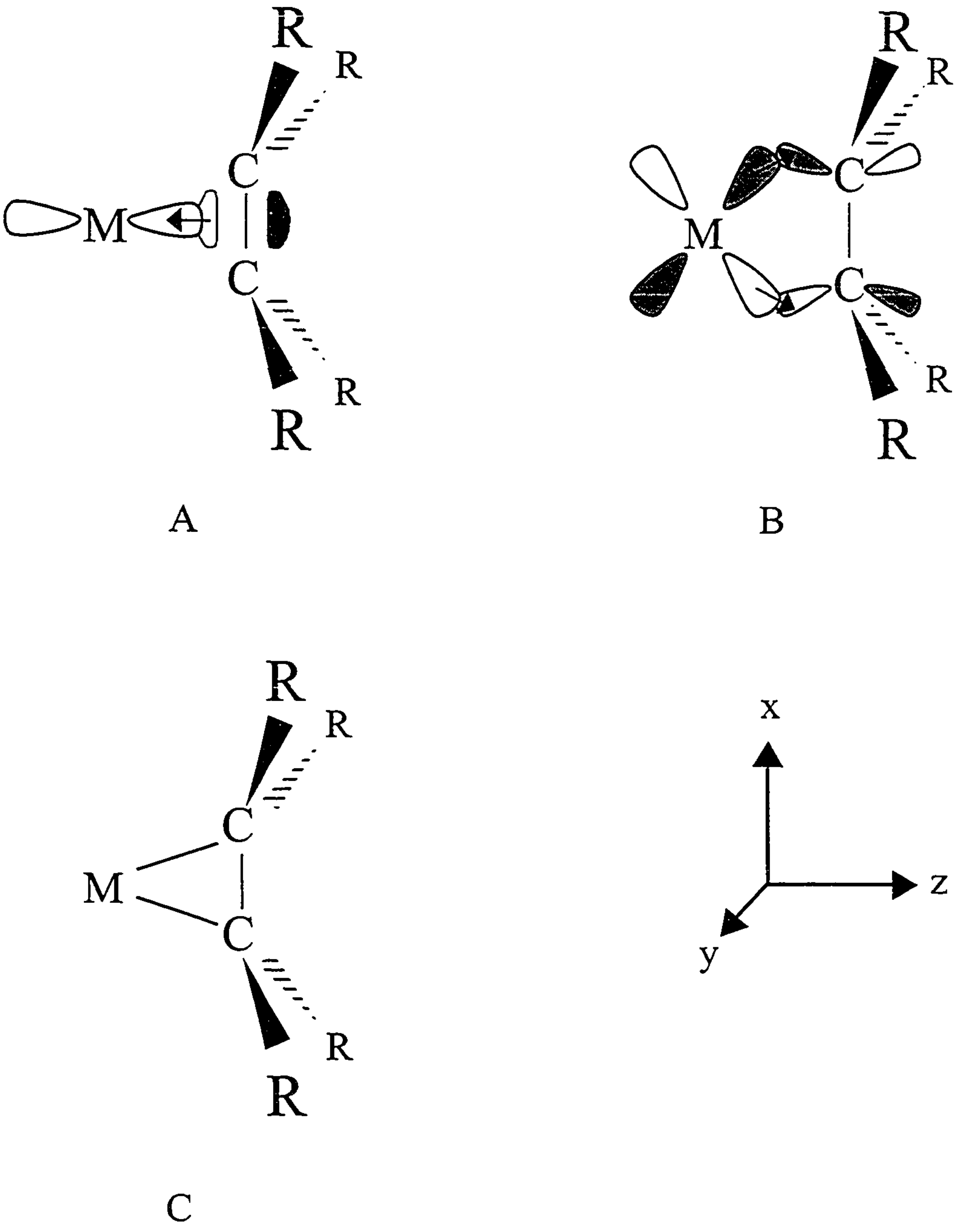
R
R
C
M
C
R
R
A
R
R
M
C
C
R
R
B
R
R
C
M
C
R
R
C
x
z
y

Figure 1.3 The Dewar, Chatt and Duncanson[28] model for the coordination of alkenes with metals: σ bonding (A) and π back bonding (B). In (C), the metallacyclopropane structure is shown.

interactions result in a weakening and hence a lengthening of the alkenyl C,C bond. The structure of the complex depends on the degree of bonding and back-bonding, which in turn depends on the metal centre, the ligand attached to the metal and on the substituents on the alkenyl carbon atoms.[1-4] Depending on the nature of the metal-alkene interaction, the complex may be considered as a metallacyclopropane (Figure 1.3 C) with σ bonds from the metal to each alkenyl carbon atom. Recent molecular orbital calculations support the electron donation and back-donation model used to describe the structure of Pt-alkene complexes.[29] However, the Dewar, Chatt and Duncanson model does not adequately explain the alkene orientations in Pt(0) and Pt(II) complexes, since *d* orbitals are available for bonding and back-bonding in both the perpendicular and planar orientations; from steric considerations, the perpendicular orientation is preferred for both Pt(0) and Pt(II) complexes.[2] However, for Pt(0) complexes, the planar orientation is favoured, since this leads to a stabilization of the electron pair in the plane containing the platinum and phosphorus atoms.[30]

The coordination of alkynes with metals has been discussed in essentially the same terms as for metal-alkene complexes.[2] However, the presence of the second pair of π electrons on the alkyne may lead to further donation of electron density to the metal d_{yz} orbitals and hence to increased electron back-donation to the π^* orbitals of the alkyne. The C,C bond of an alkyne may thus be lengthened to a greater extent than in the case of an alkene. For example, the alkynyl C,C bond length in Pt(η^2-diphenylacetylene)(PMe_3)$_2$, 1.29 ± 0.06 Å,[31] is much greater than that for uncoordinated diphenylacetylene, 1.198 ± 0.009 Å[32] and in fact within experimental error is equal to that for the alkenyl C,C bond of *trans*-stilbene, 1.327 ± 0.006 Å.[33]

1.3 Solution NMR Studies

The rapid tumbling of molecules dissolved in isotropic liquids averages the magnetic shielding interactions, giving rise to high-resolution isotropic NMR peaks. Data from such studies are used routinely to characterize organometallic complexes and to provide insight into molecular properties, such as structure or the internal dynamics of the ligand. Representative papers are reviewed here to illustrate the strengths and limitations of the technique, particularly as they pertain to η^2-coordinated platinum-alkene complexes. A compilation of ^{13}C NMR data on organometallic complexes was published in 1981.[12] Most textbooks and reviews considering ^{13}C NMR include data on organometallic complexes.[11,13,34-37]

Carbon-13 NMR data for metal-alkene complexes dissolved in isotropic liquids, as well as data for the uncoordinated ligands, are summarized in Table 1.1. A survey of the data reveals that coordination with metals increases the alkenyl carbon shielding significantly compared to the value for the uncoordinated ligand. The opposite effect is observed for the only platinum-alkyne listed in Table 1.1: the alkynyl ^{13}C nuclei of 2-butyne are deshielded on coordination with Pt in $Pt(\eta^2\text{-2-butyne})(PPh_3)_2$.[38]

The solution ^{13}C NMR studies of the series $M(C_2H_4)_3$ and $M(C_2H_4)(PPh_3)_2$, where M = Ni, Pd or Pt (Table 1.1), allow a comparison of the effect of the metal centre on the magnetic shielding of the alkenyl carbon nuclei. In both series, coordination of ethylene with platinum has a greater effect than coordination with nickel, but the effect cannot be

Table 1.1 Alkenyl or Alkynyl ^{13}C NMR Data for Some Metal Complexes in Isotropic Liquids.[a]

Compound	T/K[b]	Solvent	$\delta(^{13}C)$	$^{1}J(M,^{13}C)$	$^{2}J(^{31}P,^{13}C)$	Ref
C_2H_4			123.5	-	-	39
$Ni(C_2H_4)_3$	213	toluene-d_8	57.5	*c*	-	13
$Pd(C_2H_4)_3$	203	toluene-d_8	63.5	*c*	-	40
$Pt(C_2H_4)_3$	203	toluene-d_1	48.4	113	-	40
$Pt(C_2H_4)_2(PMe_3)$	193	toluene-d_8	37.9 33.0	139 158	-7 16	41
$Pt(C_2H_4)_2(PMe_2Ph)$	193	toluene-d_8	39.5 34.4	139 159	-6 15	41
$Pt(C_2H_4)_2(PMePh_2)$	193	toluene-d_8	42.0 36.3	137 156	-6 15	41
$Pt(C_2H_4)_2(PPh_3)$	193	toluene-d_8	45.6 38.4	137 154	-5 12	41
$Ni(C_2H_4)(PPh_3)_2$	308	toluene-d_8	49.7			13
$Pt(C_2H_4)(PPh_3)_2$		CD_2Cl_2	38.2	196	23.5[d]	42[e]
$K[Pt(C_2H_4)Cl_3]$		acetone-d_6	67.3	194	-	43[f]
trans-stilbene	304	$CDCl_3$	137.31	-	-	45
Pt(*trans*-stilbene)$(PPh_3)_2$		toluene-d_8	59.3 52.0	*c*	20.5[g] 26.7	46
Pt(tcn)$(PPh_3)_2$[h]		benzene-d_6	66.9	407.4	67 -10	47
2-butyne			73.6	-	-	48
Pt(2-butyne)$(PPh_3)_2$		CD_2Cl_2	112.8	52	*d*	38

(*continued on next page*)

Table 1.1 (*cont.*)

a. Data for the corresponding free ligand are included for comparison. Chemical shifts are in ppm relative to δ(TMS) = 0 ppm. Coupling constants are in Hz.

b. The space is left blank if temperature was not specified.

c. Not reported.

d. The sum of $^2J(^{31}P,^{13}C)_{cis}$ and $^2J(^{31}P,^{13}C)_{trans}$.

e. Similar values were reported in an early ^{13}C NMR investigation, see reference 38.

f. Values of $\delta(^{13}C)$ ranging from 67 to 75 ppm have been reported in earlier NMR studies of this complex in solution, see references 38 and 44.

g. Values shown are for $^2J(^{31}P,^{13}C)_{trans}$; the corresponding values for $^2J(^{31}P,^{13}C)_{cis}$ are 5.3 and 4.7 Hz.

h. tcn = tricyclo[3.3.1.0]non-3(7)-ene, see text.

simply correlated to the size of the metal nucleus, since the alkenyl carbon nuclei of $Pd(C_2H_4)_3$ are the least affected by metal coordination.

The series $Pt(C_2H_4)_2(PMe_{3-n}Ph_n)$ (Table 1.1) illustrates the effect on the alkenyl carbon chemical shifts of substitution of a phenylphosphine group by a methylphosphine group,[41] an important consideration for computational studies, since large ligands are sometimes replaced by smaller ones to minimize computational time (Chapter 3). Substitution of three phenyl groups by three methyl groups increases the alkenyl carbon shielding by 5 to 8 ppm. The observation of two alkenyl ^{13}C NMR peaks for these samples at 193 K, compared with single peaks for spectra acquired at room temperature, demonstrates that alkene rotation is not rapid at the lower temperature.[41] The detection of

$^1J(^{195}Pt,^{13}C)$ at all temperatures shows that exchange is a consequence of ethylene rotation rather than a dissociative process. Variable temperature ^1H NMR was used to determine the activation energy for alkene rotation; these range from 42.7 ± 1.6 kJ mol^{-1} for the PPh_3 complex to 54.4 ± 1.6 kJ mol^{-1} for the PMe_3 complex. The two peaks observed at low temperature also confirm that the ethylene ligands are coplanar (Figure 1.4 A) rather than parallel to each other (Figure 1.4 B), since equivalent alkenyl carbon chemical shifts are expected for the latter whether or not the ethylene ligands are rotating. From the values of $^2J(^{31}P,^{13}C)$, the high frequency alkenyl ^{13}C NMR peaks are attributed to the ^{13}C nuclei *cis* to the phosphorus nuclei. In later work, Wrackmeyer[42] used 1D and HETCOR[49] experiments to show that the signs of $^1J(^{195}Pt,^{13}C)$ and of the sum of the *cis* and *trans* $^2J(^{31}P,^{13}C)$ for $Pt(C_2H_4)(PPh_3)_2$ are positive.

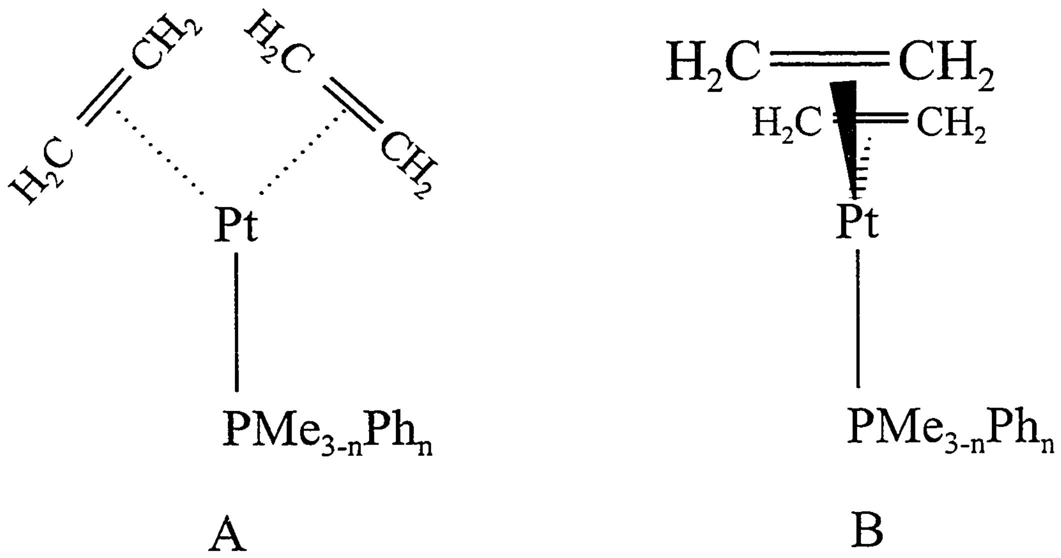

Figure 1.4 Possible orientations for the ethylene ligands in the series $Pt(C_2H_4)_2(PMe_{3-n}Ph_n)$

The vicinal coupling of the alkenyl protons of $Pt(C_2H_4)_2PMe_3$, $^3J(^1H,^1H) \approx 11.7$ and 9.2 Hz,[41] are comparable to those reported for cyclopropane (9 and 7 Hz), but significantly smaller than those for uncoordinated ethylene (19.0 and 11.6 Hz).[50] Hence, the authors[41] argue that ethylene coordination may be described in terms of the metallacyclopropane structure (Figure 1.3 C), although they acknowledge that the values of $^1J(^{195}Pt,^{13}C)$ are less than expected for a Pt,C σ bond.

Kumar and coworkers[47] investigated a highly strained tricyclononene ligand coordinated with platinum (Figure 1.5). The authors argue that the greater values of $^1J(^{195}Pt,^{13}C)$ and $^2J(^{31}P,^{13}C)$ for the nonene-platinum complex compared to those for the ethylene-platinum complex (Table 1.1) indicate greater alkenyl-carbon *s* character.

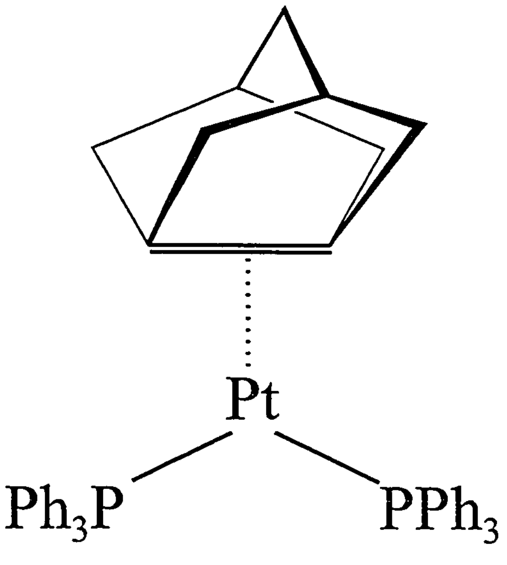

Figure 1.5 Molecular structure of Pt(η^2-tricyclo[3.3.1.0]non-3(7)-ene)(PPh_3)$_2$.

Pellizer *et al.*[51] undertook ^{31}P and ^{195}Pt NMR studies of a series of substituted-ethylene complexes, $Pt(C_2H_{4-n}X_n)(PPh_3)_2$ where X = CN or CO_2Me and n = 0 to 4. Increasing the number of CN substituents on ethylene reduces the platinum magnetic shielding monotonically, from $\delta(^{195}Pt) = -555$ ppm for the ethylene complex to $\delta(^{195}Pt) = -363$ ppm for the tetracyanoethylene complex. The effect on the platinum shielding is smaller and not monotonic for substitution of CO_2Me. These observations are discussed in terms of Ramsey's theory of nuclear magnetic shielding (Section 3.2). From the observation of nonequivalent phosphorus sites in the ^{31}P NMR spectra, the authors conclude that alkene rotation is not significant for these samples. It is noted that "significant" in this context implies an exchange process, such as rotation, which is occurring at a frequency that is equal to or greater than the chemical shift difference, in frequency units, between the two sites. The spectrometer frequency is not stated, but the chemical shift difference between the phosphorus nuclei is approximately 1 ppm. At a typical field strength of 9.4 T, this corresponds to a chemical shift difference of 160 Hz.

Carbon-13 NMR was used to investigate the influence of the ligand L in a series of platinum-alkene complexes of the type $Pt(alkene)Cl_2L$, where L = a *trans* oxygen- or nitrogen-bonded ligand, or Cl^- (the data for the ethylene complex containing the Cl^- ligand, Zeise's salt, are included in Table 1.1).[43] The authors found that the alkenyl carbon shielding decreases for the series $O < Cl^- < N$. Combined with IR data, they conclude that the shielding decreases as the *trans* influence of the ligand increases.

Zeise's salt, Zeise's dimer (Fig. 1.1) and the corresponding palladium analogues have been investigated by ^1H NMR.[52] The authors found that ethylene dissociates slowly from $[Pd(C_2H_4)Cl_3]^-$ dissolved in tetrahydrofuran (THF). In contrast, $[Pd(C_2H_4)Cl_2]_2$ and the platinum complexes are stable in THF or methanol solutions. For samples containing mixtures of the complex and uncoordinated ethylene, exchange occurs in all cases. The exchange rates are comparable for the anionic species, with second-order rate constants, k_2, on the order of 10^3 M^{-1} s^{-1}. The corresponding values for $[Pd(C_2H_4)Cl_2]_2$ and $[Pt(C_2H_4)Cl_2]_2$ are on the order of 10^6 M^{-1} s^{-1}.

1.4 Insights From Solid-State NMR

Although NMR studies of organometallic complexes in solution offer much information about molecular structure and dynamics, one must be aware of the limitations of the technique. High resolution NMR spectra are generally available for samples dissolved in isotropic liquids, but much potential information is lost (Chapter 2). Caution must be exercised when basing conclusions on isotropic chemical shifts, since nuclei with similar isotropic chemical shifts may nevertheless have very different CS tensors.

The NMR spectra of solid samples are generally not as well resolved as those of samples dissolved in solution, particularly for stationary samples. However, solid-state NMR allows for the determination of magnetic shielding tensors (Chapter 2), providing information about the orientation dependence of local magnetic fields. Such information can offer valuable insights into molecular properties, such as structure and molecular dynamics. A proper interpretation of such data requires a thorough understanding of the nuclear magnetic shielding properties of the nuclei, a major goal of the present work. Valuable insights into the origin of coordination chemical shifts can be gained by comparing carbon CS tensors for metal-ligand complexes with those for the uncoordinated ligand, particularly if the data can be related to known molecular structures.

The focus of this thesis is the investigation of the nuclear magnetic properties of ligand nuclei for organometallic complexes, but there are many other experimental considerations which lead NMR spectroscopists to examine solid samples. Many organometallic complexes are insoluble or unstable in solution. Soluble samples are affected by the solvent molecules; inter- or intra-molecular exchange processes, which often influence spectra acquired from solution NMR studies, are greatly reduced or eliminated in the solid state. It is often desirable to acquire NMR data on solid samples, since most inorganic materials are solids at room temperature. In the absence of diffraction data, solid-state NMR often offers the most reliable structural information on these compounds.

1.5 Previous Solid-State NMR Investigations of Alkenyl and Alkynyl Carbon CS Tensors

In the ensuing discussion, the solid-state NMR literature on platinum- (Section 1.5.2), copper- (Section 1.5.3), and other metal-alkene or metal-alkyne complexes (Section 1.5.4) is reviewed. In Section 1.5.5, the solid-state ^{13}C NMR investigations of solid η^5- and η^6-coordinated complexes are summarized. A compilation by Duncan summarizes the reported principal components of carbon CS tensors to 1994.[53]

1.5.1 Solid-State Carbon-13 NMR Investigations of Ethylene and Acetylene

Before discussing the ^{13}C NMR literature on organometallic complexes, it is useful to review the work of Zilm and coworkers,[54,55] who determined the carbon chemical shift tensors for several small organic molecules, including those for ethylene[54,55] and acetylene,[55] the simplest alkene and alkyne. Since the NMR properties of these compounds are thought to be representative of alkenes and alkynes in general, the data provided by these studies are invaluable. The determination of the carbon CS tensors for ethylene are of particular interest for the work presented in this thesis, since comparison of the data with that for platinum-ethylene complexes (Chapter 4) allows an assessment of the effect of metal coordination on the principal components of the carbon CS tensors.

Spectra were acquired at 20 K for samples isolated in an argon matrix (0.5 - 1 v/v % concentration). The principal components of the CS tensors for ethylene, $\delta_{11} = 234$ ppm, $\delta_{22} = 120$ ppm and $\delta_{33} = 24$ ppm, were determined from the analysis of ^{13}C NMR spectra of natural-abundance carbon[54] and $^{13}C_2$-labelled[55] samples. Since intermolecular effects are expected to be negligible, the symmetry of ethylene fixes the orientation of the carbon CS tensors such that one component is along the C,C bond, one component is perpendicular to the molecular plane, and the other component is in the plane of the molecule, perpendicular to the C,C bond. The component of the CS tensor along the C,C bond (δ_{22}) was determined from the observed ^{13}C,^{13}C dipolar splitting in the NMR spectrum of the $^{13}C_2$-labelled sample (see Section 2.4 for a discussion of dipolar-coupled NMR spectra). Since the dipolar splittings when $\mathbf{B}_0$ is in the directions of δ_{11} and δ_{33} are equal, the orientations of these components in the molecular framework were not determined from the experiment; the accepted orientation, illustrated in Figure 1.6, is based on a combination of experimental data and theoretical considerations.[55] More recent *ab* *initio* calculations confirm the orientation of the carbon CS tensors shown in Fig. 1.6.[56] The axial symmetry of acetylene allowed the determination of the carbon CS tensor orientation from the line shape of a natural-abundance carbon sample (NMR line shapes of spectra of dilute spins are discussed in Section 2.3). The direction of greatest shielding, δ_{33} (or $\delta_{\parallel}$) = -90 ppm, is along the C,C bond, with $\delta_{11} = \delta_{22}$ (or $\delta_{\perp}$) = 150 ppm.[55]

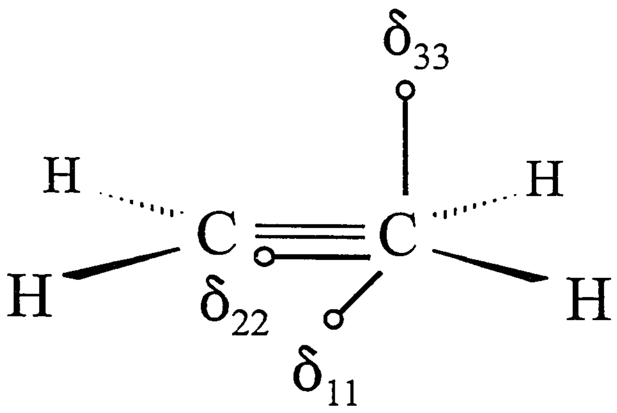

Figure 1.6 Orientation of the carbon chemical shift tensor for ethylene.[55]

1.5.2 Solid-State Carbon-13 NMR Investigations of Platinum-Alkene Complexes

Although platinum-alkene complexes have been studied extensively by ^{13}C NMR of solutions (Section 1.3), there are few corresponding studies of solids. The alkenyl carbon CS tensors for several Pt-cod (cod = cyclooctadiene) and Pt-nbd (nbd = norbornadiene) complexes have been determined through the analysis of ^{13}C NMR spectra of magic-angle spinning[57,58] (MAS) or stationary powder samples.[59] The magnitudes of

Table 1.2 Principal Components of the Alkenyl Carbon Chemical Shift Tensors for Some Platinum-Alkene Complexes.[a]

	δ_{11}	δ_{22}	δ_{33}	δ_{iso}	Ω	κ	Ref
nbd[b]	259	130	40	143	219	-0.18	59
Pt(nbd)Me$_2$	179.2(10)	77.0(7)	10.7(9)	89	168.5	-0.21	57
Pt(nbd)-[CH$_2$SiMe$_3$]$_2$[c]	171.8(12)	70.7(11)	7.4(11)	83.3	164.4	-0.23	57
	178(3)	73(2)	4(2)	85.0	174	-0.21	
	182(6)	76(5)	7(5)	88.1	175	-0.21	
	181.1(8)	81.6(7)	12.4(7)	91.7	168.7	-0.18	
Pt(nbd)(4-^{t}Bu-phenyl)$_2$[c]	195(12)	73(18)	10(10)	93.3	185	-0.33	57
	189(7)	102(6)	9(4)	100.5	180	0.03	
cod[d]	238	126	21	128	217	0.03	59
Pt(cod)Cl$_2$	182.3	104	18	103	164.3	0.02	58
Pt(cod)Cl$_2$	185	112	3	101	182	0.18	59
Pt(cod)Me$_2$[c]	179(1)	99(1)	15(1)	98.0	164	0.02	57
	185(3)	103(3)	17(2)	101.7	168	0.02	
Pt(cod)(Me)Cl[c]	159(3)	88(2)	10(2)	86.1	149	0.04	57
	203(2)	115(1)	22(2)	114.0	181	0.02	
	208(2)	122(2)	22(2)	117.2	186	0.08	
Pt(cod)-[CH$_2$SiMe$_3$]$_2$[c]	170(3)	107(2)	9(4)	95.4	161	0.22	57
	188(4)	108(3)	7(5)	100.7	181	0.12	
	187(5)	106(3)	15(5)	102.8	172	0.06	
Pt(cod)(C$_2$-^{t}Bu)$_2$[c]	192(4)	102(5)	15(4)	103.5	177	-0.03	57
	196(4)	113(5)	15(5)	106.6	181	0.11	

a. Measured at room temperature. Chemical shifts, relative to δ_{iso}(TMS) = 0, and the span, Ω, are in ppm. Where reported, the uncertainty in the last digits are given in parentheses.

b. nbd = norbornadiene. See Fig. 1.7 A for the structures of the Pt-nbd complexes.

(*continued on next page*)

Table 1.2 (*cont.*)

c. Crystallographically distinct carbon sites were reported.

d. cod = 1,5-cyclooctadiene. See Fig. 1.7 B for the structures of the Pt-cod complexes.

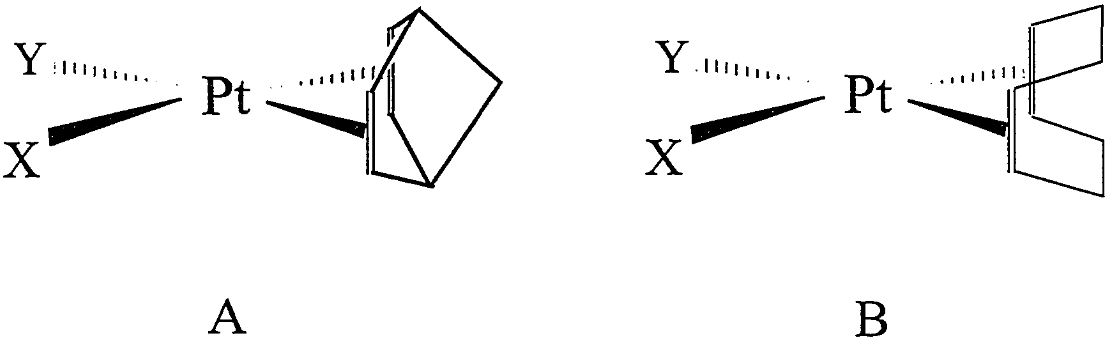

A

B

Figure 1.7 Structure of Pt-nbd complexes (A) and Pt-cod complexes (B), X,Y = Cl, Me, CH_2SiMe_3, $C_2{}^t$Bu or 4-^{t}Bu-phenyl.

the principal components of the carbon CS tensors were reported; these are summarized in Table 1.2. Carbon CS tensor orientations were not determined from these experiments; orientations for the alkenyl carbon CS tensors for Pt(cod)Cl_2 were proposed (*vide infra*), based on density functional theory (DFT) calculations.[58] In addition to the studies summarized in Table 1.2, Zeise's salt[58,60,61] and Zeise's dimer[60] have been studied by solid-state ^{13}C NMR; these experiments are discussed in detail in Section 4.1.

Some general trends are apparent from the data summarized in Table 1.2. In all cases, the isotropic shielding of the alkenyl ^{13}C nuclei increases upon coordination of the ligand with platinum; this general trend has been observed in ^{13}C NMR studies of samples in solution (Section 1.3). The most affected tensor component is δ_{11}, which is shifted to lower frequency by up to 87 ppm. The δ_{33} component is less sensitive to metal coordination, although the shielding in this direction usually is greater for the coordinated species. In general, the shielding of the alkenyl carbon nuclei is not very sensitive to the nature of the other ligands coordinated with platinum, although one of the two sites observed for Pt(nbd)(*tert*-butylphenyl)$_2$ is somewhat different. Interestingly, although the carbon CS tensors for Pt(cod)Cl$_2$ and Pt(cod)Me$_2$ are comparable, those for the non-equivalent carbon sites of Pt(cod)MeCl are significantly different, suggesting that the observed shielding cannot be explained simply by considering the ligands *trans* or *cis* to the observed nucleus.

The data summarized in Table 1.2 are a useful extension of data acquired for similar samples in isotropic liquids, demonstrating the importance of considering the principal components of CS tensors when investigating the effects of metal coordination on magnetic shielding. More information about the CS tensor orientations would be useful, since the directions of CS tensor components relative to the molecular framework are not necessarily the same for the ligand before and after coordination. However, it is noted that the alkenyl carbon CS tensor orientation calculated by Oldfield and coworkers for Pt(cod)Cl$_2$ is not very different from that for ethylene.[58] The data presented in Table 1.2 are for Pt(II)-alkene complexes; corresponding data for Pt(0)-alkene complexes would be very instructive.

1.5.3 Solid-State Carbon-13 NMR Investigations of Some Copper-Alkene Complexes

Wallraff[59] undertook a study of the alkenyl carbon CS tensors for several Cu(alkene)(OTf) complexes, where OTf = trifluoromethanesulfonate, $CF_3SO_3^-$; the results are summarized in Table 1.3. The coordination of the alkene and of the oxygen atoms about the copper atom in a typical Cu-OTf complex is illustrated in Figure 1.8. The principal components of the carbon CS tensors were determined from the analysis of ^{13}C NMR spectra of stationary powder samples at natural abundance. The reported values have significant uncertainties associated with them, a consequence of the broad ^{13}C NMR spectra. The author attributes the broadening primarily to the dipolar coupling with the $^{63/65}Cu$ nuclei. Based on the reported Cu,C bond lengths of approximately 2.07 Å for the Cu(cyclohexene)OTf complex,[62] the dipolar couplings of the alkenyl ^{13}C with ^{63}Cu ($I = 3/2$, natural abundance = 69.09 %) and with ^{65}Cu ($I = 3/2$, natural abundance = 30.91 %) are predicted to be 907 and 970 Hz, respectively. In addition to the carbon CS tensor data

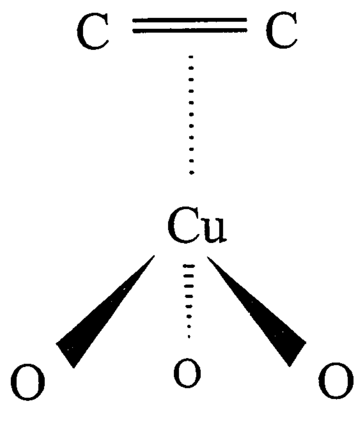

Figure 1.8 Orientation of the alkenyl C,C bond and of the oxygen atoms about the copper atom in a typical Cu-OTf complex. The oxygen atoms shown here are from separate $CF_3SO_3^-$ units. From reference 62.

Table 1.3 Principal Components of the Carbon Chemical Shift Tensors for Some η^2-Coordinated Copper(OTf)-Alkene[a] Complexes.[b]

	δ_{11}	δ_{22}	δ_{33}	δ_{iso}	Ω	κ	Ref
C_2H_4[c]	234	120	24	126	210	-0.09	54
$Cu(C_2H_4)(OTf)$	218	82	-32	90	250	-0.10	59
cis-2-butene	232	119	22	124	210	-0.07	54
Cu(*cis*-butene)(OTf)	172	116	5.4	98	166.6	0.32	59
dmb[d]	217	126	35	123	182	0.05	59
Cu(dmb)(OTf)	158	127	45	110	113	0.45	59
cis-cycloheptene	245	126	27	133	218	-0.10	54
cyclohexene				127			59
Cu(cyclohexene)(OTf)				105			59
cis-cyclooctene				131			59

a. OTf = trifluoromethanesulfonate, $CF_3SO_3^-$.

b. Measured at room temperature, unless otherwise specified. Chemical shifts, relative to $\delta_{iso}(TMS) = 0$, and the span, Ω, are in ppm.

c. Measured at 30 K.

d. dmb = 2,3-dimethyl-2-butene.

discussed above, the isotropic chemical shifts for the alkenyl carbon nuclei of solid cyclohexene- and *cis*-cyclooctadiene-copper complexes were reported (Table 1.3). Coordination of alkenes with copper results in increased shielding of the carbon nuclei in all cases.

However, unlike the data for the platinum-alkene complexes (Table 1.2), no clear trends for the CS tensor components are discerned, perhaps a consequence of the approximate nature of the data. Wallraff[59] discussed the results on the basis of the Dewar, Chatt and Duncanson model.[28]

1.5.4 Solid-State Carbon-13 NMR Investigations of Some Metal-Alkene and Metal-Alkyne Complexes

The carbon CS tensor principal components for several η^4-coordinated cyclic ligands have been determined by the analysis of ^{13}C NMR spectra of MAS[58] or stationary powder[59] samples. The data are summarized in Tables 1.2 (platinum complexes) and 1.4 (other metal centres). In general, the effects of metal coordination on the alkenyl carbon CS tensors for cyclic dienyl ligands are comparable to those observed for metal coordination of alkenes; the isotropic shielding increases, although the increased shielding is negligible in the case of the Ag-cod complex. In general, δ_{11} is the most affected component.

Data for the cyclooctadiene ligand coordinated with various metal centres (Tables 1.2 and 1.4) allow a comparison of the effect of the metal on the carbon CS tensors; for convenience the portion of the periodic table encompassing these metals is reproduced in Figure 1.9. The structures of the Cu-cod[63] and Ag-cod[64] complexes investigated by solid-state NMR are illustrated in Figure 1.10. The rhodium-, iridium-, palladium- and platinum-cod complexes are particularly instructive since they formally have d^8 valence shells with a similar environment about the metal. The isotropic shielding increases on

Table 1.4 Principal Components of the Alkenyl Carbon Chemical Shift Tensors for Some Metal-Alkene Complexes.[a]

	δ_{11}	δ_{22}	δ_{33}	δ_{iso}	Ω	κ	Ref
nbd[b]	259	130	40	143	219	-0.18	59
$[Rh(nbd)Cl]_2$	120	66	-31	52	151	0.28	59
cot[c]	234	127	43	133	191	-0.09	59
$[Rh(cot)Cl]_2$[d]	142	80	12	81	130	-0.02	59
hmdb[e]	242	147	53	147	189	0.00	65
$[Rh(hmdb)Cl]_2$	138	60	10.7	68	127.3	-0.19	59
cod[f]	238	126	21	128	217	0.03	59
$[Rh(cod)Cl]_2$	161.7	76.7	20.5	80.5	141.2	-0.08	58
$[Rh(cod)Cl]_2$	140	79	14.5	80	125.5	-0.02	59
$[Ir(cod)Cl]_2$	122	67	-1	62	123	0.12	59
$Pd(cod)Cl_2$	225	125	1	117	224	0.11	59
$[Cu(cod)Cl]_2$[g]	203.5	116.0	36.5	118.8	167.0	-0.05	58
$[Ag(cod)_2]BF_4$[h]	225	115.0	34.0	124.8	191.0	-0.15	58

a. Chemical shifts, relative to δ_{iso}(TMS) = 0, and the span, Ω, are in ppm.

b. nbd = norbornadiene.

c. cot = 1,3,5,7-cyclooctatetraene.

d. The CS tensor components for the coordinated alkenyl carbon nuclei are given here.

e. hmdb = hexamethyl dewar benzene. Measured at 87 K.

(*continued on next page*)

Table 1.4 (*cont.*)

f. cod = cyclooctadiene.

g. See Fig. 1.10 A for the molecular structure of $[Cu(cod)Cl]_2$.

h. See Figure 1.10 B for the structure of $[Ag(cod)_2]^+$.

	Group		
Period	9	10	11
4	27 Co	28 Ni	29 Cu
5	45 Rh	46 Pd	47 Ag
6	77 Ir	78 Pt	79 Au

Figure 1.9 Portion of the periodic table encompassing the metal centres discussed in Section 1.5.4.

going from period 5 to period 6, or on going from group 10 to group 9. Hence, the alkenyl carbon nuclei of the iridium-cod complex are the most affected by metal-coordination.

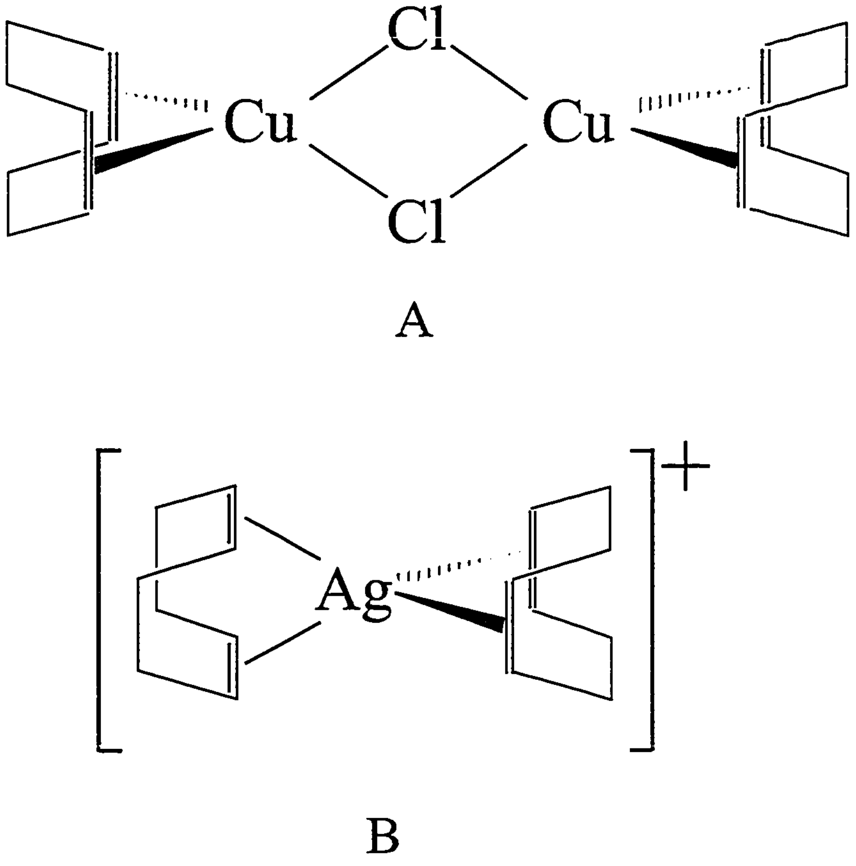

Figure 1.10 Structures of $[Cu(cod)Cl]_2$[63] (A) and of the $[Ag(cod)_2]^+$ cation[64] (B).

The effect of metal coordination on nuclear magnetic shielding is difficult to predict. Wallraff[59] considered that the principal components of a strongly coordinated complex might approach those for cyclopropane,[66] since the carbon nuclei are in strained environments in both cases. However, the author concludes that the environment about the carbon nuclei for cyclopropane and the metallacyclopropane structure are too different to allow a meaningful comparison. Nuclear magnetic shielding is very sensitive to small structural differences. For example, in a computational study, Chesnut and Wright found that the carbon magnetic shielding derivative with respect to C,C bond extension for ethylene is -177 ppm/Å.[67] As well, relativistic effects,[68-70] significant for heavier elements, also affect the magnetic shielding of ligands directly coordinated with them.[71,72] Nevertheless, the fact that the CS tensor components for the Pd-cod complex are not significantly different from the corresponding values for the uncoordinated cyclooctadiene ligand suggests that this is a very weak coordination complex. Calculations using DFT suggest that the coordination energy for a neutral palladium-ethylene complex is significantly less than that for the corresponding platinum-ethylene complex.[29] The alkenyl carbon CS tensors for the Cu- and Ag-cod complexes (both metals formally with d^{10} electronic configurations) also do not differ significantly from that for the uncoordinated ligand.

DFT calculations suggest that alkenyl carbon CS tensor orientations, not determined experimentally, are generally sensitive to the degree of metal to ligand back bonding.[58] Increased back bonding leads to a rotation of the CS tensor about the δ_{11} component. For $[Rh(cod)Cl]_2$, the δ_{22} and δ_{33} components form angles of 37.5° and 107.3°, respectively, with the alkenyl C,C bond.

Principal components of the alkynyl carbon CS tensors for metal-alkyne complexes have not been reported, but Wallraff reported the isotropic carbon chemical shifts for some solid copper-alkyne complexes[59] determined by ^{13}C NMR of MAS samples. The data, summarized in Table 1.5, show that coordination of alkynes with copper has a small effect on δ_{iso}. Caution should be used in reaching conclusions from this observation, since the invariance of δ_{iso} may reflect opposing changes to the CS tensor components. Hence, coordination with copper may have a greater effect on the magnetic shielding of the alkynyl nuclei than is suggested by the data presented in Table 1.5.

Table 1.5 Isotropic Carbon Chemical Shifts for Some Solid Alkynes and Copper-Alkyne Complexes.[a]

	δ_{iso}/ppm	Ref		δ_{iso}/ppm	Ref
acetylene[b]	70	55	DPA[c]	89.8	this work
Cu(acetylene)(OTf)[d]	77	59	Cu(DPA)(OTf)	93	59
2-butyne	74.8	73	btsa[e]	114	59
Cu(2-butyne)(OTf)	81	59	Cu(btsa)(OTf)	114	59

a. Chemical shifts are in ppm, relative to δ_{iso}(TMS) = 0.

b. Measured at 15 K.

c. DPA = diphenylacetylene. See Section 6.3.1 for a discussion of the experimental results.

d. OTf = trifluoromethanesulfonate.

e. btsa = *bis*-(trimethylsilyl) acetylene.

1.5.5 Solid-State Carbon-13 NMR Investigations of Some η^5- and η^6-Coordinated Metal Complexes.

Solid-state ^{13}C NMR investigations of η^5- and η^6-metal complexes provide useful insights into nuclear magnetic shielding of unsaturated carbon ligands coordinated with metals. Such experiments also demonstrate how information about internal dynamics is available from standard one-dimensional NMR experiments. Representative data are summarized in Table 1.6.

The determination by Orendt and coworkers[74] of the carbon CS tensors for rigid ferrocene, measured at 9 K and higher, has provided some fundamental information about the internal dynamics of the cyclopentadienyl ligands in these complexes. The investigation also provided experimental evidence for the CS tensor orientations in the absence of motion, allowing a comparison of the magnetic shielding in specific directions with those for the cyclopentadienyl ligand.[75] The average of the two CS tensor components approximately in the plane of the cyclopentadienyl ligand, δ_{11} = 121 ppm and δ_{22} = 71 ppm, corresponds to the value of $\delta_{\perp}$ determined from spectra acquired at 77 K[76] and at room temperature.[74,77,78] The experiment of Orendt and coworkers confirmed the earlier conclusion that the direction of greatest shielding is approximately perpendicular to the plane of the cyclopentadienyl ligand.[77] By obtaining ^{13}C NMR spectra as a function of temperature, the authors showed that motion of the ring about the ligand C_5 symmetry axis is not significant at temperatures below 45 K.[74] The orientation of δ_{33} relative to the ligand C_5 axis was determined by comparing the magnitudes of δ_{33} measured in the absence ofmotional averaging, δ_{33} = 13 ppm, with those obtained at room temperature, δ_{33} = 18 ppm. The authors found that δ_{33} forms an angle of ±12.4 ± 0.7° with the ligand C_5 axis; the sign of this angle is unavailable from the experiment (Figure 1.11). NMR shielding calculations using density functional theory were undertaken on optimized structures and on the three known structures of solid ferrocene.[74] These calculations accurately predict the magnitudes of the CS tensor principal components and suggest that δ_{33} is oriented as shown in Figure 1.11. The proposed orientation for the carbon CS tensor is comparable

Table 1.6 Principal Components of the Carbon Chemical Shift Tensors for Some η^5- and η^6-Coordinated Metal Complexes.[a]

	δ_{11}	δ_{22}	δ_{33}	δ_{iso}	Ω	κ	Ref
$[Cp^-]^b$	182	114	21	106	161	0.15	75
$FeCp_2{}^c$	121(3)	71(2)	13(2)	68(2)	108	0.08	74
$FeCp_2$	96	96	18	70	78	1.00	74
$FeCp_2{}^d$	94	94	18	69	76	1.00	76
$FeCp_2$	94	94	17	68	77	1.00	77
$FeCp_2$	95.0(5)	95.0(5)	17.8(5)	69.3(9)	77.2	1.00	78
$Fe(C_5Me_5)_2{}^e$	128.0(10)	85.5(10)	22.9(10)	78.8	105.1	0.19	82
$C_6H_6{}^f$	217.2(32)	141.0(20)	1.3(30)	119.8	215.9	0.29	79
$Cr(C_6H_6)_2{}^d$	114	114	0	76	114	1.00	76
$Cr(C_6H_6)(CO)_3$	152(5)	138(5)	7(5)	99	145	0.81	80
$C_6Me_6{}^g$	227(4)	155(4)	19(4)	133(4)	208	0.32	81
$Cr(C_6Me_6)(CO)_3$	170(5)	138(5)	25(5)	111	145	0.56	80
$C_6Et_6{}^h$	220.1(7)	164.2(7)	21.4(7)	135.2(10)	198.7	0.44	81
$Cr(C_6Et_6)(CO)_3{}^i$	170(5)	161(5)	29(5)	120	141	0.87	80
	168(5)	146(5)	22(5)	112	146	0.70	

a. Chemical shifts, relative to δ_{iso}(TMS) = 0, and the span, Ω, are in ppm. Spectra were acquired at room temperature unless otherwise specified. The uncertainties in the last digits, where reported, are given in parentheses.

(*continued on next page*)

Table 1.6 (*cont.*)

b. Cp = cyclopentadienyl. The sample was prepared by dissolving cyclopentadiene in $NH_3(l)$ from excess $NaNH_2$ and cooling to 20 K.

c. Average values for spectra acquired at 9, 15 and 25 K were reported.

d. Measured at 77 K.

e. Measured at 113 K.

f. Measured at 14 K.

g. Measured at 87 K.

h. Et = ethyl. The average of the three observed values for each tensor component are reported here.

i. Non-equivalent carbon sites were reported.

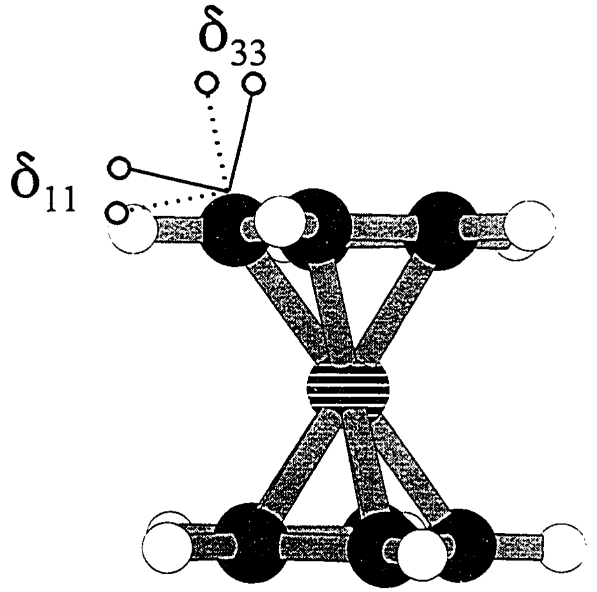

Figure 1.11 Orientation of the carbon CS tensors for ferrocene.[74] The solid lines indicate the orientation assigned on the basis of experimental and theoretical data, the dotted lines represent an alternative orientation from the experimental results. The δ_{22} component is tangential to the cyclopentadienyl ring, perpendicular to the page here.

to that found for permethyl ferrocene.[82] Comparison of the carbon CS tensor components for ferrocene[74] with those for the cyclopentadienyl anion[75] (Table 1.6) shows that the effect of metal coordination is comparable to that observed for the metal-alkene complexes discussed above: the shielding in the direction of δ_{11} increases significantly, while the shielding in the direction of δ_{33} is virtually unchanged.

Carbon-13 NMR data for the η^6-coordinated complexes are also summarized in Table 1.6. The carbon CS tensors for $Cr(C_6H_6)_2$, determined by Wemmer and Pines,[76] are axially symmetric at 77 K, demonstrating that the benzene ligands rotate rapidly about the C_6 axis at this temperature; the direction of greatest shielding is perpendicular to the ring plane. Comparison of the CS tensors for this complex with those for benzene[79] show that the magnetic shielding perpendicular to the ring is unaffected by coordination, but the in-plane components are shielded significantly. The CS tensor principal components for the ring carbon nuclei of the corresponding arene chromium tricarbonyl complexes, determined by the method of moments,[83] were reported by Maricq and coworkers.[80] The study showed that the increased isotropic shielding of 15 to 20 ppm relative to that for benzene arises almost entirely from the increased shielding in the direction of δ_{11}. The methyl and ethyl substituted derivatives of the arene chromium tricarbonyl complex exhibit similar behaviour. Orientations for the carbon CS tensors were not determined, but the authors[80] speculate that these are the same as those of benzene, illustrated in Fig. 1.12.

1.6 Outline of the Thesis

There are two facets to the work presented in this thesis: the acquisition and

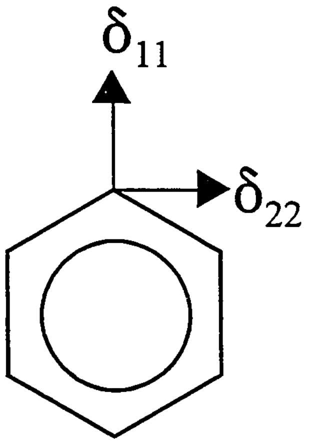

Figure 1.12 Orientation of the carbon CS tensor for benzene.[79] The δ_{33} component is perpendicular to the molecular plane.

analysis of solid-state NMR spectra of platinum-alkene or platinum-alkyne complexes, and the application of *ab initio* methods to assist in the assignment of CS tensor orientations. In Chapter 2, the theoretical background for the NMR experiments is presented, emphasizing the interpretation of NMR spectra acquired in this work. This section also includes a general outline of the experimental procedures; specific experimental details are given in the relevant sections. Before presenting a detailed discussion of the experimental results, it is useful to consider the various computational techniques employed in the course of this work. Calculations on the platinum complexes considered in this work and on some related complexes are summarized in Chapter 3. In subsequent sections, *ab initio* calculations are considered only to the extent needed to assign CS tensor orientations. The experimental work is presented in three sections: the investigation of the alkenyl carbon CS tensors and internal dynamics of Pt(0)- and Pt(II)-ethylene complexes (Chapter 4), the determination of the carbon CS tensors for *trans*-stilbene and Pt(η^2-*trans*-stilbene)(PPh_3)$_2$ (Chapter 5) and the determination of the alkynyl carbon CS tensors for diphenylacetylene and Pt(η^2-diphenylacetylene)(PPh_3)$_2$ (Chapter 6). Proposals for extensions of this work and concluding remarks are presented in Chapters 7 and 8, respectively.

Chapter 2

Solid-State NMR—Background

The basic pulsed Fourier transform NMR experiment can be summarized as follows: *i*) a thermal equilibrium between magnetically active nuclei in different spin states is established by placing a sample in a strong external applied magnetic field, $\mathbf{B}_0$; *ii*) the equilibrium is perturbed by the application of a radio-frequency (rf) pulse; and *iii*) the response of the spin system as a result of the perturbation is monitored through the acquisition of a free induction decay (FID). The reader is referred to several introductory texts for a detailed description of nuclear magnetic resonance.[84-90] A brief overview of some fundamental concepts and terms is presented here.

2.1 Interactions in the Solid State

In this work, the NMR properties of solid samples are investigated. In an applied magnetic field, such samples are subject to numerous interactions, summarized by the Hamiltonian ($\mathcal{H}$):[14-17,91-93]

$$\mathcal{H} = \mathcal{H}_Z + \mathcal{H}_S + \mathcal{H}_J + \mathcal{H}_{DD} + \mathcal{H}_Q. \qquad 2.1$$

The terms in eq 2.1 describe the Zeeman, $\mathcal{H}_Z$, magnetic shielding, $\mathcal{H}_S$, indirect coupling, $\mathcal{H}_J$, direct dipolar coupling, $\mathcal{H}_{DD}$ and quadrupolar coupling, $\mathcal{H}_Q$, interactions, discussed in detail below.

2.1.1 The Zeeman Interaction

A fundamental property of a nucleus is its spin angular momentum, P. The magnitude of P, a vector quantity, is given by:

$$P = \hbar[I(I + 1)]^{1/2} \qquad 2.2$$

where $\hbar$ is the Planck constant, h, divided by 2π, and I is the nuclear spin quantum number, $I = 0, \frac{1}{2}, 1, \ldots$ Nuclei with spin number $I > 0$ have associated with them a nuclear magnetic moment, μ, which is also a vector quantity. The magnetic moment is proportional to spin angular momentum:

$$\mu = \gamma \mathbf{P} \qquad 2.3$$

where the proportionality constant γ is known as the magnetogyric ratio. Quantum theory requires that the allowed components of the nuclear spin vector be quantized. For a nucleus of spin I, there are $2I + 1$ components of the spin vector, where the quantum number m_I may take discrete values between $-I, -I + 1, -I + 2, \ldots I$. The energy, or Zeeman levels for a nucleus placed in an applied magnetic field along the z-axis is described by the Hamiltonian $\mathcal{H}_Z$ (eq 2.4).

$$\begin{aligned} \mathcal{H}_Z &= -\mu \cdot \mathbf{B}_0 \\ &= -\gamma \hbar I_z \mathbf{B}_0. \end{aligned} \qquad 2.4$$

In eq 2.4, I_z describes the component of the angular momentum operator in the direction of $\mathbf{B}_0$. For isolated nuclei, it is easy to show[85-90] that NMR transitions will take place at a frequency, ν_0, known as the Larmor frequency:

$$\nu_0 = \frac{|\gamma| B_0}{2\pi}. \qquad 2.5$$

2.1.2 Nuclear Magnetic Shielding

If eq 2.5 described the magnetic resonance frequencies of all nuclei, applications of NMR would be very limited, since the technique would only distinguish between isotopes. In fact, the magnetic resonance frequency of a nucleus is very sensitive to its electronic environment. The Zeeman interaction between nucleus *A* and $\mathbf{B}_0$ must include another interaction, described by the Hamiltonian:[14-17,93]

$$\mathcal{H}_S = \gamma \hbar \mathbf{I}_A \cdot \boldsymbol{\sigma} \cdot \mathbf{B}_0. \qquad 2.6$$

where $\mathbf{I}_A$ is the nuclear spin angular momentum operator of spin *A*. The magnetic shielding tensor, $\boldsymbol{\sigma}$, is defined by:

$$\boldsymbol{\sigma} = \begin{bmatrix} \sigma_{xx} & \sigma_{xy} & \sigma_{xz} \\ \sigma_{yx} & \sigma_{yy} & \sigma_{yz} \\ \sigma_{zx} & \sigma_{zy} & \sigma_{zz} \end{bmatrix} \qquad 2.7$$

The magnetic shielding tensor in eq 2.7 is the sum of the symmetric, $\boldsymbol{\sigma}^{\mathrm{symm}}$, and antisymmetric, $\boldsymbol{\sigma}^{\mathrm{anti}}$, tensors.[94] The former consists of 3 diagonal elements, $\sigma_{ii}^{\mathrm{symm}}$ and six off-diagonal elements, $\sigma_{ij}^{\mathrm{symm}} = \sigma_{ji}^{\mathrm{symm}}$, such that the magnetic shielding tensor may be described by 6 independent parameters. Since $\sigma_{ii}^{\mathrm{anti}} = 0$ and $\sigma_{ij}^{\mathrm{anti}} = -\sigma_{ji}^{\mathrm{anti}}$, $\boldsymbol{\sigma}^{\mathrm{anti}}$ is described by at most three independent parameters. To a good approximation, the line shapes observed in the NMR spectra of solids are only dependent on $\boldsymbol{\sigma}^{\mathrm{symm}}$.[88,95,96] Hence, $\boldsymbol{\sigma}^{\mathrm{anti}}$ is not considered further here. In its PAS, the off-diagonal elements of the symmetric magnetic shielding tensor are zero:

$$\sigma_{PAS} = \begin{bmatrix} \sigma_{11} & 0 & 0 \\ 0 & \sigma_{22} & 0 \\ 0 & 0 & \sigma_{33} \end{bmatrix} \qquad 2.8$$

Hence, $\boldsymbol{\sigma}$ may be described by the principal components, σ_{ii} (i = 1,2,3) and by three Euler angles, α, β and γ, which describe the orientation of the PAS of the magnetic shielding tensor relative to the molecular framework.[88,97] These parameters may be determined by investigating the magnetic shielding of nuclei in single crystals as a function of the crystal orientation in the magnetic field,[98-103] but such experiments are time-consuming, and single crystals of sufficient size and quality are not always available.

The resonance frequency, ν_A, of a nucleus in an applied magnetic field is given by:[104]

$$\nu_A = \nu_0[1 - (\sigma_{11}\sin^2\theta\cos^2\phi + \sigma_{22}\sin^2\theta\sin^2\phi + \sigma_{33}\cos^2\theta)]. \qquad 2.9$$

The angles θ and ϕ orient the magnetic field in the principal axis system (PAS) of the magnetic shielding tensor (Fig. 2.1). For powder samples, the observed spectrum is the sum of the resonance frequencies from all crystallites in the sample. Eqs 2.5 and 2.9 demonstrate an important feature of nuclear magnetic resonance: the resonance frequency of a nucleus is proportional to $\mathbf{B}_0$.

2.1.3 Indirect Nuclear Spin-Spin Coupling

Indirect spin-spin coupling defines the electron-mediated interaction between two nuclear magnetic moments. The strength of this interaction depends on the electronic structure of the molecule and in particular on the nature of the bonding between the nuclei. The

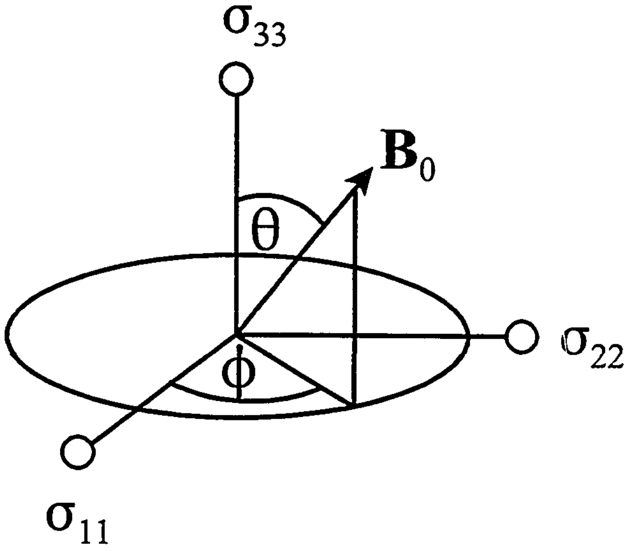

Figure 2.1 Orientation of the applied magnetic field, $\mathbf{B}_0$, relative to the PAS of the magnetic shielding tensor.

Hamiltonian describing indirect coupling is:[14,95]

$$\mathcal{H}_{DD} = \hbar \mathbf{I}_A \cdot \mathbf{J} \cdot \mathbf{I}_B \qquad 2.10$$

where **J** is the indirect coupling tensor. Similar to the magnetic shielding tensor, the off-diagonal elements of the symmetric portion of **J** are zero in its PAS:

$$\mathbf{J} = \begin{bmatrix} J_{11} & 0 & 0 \\ 0 & J_{22} & 0 \\ 0 & 0 & J_{33} \end{bmatrix} \qquad 2.11$$

In contrast to the direct coupling (*vide infra*), the trace of **J** is not zero and hence the isotropic indirect coupling, $J_{iso} = \frac{1}{3}\mathrm{Tr}\mathbf{J}$, is observed in solution or under conditions of magic angle spinning. The anisotropy in **J**, ΔJ, is:

$$\Delta J = J_{33} - \frac{1}{2}(J_{11} + J_{22}) \qquad 2.12$$

For an axially symmetric **J** tensor, eq 2.12 simplifies to:

$$\Delta J = J_{\parallel} - J_{\perp}. \qquad 2.13$$

Since in most cases only J_{iso} is determined, **J** is often assumed to be axially symmetric regardless of the local symmetry. Recent high-level calculations in this lab have shown that this assumption is questionable.[105]

2.1.4 Direct Dipolar Coupling

Two magnetically active nuclei A and B separated by r_{AB}, will experience a direct dipole-dipole interaction, a consequence of the relatively small magnetic fields arising from the nuclei.[14,93,104,106] The Hamiltonian that describes this interaction may be written as:[106]

$$\mathcal{H}_{\text{DD}} = \hbar R_{\text{DD}} \mathbf{I}_{\text{A}} \cdot \mathbf{D} \cdot \mathbf{I}_{\text{B}}. \qquad 2.14$$

The direct dipolar tensor, **D**, is symmetric with a trace of zero. Hence $D_{11} = D_{22}$ and $D_{33} = -2D_{11}$. Consequently, the dipolar interaction is not observed for samples in isotropic fluids, or in general, for solid samples spinning at the magic angle. The direct dipolar coupling constant, R_{DD}, is described by:

$$R_{\text{DD}} = \left(\frac{\mu_o}{4\pi}\right)\left(\frac{\hbar}{2\pi}\right)\gamma_{\text{A}}\gamma_{\text{B}}\langle r_{\text{AB}}^{-3}\rangle \qquad 2.15$$

The angular brackets in eq 2.15 indicate that r_{AB}, and hence the observed dipolar coupling, are subject to motional averaging.[107]

Experimentally the dipolar coupling is modified by ΔJ (eq 2.12), and an effective dipolar coupling is observed:[106]

$$R_{\text{eff}} = R_{\text{DD}} - \frac{\Delta J}{3}. \qquad 2.16$$

In principle, the contribution of ΔJ to R_{eff} should be considered if conclusions are to be reached about r_{AB} from a measured dipolar coupling, but this value is rarely known. $\Delta^1J(^{13}C,^{13}C)$ has not been determined for any of the compounds considered in this work, but it is thought to be small. For example, a recent experimental study of ethylene oriented in liquid crystal solvents reported values $\Delta^1J(^{13}C,^{13}C)$ ranging from 3 to 21 Hz.[50] For benzene-$^{13}C_6$, $\Delta^1J(^{13}C,^{13}C)$ is 17 to 21 Hz.[108] These results have been corroborated by high-level *ab initio* calculations.[50,108] In contrast, the $^{13}C,^{13}C$ dipolar coupling expected for ethylene, based on $r_{\text{CC}} = 1.3384$ Å,[25] is 3170 Hz. Hence, the contribution of $\Delta J/3$ is expected to be negligible and $R_{\text{eff}} \approx R_{\text{DD}}$.

In the absence of other interactions or of rapid motion, the contribution to an NMR spectrum from a pair of magnetically-active nuclei consists of a doublet with a splitting that depends on the magnitude of R_{eff} and on the orientation of the dipolar vector relative to $\mathbf{B}_0$. The orientation dependence is given by $(3\cos^2\theta_D - 1)$ where θ_D is the angle between the dipolar vector and the applied magnetic field. For a powder sample, the sum of the peaks from these transitions gives rise to the characteristic Pake doublet (Figure 2.2).[109] The line shapes of the spectra predicted by this basic model are the same for all nuclei, but the breadth of the spectra depends on the nature of the spin system. For an AX spin system consisting of

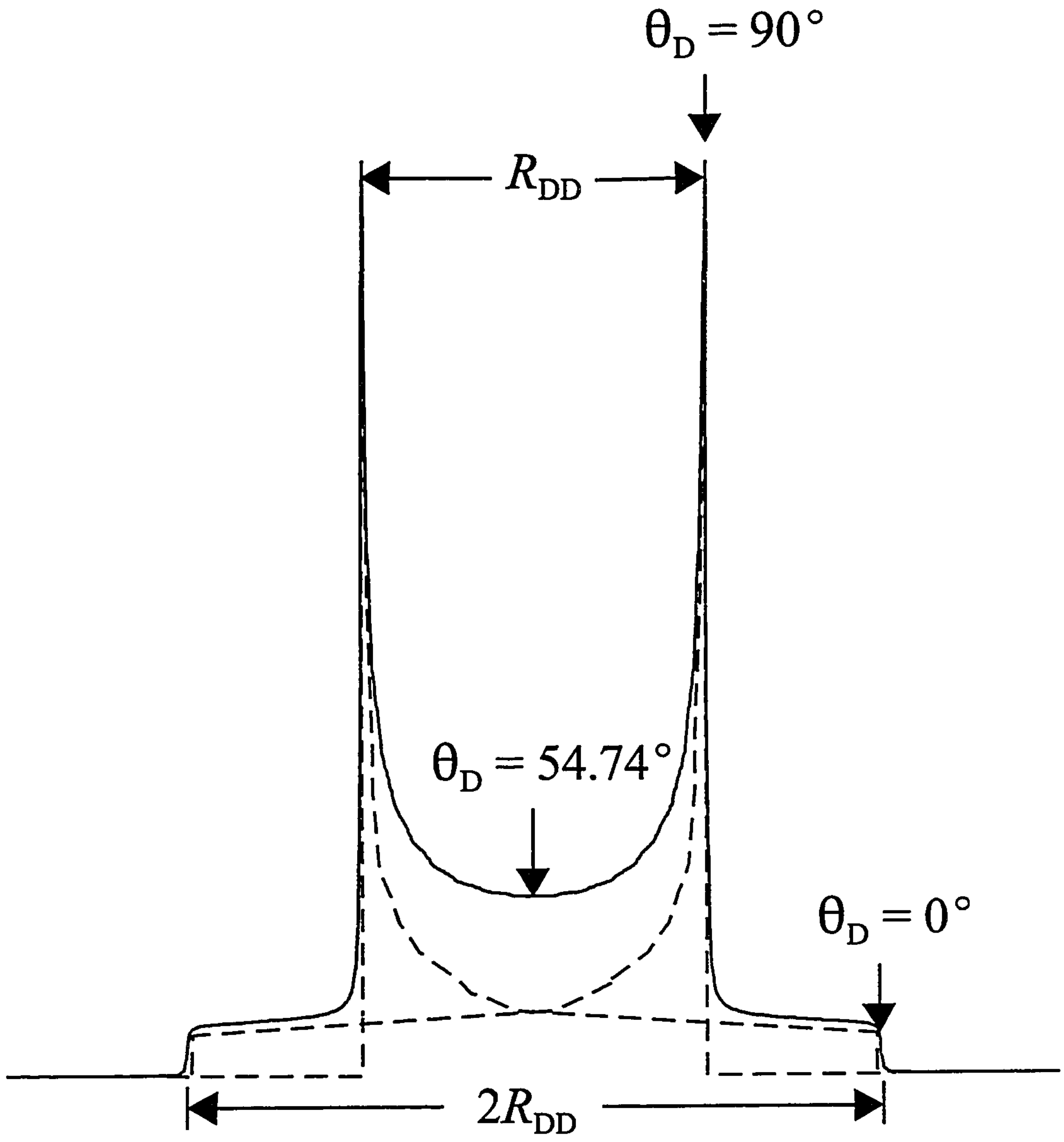

Figure 2.2 The Pake doublet powder pattern expected for a dipolar-coupled *AX* spin pair in the absence other spin interactions. The angle θ_D defines the orientation of the dipolar vector relative to $\mathbf{B}_0$; note that the orientation labelled 90° contains a contribution to the total intensity from the other transition, corresponding to $\theta_D \approx 35.3°$. The dotted lines represent the two subspectra contributing to the total line shape.

a pair of spin-½ nuclei, the "horns" and the outer shoulders of the spectrum are separated by R_{DD} and $2R_{DD}$, respectively, as illustrated in Figure 2.2. The powder pattern for a spin pair in which one of the nuclei has spin $I \geq 1$ is more complex; such spectra have been described elsewhere.[110] For a pair of magnetically equivalent nuclei (*i.e.*, an A_2 spin system), the horns and shoulders of the Pake doublet are separated by $1.5R_{DD}$ and $3R_{DD}$, respectively. The difference between the dipolar splitting for the AX and A_2 spin systems is a consequence of the "flip-flop" term in the dipolar Hamiltonian.[106] Pake powder patterns are generally not observed since other interactions, particularly anisotropic magnetic shielding, also contribute to the line shapes of NMR spectra, resulting in more complex powder patterns.[104,111]

2.1.5 Nuclear Quadrupolar Coupling

Nuclear quadrupolar interactions are important when considering the line shapes of nuclei with spin $I > ½$, or when describing the line shapes of spin-½ nuclei that are subject to spin-spin coupling with quadrupolar nuclei. The concepts describing NMR of quadrupolar nuclei have been presented in several texts and review articles.[7,93,95,112,113] A general overview of nuclear quadrupolar coupling is presented here. Specific expressions describing the line shapes of ^{2}H NMR spectra are given in Section 2.6.

Nuclei with spin $I > ½$ have an asymmetric distribution of charge, described by the nuclear quadrupole moment, Q. The symmetry of the charge distribution is described by the sign of Q: for a "cigar"-shaped or prolate charge distribution, Q is defined as positive, while a disc-like or oblate charge distribution leads to a negative Q. For deuterium ($I = 1$), $Q = +2.8 \times 10^{-31}$ m^2. Quadrupolar nuclei located in an inhomogeneous electric field are subjected to an interaction between the electric field gradient (EFG) and Q. The EFG is described by a symmetric, traceless second rank tensor, **V**. In its PAS, **V** is described by three principal components, with the convention $|V_{33}| \geq |V_{22}| \geq |V_{11}|$. The asymmetry, η, of **V** is:

$$\eta = \frac{V_{22} - V_{11}}{V_{33}} \qquad 2.17$$

such that $0 \leq \eta \leq 1$. The interaction between **V** and Q, $\mathcal{H}_Q$, is:

$$\mathcal{H}_Q = \mathbf{I} \cdot \mathbf{Q} \cdot \mathbf{I} \qquad 2.18$$

where

$$\mathbf{Q} = \frac{eQ}{6I(2I - 1)h} \cdot \mathbf{V} \qquad 2.19$$

The quadrupolar interaction is described by the quadrupolar coupling constant, C_Q, in terms of the largest component of the EFG, $eq_{zz} = V_{33}$:

$$C_Q = \frac{e^2 Q q_{zz}}{h} \qquad 2.20$$

where e is the elementary charge and C_Q has frequency units. The direction of quantization when a quadrupolar nucleus is placed in an applied magnetic field depends on the relative magnitudes of $\mathcal{H}_Z$ and $\mathcal{H}_Q$. For ^{2}H, $\mathcal{H}_Q$ is sufficiently small that the quadrupolar interaction may be considered a weak perturbation of the Zeeman interaction.

2.2 Nuclear Magnetic Shielding and Chemical Shifts

Before considering how the combined interactions discussed above manifest themselves in NMR spectra, it is useful to summarize the notation that will be used henceforth. In the preceding sections, nuclear magnetic properties have been discussed in terms of the magnetic *shielding* σ_{ii} relative to the bare nucleus, with the convention $\sigma_{33} \geq \sigma_{22} \geq \sigma_{11}$. While *ab initio* methods calculate magnetic shielding tensors (Chapter 3), experimentally one measures a chemical *shift*, δ_{ii}, relative to a chosen reference with the convention $\delta_{11} \geq \delta_{22} \geq \delta_{33}$. The two sets of tensor components are related by:

$$\begin{aligned}\delta_{ii} &= \frac{\nu_{ii} - \nu_{ref}}{\nu_{ref}} \cdot 10^6 \\ &= \frac{\sigma_{ref} - \sigma_{ii}}{1 - \sigma_{ref}}\end{aligned} \qquad 2.21$$

where ν_{ii} and ν_{ref} are the resonance frequencies of the *ii*th tensor component and of the reference, respectively. For carbon, $1 - \sigma_{ref} \approx 1$, and hence $\delta_{ii} \approx \sigma_{ref} - \sigma_{ii}$. To relate experimental data to those calculated by *ab initio* methods, one requires an absolute shielding scale for the nucleus of interest.[114] Jameson and Jameson have shown that the absolute shielding of the carbon nuclei of TMS, the standard reference for ^{13}C NMR, is 188.1 ± 1.2 ppm.[115] Thus, the calculated magnetic shielding, σ(calc), can be converted to chemical shifts, δ(calc) according to:

$$\delta(\text{calc}) = 188.1 - \sigma(\text{calc}) \qquad 2.22$$

Although experimental data presented in this thesis are discussed in terms of chemical shifts, it is convenient, when comparing NMR data, to discuss the relative shielding of the nuclei; the reader is reminded that a *decrease* in the chemical shift implies *increased* shielding and a *decreased* resonance frequency, as shown graphically in Figure 2.3.

The choice of notation to describe magnetic shielding or chemical shift tensors remains contentious.[116] In this report, the "Maryland" convention described by Mason will be used

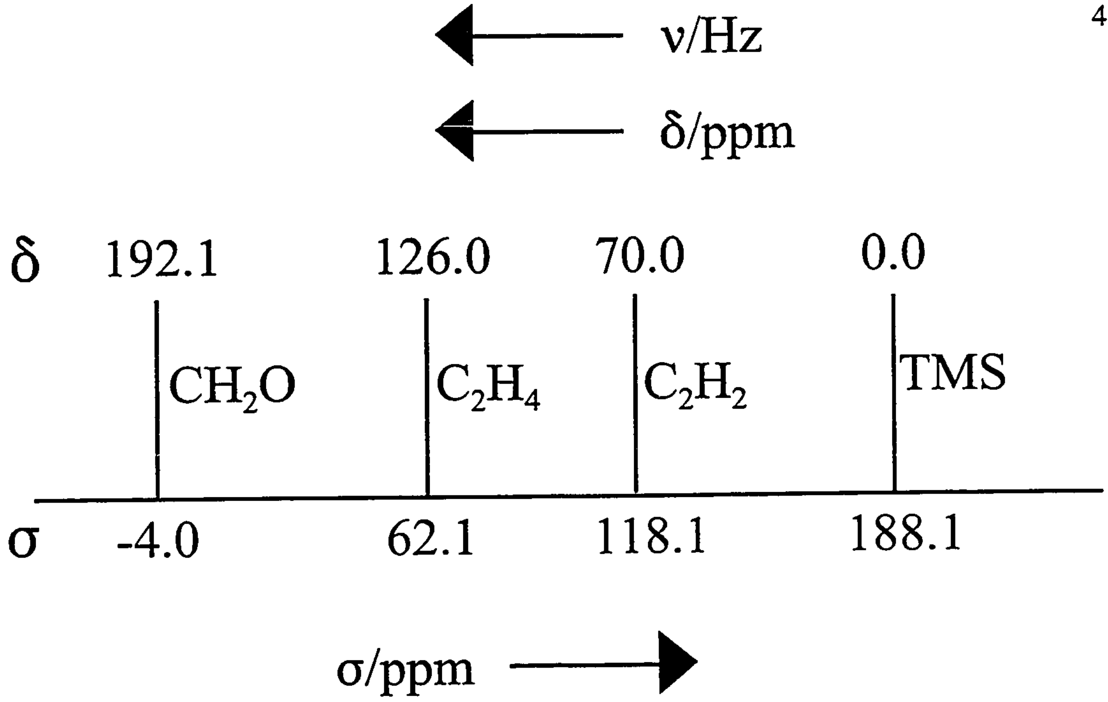
ν/Hz
δ/ppm
δ 192.1 126.0 70.0 0.0
CH_2O
C_2H_4
C_2H_2
TMS
σ -4.0 62.1 118.1 188.1
σ/ppm

Figure 2.3 The shielding, σ, and chemical shift, δ, scales for ^{13}C. Isotropic values for some representative compounds are included.

to describe NMR data.[117] Magnetic shielding tensors will be discussed in terms of the isotropic magnetic shielding or shift, σ_{iso} or δ_{iso}, respectively, and of their span, Ω, and skew, κ:

$$\sigma_{iso} = \frac{1}{3}(\sigma_{11} + \sigma_{22} + \sigma_{33}) \tag{2.23}$$

or

$$\delta_{iso} = \frac{1}{3}(\delta_{11} + \delta_{22} + \delta_{33}), \tag{2.24}$$

$$\begin{aligned}\Omega &= \sigma_{33} - \sigma_{11} \\ &= \delta_{11} - \delta_{33}\end{aligned} \tag{2.25}$$

and

$$\kappa = \frac{3(\sigma_{iso} - \sigma_{22})}{\Omega} = \frac{3(\delta_{22} - \delta_{iso})}{\Omega} \qquad 2.26$$

Although only three parameters are needed to describe the principal components of a chemical shift tensor, either δ_{iso}, Ω and κ, or δ_{11}, δ_{22} and δ_{33}, all six are presented to facilitate comparison with data reported using other conventions.

2.3 NMR of an Isolated Spin-1/2 Nucleus

In a stationary powder sample, crystallites are oriented randomly in the applied magnetic field, giving rise to a powder NMR pattern. In the absence of interactions with other magnetic nuclei (*i.e.*, an isolated spin), the line shape of an NMR spectrum will reflect the orientation dependence of the magnetic shielding (eq 2.9). As an example, the ^{13}C NMR spectrum expected for a stationary powder sample of ethylene is shown in Figure 2.4 A.[54,55] The magnitudes of the principal components of the CS tensor can be determined from the discontinuity and shoulders of the spectrum, but information about the tensor orientation in the molecular framework is usually unavailable—the orientation illustrated here was determined from a different experiment, discussed in Section 1.5.1.[55] Information about the CS tensor orientation may sometimes be surmised from molecular symmetry. For example, Figure 2.4 B illustrates the ^{13}C NMR spectrum expected for a stationary sample of acetylene, based on the parameters reported by Zilm and Grant.[55] The line shape of the spectrum, with $\kappa = 1.0$, arises from the symmetry of the molecule: the chemical shift when the C,C bond is perpendicular to $\mathbf{B}_0$, $\delta_\perp$, corresponds to the discontinuity in the spectrum, while the shoulder

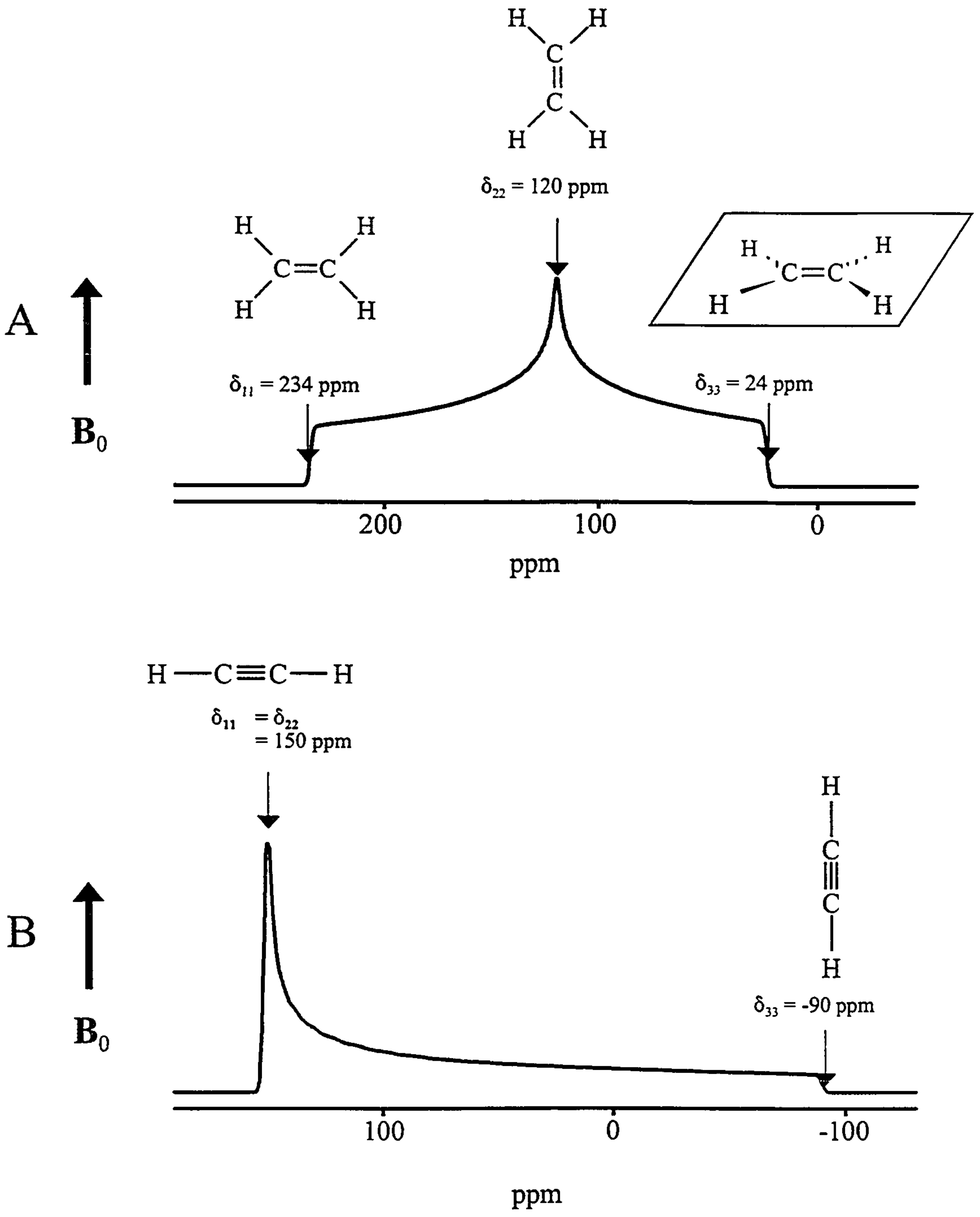

Figure 2.4 Simulated ^{13}C NMR spectra expected for stationary powder samples of ethylene (A) and acetylene (B), both at natural abundance. The orientation of the molecule relative to B_0 is illustrated for each of the principal components of the tensor.

corresponds to the chemical shift when the C,C bond is parallel to $\mathbf{B}_0$, $\delta_{\parallel}$. Axially symmetric powder patterns are observed for nuclei that lie on a C_n symmetry axis, with $n \geq 3$.

At MAS frequencies greater than the total breadth, Ω, of the magnetic shielding tensor expressed in Hz, the NMR spectrum of an isolated spin consists of a single peak. However, if the MAS frequency is significantly less than Ω, a spinning sideband pattern consisting of a series of sharp peaks separated by the spinning frequency is observed. The sideband pattern is a consequence of the anisotropy in the shielding and hence encompasses information about the principal components of the CS tensor. Herzfeld and Berger[118] have shown that the relative intensities of the spinning sidebands may be used to extract the principal components of the CS tensor. The method, which has been used extensively to partially characterize carbon CS tensors, is particularly useful for the analysis of spectra with several carbon sites. In general, accurate CS tensor components are obtained, but values are less reliable for spectra which approach axial symmetry.[119] In addition, the method cannot readily be applied to a spin pair, since dipolar interactions affect the intensities of the spinning sidebands. Information about CS tensor orientations is generally not available from standard Herzfeld-Berger analyses. Alternatively, the principal components can be determined from a moment analysis of the spectra of MAS samples.[83]

2.4 NMR Spectra of an Isolated Spin Pair

2.4.1 The Dipolar-Chemical Shift Method

The dipolar-chemical shift method has been used to elucidate CS tensors for nuclei in several solid samples.[55,120-122] An overview of the underlying concepts for this technique is presented here. By placing two spins in close proximity to one another (*e.g.*, by isotopic labelling in the case of ^{13}C), one obtains an isolated spin pair. In general, when the two coupled spins are not magnetically equivalent, there are four NMR transitions associated with each particular orientation of the spin pair in the applied magnetic field.[55,106,111,122-125] The frequencies, ν_i, and relative intensities, P_i, of these transitions are:

$$\nu_1 = \frac{1}{2}(\nu_A + \nu_B + d + a); \qquad P_1 = 1 - \frac{b}{d} \tag{2.27}$$

$$\nu_2 = \frac{1}{2}(\nu_A + \nu_B + d - a); \qquad P_2 = 1 + \frac{b}{d} \tag{2.28}$$

$$\nu_3 = \frac{1}{2}(\nu_A + \nu_B - d + a); \qquad P_3 = 1 + \frac{b}{d} \tag{2.29}$$

$$\nu_4 = \frac{1}{2}(\nu_A + \nu_B - d - a); \qquad P_4 = 1 - \frac{b}{d} \tag{2.30}$$

where

$$a = J_{iso} - R_{eff}(3\cos^2\zeta - 1), \tag{2.31}$$

$$b = J_{iso} + \frac{1}{2}R_{eff}(3\cos^2\zeta - 1), \tag{2.32}$$

and

$$d = [(\nu_A - \nu_B)^2 + b^2]^{1/2}. \tag{2.33}$$

In eqs 2.27 - 2.33, ν_A and ν_B are the resonance frequencies, in the absence of the dipolar interaction, of spins *A* and *B*, respectively, and ζ is the angle between the applied magnetic field and the dipolar vector $\mathbf{r}_{AB}$—the alkenyl or alkynyl C,C bond for the compounds considered in this thesis.

The NMR spectrum of a stationary sample containing an isolated spin pair reflects the anisotropy in the magnetic shielding as well as the magnitude of R_{eff} and the orientation of the dipolar vector relative to the PAS of the CS tensor. The magnitude of the dipolar interaction for crystallites oriented such that a given CS tensor principal component is parallel to the applied magnetic field allows the determination of the angle between that component and $\mathbf{r}_{AB}$.[122] However, because $\mathbf{r}_{AB}$ is axially symmetric, the angle α, which defines the rotation of the CS tensor about $\mathbf{r}_{AB}$, is not known, although the relative value of α for the two CS tensors is determined. The calculated spectrum is therefore invariant to simultaneous rotation of the two CS tensors about the dipolar vector. In addition, the supplement of a given angle will yield the same calculated spectrum. Hence, a calculated spectrum based on the dipolar-chemical shift method yields an infinite set of solutions, with the tensor components oriented about two cones (Figure 2.5).

If the indirect coupling is negligible, the NMR spectrum of a dipolar-coupled spin pair is defined by up to 13 parameters: besides R_{eff}, there are three principal components and three Euler angles for each CS tensor. Comparison of NMR spectra acquired at different applied magnetic fields differentiates between spectral features arising from magnetic shielding and dipolar interactions, since the latter are independent of the applied magnetic field strength.

Parameters obtained from other experiments may be used in concert with the dipolar-chemical shift method. If not complicated by other nuclei, the principal components of the CS tensor can be determined from the NMR spectrum of a stationary sample containing a

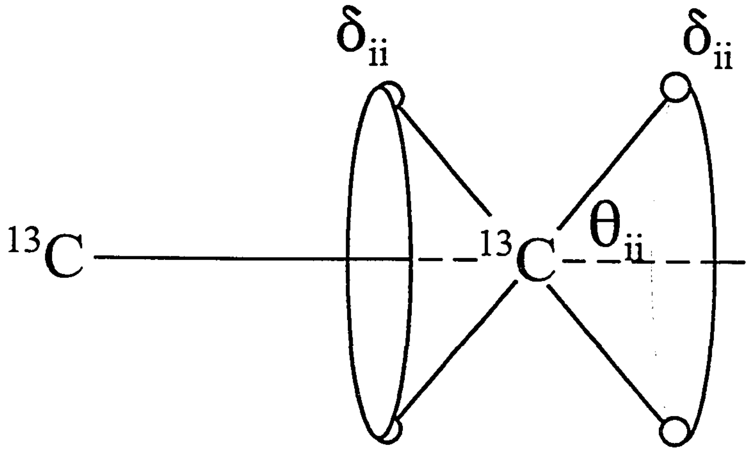

Figure 2.5 Possible orientations of a CS tensor component relative to the ^{13}C,^{13}C dipolar vector, as determined by the dipolar-chemical shift method. θ_{ii} defines the orientation of the tensor component δ_{ii} relative to the dipolar vector.

dilute spin (Section 2.3). The spectrum of a slow MAS sample yields δ_{iso} and provides insight into the values of Ω and κ. For example, spectra with small spans have a negligible spinning sideband pattern. For a dilute spin it may be possible to obtain the principal components of the CS tensor through the analysis of the spinning sideband pattern as discussed above (Section 2.3). Two-dimensional spin-echo experiments (Section 2.5) provide reliable values of R_{eff} and corroborate other parameters obtained from the fit of the NMR spectra of the isolated spin pair.

Information about the CS tensor is also available from other sources. Molecular symmetry aids in the assignment of CS tensor parameters, since the magnitudes of the CS tensor principal components for crystallographically equivalent nuclei are equal and their orientations have the same symmetry relationship as the nuclei of the spin pair. Even if the nuclei are not chemically equivalent, molecular symmetry may fix the orientations of one or more CS tensor components. For example, nuclei lying in a mirror symmetry plane must have a component perpendicular to the plane. The known CS tensor orientations for closely related compounds may be used to propose CS tensor orientations for the nuclei of interest. As well, there is growing evidence that *ab initio* calculations accurately predict CS tensor orientations.[103,120,126-132]

In summary, information about the orientations of the CS tensor components relative to $\mathbf{r}_{AB}$ is available from the NMR spectrum of an isolated spin pair. Further insight into CS tensor orientations may be gained from molecular symmetry, CS tensor orientations for closely related compounds, or from *ab initio* calculations.

2.4.2 Line Shapes of *AB* Spin Systems Under Conditions of Magic-Angle Spinning.

Under rapid MAS conditions, the NMR spectrum of an isolated spin consists of an isotropic peak. However, in the case of a homonuclear spin pair, the direct dipolar interaction may not be completely averaged by MAS,[83] giving rise to a distribution of NMR frequencies.[133-136] This can be exploited to gain information about the orientation of the CS tensor, although the same information is generally more readily available from an analysis of the spectrum of the stationary sample.

The Hamiltonian describing the NMR spectrum of an MAS sample is time-dependent.[137] By use of average-Hamiltonian theory,[83] equations describing the spectral line shapes of MAS samples have been derived.[133,138] Floquet theory[139,140] has also been used to describe the NMR line shapes of spinning samples. Similar to spectra of stationary samples, the observed spectrum of an MAS sample is a consequence of four NMR transitions. However, since ${}^1J_{\mathrm{iso}}({}^{13}\mathrm{C},{}^{13}\mathrm{C})$ is generally not resolved for the molecules considered here, the observed peaks in spectra of MAS samples may be described by two transitions:

$$\nu_{\pm} = \frac{1}{2}(\nu_{\Sigma} \pm d') \qquad 2.34$$

where

$$d' = [(\nu_{\Delta} - G)^2 + F^2 + K^2]^{1/2} \qquad 2.35$$

The terms ν_{Σ} and ν_{Δ} are the sum and difference, respectively, of the isotropic resonance frequencies of spins A and B. The parameters G, F and K are higher-order corrections to the average Hamiltonian:

$$G = \sum_{n=1}^{+\infty} \frac{g_{2n}}{(2\pi\nu_{\mathrm{rot}})^{2n}}; \qquad F = \sum_{n=1}^{+\infty} \frac{f_{2n}}{(2\pi\nu_{\mathrm{rot}})^{2n}}; \qquad K = \sum_{n=0}^{+\infty} \frac{k_{2n+1}}{(2\pi\nu_{\mathrm{rot}})^{2n+1}} \qquad 2.36$$

where ν_{rot} is the MAS frequency. The terms g_{2n}, f_{2n} and k_{2n+1} are correction coefficients which are related to the instantaneous chemical shift difference, $\Delta\nu$:

$$g_{2n} \propto R_{\mathrm{DD}}^{2n}(\Delta\nu); \qquad f_{2n} \propto R_{\mathrm{DD}}(\Delta\nu)^{2n}; \qquad k_{2n+1} \propto R_{\mathrm{DD}}(\Delta\nu)^{2n+1} \qquad 2.37$$

Exact expressions for these coefficients are given elsewhere.[141] They depend on the principal components of the CS tensors, R_{DD}, and on the orientation of the dipolar vector relative to the CS tensors. Eq 2.36 explains the observed dependence of the line shapes of MAS samples on ν_{rot}. At high MAS frequencies, the terms G, F and K approach zero, and the separation between the peaks is ν_{Δ}, the difference in the isotropic chemical shifts. However, eq 2.37

shows that the peak positions also depend on $\Delta\nu$, which increases with B_0. Hence, NMR line shapes of MAS samples also exhibit a dependence on the applied magnetic field. Since eqs 2.34 - 2.37 describe the *total* line shape, it is necessary to sum the spinning sidebands into the isotropic peak when considering these equations.[134] Efficient computer programs have been developed to calculate the NMR line shapes expected for samples containing spin pairs at any spinning frequency.[142,143]

2.5 Two-Dimensional NMR—Spin Echo Techniques

Two-dimensional (2D) NMR spectroscopy has developed into a powerful technique for the investigation of molecular properties.[88,144] The technique is an extension of the basic 1D NMR experiment discussed in the introduction to this section. In general, a time-dependent signal in the second dimension is achieved by inserting a variable delay, τ_1, and a second pulse between the first rf pulse and the detection period. The spectrum in the second dimension ($F1$) thus contains information about the interaction giving rise to the time dependence.

The use of echoes in NMR is well known.[145] The impetus for the development of two-dimensional spin-echo NMR techniques was the desire to separate $J(^{13}C,^{1}H)$ from the magnetic shielding in samples dissolved in isotropic liquids.[146] In solid-state NMR, the spin-echo technique has been used to investigate the direct dipolar and indirect J-coupling for isolated spin pairs and to provide information about anisotropic chemical shielding.[121,147-150] Figure 2.6 illustrates the pulse sequence used for the 2D spin-echo method.

Nakai and McDowell have presented expressions for the six transitions expected for

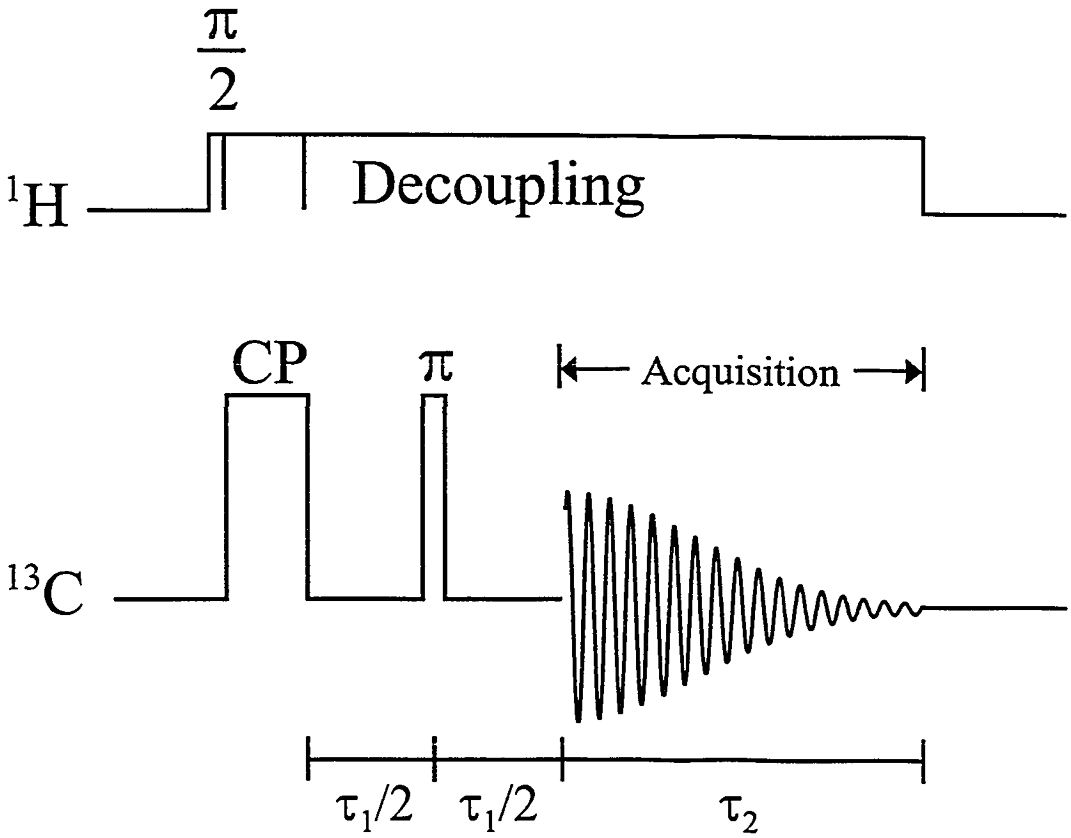

$\frac{\pi}{2}$
^{1}H
Decoupling
CP
π
Acquisition
^{13}C
τ1/2
τ1/2
τ2

Figure 2.6 Pulse sequence for the 2D spin-echo NMR experiment. The π and π/2 pulses are not drawn to scale.

the *F*1 projection of a 2D spin-echo spectrum.[148] These transitions, ν_i, and their relative intensities, P_i, are:

$$\nu_{1,2} = \pm\left(a' - \frac{1}{2}d\right) \qquad P_{1,2} = \frac{1}{2}\frac{b}{d}\left(1 + \frac{b}{d}\right) \tag{2.38}$$

$$\nu_{3,4} = \pm\left(a' + \frac{1}{2}d\right) \qquad P_{3,4} = \frac{1}{2}\frac{b}{d}\left(1 - \frac{b}{d}\right) \tag{2.39}$$

$$\nu_{5,6} = \pm a' \qquad P_{5,6} = \frac{(\nu_A - \nu_B)^2}{d^2} \tag{2.40}$$

where

$$a' = \frac{1}{2}\left[J_{\mathrm{iso}} - R_{\mathrm{eff}}(3\cos^2\zeta - 1)\right]. \qquad 2.41$$

The terms b and d have been presented earlier (eqs 2.32 and 2.33).

To understand the line shapes expected for the $F1$ projection, it is useful to consider the A_2 and AX spin systems where J_{iso} is negligible. In the former, $\nu_A = \nu_B$ at all orientations, and hence $\nu_A - \nu_B = 0$ and $d = \pm b$ (eq 2.33). For $d = +b$, P_3 to $P_6 = 0$ and the frequencies of $\nu_{1,2} = \pm\frac{3}{4}R_{\mathrm{eff}}(3\cos^2\zeta - 1)$; this describes the Pake doublet expected for an A_2 spin system. The same result obtains for $d = -b$, except that here only ν_3 and ν_4 have nonzero intensity. For an AX spin system, $d \approx (\nu_A - \nu_B) \gg b$, so only ν_5 and ν_6 have nonzero intensity. The transitions here, $\pm\frac{1}{2}R_{\mathrm{eff}}(3\cos^2\zeta - 1)$, describe the Pake doublet expected for an AX system (Figure 2.2). However, for AB spin systems, the $F1$ projection is expected to be significantly more complicated, since the relative value of $(\nu_A - \nu_B)$ can vary significantly depending on crystallite orientations. In considering 2D spin-echo NMR spectra, one should consider that $(\nu_A - \nu_B)$ describes the instantaneous chemical shift difference between two nuclei: a large isotropic chemical shift difference between two nuclei does not preclude crystallite orientations for which $(\nu_A - \nu_B)$ is small.

2.6 Deuterium NMR

The deuterium quadrupole interaction is sufficiently small ($C_Q < 300$ kHz) to allow acquisition of ^{2}H NMR powder spectra and yet is large enough to be a sensitive probe of molecular dynamics;[151-154] the underlying theory has been summarized in several articles.[95,155-158]

If the asymmetry in the EFG, η, is zero (in general, for a C,^{2}H bond, η is less than 0.1)[159] and dipolar or indirect spin-spin coupling interactions are negligible, the contribution to the solid-state ^{2}H NMR spectrum from a single deuteron is two transitions with a separation that depends on the magnitude of C_Q and on the orientation of the largest component of the EFG tensor relative to $\mathbf{B}_0$.[95,155-159] Analysis of single crystals is possible if suitable crystals can be grown,[160-162] but it is more common to measure ^{2}H NMR spectra of powder samples. The random orientation of crystallites in such samples gives rise to the characteristic Pake doublet, similar to that discussed for dipolar-coupled spins (Figure 2.2). If motion is not significant, the splitting from crystallites contributing to the "horns" and outer shoulders of the spectrum are $.75C_Q$ and $1.5C_Q$, respectively. The actual line shape of experimental spectra will reflect the magnitudes of C_Q and η (Fig. 2.7); further complications arise if there are contributions to the spectra from non-equivalent deuteron sites and if motional averaging of C_Q is a factor (*vide infra*). Other interactions, such as the anisotropy in the magnetic shielding as well as direct or indirect coupling with the deuterons, may also complicate the spectra, although these interactions are usually much less than C_Q and hence generally are not significant for spectra of stationary samples. The theory for these more complex spectra have been discussed by Haeberlen[95] and Spiess.[163] In the absence of other interactions, the quadrupolar parameters may be calculated from the observed line shape (Figure 2.7) according to:[164]

$$\Delta \nu_1 = \frac{3}{4} C_Q (1 - \eta) \qquad 2.42$$

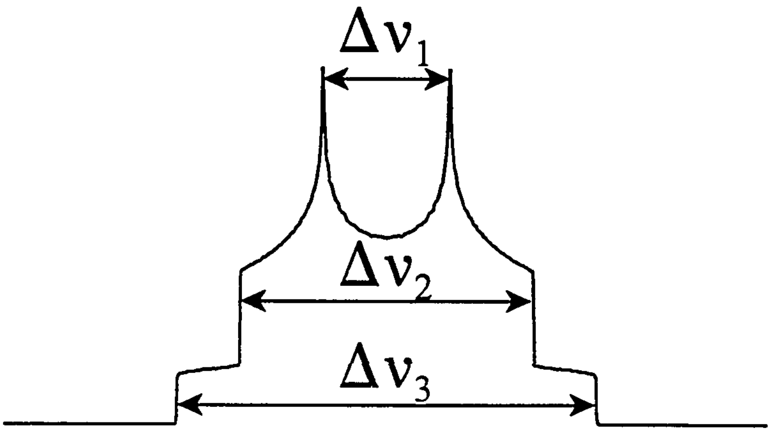

Figure 2.7 Line shape of ^{2}H NMR spectrum as defined by η and C_Q.

$$\Delta\nu_2 = \frac{3}{4}C_Q(1 + \eta) \qquad 2.43$$

$$\Delta\nu_3 = \frac{3}{2}C_Q \qquad 2.44$$

The natural abundance of deuterium (0.015 %) generally precludes the analysis of samples at natural abundance, but the synthesis of compounds with deuterium labels at specific sites is usually relatively straightforward.[165,166] If the molecule or ligand reorients on a timescale comparable to C_Q, the motional averaging of the quadrupolar interaction will be reflected in the observed ^{2}H NMR line shape. For an axially symmetric (*i.e.*, $\eta = 0$) ^{2}H powder pattern, the ^{2}H NMR line shape for motion about a C_n ($n \geq 3$) axis is defined by:[157]

$$\Delta_n = \frac{C_Q}{2}(3\cos^2\theta_Q - 1). \qquad 2.45$$

In eq 2.45, θ_Q defines the angle between the rotation axis and the direction of the largest component of the EFG and Δ_n is a scaling factor defining the ratio between the observed quadrupolar splitting and that expected in the absence of motion. Hence, if the latter is known or can be predicted, insight about the motion of the molecule or ligand is available. Expressions describing the line shapes expected for ^{2}H NMR spectra of molecules undergoing more complex motion, or those with a non-axially symmetric EFG tensor, have been given elsewhere.[95,163]

The observed line shapes depend on the type of motion.[157] For example, the ^{2}H NMR line shape for a molecule or ligand undergoing C_2 motion depends on whether the type of motion is diffusion or discrete jumps.[157] For motion about a symmetry axis C_n, $n \geq 3$, the examination of the ^{2}H NMR line shapes will not distinguish between diffusion or discrete jumps, but the nature of the motion can be ascertained through the measurement of the anisotropy in T_1.[167] As well, one must be aware that different types of motion may yield similar spectra.[160] This discrepancy may be resolved by a careful measurement of the relaxation using the inversion-recovery experiment.[168,169]

The broad spectra encountered in ^{2}H NMR of stationary powders leads to free induction decay times comparable to the time required for the probe to recover from the excitation pulse. To avoid severe distortions of the spectra,[170,171] a quadrupolar echo pulse sequence is used. These sequences refocus the signal after a suitable delay to allow for probe recovery.[172,173] The pulse sequence proposed by Davis *et al.*[173] is shown in Figure 2.8, along with a schematic representation of the evolution of the magnetization. The delays may be set such that acquisition begins at the echo maximum, but in practice the delays are set such that $\tau_1 > \tau_2$, allowing the observation of the full echo (see the FID at the right of Figure 2.8). Before Fourier transformation, the FID must be left-shifted such that the echo maximum is the first point of the FID. Fractional left-shifting[174,175] or interleaving[176] may also be used to ensure that there is a point at the echo maximum.

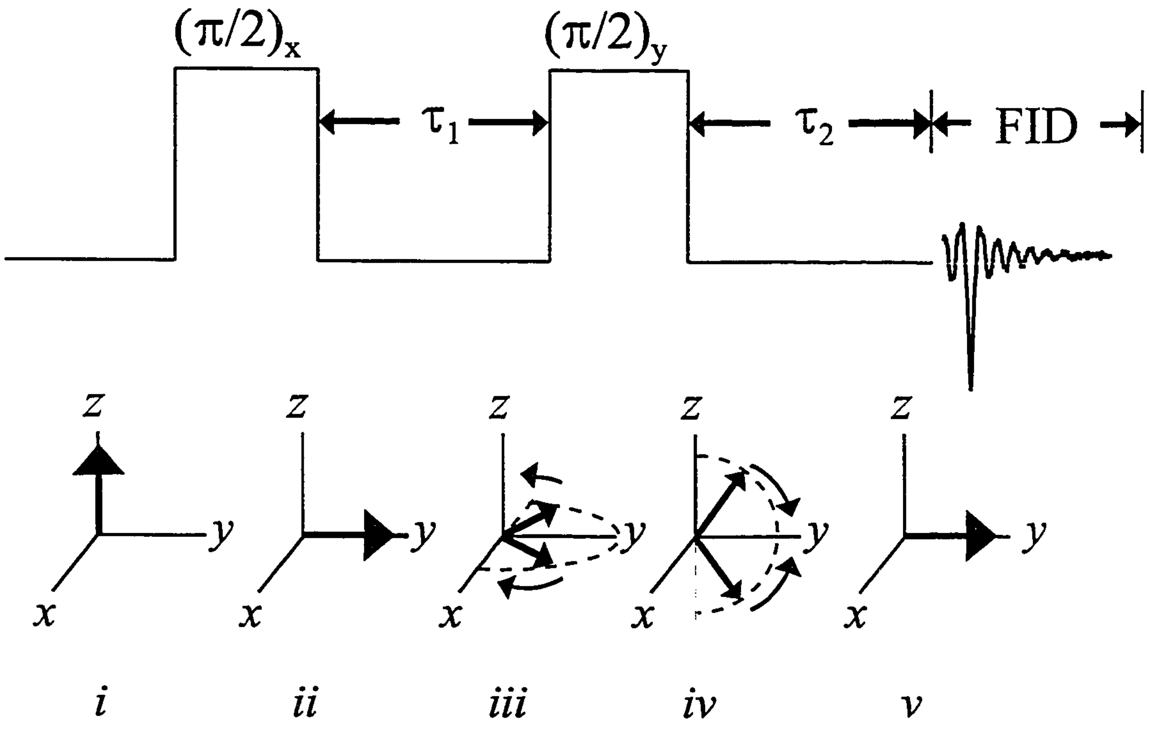

Figure 2.8 Quadrupolar echo pulse sequence (top). The lower diagram illustrates the evolution of the magnetization.

2.7 Experimental Procedure

To avoid redundancy in later sections, the basic experimental procedures used to acquire solid-state NMR spectra are summarized here. Specific details are presented in Chapters 4 to 6.

Solid-state ^{13}C NMR spectra were obtained at 300 K on Bruker MSL-200 or Chemagnetics CMX Infinity 200 (B_0 = 4.7 T, $\nu_0(^{13}C)$ = 50.3 MHz for both) and Bruker AMX-400 (B_0 = 9.4 T, $\nu_0(^{13}C)$ = 100.6 MHz) NMR spectrometers. Cross polarization under the Hartmann-Hahn match condition[177,178] with recycle times of 20 - 300 s were used to acquire all ^{13}C NMR spectra. Contact times, ranging from 0.5 to 6.0 ms, were those that gave the maximum intensity isotropic peaks in spectra of MAS samples. High-power proton decoupling with ^{1}H 90° pulse widths of 3.5 to 5.0 μs was accomplished using the two-pulse phase modulation (TPPM) sequence of Griffin and coworkers.[179] Samples were packed in 4, 5 or 7 mm o.d. zirconium oxide rotors. All ^{13}C NMR spectra were referenced to TMS (δ_{iso} = 0 ppm) by setting the high-frequency peak of an external adamantane sample to 38.56 ppm.[180] The magic angle was checked routinely. This was accomplished by setting the angle such that a maximum number of spinning sidebands was observed in the ^{23}Na NMR spectra of an MAS sample of $NaNO_3$.

Carbon-13 NMR spectra of stationary $^{13}C_2$-labelled samples containing phenyl groups were complicated by the contribution to the spectra from the aromatic ^{13}C in natural abundance. For $Pt(C_2H_4)(PPh_3)_2$ and $Pt(diphenylacetylene)(PPh_3)_2$, this was removed by acquiring a spectrum of the unlabelled sample under identical conditions as for the labelled sample and subtracting the FID of the former from the latter.

Spectra of stationary powder samples were calculated using a program developed in this laboratory which incorporates the POWDER routine of Alderman *et al.*[181] Spectra were analyzed on the basis of the dipolar-chemical shift method (Section 2.4.1). Although $^1J(^{13}C,^{13}C)$ was not resolved for most spectra, an estimate of its value, based on reported values from solution studies or from analogous compounds, was included in the simulations. All other spin-spin interactions were assumed to be negligible and were not included in the simulation of the spectra of stationary samples. Unless otherwise noted, uncertainties in the principal components of the CS tensors and in the orientations of these components relative to the dipolar vector were estimated by visual inspection of the calculated and experimental spectra.

The relationship between two tensors is described mathematically by Euler angles;[95] however, it is convenient to discuss CS tensor orientations in terms of the angle θ_{ii}, which defines the angle formed by the CS tensor component δ_{ii} with the $^{13}C,^{13}C$ dipolar vector (Figure 2.5). By arbitrarily setting one Euler angle to zero, the relative orientations of the two CS tensors are described by the value of α at the other nucleus; this value is equivalent to the torsion angle between the two δ_{33} components.

Chapter 3

Calculation of Magnetic Shielding From First Principles

3.1 Introduction

With the commercial availability of efficient quantum-chemical computer programs and the increasing capacity of computers, calculation of magnetic shielding from first principles has become common. Information from such calculations has been used to provide fundamental information about nuclear magnetic shielding[126-132,182] and is also used for computer-assisted NMR studies of molecular structure.[183] As well, the results of *ab initio* calculations have been used to determine magnetic shielding tensor orientations,[58,74,120] the impetus for the calculations presented in this work. The literature on *ab initio* calculations of magnetic shielding tensors is reviewed annually.[131]

The calculated magnetic shielding tensor principal components for various alkenes, alkynes and the corresponding metal complexes, including those investigated experimentally in this work, are summarized in this chapter. The results of *ab initio* calculations are compiled in a single chapter to establish any trends and to present the computational strategy used for the calculations. Experimental results, discussed in detail in Chapters 4 to 6, are presented here for comparison with calculated data. Orientations for calculated magnetic shielding tensors are generally invariant to basis set size or to computational technique; this aspect of the calculated results is discussed with the experimental data in Chapters 4 to 6. Since computational methods calculate absolute shielding, data presented in this section are discussed in terms of magnetic shielding rather than chemical shifts. To facilitate comparison, some data appear in more than one table.

3.2 Background

It is useful to consider nuclear magnetic shielding in terms of theories advanced 50 years ago by Ramsey.[184] In this theory, the magnetic shielding is partitioned into diamagnetic (σ^d) and paramagnetic (σ^p) contributions:[185-188]

$$\sigma_{ii} = \sigma_{ii}^{d} + \sigma_{ii}^{p} \tag{3.1}$$

where

$$\sigma_{ii}^{d} = \frac{\mu_o}{4\pi}\frac{e^2}{2m}\langle 0|\sum_{k}\frac{r_k^2 - r_{ki}^2}{r_k^3}|0\rangle \tag{3.2}$$

and

$$\sigma_{ii}^{p} = -\frac{\mu_0}{4\pi}\frac{e^2}{2m^2}\sum_{n>0}\frac{1}{E_n - E_0}\left[\langle 0|\sum_{k}\frac{l_{ki}}{r_k^3}|n\rangle\langle n|\sum_{k} l_{ki}|0\rangle + \langle 0|\sum_{k} l_{ki}|n\rangle\langle n|\sum_{k}\frac{l_{ki}}{r_k^3}|0\rangle\right] \tag{3.3}$$

In the above equations, μ_0 is the permeability of free space, e and m are the electron charge and rest mass, respectively while $\langle 0|$ and $\langle n|$ represent ground and excited singlet electronic states of the molecule, with electronic energy E_0 and E_n, respectively. The position vector for electron k is defined by r_k and l_{ki} is the angular momentum operator. Eqs 3.1 - 3.3 describe the shielding in the directions of the principal components of the magnetic shielding tensor and are valid only if the nucleus of interest is chosen as the gauge origin. Expressions for the off-diagonal elements of the magnetic shielding tensor and for different gauge origins have been derived.[126,186,188]

The contribution to shielding from σ^d (eq 3.2) is always positive, leading to increased shielding relative to the bare nucleus. Because σ^d depends only on the ground electronic state of the molecule, it can be calculated accurately at relatively low levels of theory and hence is expected to be essentially invariant to basis set size or to the effects of electron correlation. Gierke and Flygare have shown that σ^d may be approximated if the molecular structure is known.[189] For example, the shielding for nucleus *A* in the *x*-direction may be approximated by:[186]

$$\sigma^d_{xx} \approx \sigma^d_{av}(\text{free atom}) + \frac{\mu_o}{4\pi}\frac{e^2}{2m}\sum_{B \neq A}\frac{Z_B}{r^3_{AB}}(y^2_B + z^2_B) \qquad 3.4$$

where σ^d_{av}(free atom) is the shielding expected for an isolated single atom. For carbon, σ^d_{av}(free atom) = 260.7 ppm.[190] The summation is carried out over all other atoms in the molecule, Z_B is the atomic number of atom B, with Cartesian coordinates y_B and z_B, and r_{AB} is the distance from the origin, the site of the observed nucleus. The remaining tensor components follow from cyclic permutations of eq. 3.4.

The paramagnetic contribution to nuclear magnetic shielding (eq 3.3) is a second-order electronic property which depends on the mixing of ground and excited electronic states of the molecule. These states correspond approximately to the occupied and unoccupied molecular orbitals (MOs).[185,187,191] The paramagnetic term is usually negative and is inversely proportional to the difference in the electronic energy of the MOs undergoing mixing. Contributions to σ^p arise from induced electron motion in the plane perpendicular to the direction of the applied magnetic field such that charge appears to rotate.[185,187,191] This can be understood by considering the action of the angular momentum operators on atomic orbitals. For example, $l_z|p_x\rangle = i|p_y\rangle$; thus l_z "rotates" p_x by 90° about the z-axis, resulting in an effective mixing between p_x and p_y. Mixing of MOs can only occur between occupied and unoccupied MOs with magnetic-dipole allowed symmetry. Fig. 3.1 illustrates MOs for a hypothetical diatomic molecule. Mixing of π_u and σ_u^* (Fig. 3.1 A) is magnetic-dipole allowed, but mixing of π_u and π_g^* (Fig. 3.1 B) is forbidden by symmetry. In summary, significant

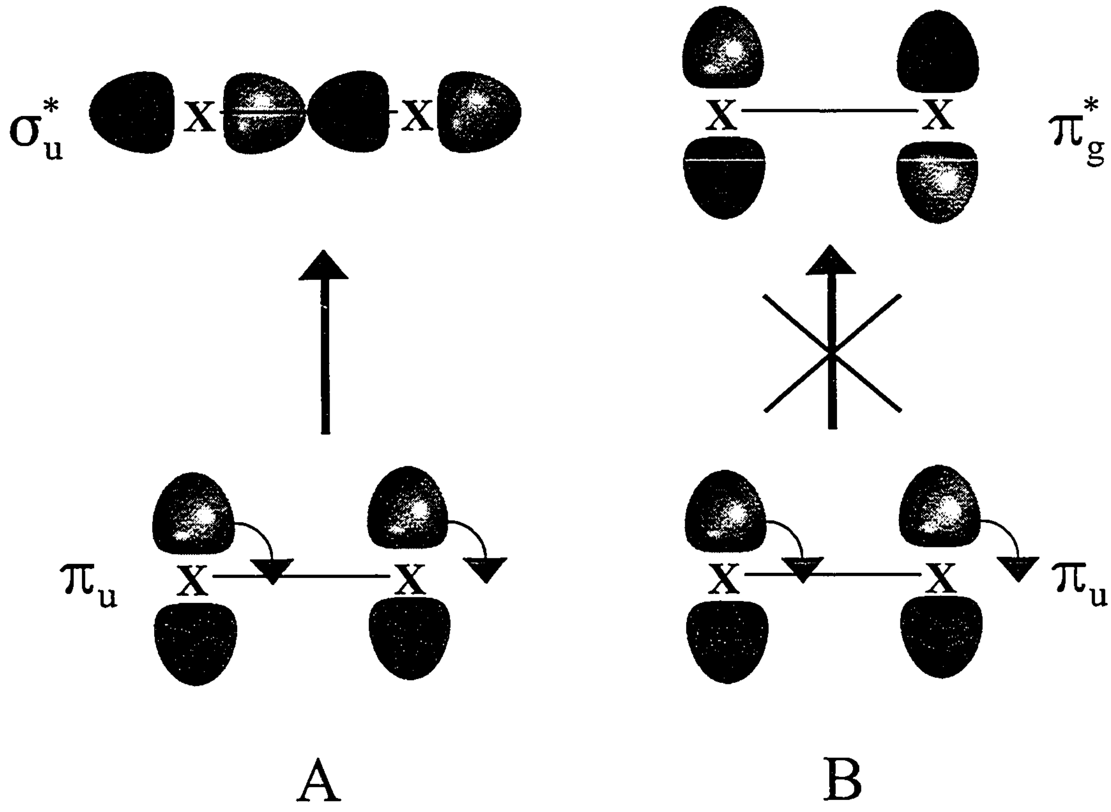

Figure 3.1 Examples of magnetic-dipole allowed (A) and forbidden (B) mixing of molecular orbitals for a hypothetical diatomic molecule with the applied magnetic field perpendicular to the page.

deshielding is expected in directions perpendicular to the symmetry planes of occupied and virtual MOs that have the proper symmetry for mixing, and that are separated by a small energy difference. It is noted that a discussion of nuclear magnetic shielding in terms of electronic current density leads to equivalent partitioning of the diamagnetic and paramagnetic terms (eqs 3.1 - 3.3).[182]

Table 3.1 Diamagnetic and Paramagnetic Contributions to the Principal Components of the Magnetic Shielding Tensors for Ethane, Ethylene and Acetylene.[a]

	σ_{xx}			σ_{yy}			σ_{zz}		
	σ^d	σ^p	σ	σ^d	σ^p	σ	σ^d	σ^p	σ
Ethane	290	-111	179	340	-168	172	340	-168	172
Ethylene	280	-217	63	331	-382	-51	337	-178	159
Acetylene	273	0	273	331	-298	33	331	-298	33

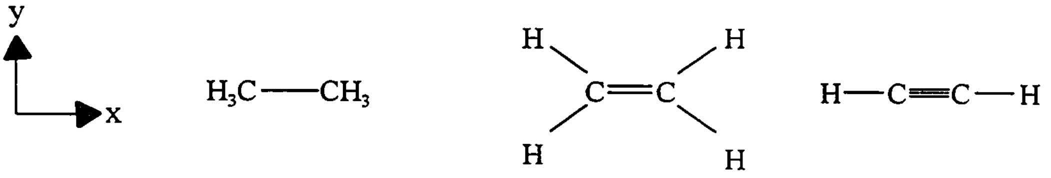

---

a. From reference 193. The values of σ^p are derived from experimental values (reference 192 for ethane and reference 54 for ethylene and acetylene) and eq 3.1. Note that reported data are based on an earlier absolute shielding scale for carbon, σ_{iso}(TMS) = 183 rather than the currently accepted value, 188.1 ppm.

Contributions from σ^d and σ^p to the total carbon magnetic shielding, σ, for ethane, ethylene and acetylene are summarized in Table 3.1. The diamagnetic contribution was reported by Zilm and Duchamp,[193] based on the empirical procedure of Gierke and Flygare.[189]

The data presented in Table 3.1 demonstrate some important properties of nuclear magnetic shielding. Despite the different environments about the carbon nuclei, σ^d is relatively insensitive to orientation and has comparable values for all three compounds. In contrast, σ^p is very sensitive to the local environment and to orientation. For example, the span of σ^d for ethylene is 57 ppm, much less than the corresponding value for σ^p, 204 ppm. Hence, qualitative explanations for observed differences in magnetic shielding within a molecule or between related molecules are often based on the assumption that the different shielding is a consequence of the paramagnetic term.[194]

For linear molecules, $\sigma^p_\parallel = 0$ and hence, from eq 3.4, $\sigma_\parallel = \sigma^d_\parallel \approx \sigma^d_{av}$(free atom). The magnetic shielding in directions perpendicular to the C,C bond of acetylene is a consequence of the efficient mixing of σ and π^* MOs.[195] Likewise, for ethylene, mixing of π and σ^* or σ and π^* MOs explains the large paramagnetic components in the direction of the C,C bond or perpendicular to this bond in the molecular plane. However, mixing of occupied and unoccupied MOs about an axis perpendicular to the molecular plane of ethylene is magnetic-dipole forbidden and there is a large difference in the energies of the MOs. Consequently the magnitude of σ^p is small in this direction. Likewise, the absence of low-lying excited electronic states for ethane results in small values for σ^p.[191] Since the largest components of σ^d and σ^p for ethane are both perpendicular to the C,C bond, offsetting each other, the span of the carbon magnetic shielding tensor for ethane is very small, 7 ppm.

3.3 Computational Techniques

A general overview of *ab initio* methods of calculating magnetic shielding is presented here. Progress in computational NMR has been discussed in several articles.[131,132,185,188,196,197] The reviews of Jameson and Mason[185] and of Fleischer and coworkers[197] were particularly useful in the preparation of this section.

Contributions to nuclear magnetic shielding arise from a summation of the energy differences between the ground and all excited electronic states of the molecule. Hence, accurate first principles calculation of magnetic shielding is very challenging,[188] and in fact is one of the most rigorous tests of computational techniques.[126-131] Modern programs do not calculate magnetic shielding according to eqs 3.1 - 3.3. The α,β principal components of the nuclear magnetic shielding tensor are calculated according to:[126]

$$\sigma_{\alpha,\beta} = \left[\frac{\partial^2 E}{\partial \mu_\alpha \partial \mathbf{B}_\beta}\right]_{\mu,B=0} \qquad 3.5$$

where α, β are the Cartesian coordinate components (*i.e.*, α,β = x, y, z), E is the total electronic energy, μ is the nuclear magnetic moment and **B** is the applied magnetic field. Some programs provide a breakdown of the magnetic shielding into diamagnetic and paramagnetic shielding contributions; these values should be regarded as approximate, since the breakdown is somewhat arbitrary.[196,197]

Ab initio calculations of CS tensors use perturbation theory to describe the contribution to the total electronic energy of the molecule arising from the applied magnetic field. The perturbation is described by an orbital angular momentum operator that is not invariant to translations, so that the influence of this operator on the wave function depends on where it is evaluated (*i.e.*, the gauge origin),[188,197] unless the Schrödinger equation is solved exactly. Approximate methods yield gauge-dependent results unless the gauge origin is at the nucleus of interest.[197] This approach, known as the common origin method, has yielded magnetic shielding tensors for small hydrocarbons that are in agreement with experiment[198,199] if large basis sets are used.

Since calculations with very large basis sets are impractical for most molecules, alternative computational techniques, known as distributed-origin methods, have been devised.[126-131,197] The gauge independent atomic orbitals (GIAO) technique[200-203] yields results that are independent of the gauge origin by including a gauge factor into the atomic orbitals. In another approach, known as individual gauge for localized orbitals (IGLO), gauge factors are introduced into the molecular orbitals.[204-208] These techniques are essentially variants of the common origin method, since the gauge origin is placed on each nucleus in turn. Another method, known as CSGT, achieves gauge invariance by performing a continuous set of gauge transformations.[209]

Density functional theory (DFT) has been developed to efficiently include electron correlation effects.[210] Application of DFT to the calculation of magnetic shielding properties is very challenging;[211] this is the focus of research by several groups.[212-216]

Calculation of magnetic shielding tensors from first principles is particularly daunting in the case of organometallic complexes, since all-electron calculations on molecules with heavy nuclei are computationally demanding,[217] and relativistic effects[69,70] must be considered, even for the magnetic shielding of ligand nuclei.[71,72] The development of pseudopotentials, also known as effective core potentials (ECPs), has greatly reduced the computational time by replacing the core electrons of heavy nuclei with parameterized functions which account for relativistic effects.[211] While the use of ECPs is not recommended for the calculation of the magnetic properties of the metal, since the orbitals at the metal centre are not properly described, accurate magnetic shielding parameters for organometallic ligand atoms have been achieved using ECPs for the heavy nuclei.[218-222] Effective core potentials that use "small cores" (*i.e.,* the valence shell includes the high-level *s* and *p* orbitals for transition-metal elements) improves the accuracy of the calculated shielding for the ligand nuclei.[197] Inclusion of electron correlation effects is also important[223,224] but generally is not practical for calculations on large organometallic compounds.

Because of the difficulties cited above, there have been few reports of calculated magnetic shielding tensors for the ligand nuclei of organometallic complexes. The work of Oldfield *et al.*,[58] who reported the only calculated alkenyl carbon magnetic shielding tensors apart from the work presented in this thesis, has been discussed in Section 1.5. The calculation of the carbon magnetic shielding tensor for ferrocene by Orendt and workers[74] has also been discussed previously. The carbon magnetic shielding tensors for some metal-carbonyl complexes have been calculated by several groups, using DFT and ECPs.[218,220,225,226] Calculated isotropic values are generally within 20 ppm of experimental values. Ziegler and coworkers showed that the DFT calculations accurately predict the difference in the carbon magnetic shielding for uncoordinated CO and the carbonyl groups coordinated with Cr, Mo, W, Fe and Ni.[225]

Accurate calculation of magnetic resonance properties requires large basis sets on the nuclei of interest. Chesnut has shown that calculated magnetic shielding using locally-dense basis sets are virtually identical to those obtained using large basis sets for the complete molecule.[227,228] The technique entails calculating the shielding with a large basis set for the nuclei of interest, but placing a much smaller basis set on the neighbouring nuclei.

3.4 Computational Details

Ab initio calculations of the carbon magnetic shielding tensors were performed with the Gaussian 94[229] or Gaussian 98[230] suite of programs mounted on IBM RS/6000 computers. The magnetic shielding tensors for all compounds were calculated at the restricted Hartree-Fock (RHF) level of theory using the GIAO method.[201,202] Locally-dense basis sets[228] were used; those used for the alkenyl or alkynyl carbon atoms are summarized in Table 3.2. The same basis sets were used for the adjacent atoms, apart from the metal centre, for which the LANL2DZ ECPs of Hay and Wadt,[231] as currently configured for Gaussian 98, were used. The LANL2DZ ECP uses a 'small core', which includes *s* and *p* electrons in the valence shell, as summarized in Table 3.2. The 3-21G basis set was used for the remaining atoms. Basis sets were obtained from the basis set library of the programs or from an online data base.[232] Where practical, the effects of electron correlation were investigated by calculating the magnetic shielding tensors at the second-order Møller-Plesset (MP2) level of theory.[233] For comparison, calculations were also undertaken using DFT, although it is noted that functionals currently available with the Gaussian programs do not specifically include a magnetic field dependence and hence will not systematically yield more accurate results than those calculated using RHF theory.[234] The DFT calculations used Becke's three parameter hybrid functional[235] with the correlation functional of Lee, Yang and Parr[236] (B3LYP). To facilitate comparison, experimental chemical shifts are converted to magnetic shielding according to eq 2.22.

Table 3.2 Basis Sets Used for the *Ab Initio* Calculations.

Nucleus	Basis Set	Uncontracted	Contracted	Ref.
C	3-21G	6s,3p	3s,2p	237
C	6-31G*	10s,4p,1d	3s,2p,1d	238
C	6-311+G*	12s,6p,1d	5s,4p,1d	239
C	cc-pVTZ	10s,5p,2d,1f	4s,3p,2d,1f	240
C	aug-cc-pVTZ	11s,6p,3d,2f	5s,4p,3d,2f	240
C	cc-pVQZ	12s,6p,3d,2f,1g	5s,4p,3d,2f,1g	240
C	cc-pV5Z	14s,8p,4d,3f,2g,1h	6s,5p,4d,3f,2g,1h	241
Ni	LANL2DZ	5s,5p,5d	3s,3p,2d	231
Pd	LANL2DZ	5s,6p,4d	3s,3p,2d	231
Pt	LANL2DZ	5s,6p,3d	3s,3p,2d	231

Calculations were undertaken on several alkenes and alkynes, and on these ligands coordinated with several metals. The compounds and the structures about the alkenyl or alkynyl carbon atoms are summarized in Table 3.3. The molecular structures used for these calculations were obtained by diffraction methods for all molecules, except ethylene and $[Pd(C_2H_4)Cl_3]^-$. The molecular structure of ethylene is that reported by Duncan, determined by infrared spectroscopy.[25] That of $[Pd(C_2H_4)Cl_3]^-$ was determined by a geometry optimization at the RHF level, with the cc-pVTZ basis set for all atoms except palladium, for which the LANL2DZ ECP was used. The structure for the heavy atoms of Zeise's salt is that reported for the anhydrous form reported by Eller *et al.*[242] The positions of the hydrogen atoms are from a neutron diffraction study of the hydrated salt.[27] Apart from Zeise's salt, alkenyl or alkynyl hydrogen atom positions for structures determined by X-ray

Table 3.3 Structural Parameters for the Compounds Investigated by *Ab Initio* Methods.[a]

Ligand	Metal	$r_{C,C}$/Å	$r_{M,C}$/Å[b]	Θ[c]/°	Ref.
Ethylene	uncoordinated	1.3384(10)	-	0.0	25
Ethylene	Ni(0)	1.391(5)	1.969(6)	29.9[d]	243
Ethylene	Pd(0)	1.366(11)	2.121(8)	20.7[d]	244
Ethylene	Pd(II)	1.3344[d]	2.445[d]	2.8[d]	This work
Ethylene	Pt(0)	1.434(13)	2.111(9)	28.1[d]	24
Ethylene	Pt(II)	1.375(4)	2.132(3)	16.3	27, 242
trans-stilbene	uncoordinated	1.327(2)	-	0.0	33
trans-stilbene[e]	Pt(0)	1.416(15)	2.129(12)	33,5[f]	245
diphenylacetylene	uncoordinated	1.198(3)	-	0.0	32
diphenylacetylene	Pt(0)	1.29(2)	2.05(1)	38.4(12)	31
diphenylacetylene	Ni(0)	1.290(3)	1.877(2)	34.0(2)	246
phenylacetylene	uncoordinated	1.048	-	0.0	247
phenylacetylene	Pt(II)	1.23(1)	2.13(1)	35.2(9)[g]	248

a. Experimental data unless otherwise noted, see text. Where reported, the estimated standard deviations in the last digits are given in parentheses.

b. Average of the two C-metal bond lengths.

c. Angle formed by the substituents on the alkenyl or alkynyl carbon atom relative to the plane defined by the uncoordinated ligand.

d. Determined from a geometry optimization, see text.

(*continued on next page*)

Table 3.3 (*cont.*)

e. The X-ray structure of the 4-4'-dinitro derivative of Pt(*trans*-stilbene)$(PPh_3)_2$ was used in the calculations; the nitro groups were replaced with hydrogen atoms.

f. The alkenyl phenyl groups have significantly different orientations.

g. Orientation of the phenyl group; $\Theta = 36.7°$ for the alkynyl hydrogen atom.

crystallography were obtained by a geometry optimization at the RHF/6-31G* level. To keep computational time within reasonable limits, phenyl groups on the substituted phosphine ligands of the metal complexes were replaced with methyl groups. The P,C bond lengths are those reported for the experimental structure; tetrahedral geometry was assumed for the methyl groups, with the C,H bond length fixed at 1.086 Å. Carbon-13 NMR spectra of samples in solution show that replacement of PPh_3 with PMe_3 has a small effect on the observed isotropic magnetic shielding.[41]

Within the Gaussian suite of programs, magnetic shielding tensors may be calculated with the GIAO, CSGT or IGAIM[249] methods; the latter technique is a variation of CSGT.[234] Calculations in this laboratory and elsewhere[250] have shown that GIAO and CSGT yield similar results. Hence, only the GIAO method was used for the calculations reported here. The IGLO[204-208] method is not available with Gaussian 98; calculations have shown that results obtained using IGLO and GIAO are comparable.[197] Likewise, the dependence of the calculated shielding on the choice of density functional was not investigated. Rauhut and coworkers calculated the magnetic shielding for several small hydrocarbon molecules using B3LYP and several other functionals; the calculated results are similar for all DFT methods.[202]

In principle, factors such as vibrational motion or packing effects should be considered when comparing calculated and experimental NMR data,[131] since the former are for an isolated molecule. Such effects are difficult to predict for large molecules but are expected to be relatively small. For example, Jameson and Jameson[115] found that the isotropic carbon magnetic shielding for small organic molecules is 1 to 10 ppm less for solid samples than the estimated values for the samples in the gas phase at the zero pressure limit.

3.5 Results and Discussion

3.5.1 Convergence

Calculated magnetic shielding tensor components are expected to converge to a basis set limit as the size of the basis set is increased.[197] To determine whether this limit has been reached with the basis sets used in this work, the carbon magnetic shielding tensors for ethylene were calculated at various levels of theory; the results are summarized in Table 3.4 and shown graphically in Figure 3.2. To quantify the deviation from experimental values of the calculated magnetic shielding tensor components, a modified sample standard variance,[251] s, is introduced:

$$s = \left[\frac{1}{n - 1}\sum_{i=1}^{3}\left(\sigma_{ii}(\mathrm{calc}) - \sigma_{ii}(\mathrm{exp})\right)^2\right]^{1/2} \qquad 3.6$$

where n is the number of components (3) being compared. The variance of the calculated magnetic shielding tensor principal components for ethylene is summarized in Table 3.4.

There is no clear trend in the calculated principal components of the magnetic shielding (Table 3.4) apart from the observation that using a small basis set results in

Table 3.4 Calculated Carbon Magnetic Shielding Tensor Components for Ethylene.[a]

	σ_{11}	σ_{22}	σ_{33}	σ_{iso}	Ω	κ	s
Experimental[b]	-46	68	164	62	210	-0.10	-
			B3LYP				
3-21G	-17	98	187	89	204	-0.13	34
6-31G	-39	82	173	72	212	-0.14	13
6-311+G*	-71	65	167	54	238	-0.14	18
cc-pVTZ	-73	62	170	53	243	-0.11	20
aug-cc-pVTZ	-74	62	166	51	240	-0.14	20
cc-pVQZ	-81	59	167	48	248	-0.13	26
cc-pV5Z	-87	55	164	44	251	-0.13	30
			RHF				
3-21G	-36	112	199	92	235	-0.26	40
6-31G	-53	98	185	77	238	-0.26	26
6-311+G*	-76	88	179	64	255	-0.28	28
cc-pVTZ	-79	85	180	62	259	-0.27	29
aug-cc-pVTZ	-79	84	177	61	256	-0.27	28
cc-pVQZ	-84	83	178	59	262	-0.27	31
cc-pV5Z	-88	80	176	56	264	-0.27	32
			MP2				
3-21G	15	125	200	113	185	-0.19	64
6-31G	-10	104	188	94	198	-0.15	40
6-311+G*	-40	91	182	78	222	-0.18	21
cc-pVTZ	-45	84	185	75	230	-0.12	19
aug-cc-pVTZ	-45	83	181	73	226	-0.13	16
cc-pVQZ	-52	80	182	70	234	-0.13	16

(*continued on next page*)

Table 3.4 (*cont.*)

a. Principal components of the magnetic shielding tensors and the span, Ω, are in ppm.

b. From reference 54.

calculated magnetic shielding in all directions that is much greater than experimental values. Beyond 6-311+G*, calculated values have almost converged, but increasing the basis set from cc-pVQZ to cc-pV5Z results in a slightly reduced shielding in all directions for the RHF calculations, suggesting that the basis set limit has not quite been achieved at this level. Agreement between experiment and theory is actually best at the B3LYP/6-31G* level, but this is fortuitous, since the basis set limit clearly has not yet been reached. Calculated values improve significantly if electron correlation effects are considered: MP2 calculations are converging to values that are closer to experimental values. In particular, the shielding in the direction of σ_{11}, which is expected to have the greatest contribution from σ^p (see Table 3.1), is only calculated accurately if electron correlation effects are considered. The data illustrate the importance of considering magnetic shielding tensors when assessing computational techniques, since apparently accurate isotropic values may be a consequence of cancellation of errors. For example, the calculated isotropic shielding obtained with RHF/cc-pVTZ is in agreement with experiment, but the individual tensor components deviate significantly: the underestimate of σ_{11} is offset by an overestimate of σ_{22} and σ_{33}. The magnetic shielding principal components calculated at the RHF level are converging to values that are similar to those reported by Orendt *et al.* using IGLO.[56] Cheeseman and coworkers reported comparable isotropic magnetic shielding values for ethylene, calculated using various density

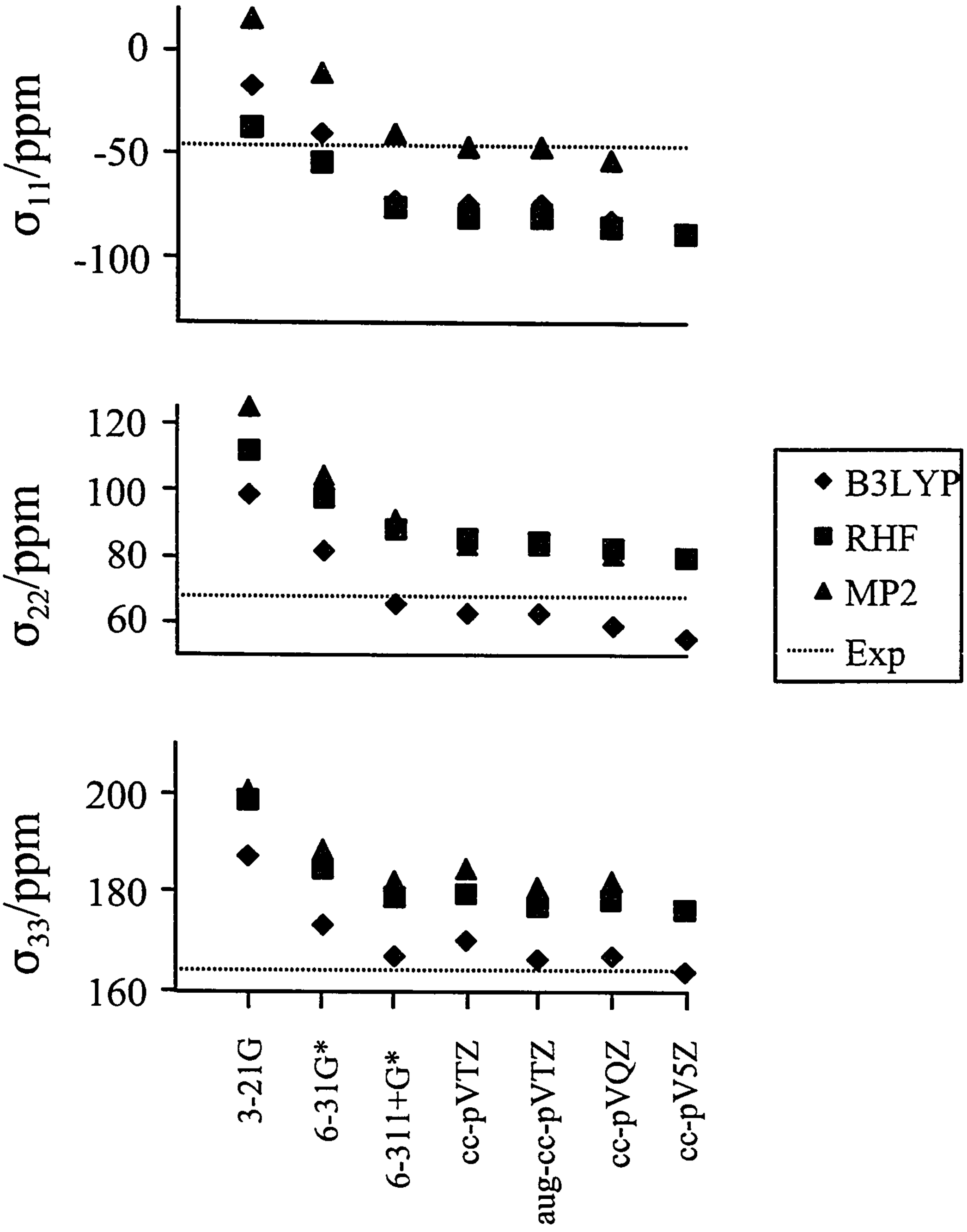

Figure 3.2 Calculated carbon magnetic shielding tensor components for ethylene as a function of basis set. The scale for the abscissa is qualitative. Experimental values are from reference 54.

functionals, including B3LYP.[250] Recently, Kaski *et al.*[50] calculated the magnetic shielding for ethylene using multi configuration self-consistent field (MCSCF) theory; the calculated components of the magnetic shielding tensor are similar to those obtained at the MP2 level of theory.

A similar series of calculations was undertaken for diphenylacetylene, although it was not practical to calculate the shielding at the MP2 level of theory; the results are illustrated in Figure 3.3. Both RHF and B3LYP calculations underestimate the magnitude of the shielding in the directions of σ_{11} and σ_{22} but overestimate the shielding in the direction of σ_{33}. Hence, the σ_{iso} are closer to experimental values than are the individual tensor components. The trend in the magnetic shielding tensor components calculated with B3LYP is comparable to that observed for calculations on ethylene: agreement between experiment and theory is good with the 6-31G* basis but calculations with larger basis sets are significantly different from experimental values.

Figure 3.4 illustrates the calculated shielding, at the RHF level, as a function of basis set size for two platinum-ethylene complexes: $Pt(C_2H_4)(PPh_3)_2$ and $[Pt(C_2H_4)Cl_3]^-$; the data are summarized in Table 3.5. Calculations for $Pt(C_2H_4)(PPh_3)_2$ are in qualitative agreement with experiment, but the principal components are overestimated. In contrast, the calculated shielding for $[Pt(C_2H_4)Cl_3]^-$ is in agreement with experiment. It is not clear why calculations for the latter converge to the experimental values while those for $Pt(C_2H_4)(PPh_3)_2$ are shielded compared with experiment. The ethylene ligand is modified much more upon coordination with Pt(0)[24] than with Pt(II).[248] However, if weak coordination of the ethylene with platinum results in calculated magnetic shielding tensors that are closer to experimental

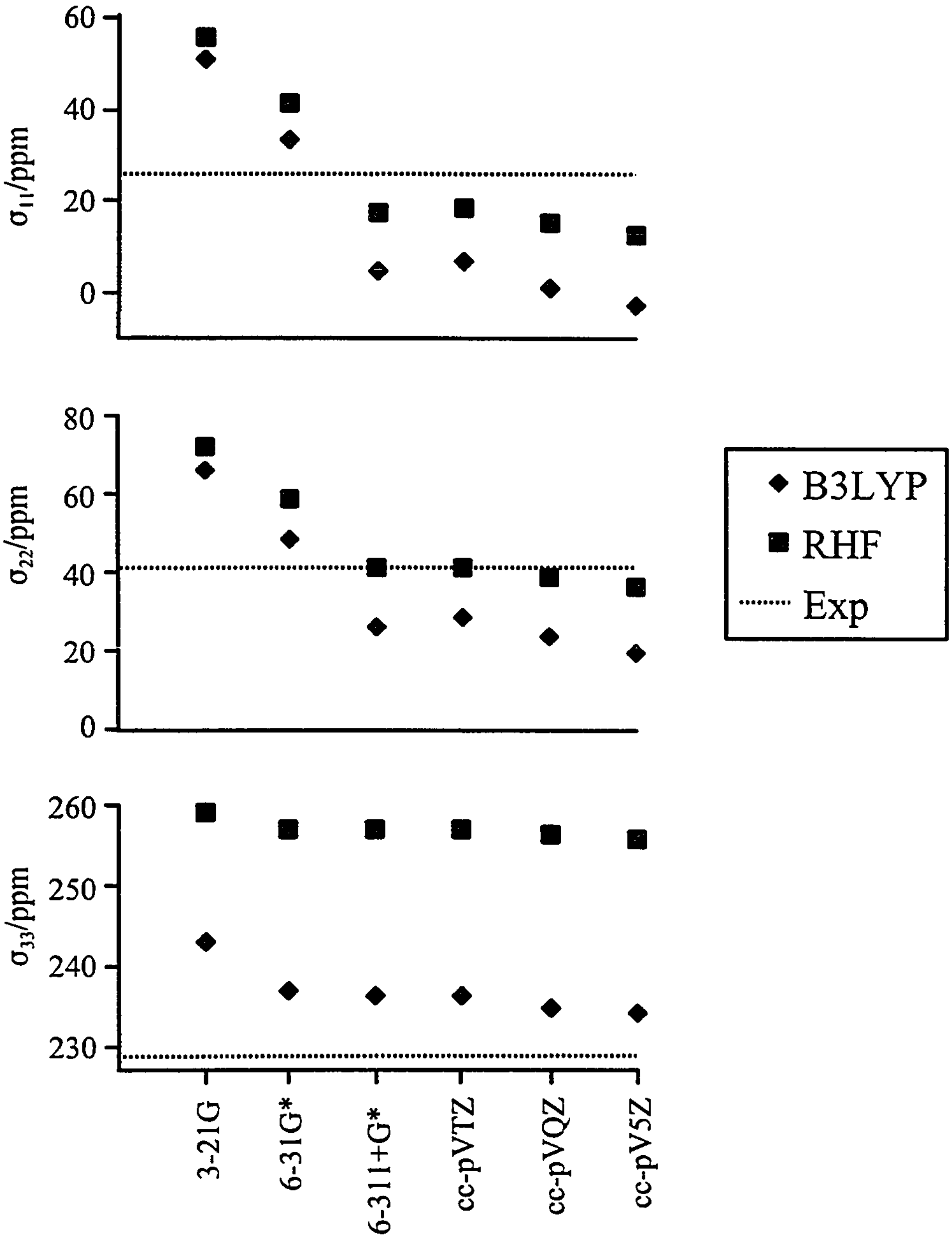

Figure 3.3 Calculated magnetic shielding tensor components for the alkynyl carbon nuclei of diphenylacetylene as a function of basis set. The scale for the abscissa is qualitative. Experimental values are from this work (see Chapter 6).

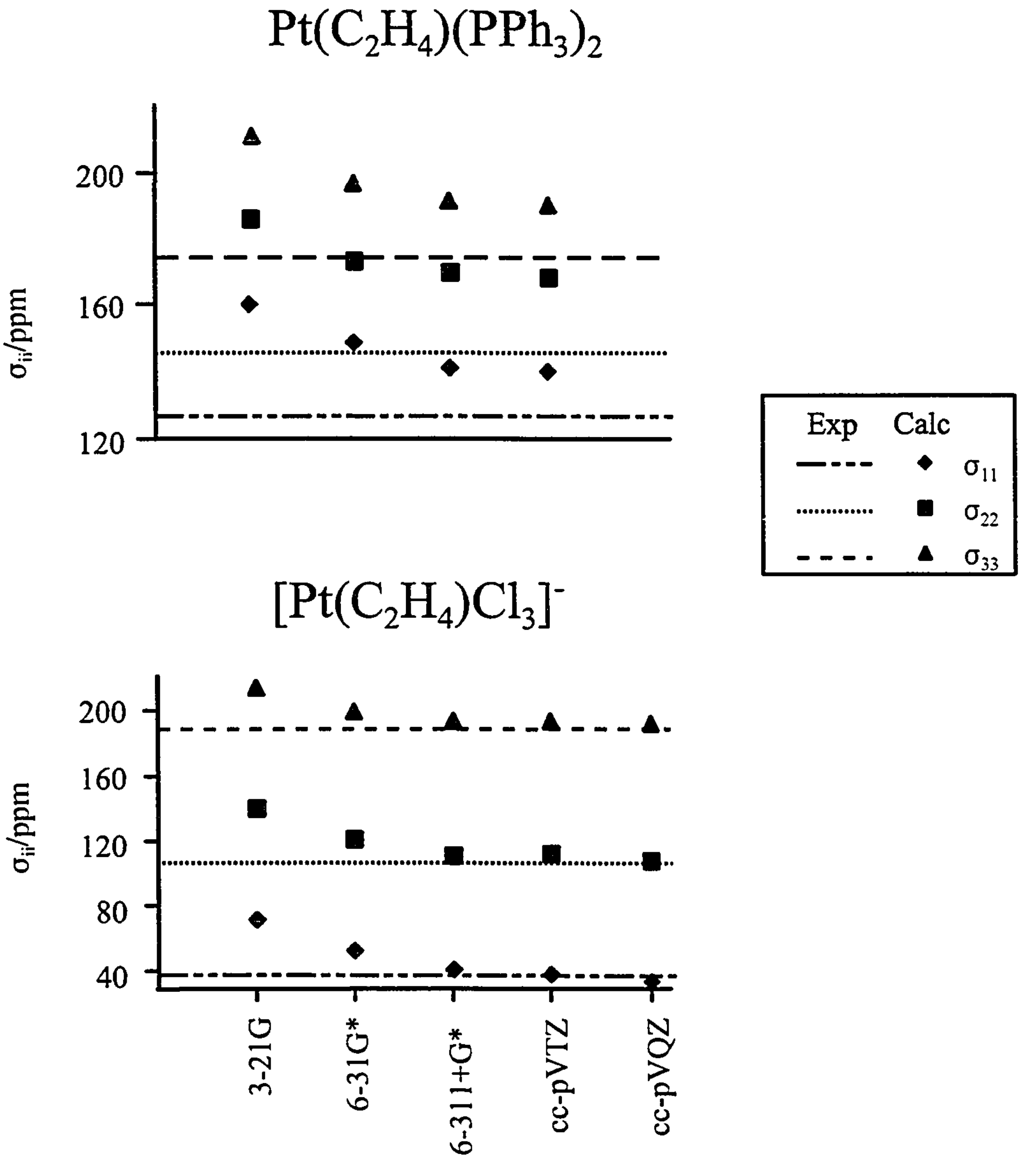

Figure 3.4 Calculated carbon magnetic shielding tensor components for $Pt(C_2H_4)(PPh_3)_2$ and $[Pt(C_2H_4)Cl_3]^-$. The scale for the abscissa is qualitative.

Table 3.5 Calculated Carbon Magnetic Shielding Tensor Components for $Pt(C_2H_4)(PPh_3)_2$ and $[Pt(C_2H_4)Cl_3]^-$.[a]

	σ_{11}	σ_{22}	σ_{33}	σ_{iso}	Ω	κ	*s*
			$Pt(C_2H_4)(PPh_3)_2$				
Experimental[b]	125	145	177	149	52	0.23	-
3-21G	160	185	211	185	51	0.00	45
6-31G*	149	172	197	173	48	0.06	29
6-311+G*	142	169	193	168	51	-0.06	24
cc-pVTZ	141	167	192	167	51	0.00	22
aug-cc-pVTZ	141	168	191	167	50	-0.06	22
			$[Pt(C_2H_4)Cl_3]^-$				
Experimental[b]	38	109	188	112	150	0.06	-
3-21G	70	141	214	142	144	0.02	37
6-31G*	51	122	199	124	148	0.04	15
6-311+G*	38	112	193	114	155	0.04	4
cc-pVTZ	37	113	192	114	155	0.02	4
cc-pVQZ	32	109	191	111	159	0.04	5

a. Magnetic shielding and the span, Ω, are in ppm. Average values for nonequivalent alkenyl carbon sites are reported.

b. This work.

values, one would expect agreement between calculated and experimental values for uncoordinated ethylene; this is not the case (see Table 3.4). Higher level calculations would be instructive, but are not practical at this time.

3.5.2 Calculations on Metal-Alkene Complexes

As stated above, the magnetic shielding tensor orientations will not be considered in detail in this chapter. However, it is noted that, with one exception discussed below, all calculated alkenyl magnetic shielding tensors have orientations similar to that illustrated for ethylene in Fig. 1.6: σ_{22} is approximately along the C,C bond with σ_{33} perpendicular to C,C bond in the plane defined by the metal and the alkenyl carbon atoms. The principal components of the calculated alkenyl magnetic shielding tensors are summarized in Table 3.6. For comparison, calculated results shown here were all obtained with the same basis set, cc-pVTZ.

The availability of experimental NMR data for the Pt(0) and Pt(II)-ethylene complexes allows a comparison of experimental and calculated shielding tensor data. Qualitatively, the calculations reproduce experimental trends, predicting that: the shielding in the directions of σ_{11} and σ_{22} is much greater for $Pt(C_2H_4)(PPh_3)_2$ than for $[Pt(C_2H_4)Cl_3]^-$; the span of the latter is larger; and the shielding in the direction of σ_{33} is virtually unaffected by metal coordination. Table 3.6 also summarizes the calculated alkenyl carbon magnetic shielding tensors for Pt(η^2-*trans*-stilbene)$(PPh_3)_2$. The effect on the carbon magnetic shielding of coordination of *trans*-stilbene with platinum is similar to that discussed above for the platinum-ethylene complexes. The principal components of the carbon magnetic shielding tensors for Pt(η^2-*trans*-stilbene)$(PPh_3)_2$ calculated using B3LYP/cc-pVTZ are closer to experimental values than are those calculated with RHF/cc-pVTZ, but it is uncertain if the basis set limit has been reached for the former.

Table 3.6 Calculated Carbon Magnetic Shielding Tensor Components for Some Metal-Alkene Complexes.[a,b]

		σ_{11}	σ_{22}	σ_{33}	σ_{iso}	Ω	κ
C_2H_4	Exp[c]	-46	68	164	62	210	-0.10
	Calc	-79	85	180	62	259	-0.27
$Ni(C_2H_4)(PMe_3)_2$	Exp[d]				138		
	Calc	175	195	226	199	51	0.24
$Pd(C_2H_4)(PMe_3)_2$	Calc	111	164	190	155	79	-0.34
$Pt(C_2H_4)(PMe_3)_2$	Exp[e]	125	145	177	149	52	0.23
	Calc	141	167	192	167	51	0.00
$[Pd(C_2H_4)Cl_3]^-$	Calc	-44	98	186	80	230	-0.23
$[Pt(C_2H_4)Cl_3]^-$	Exp[e]	38	109	188	112	150	0.06
	Calc	37	113	192	114	155	0.02
trans-stilbene	Exp[e]	-27	68	139	60	166	-0.14
	Calc	-47	85	152	63	199	-0.33
Pt(*trans*-stilbene)$(PMe_3)_2$	Exp[e]	96	117	147	120	51	0.18
	Calc	130	148	157	145	27	-0.33
	Calc[f]	104	127	138	123	34	-0.35

a. Magnetic shielding and the span, Ω, are in ppm.

b. Unless otherwise indicated, calculated values were determined at the RHF/cc-pVTZ level of theory. Average values are reported for crystallographically nonequivalent nuclei.

c. From reference 54.

d. Experimental value, from reference 13, is for $Ni(C_2H_4)(PPh_3)_2$.

(*continued on next page*)

Table 3.6 (*cont.*)

e. This work. Experimental values are for the triphenylphosphine derivatives of the Pt(0) complexes.

f. Calculated at the B3LYP/cc-pVTZ level of theory.

The limited experimental ^{13}C NMR data for the nickel- and palladium-ethylene complexes preclude a detailed comparison of calculated and experimental data. Comparison of the calculated magnetic shielding tensors for the Pd(0)- and Pd(II)-ethylene complexes suggests that the effect of coordination of ethylene with palladium is comparable to that of coordination with platinum. The magnetic shielding of the alkenyl carbon nuclei is much more sensitive to coordination with Pd(0) than to coordination with Pd(II). In fact, the carbon shielding tensor for the Pd(II)-ethylene complex is not very different from that for uncoordinated ethylene, consistent with the fact that the calculated structure of the ethylene ligand in this complex is not greatly modified (Table 3.3) from that for uncoordinated ethylene. For both complexes, σ_{33} is relatively unaffected by coordination with palladium.

The carbon magnetic shielding tensor for the nickel-ethylene complex is interesting in that the predicted tensor orientation is different from other alkenyl carbon tensors: the directions of greatest and least shielding are approximately interchanged. Since the magnitude of σ_{33} for ethylene is comparable to that of σ_{11} for $Ni(C_2H_4)(PMe_3)_2$, the effect of metal coordination is in fact similar to that observed or predicted for the palladium- and platinum-ethylene complexes. The magnetic shielding tensor component perpendicular to the molecular plane of uncoordinated ethylene is relatively unaffected by metal coordination, but the shielding in the remaining directions increases significantly. However, considering the discrepancy between the calculated isotropic magnetic shielding and the experimental value[13] and in view of the small span of the shielding tensor, the proposed orientation must be regarded as tentative. Accurately calculating orientations for magnetic shielding tensors with small spans is particularly challenging, since the shielding is relatively insensitive to orientation. It is noted that calculations on the nickel analogue of Zeise's salt were not undertaken, since this anion has never been prepared.[29]

Summarizing, the effect on the magnetic shielding tensor of coordination of alkenes with nickel, palladium or platinum generally is orientation dependent. Metal coordination results in a large increase in the magnetic shielding perpendicular to the plane defined by the metal and the alkenyl carbon atoms. The shielding along the alkenyl C,C bond also increases significantly following metal coordination, but the shielding in the direction perpendicular to the plane of the alkene is relatively unaffected.

These effects may be qualitatively rationalized by considering Ramsey's theory,[184] discussed in Section 3.2. The carbon magnetic shielding perpendicular to the plane of ethylene is dominated by σ^d (Table 3.1). Since σ^d is less sensitive to orientation than σ^p, it is expected to be less sensitive to metal coordination, as observed experimentally and predicted theoretically. The shielding in the direction of σ_{11} for ethylene, in the molecular plane perpendicular to the C,C bond, is dominated by σ^p and hence is particularly sensitive to metal coordination.

The calculated and experimental results are consistent with the expectation that alkenes coordinated with a metal centre have properties intermediate between those of alkenes and alkanes;[1] the carbon magnetic shielding tensor for the metal-ethylene complexes are generally approaching those for ethane, $\sigma_{11} = \sigma_{22} = 172$ ppm and $\sigma_{33} = 179$ ppm.[192] Likewise, the increased shielding in the direction of σ_{11} (σ_{33} for $Ni(C_2H_4)(PMe_3)_2$), suggests that the tensors for the metal complexes are approaching those for ethane, since the magnetic shielding in this direction for ethane is dominated by σ^d.

3.5.3 Calculations on Metal-Alkyne Complexes

Table 3.7 summarizes the calculated principal components of the alkynyl carbon magnetic shielding tensors for some alkynes coordinated with Ni(0), Pt(0) and Pt(II), as well as the values for the uncoordinated ligands. The calculations are qualitatively in agreement with experiment. Calculations accurately predict a non-axially symmetric shielding tensor for diphenylacetylene (DPA), and the decreased shielding in the directions of σ_{11} and σ_{33} following coordination with platinum is also accurately predicted. However, the calculations predict significant increased shielding in the direction of σ_{22}, contrary to experimental observations.

Similar magnetic shielding tensor components are predicted for the platinum- and nickel-diphenylacetylene complexes; the calculated isotropic magnetic shielding of the latter is calculated accurately. The magnetic shielding tensor components for the terminal carbon nucleus of phenylacetylene were determined by measuring the spin relaxation rates for the ^{13}C nucleus of a ^{13}C-labelled sample dissolved in toluene and in 50/50 mixtures of toluene/methanol and toluene/2-propanol.[252] The carbon magnetic shielding tensor was assumed to be axially symmetric; calculations suggest that this may not be the case. It is

Table 3.7 Calculated Carbon Magnetic Shielding Tensor Components for Some Metal-Alkyne Complexes.[a,b]

		σ_{11}	σ_{22}	σ_{33}	σ_{iso}	Ω	κ
Ph-C≡C-Ph	Exp[c]	23	41	230	98	207	0.83
	Calc	18	41	257	105	239	0.80
Pt(Ph-C≡C-Ph)(PMe$_3$)$_2$	Exp[c]	-33	46	159	57	192	0.17
	Calc	-54	94	188	76	242	-0.22
Ni(Ph-C≡C-Ph)dmpe[d]	Exp[e]				50		
	Calc	-87	20	202	45	289	-0.26
H-C*≡C-Ph	Exp[f]	56	56	216	109	160	1.00
	Calc	62	71	247	127	185	0.91
H-C≡C*-Ph	Calc	22	36	303	120	281	0.90
[Pt(H-C*≡C-Ph)Cl$_3$]$^-$	Calc	10	117	243	123	233	0.08
[Pt(H-C≡C*-Ph)Cl$_3$]$^-$	Calc	-13	66	318	124	331	0.53

a. Magnetic shielding and the span, Ω, are in ppm. Data for the uncoordinated ligands are included for comparison.

b. Calculated values were determined at the RHF/cc-pVTZ level of theory.

c. This work; the average magnetic shielding for the four alkynyl carbon sites of Pt(Ph-C≡C-Ph)(PMe$_3$)$_2$ are given here (see Chapter 6).

d. dmpe = PMe$_2$-CH$_2$-CH$_2$-PMe$_2$

e. From reference 245.

f. From reference 252.

interesting to note that calculations predict significantly greater shielding in the direction of the C,C bond for the phenyl-bonded alkynyl carbon nucleus than for the terminal carbon nucleus, implying a smaller contribution from σ^p for the former despite the proximity to the phenyl ring.

Unlike the calculations for the metal-alkene complexes, the orientations for the alkynyl carbon magnetic shielding tensors of diphenylacetylene coordinated with nickel and platinum are significantly different from those for the uncoordinated ligand. This is thought to be a consequence of the large difference in the structure of the diphenylacetylene ligand before and after coordination. A detailed discussion of this effect for the platinum-diphenylacetylene complex is presented in Section 6.3.6. In contrast, coordination of phenylacetylene with Pt(II) has a negligible effect on the orientation of the magnetic shielding tensor: the direction of greatest shielding is along the alkynyl C,C bond for both the uncoordinated ligand and the complex. The alkynyl C,C bond lengths for the phenylacetylene ligand before and after coordination are shorter than the corresponding values for diphenylacetylene.

3.6 Summary

Carbon magnetic shielding tensors for several alkenes and alkynes, as well as those for the nickel, palladium or platinum complexes of these ligands, have been calculated. A comparison of the magnetic shielding tensor components for ethylene, calculated at the DFT, RHF and MP2 levels of theory, reveals that the inclusion of electron correlation effects at the MP2 level improves agreement between experiment and theory significantly. With small basis sets, the magnetic shielding tensors calculated using DFT are close to experimental values, but the basis set limit has not been achieved at this level; calculations converge to values that are significantly deshielded compared to experimental values. Since the DFT calculations do not yield results that are consistently closer to experimental values than those obtained at the RHF level of theory, the latter was chosen to calculate the magnetic shielding tensors for the metal-alkene and metal-alkyne complexes. Calculations at all levels of theory demonstrate the importance of considering magnetic shielding tensor components rather than merely isotropic shielding values when assessing the quality of a computational technique, since cancellation of errors may lead to misleading results.

The calculated principal components of the magnetic shielding tensors for metal-alkene and metal-alkyne complexes are qualitatively in agreement with experimental values. In general, agreement between experimental and calculated magnetic shielding tensors improves as the shielding increases, reflecting the greater difficulty of calculating the paramagnetic component of the shielding. In the case of the anion of Zeise's salt, agreement with experiment is excellent. For other compounds, the principal components of the magnetic shielding tensors are generally overestimated. Nevertheless, calculations qualitatively predict the effect of metal coordination on the principal components of the shielding tensors. Calculation of the magnetic shielding tensor components for $Ni(C_2H_4)(PMe_3)_2$ suggest that the σ_{11} and σ_{33} components for the alkenyl carbon shielding tensor are approximately interchanged. If accurate, this represents the first known example of an alkenyl shielding tensor for which the direction of greatest shielding is not perpendicular to the pseudo-plane of the alkene.

Calculated tensor orientations are virtually invariant to basis set size or to computational technique. Single-crystal ^{13}C NMR data for an organometallic complex would be instructive, allowing a comparison of calculated and experimental alkenyl carbon shielding tensor orientations. Such data are unavailable. It is noted that the calculated orientation of the carbon magnetic shielding tensor for ferrocene is in agreement with the experimental value.[74] In a combined theoretical and single-crystal ^{31}P NMR investigation of a phosphole tretramer, agreement between calculated and experimental phosphorus magnetic shielding tensor orientations is excellent, although the magnitudes of the calculated principal components deviate from experimental values.[103] Hence, it is felt that magnetic shielding tensor orientations may be proposed with reasonable confidence based on the combination of experimental and theoretical data.

Finally it is noted that the computer resources required for routine calculations on large molecules have only become available in this lab in the past year. Extensions of the work discussed in this section are presented in Chapter 7.

Chapter 4

A Solid-State NMR Investigation of Platinum-Ethylene Complexes: $Pt(C_2H_4)(PPh_3)_2$ and Zeise's Salt, $K[Pt(C_2H_4)Cl_3]$

4.1 Introduction

Although Zeise's salt has been known for nearly two centuries, its physical and electronic properties, as well as those of its Pt(0) analogue, ethylene*bis*(triphenylphosphine)platinum(0), $Pt(C_2H_4)(PPh_3)_2$, are not fully understood.[1-3] The structures of these complexes have been discussed in Section 1.2 and are illustrated in Figures 1.1 A and 1.2. Since the carbon CS tensor for ethylene is known,[54,55] the characterization of the alkenyl carbon CS tensors for these fundamental platinum-alkene complexes allows a determination of the effect of coordination with platinum when it formally has either a d^8 or d^{10} electronic configuration.

A further goal of this study is to investigate the internal dynamics of the ethylene ligand in Zeise's salt; that of $Pt(C_2H_4)(PPh_3)_2$ is thought to be rigid at room temperature but is investigated for completeness. Understanding the internal dynamics of molecules, an important molecular property in itself, is particularly important here since a proper interpretation of the ^{13}C NMR data requires knowledge of the motion of the ligand under investigation. By preparing ethylene-$^2H_4$ derivatives of Zeise's salt and $Pt(C_2H_4)(PPh_3)_2$, the dynamics of the ethylene ligand in these complexes were investigated by ^2H NMR. The dynamic properties derived from this study are corroborated by *ab initio* calculations.

Summarizing, this study was undertaken to characterize the alkenyl carbon CS tensors for Zeise's salt and $Pt(C_2H_4)(PPh_3)_2$, and to investigate the internal dynamics of the ethylene ligands in these fundamental platinum-alkene complexes. Before presenting the experimental results, it is useful to review earlier NMR investigations of these and related compounds.

Previous NMR Studies. There have been numerous solution ^{13}C NMR studies of Zeise's salt; the isotropic carbon chemical shifts determined from these studies range from 67.1 to 75.1 ppm,[38,43,44] compared to an isotropic carbon chemical shift of 126 ppm for ethylene.[54,55] There have also been some natural-abundance ^{13}C NMR studies of solid magic-angle-spinning (MAS) samples of Zeise's salt. Huang and coworkers,[60] as well as Oldfield *et al.*,[58] reported the magnitudes of the principal components of the carbon CS tensors for Zeise's salt based on an analysis of the spinning sideband patterns of slow MAS samples. The analyses were based on the method of Herzfeld and Berger,[118] which does not provide any information about the orientation of the CS tensor. Ding and McDowell have carried out ^{13}C NMR studies of slow MAS samples of Zeise's salt.[61] It appears that the authors have used the $^{35/37}Cl,^{13}C$ dipolar interaction to obtain information about the anisotropy and orientation of the carbon CS tensors. Given that splittings due to $^{35/37}Cl,^{13}C$ spin-spin coupling interactions are not resolved in the ^{13}C NMR spectra of either spinning or stationary samples, it is unclear how reliable the orientation information is. There has been no ^{13}C NMR study of stationary solid samples of Zeise's salt. In contrast to the various solid-state ^{13}C NMR studies of Zeise's salt, the principal components of the carbon CS tensors for $Pt(C_2H_4)(PPh_3)_2$ have not been reported; Challoner and Sebald reported the isotropic chemical shift of the alkenyl carbon nuclei, determined from ^{13}C NMR spectra of MAS samples.[253]

Dynamics of the Ethylene Ligands of Pt(C_2H_4)(PPh_3)$_2$ and Zeise's Salt. The internal ligand dynamics for metal-alkenes have been investigated in solution,[254] but the dynamics of the ethylene ligand in the solid state have rarely been investigated. Vierkötter and Barnes studied the dynamics of the ethylene ligand in solid Rh(acetylacetonato)(C_2H_4)$_2$ by ^{2}H NMR and variable temperature ^{13}C NMR, concluding that the ethylene undergoes both librational motion and 180° flips.[255] In their ^{13}C NMR investigation of solid osmium-ethylene complexes, Lewis and coworkers concluded that the ethylene ligand undergoes rotation about the axis perpendicular to the C,C bond, and that the barrier to internal rotation is similar to that measured in solution.[256]

The dynamics of the ethylene ligand for solid samples of Zeise's salt and Zeise's dimer (Figure 1.1 B) have been studied by ^{1}H NMR. Through a second moment analysis[92] of the ^{1}H NMR spectra of Zeise's dimer, Reeves concluded that the ethylene ligand undergoes a rocking motion about the axis perpendicular to the C,C bond.[257] In a later ^{1}H NMR study of Zeise's salt, Maričić *et al.*[258] concluded that, besides the rocking motion, the ethylene ligand also undergoes large amplitude oscillations about the axis parallel to the C,C bond.

There appears to be uncertainty in the literature about the interpretation of these experimental results. For example, it has recently been stated that the ethylene ligand of Zeise's salt "rotates rapidly" in the solid state.[61] To clarify this point, and to properly interpret our ^{13}C NMR data, a ^{2}H NMR study of the internal dynamics of the ethylene ligands in Pt($C_2{}^2H_4$)(PPh_3)$_2$ and Zeise's salt-$^2H_4$ was undertaken.

4.2 Experimental

Sample preparation. Samples were prepared with the assistance of Mr. A. Phillips. For both $Pt(C_2H_4)(PPh_3)_2$ and Zeise's salt, the procedures were modified from those suggested in the literature, since these entailed bubbling ethylene through a solution, which is impractical for labelled ethylene. Samples were prepared with ethylene at natural abundance, $^{13}C_2$-labelled (Isotec, 99 % ^{13}C) or $^2H_4$-labelled (Isotec, 99 % ^2H); representative syntheses are outlined below.

A procedure based on that of Blake and Roundhill[259] was used for the preparation of $Pt(C_2H_4)(PPh_3)_2$. This entails the preparation of $Pt(CO_3)(PPh_3)_2{\cdot}C_6H_6$ by bubbling O_2 and CO_2 for 30 minutes through a solution of $Pt(PPh_3)_4$ dissolved in benzene. The product precipitates quickly and is dissolved in CH_2Cl_2 to which PPh_3 is added. After refluxing for six hours, the solution is placed in a rotary evaporator until the volume is reduced by approximately one half. The final product is filtered. 1.2 g (70 % yield) was prepared for this and other syntheses. $Pt(C_2H_4)(PPh_3)_2$ was prepared by dissolving 0.395 g of $Pt(CO_3)(PPh_3)_2{\cdot}C_6H_6$ in 25 ml of ethanol. The solution was placed in a 125 ml 2-neck reaction flask, to which a stirring bar had been added. Before transferring the ethylene, 20 ml of a 0.1 M solution of $NaBH_4$ was placed in a syringe which was inserted through a rubber septum in the neck of the flask; to prevent leaks the insertion point was sealed with epoxy glue and the septum was secured with a wire. Approximately 5.5 mmol of ethylene was condensed into the reaction flask; after thawing, the ethylene was at approximately 2 atm pressure. The 0.1 M $NaBH_4$ was transferred dropwise over a period of approximately 20 minutes, with vigorous stirring. After 48 hours, 0.315 g of a fine white powder was recovered, corresponding to a yield of 90 %. $Pt(C_2H_4)(PPh_3)_2$ was characterized by its melting point, 117 to 118° C, and by IR and solid-state NMR.

Zeise's salt was prepared based on a procedure proposed by Chock *et al.*[260] Approximately 2 g of potassium tetrachloroplatinate (K_2PtCl_4) was dissolved in 20 mL of 5M hydrochloric acid and transferred to a 125 mL reaction flask containing a stirring bar. Approximately 0.02 g of tin chloride hydrate ($SnCl_2{\cdot}2H_2O$) was dissolved in 2.75 mL H_2O and transferred to the reaction flask. The resulting solution was degassed by 3 cycles of the freeze-pump-thaw cycle. The solution was frozen by immersing the flask in $N_2(\ell)$, the flask was evacuated, then approximately 5.5 mmol of ethylene was transferred by condensation. The initial pressure in the reaction flask, after thawing the ethylene, was approximately 2 atm. After stirring for 24 hours, the solution, which was initially dark red with undissolved solid K_2PtCl_4, became a clear yellow solution. The reaction was stopped after 2 days. Upon cooling the solution, yellow needle-like crystals precipitated; 0.6 g was recovered corresponding to a yield 40 %. The samples were characterized by their melting points (decomposes at 190° C), solution and solid-state NMR spectra, and for the sample at natural abundance, by electro-spray mass spectrometry. To ensure consistent Zeise's salt samples, these were dehydrated by placing them under dynamic vacuum (10^{-3} Torr) for 16 to 20 hours.[260] Anhydrous samples were packed in sealed NMR rotors in a dry nitrogen atmosphere.

NMR. The acquisition of ^{13}C NMR spectra has been summarized in Section 2.7. Contact times of 0.5 to 1.0 ms with ^{1}H 90° pulses of 3.5 to 4.5 μs and recycle times of 100 - 300 s were used to acquire all ^{13}C NMR spectra. NMR spectra of $^{13}C_2$-labelled samples were analyzed with the dipolar-chemical shift method (Section 2.4.1).

Carbon-13 2D spin-echo NMR spectra were acquired on a Bruker AMX 400 spectrometer using a standard spin-echo pulse sequence,[261,262] with experimental parameters similar to those used for the 1D experiments. The data size was 1024 × 128 after zero filling in both dimensions. The final spectra were displayed in the magnitude mode following the application of window functions in both dimensions. The *F*1 projections were simulated using the program Spinecho, written in this laboratory. The *F*1 projections contain a sharp central peak, a consequence of incomplete refocusing of the magnetization following the π pulse; the length of the experiment made it impractical to optimize this parameter.

Deuterium NMR spectra of stationary powder samples were acquired at 300 K on the Bruker AMX-400 spectrometer operating at a ^{2}H NMR frequency of 61.4 MHz. A quadrupolar echo pulse sequence,[173] with delays τ_1 and τ_2 (Figure 2.6) of 15.0 and 20.0 μs, respectively, was used; 90° pulse widths were 2.3 μs. Recycle delays of up to 90 minutes were required to obtain spectra with an acceptable signal-to-noise ratio. The spectrum of $Pt(C_2H_4)(PPh_3)_2$ was symmetrized, yielding a $2^{1/2}$ enhancement in the signal-to-noise ratio.[170] NMR spectra were calculated with the program WSolids, written in this laboratory; corrections for finite pulse lengths were not included in the simulation.

***Ab initio* Calculations.** Details of the calculation of the carbon CS tensors have been summarized in Section 3.4. The barrier to internal rotation of the ethylene ligand of Zeise's salt was calculated at the MP2 level of theory[233] using the LANL2DZ ECP for platinum and the 6-31G* basis set for the remaining atoms. All structural parameters were optimized except the angle φ, which defines the orientation of the C,C bond relative to the plane containing the platinum and chlorine atoms. This angle was fixed at 15° increments between 0 and 90°. Similar calculations on $Pt(C_2H_4)(PPh_3)_2$ were not practical because of its size, but single-point RHF calculations at the 6-31G* level were performed, with the ethylene oriented in and at 90° to the plane defined by the platinum and phosphorus atoms.

4.3 Results and Discussion

4.3.1 Carbon-13 NMR Spectra of $Pt(\eta^2\text{-}C_2H_4)(PPh_3)_2$

Carbon-13 NMR spectra of MAS samples of $Pt(C_2H_4)(PPh_3)_2$ are shown in Figure 4.1. The lower trace, a spectrum of the unlabelled sample, illustrates the large contribution from the phenyl ^{13}C nuclei at natural abundance. Although of relatively low intensity, the contributions from the alkenyl carbon nuclei are apparent at approximately 39 ppm, in agreement with previous solid-state[253] and solution[38,42] NMR studies. The expansion of this region shows that there are two peaks. This is consistent with the crystal structure of the molecule (space group $P2_1/a$, $Z = 4$, density = 1.58 g cm^{-3}) which indicates crystallographically distinct alkenyl carbon atoms.[24] Spinning sidebands, indicated with asterisks in Figure 4.1, are barely distinguishable at an MAS frequency (ν_{rot}) of 3725 Hz, demonstrating that the spans of the alkenyl carbon nuclei are not large. The spectrum of the $^{13}C_2$-labelled sample is shown in the upper trace of Figure 4.1; the expansion of the alkenyl region indicates the presence of two peaks; these are invariant to ν_{rot} or B_0. The line widths at half-height ($\nu_{1/2}$) of the isotropic alkenyl peaks of the $^{13}C_2$-labelled MAS samples are broadened to approximately 250 Hz. There is no evidence of indirect spin-spin coupling to ^{195}Pt (natural abundance, 33.8 %) or ^{31}P; this is not surprising since the reported values of $^1J(^{195}Pt,^{13}C)$ and

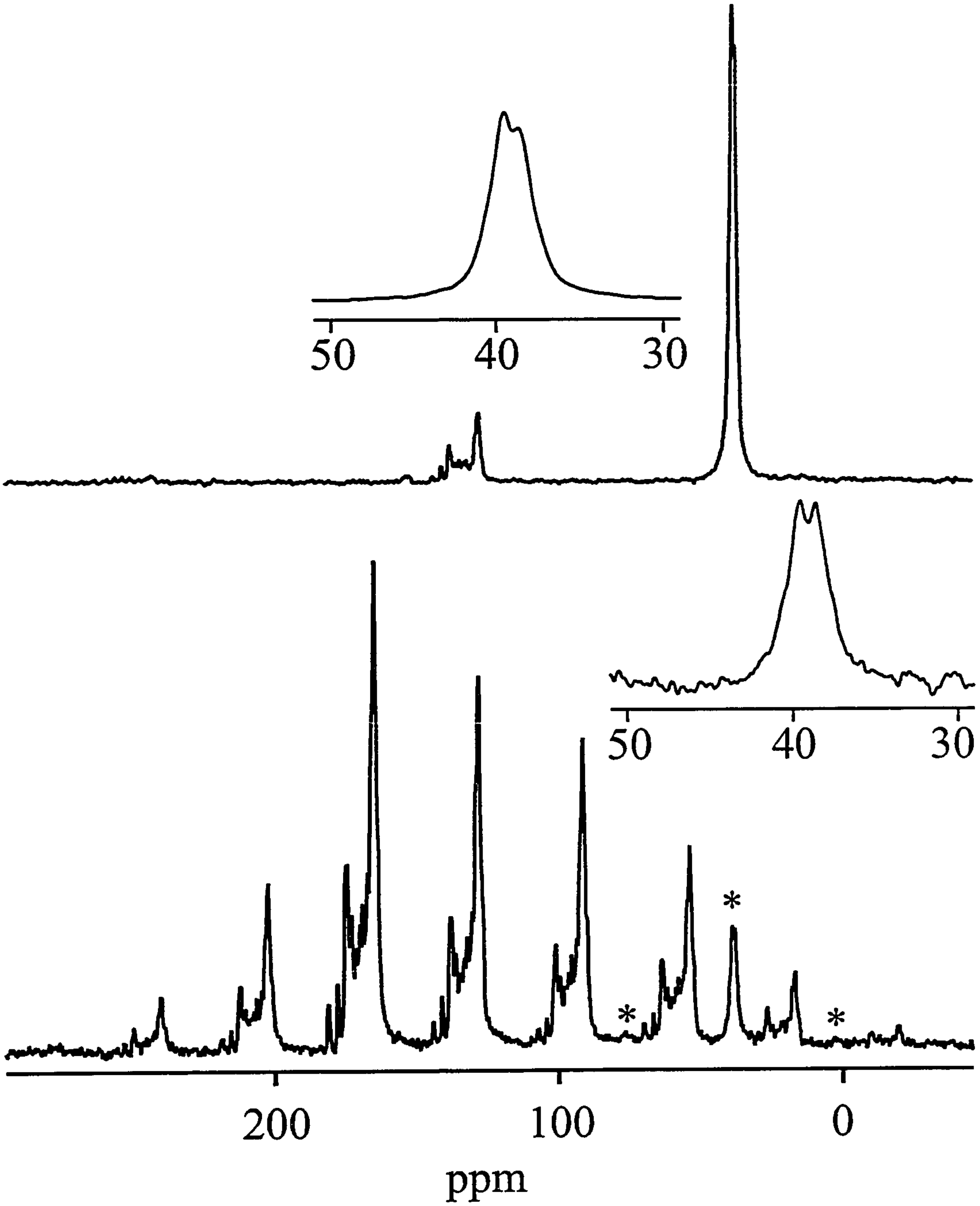

Figure 4.1 Carbon-13 NMR spectra of MAS samples of $Pt(C_2H_4)(PPh_3)_2$. The lower trace is a spectrum of the unlabelled sample, acquired at 9.4 T with ν_{rot} = 3725 Hz; 476 transients were added. The isotropic peak and first-order spinning sidebands of the alkenyl carbon nuclei are indicated with asterisks. The upper trace is that of the $^{13}C_2$-labelled sample acquired at 9.4 T with ν_{rot} = 11500 Hz; 24 transients were added. The alkenyl carbon regions are shown in the expansions.

${}^{2}J({}^{31}\mathrm{P},{}^{13}\mathrm{C})$ measured in solution, 194 and 24 Hz, respectively,[38] are significantly less than the line widths of the spectra of the MAS samples.

Figure 4.2 illustrates the 2D ${}^{13}\mathrm{C}$ spin-echo NMR spectrum of $\mathrm{Pt(C_2H_4)(PPh_3)_2}$. The simulated $F1$ projection, shown at the bottom, was calculated with the same parameters as for the calculation of the 1D NMR spectra, discussed below. The calculated spectrum is very sensitive to R_{eff} (eq 2.16). Assuming $\Delta J({}^{13}\mathrm{C},{}^{13}\mathrm{C})$ for $\mathrm{Pt(C_2H_4)(PPh_3)_2}$ is negligible (Section 2.1.4) and hence $R_{\mathrm{DD}} \approx R_{\mathrm{eff}}$, r_{CC} may be estimated from eq 2.15. The experimental value of R_{eff}, 2475 ± 50 Hz, corresponds to $r_{\mathrm{CC}} = 1.453 \pm 0.010$ Å. This value is within experimental error of that determined from X-ray crystallography, 1.434 ± 0.039 Å.[24] The close agreement of the values of r_{CC} determined from R_{eff} and from X-ray diffraction suggests that motional averaging of the dipolar interaction is not significant (*vide infra*).

The simulated and experimental ${}^{13}\mathrm{C}$ NMR spectra of stationary samples of $\mathrm{Pt(C_2H_4)(PPh_3)_2}$ are shown in Figure 4.3; the parameters derived from the simulation are summarized in Table 4.1. The small chemical shift difference between the two alkenyl carbon nuclei results in a complex powder pattern, since most crystallites are oriented such that the two carbon nuclei comprise an *AB* spin system.[263]

The orientations of the alkenyl carbon CS tensor components for $\mathrm{Pt(C_2H_4)(PPh_3)_2}$ relative to the ${}^{13}\mathrm{C},{}^{13}\mathrm{C}$ dipolar vector are summarized in Table 4.1. Molecules with mirror symmetry planes which include the nuclei of interest have one CS tensor component perpendicular to this plane while the remaining two components lie in the plane. For $\mathrm{Pt(C_2H_4)(PPh_3)_2}$, none of the principal components of the carbon CS tensors are oriented perpendicular to the plane defined by the platinum and alkenyl carbon atoms. This is

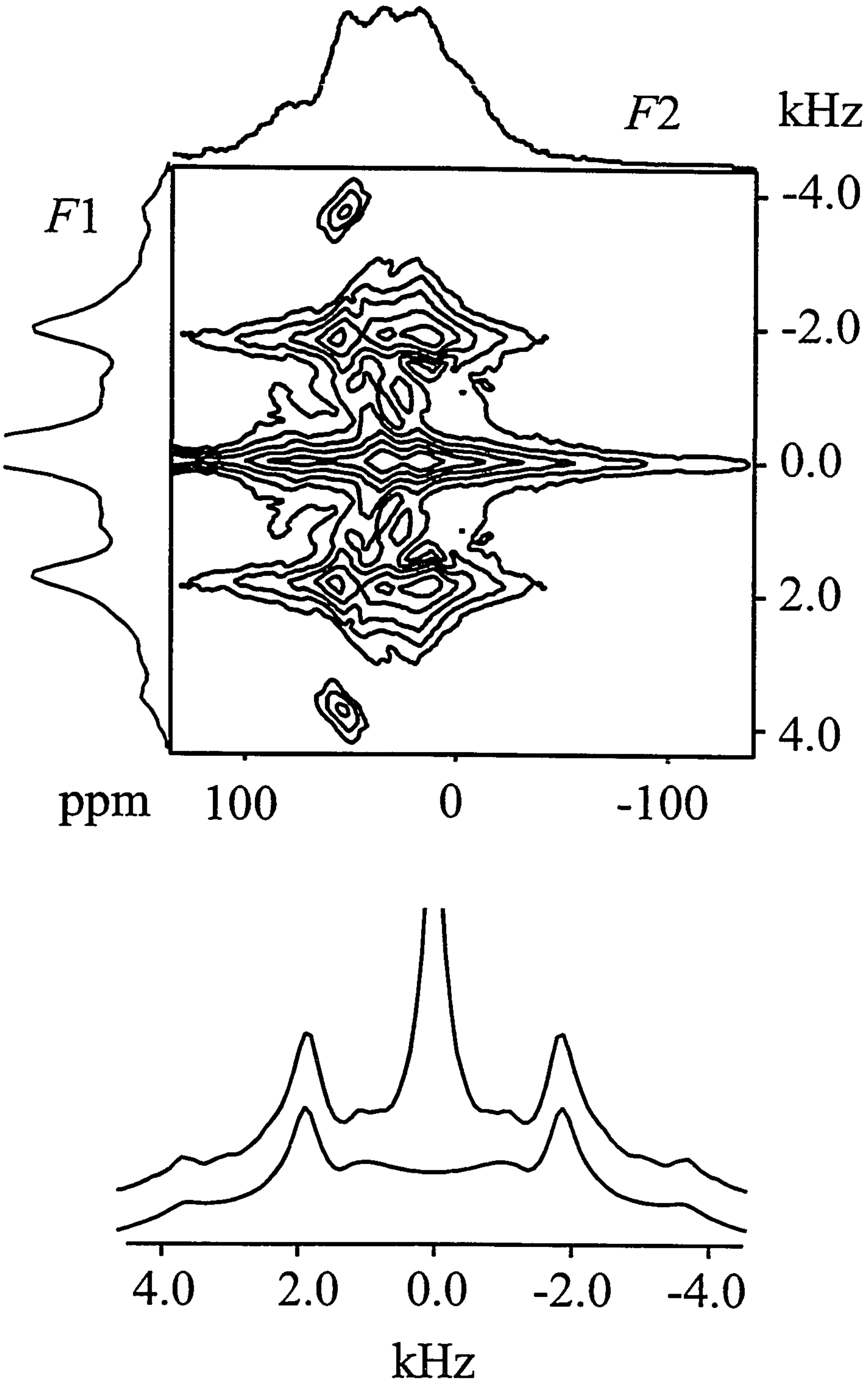

Figure 4.2 Two-dimensional ^{13}C spin-echo NMR spectrum of Pt(^{13}C$_2$H$_4$)(PPh$_3$)$_2$ acquired at 9.4 T (top); 32 transients were added for each of 64 increments. At the bottom, the experimental (upper trace) and calculated (lower trace) *F*1 projections are shown. The central peak is an experimental artifact.

Table 4.1 Experimental and Calculated Principal Components of the Carbon Chemical Shift Tensors for Ethylene, $Pt(C_2H_4)(PPh_3)_2$ and Zeise's Salt.[a]

	δ_{11}	δ_{22}	δ_{33}	δ_{iso}[b]	Ω	κ	θ_{11}	θ_{22}	θ_{33}	α[c]
					Ethylene					
Exp[d]	234	120	24	126	210	-0.10	90.0	0.0	90.0	0
Calc	267	104	11	127	256	-0.27	90.0	0.0	90.0	0
					$Pt(C_2H_4)(PPh_3)_2$					
Exp[e]	65	44	10	39.7	55	0.23	42	52	75	0
Exp[e]	61	42	13	38.7	48	0.21	36	56	80	0
Calc	48	22	-3	22.3	51	0.00	81	15	78	0
Calc	47	19	-3	21.0	50	-0.12	86	18	73	2
					Zeise's Salt (anhydrous)					
Exp[e]	150	79	0	76	150	0.06	84	14	103	0
Calc[f]	159	78	-3	78	162	0.00	89	4	94	0
Calc[f]	153	80	-3	76.7	156	0.06	90	3	94	0
					Zeise's Salt (hydrate)					
Calc[f]	145	69	-6	69.3	151	0.00	90	4	94	0
Calc[f]	158	77	-5	76.7	163	0.01	89	5	94	0

a. Chemical shifts, relative to δ_{iso}(TMS) = 0, and the span, Ω, are in ppm.

b. δ_{iso} is not necessarily exactly equal to $⅓(\delta_{11} + \delta_{22} + \delta_{33})$ since the former is determined with greater accuracy from MAS NMR experiments.

c. The torsion angle between δ_{33} components of the spin pair, see text.

d. From reference 54. Uncertainties are ± 2.5 ppm.

e. This work. Uncertainties are estimated to be ± 5 ppm for the principal components of the CS tensor and ± 0.5 ppm for δ_{iso}. The θ_{ii} and α are in degrees, with an estimated uncertainty of ± 10°.

f. Non-equivalent carbon CS tensors were calculated.

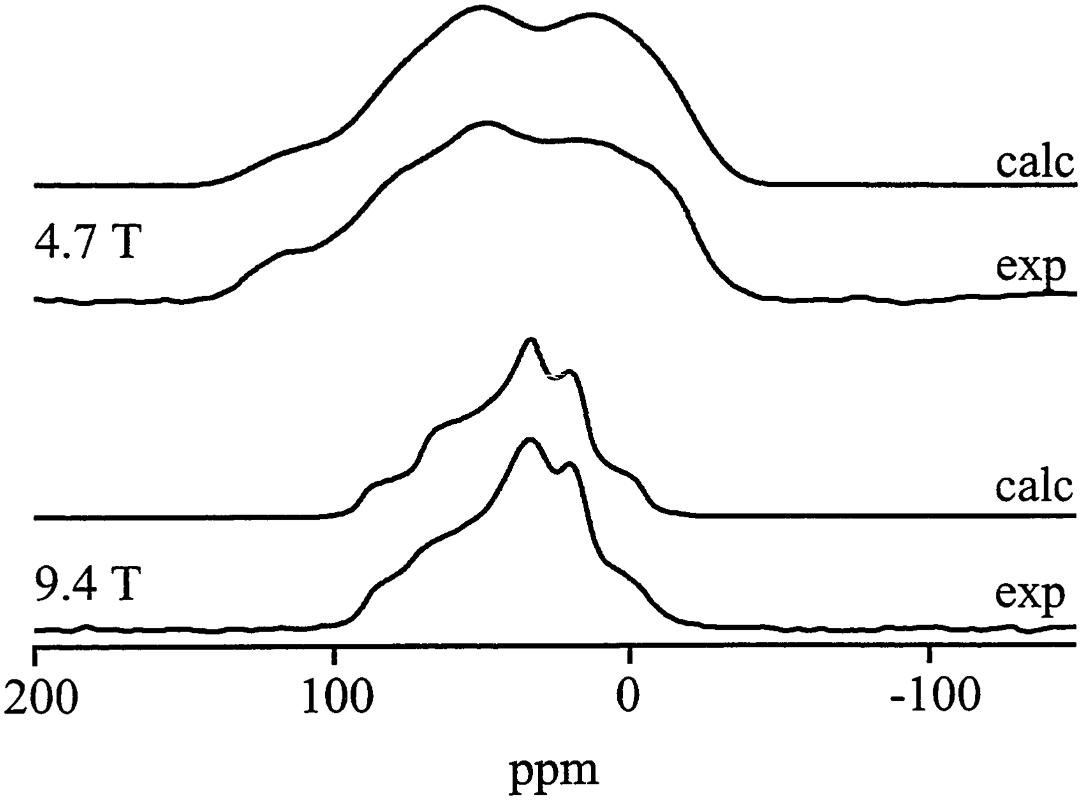

Figure 4.3 Calculated and experimental ^{13}C NMR spectra of stationary samples of $Pt(^{13}C_2H_4)(PPh_3)_2$. 276 and 174 transients were added for spectra acquired at 4.7 and 9.4 T, respectively.

attributed to the fact that $Pt(C_2H_4)(PPh_3)_2$ does not have a mirror plane in the solid state.[24] Since carbon shielding is sensitive to small differences in the local environment (*vide infra*) and the magnitudes of the principal components are comparable, small deviations from planarity can lead to significant changes to θ_{ii}.

The calculation of the alkenyl carbon CS tensors for $Pt(C_2H_4)(PPh_3)_2$ from first principles has been discussed in Section 3.5.2; for comparison, the parameters calculated with the cc-pVQZ basis set are summarized in Table 4.1. While the calculated values of θ_{33} are within error of the experimental values, the calculated values of θ_{11} and θ_{22} are significantly different from experimental values. Accurately calculating orientations for CS tensors with principal components that have similar magnitudes is particularly challenging. As well, it is important to recognize that the calculations are carried out on an isolated molecule while experimentally the molecule is subject to numerous intermolecular interactions.

As discussed above, the absence of a component perpendicular to the Pt,C,C plane is not surprising. One is tempted to assume that the δ_{33} components are in this general direction, since θ_{33} is close to 90°; however, results of *ab initio* calculations on $Pt(C_2H_4)(PMe_3)_2$ suggest that this component is actually in the Pt,C,C plane, oriented such that it is approximately perpendicular to the plane defined by the methylene group. This is consistent with earlier observations: δ_{33} is perpendicular to the molecular plane for all the alkenyl carbon CS tensors that have been reported.[55,163,264-266] Thus, based on the combined experimental/theoretical results, the orientation for δ_{33} is assigned as shown in Figure 4.4 A. The orientations for δ_{11} and δ_{22} follow from that of δ_{33} and the experimental values of θ_{11} and θ_{22}, as shown in Figure 4.4 B.

4.3.2 Carbon-13 NMR Spectra of $K[Pt(\eta^2\text{-}C_2H_4)Cl_3]$, Zeise's Salt

Carbon-13 NMR spectra of MAS samples of unlabelled and $^{13}C_2$-labelled samples of Zeise's salt are shown in Figures 4.5 A and B, respectively. The spectrum of the unlabelled sample is similar to that of the $^{13}C_2$-labelled sample except that the line shapes of the latter exhibit some spinning-frequency dependence. This is often observed in samples containing a spin pair with crystallographically equivalent but magnetically nonequivalent sites (Section

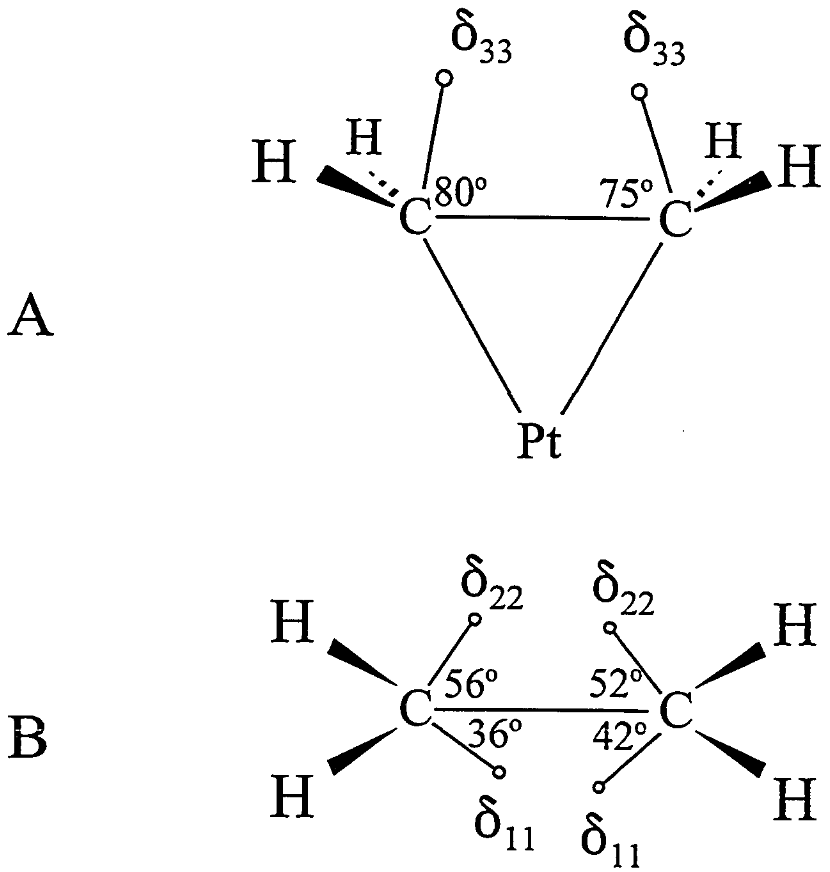

Figure 4.4 Orientation of the alkenyl carbon CS tensors for $Pt(C_2H_4)(PPh_3)_2$. In (A), the δ_{33} components are shown with the molecule oriented such that the platinum and alkenyl carbon atoms are in the plane of the page. The remaining components are shown in (B), with the Pt,C,C plane perpendicular to the page. Note that δ_{11} and δ_{22} are not exactly in the plane of the page. The angles formed by the tensor components relative to r_{CC} are indicated.

2.4.2).[133] The half-height line width of the isotropic peak of the unlabelled MAS sample is approximately 250 Hz. The fact that these peaks are broader than expected (for example, they are as broad as that observed for the crystallographically distinct sites of the spectra of MAS samples of $Pt(C_2H_4)(PPh_3)_2$) suggests that there are contributions to the observed line

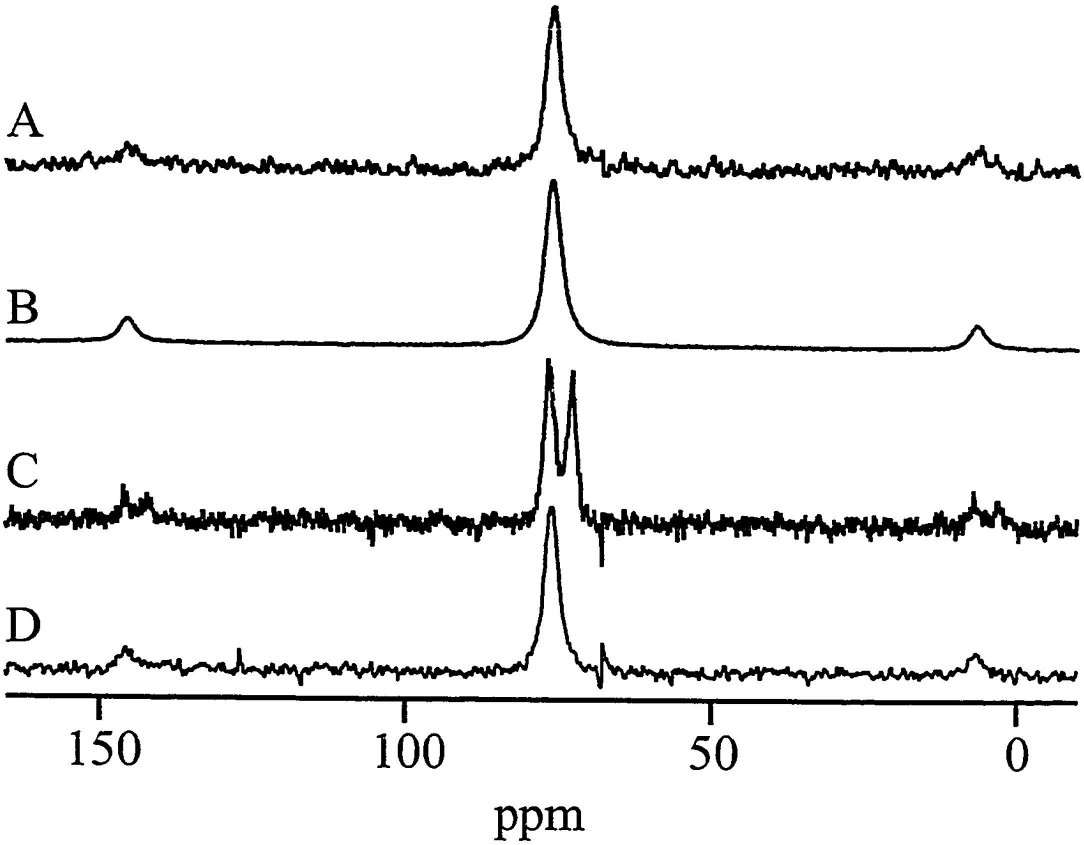

Figure 4.5 Carbon-13 NMR spectra of MAS samples of Zeise's salt: that of a locally prepared sample at natural abundance (A), that of the $^{13}C_2$-labelled sample (B) and those of a commercial sample before (C) and after (D) dehydration. Spectra were acquired at 9.4 T with ν_{rot} = 7 kHz; 104 (A), 64 (B), and 72 transients for both (C) and (D) were added.

shapes from the dipolar interactions with the chlorine atoms, which are not completely averaged by MAS.[267,268] For the $^{13}C_2$-labelled samples, $\nu_{1/2} \approx 700$ Hz at $B_0 = 9.4$ T and ν_{rot} = 3 kHz; at ν_{rot} = 12 kHz, the line width is comparable to that observed for the unlabelled sample. The line widths observed for spectra of MAS samples acquired at 4.7 T are similar to those observed at twice the spinning frequency at 9.4 T, as expected (Section 2.4.2). Considering the line widths for these samples, it is not surprising that $^1J(^{195}Pt,^{13}C)$, approximately 195 Hz in solution NMR studies,[38,43,44] is not observed in solid-state NMR spectra.

There are two striking differences between the spectra of the MAS samples shown here (Figure 4.5 A and B), and those reported by Huang *et al.*[60] The latter observed two isotropic peaks for the ^{13}C NMR spectrum of an unlabelled sample, attributed to nonequivalent carbon sites, and the values of δ_{iso} for these two peaks (63 and 61 ppm) are approximately 14 ppm to low frequency of the single peak, $\delta_{iso} = 76$ ppm, observed in the spectrum shown in Figures 4.5 A and B. Zeise's salt is known to crystallize in a hydrate form (space group $P2_1/c$, $Z = 4$, density = 2.94 g cm^{-3})[27,269] and in an anhydrous form (space group $Pmab$, $Z = 4$, density = 3.129 g cm^{-3}).[242] Suspecting that the two peaks observed by Huang *et al.* are separate peaks from each of the two crystal forms, a sample of Zeise's salt was obtained from the same supplier; the ^{13}C NMR spectrum of this sample is shown in Figure 4.5 C. Two isotropic peaks separated by 2 ppm are observed, as reported by Huang *et al.*, but the spectrum is shifted to higher frequencies, $\delta_{iso} = 74$ and 76 ppm; the high frequency peak corresponds to the position of the single peak observed for samples prepared in this laboratory (Figure 4.5 A and B). This experiment has been repeated several times; a value of $\delta_{iso} = 76$ ppm is consistently observed. Oldfield and coworkers[58] also reported a value of $\delta_{iso} = 76$ ppm for Zeise's salt; it is not clear if their value is for a single peak or the average of two peaks. The ^{13}C NMR spectrum of the commercial sample following dehydration is shown in Figure 4.5 D. A single peak remains, at the same frequency as that observed for the locally-prepared samples. The two peaks observed for the sample before dehydration may arise from separate peaks for the hydrate and anhydrous forms present in the sample or from two peaks for nonequivalent carbon nuclei of a sample that is predominantly the hydrate form.

Summarizing, the ^{13}C NMR spectrum of the anhydrous form of Zeise's salt contains a single peak at δ_{iso} = 76 ppm. The isotropic chemical shifts reported by Huang *et al.*[60] are at significantly lower frequencies than those measured in this lab and by Oldfield and coworkers.[58] Finally, it is noted that Huang and coworkers reported a value of δ_{iso} = 76 ppm for the alkenyl carbon nuclei of Zeise's dimer.

The carbon magnetic shielding was calculated from first principles using the reported structures for the hydrate[27,269] and anhydrous[242] forms of Zeise's salt to determine whether different chemical shifts are predicted. The results of these calculations are summarized in Table 4.1. These results are qualitatively in agreement with experiment: calculations predict a small isotropic chemical shift difference for the two carbon nuclei of the anhydrous form and a much larger difference for the two peaks of the hydrate form.

Figure 4.6 illustrates the ^{13}C NMR spectrum of a stationary sample of Zeise's salt at natural abundance. Although it was not possible to obtain a spectrum with a high signal-to-noise ratio, reasonable estimates of the magnitudes of the CS tensor components are possible from this spectrum. Principal components obtained from a visual inspection of this spectrum were used as initial parameters in the fit of the spectra of the $^{13}C_2$-labelled samples (*vide infra*). The calculated spectrum illustrated here is that obtained with parameters that gave the best fit for all ^{13}C NMR spectra of this sample. The experimental spectrum (Fig. 4.6) contains an extra peak at approximately 126 ppm. Since the spectrum of an isolated spin is defined solely by the magnetic shielding interaction, this peak must be an impurity, perhaps ethylene, which has an isotropic chemical shift of 126 ppm.[55]

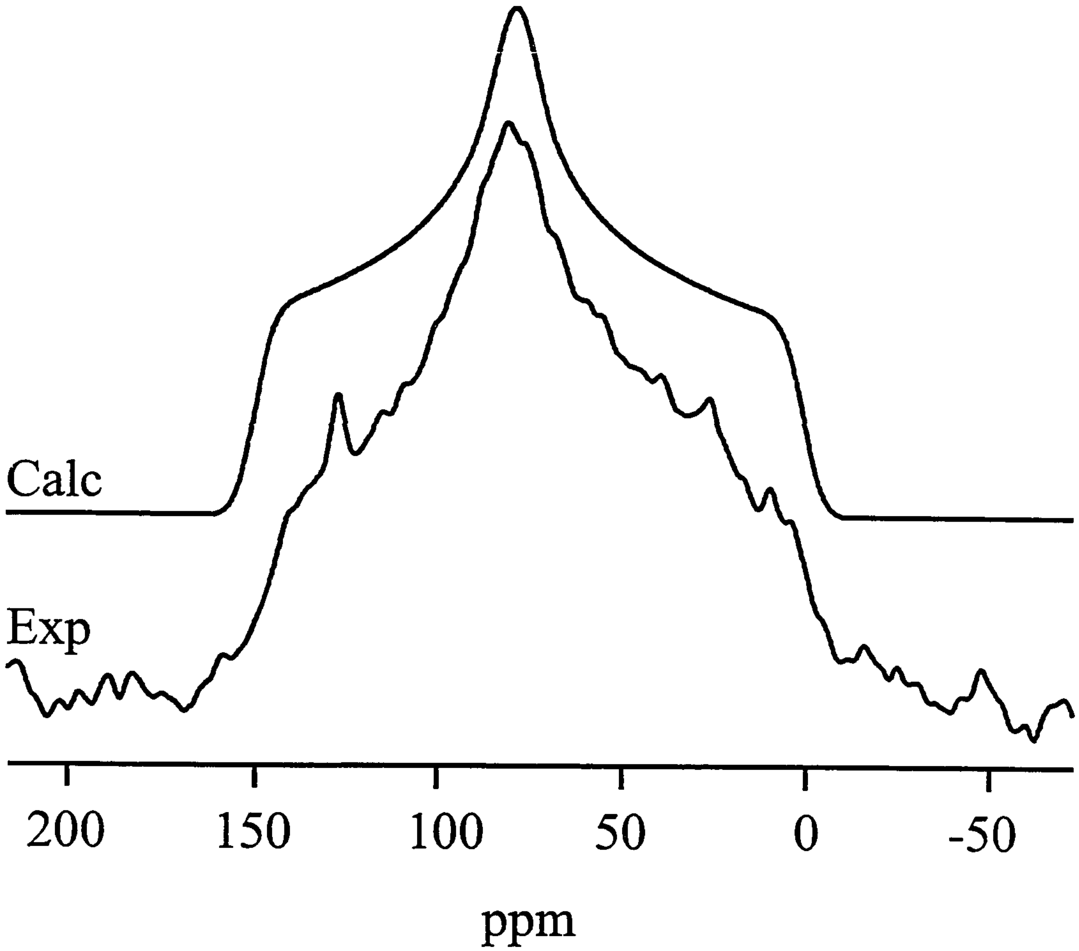

Figure 4.6 Calculated (upper trace) and experimental ^{13}C NMR spectra of a stationary sample of Zeise's salt at natural abundance, acquired at 9.4 T; 642 transients were added.

The two-dimensional ^{13}C spin-echo NMR spectrum of Zeise's salt-$^{13}C_2$ is shown in Figure 4.7. Although the centre of the *F*1 projection is dominated by an experimental artifact, the "horns" arising from $R_{\text{eff}}(^{13}C,^{13}C)$ are well resolved. The positions of these peaks are very sensitive to the magnitude of $R_{\text{eff}}(^{13}C,^{13}C)$, but insensitive to CS tensor parameters, allowing an accurate determination of this value. The fit of the *F*1 projection, shown at the bottom of Figure 4.7, was achieved with $R_{\text{eff}}(^{13}C,^{13}C) = 2575 \pm 100$

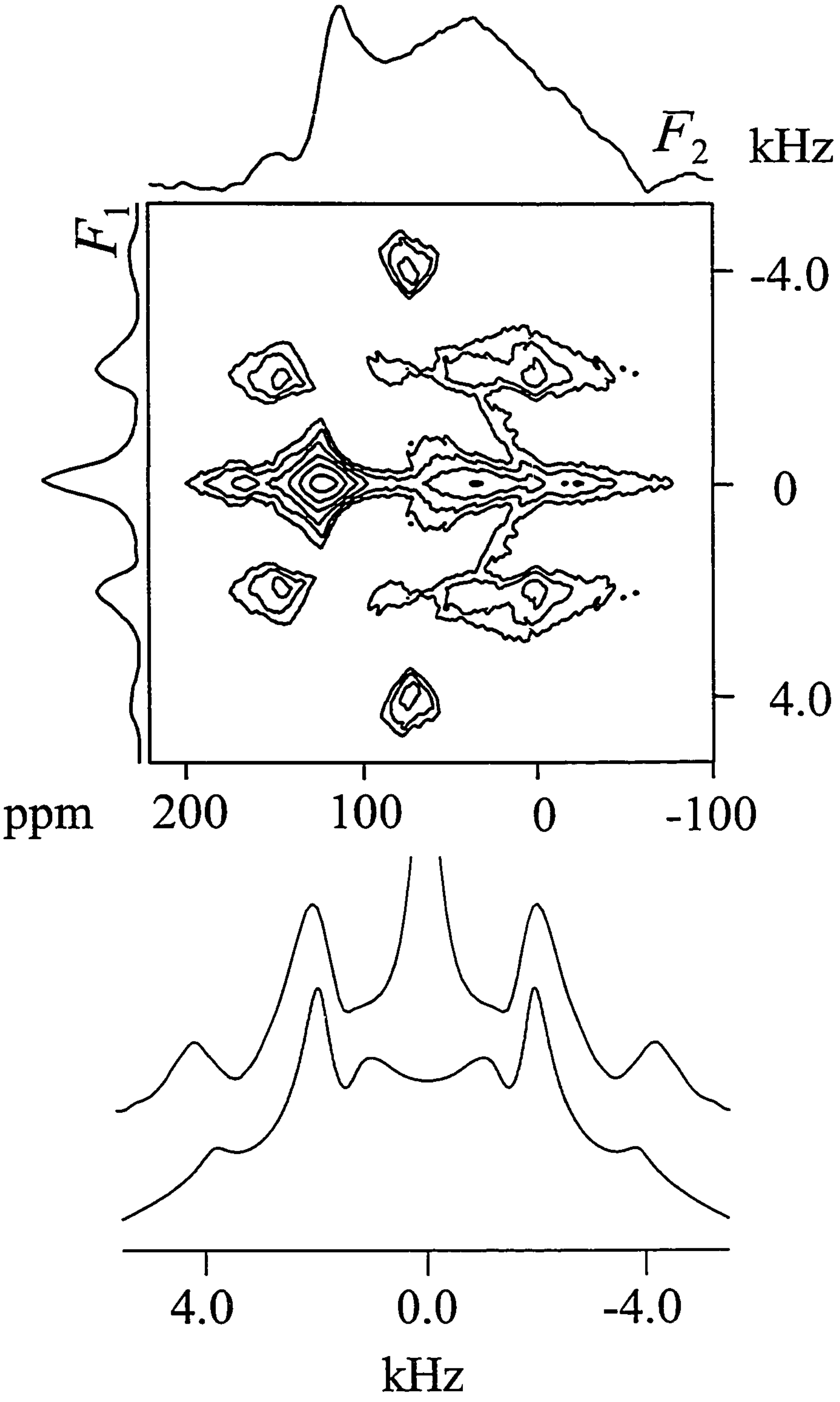

Figure 4.7 Two-dimensional ^{13}C spin-echo NMR spectrum of Zeise's salt-$^{13}C_2$ acquired at 9.4 T; 32 transients were added for each of 64 τ_1 increments. At the bottom, the experimental (upper trace) and calculated (lower trace) *F*1 projections are shown. The central peak is an experimental artifact.

Hz; the uncertainty here is based on the spectral resolution of 187.5 Hz/point in the *F*1 dimension. The value of $R_{eff}(^{13}C,^{13}C)$ is less than the value predicted from the C,C bond length of 1.37 ± 0.09 Å,[242] 2950 ± 500 Hz (eq 2.15). Factors that might contribute to the reduced experimental value include vibrational motion of the C,C bond[107] and small amplitude torsional oscillations of the C,C bond (*vide infra*).[55]

The shoulders of the *F*1 projection at ±4.0 kHz are not as well reproduced. Before considering this, it is useful to review the information available from the ^{13}C NMR experiments discussed above and the insight provided by the symmetry of the molecule. The observation of a single isotropic peak in spectra of MAS samples indicates that the two ^{13}C nuclei are crystallographically equivalent and hence will have the same principal components—these are known from the spectrum of the natural abundance sample (Figure 4.6). The two CS tensors have the same symmetry relation as the carbon nuclei, C_2. This fixes the angle α, which defines the relative orientation of the two CS tensors, to 0°. With a known $R_{eff}(^{13}C,^{13}C)$, the only undetermined parameters are the Euler angles β and γ. The shoulders of the calculated *F*1 projection are very sensitive to γ and virtually insensitive to changes in the other CS tensor parameters. Since the one-dimensional spectra, discussed below, are also sensitive to this parameter, the parameters used to calculate the *F*1 projection are those that give the best fit to the latter, which have a much higher digital resolution. The discrepancy is thought to arise from the low digital resolution of the *F*1 projection. Complications may also arise from contributions to the experimental spectrum from the other magnetically active nuclei of the molecule ($^{35/37}Cl$, $I = 3/2$, natural abundance = 75.77 and 24.23 %, respectively, and ^{195}Pt). It is noted that even in cases where all parameters are known from a single-crystal experiment, minor features of the *F*1 projection are not calculated exactly.[103]

Carbon-13 NMR spectra of a stationary ^{13}C-labelled sample of Zeise's salt, with the corresponding calculated spectra, are shown in Fig. 4.8; the CS tensor parameters derived from the simulation are summarized in Table 4.1. The spectra exhibit features characteristic of dipolar-coupled *AB* spin systems. Spectral features are broadened, a consequence of the direct dipolar interactions with other magnetic nuclei of Zeise's salt, $^{35/37}$Cl and ^{195}Pt. For

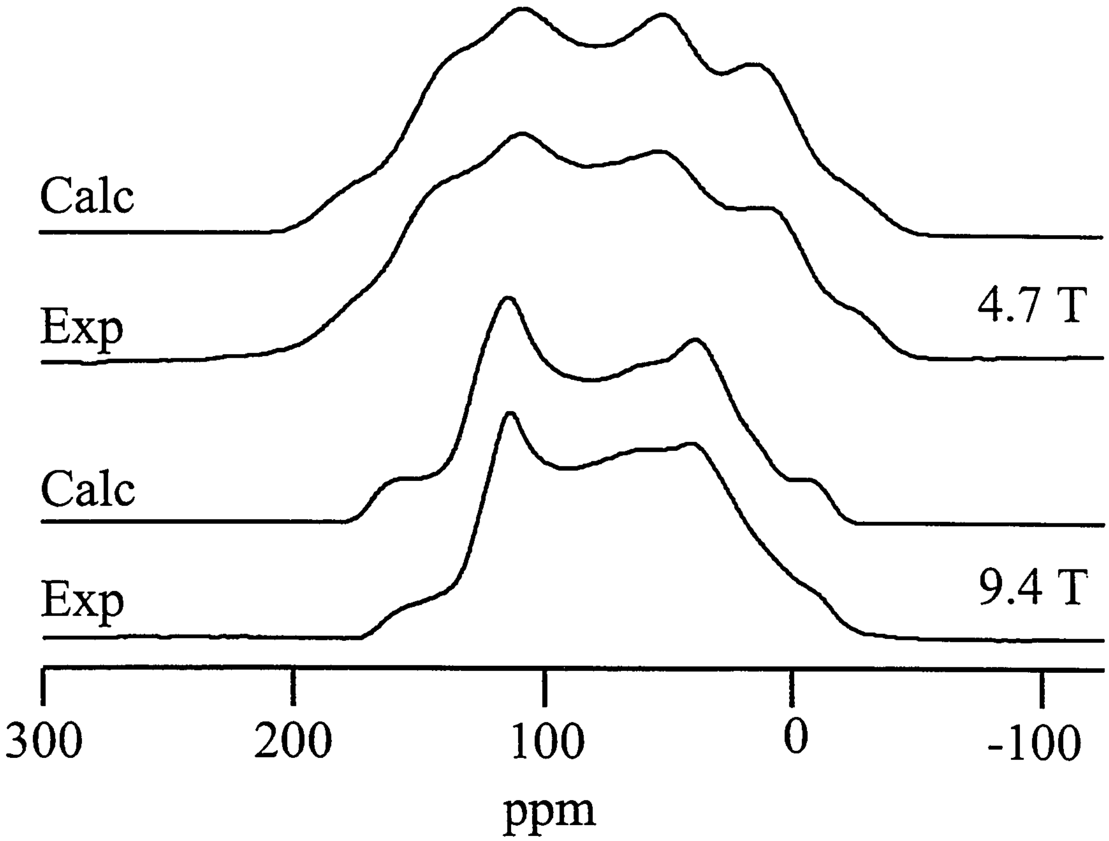

Figure 4.8 Calculated and experimental ^{13}C NMR spectra of a stationary ^{13}C$_2$-labelled sample of Zeise's salt, acquired at 4.7 and 9.4 T; 352 and 302 transients, respectively, were added.

example, based on $r_{Pt,C} = 2.14$ Å,[248] $R_{DD}(^{195}Pt,^{13}C) \approx 670$ Hz. This is expected to produce significant broadening to the base of the spectra. The effect is less evident in the spectrum acquired at 9.4 T because the anisotropy in the shielding is relatively larger (in frequency units).

The orientation of the principal components of the carbon CS tensors calculated from first principles are summarized in Table 4.1. Agreement between calculated and experimental values is good; hence, orientations for the carbon CS tensors are proposed based on combined experimental/theoretical results, as shown in Figure 4.9. Comparison of the carbon CS tensor orientations for Zeise's salt with those for ethylene (Fig. 1.6) demonstrates that coordination with Pt(II) has a minimal effect on the CS tensor orientation: δ_{11} is unchanged while the other components are oriented such that δ_{33} is approximately in the direction of the platinum atom.

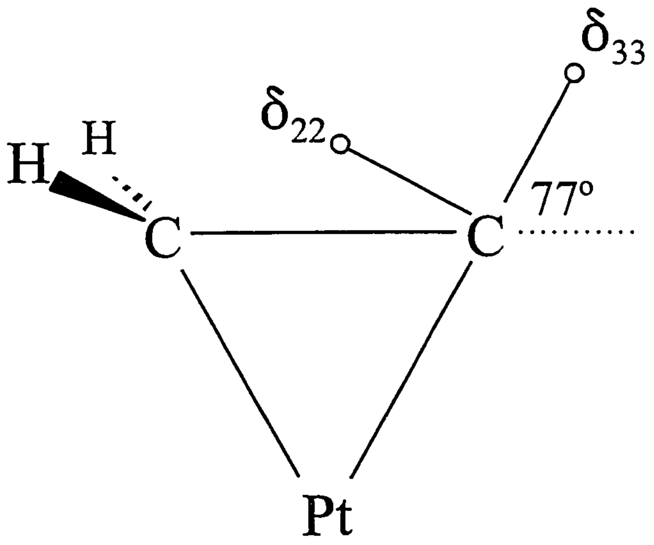

Figure 4.9 Orientation of the carbon CS tensor for Zeise's salt; δ_{11} is perpendicular to the page.

The magnitudes of the principal components (Table 4.1) are similar to those reported by Oldfield *et al.*[58] The authors also reported orientations for the CS tensor components calculated with DFT; these are comparable to those reported here. Ding and McDowell have reported the anisotropy, asymmetry and orientation of the carbon CS tensor for Zeise's salt.[61] Unfortunately it is not possible to compare the results presented here with those of Ding and McDowell, since they do not report the chemical shifts or explain how the reported parameters are defined.

4.3.3 Comparison of the Alkenyl Carbon Chemical Shift Tensors for $Pt(\eta^2-C_2H_4)(PPh_3)_2$ and Zeise's Salt

The effect on the principal components of the carbon CS tensors of coordinating ethylene with Pt(0) and Pt(II) is shown graphically in Figure 4.10. For comparison, the carbon CS tensor components of ethane[192] are included. The magnitudes of δ_{11} and δ_{22} decrease significantly; δ_{11} for $Pt(C_2H_4)(PPh_3)_2$ is most affected, being shielded by 169 ppm compared to δ_{11} for ethylene. In contrast, δ_{33} is relatively insensitive to coordination. The orientations of the three principal components of the carbon CS tensor for Zeise's salt (Figure 4.9) as well as that of δ_{33} for $Pt(C_2H_4)(PPh_3)_2$ (Figure 4.4 B) are similar to those for uncoordinated ethylene (Figure 1.6); the orientations of δ_{11} and δ_{22} for $Pt(C_2H_4)(PPh_3)_2$ (Figure 4.4 C) are significantly different from those for ethylene. Considering the small chemical shift difference between δ_{11} and δ_{22}, approximately 20 ppm, the different orientations for these components does not indicate a large change in the magnetic shielding properties of the alkenyl carbon nuclei of $Pt(C_2H_4)(PPh_3)_2$.

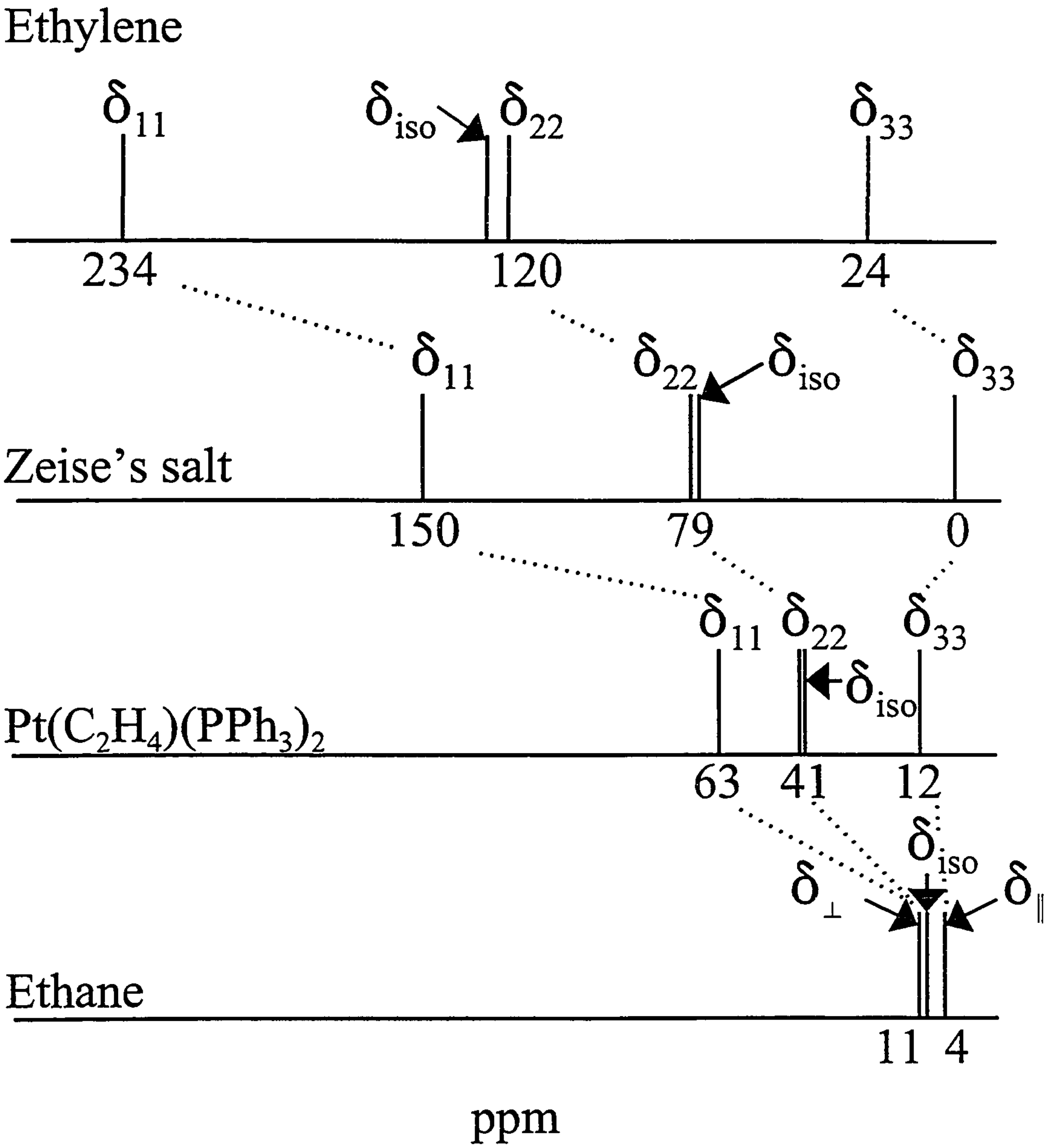
Ethylene
δ11
δiso
δ22
δ33
234
120
24
δ11
δ22
δiso
δ33
Zeise's salt
150
79
0
δ11
δ22
δ33
δiso
Pt(C2H4)(PPh3)2
63
41
12
δiso
δ⊥
δ∥
Ethane
11
4
ppm

Figure 4.10 Comparison of the principal components of the carbon CS tensors for ethylene, ethane and the platinum-ethylene complexes. The average values for the non-equivalent alkenyl carbon nuclei of $Pt(C_2H_4)(PPh_3)_2$ are shown.

A qualitative explanation for the effects of metal coordination on alkenyl carbon magnetic shielding has been presented in Section 3.5.2. In light of the ensuing discussion on the dynamics of the ethylene ligand in these complexes, it may be assumed that the carbon CS tensors for these compounds are not subject to the effects of motional averaging.

4.3.4 The Internal Dynamics of the Ethylene Moiety of $Pt(\eta^2\text{-}C_2H_4)(PPh_3)_2$ and Zeise's Salt

Deuterium NMR. The calculated and experimental ^2H NMR spectra of stationary samples of $Pt(C_2{}^2H_4)(PPh_3)_2$ and Zeise's salt-$^2H_4$ are shown in Figure 4.11. The ^2H magnetization is slow to relax (*vide infra*), particularly for $Pt(C_2{}^2H_4)(PPh_3)_2$ which requires a 1.5 hour recycle delay between excitation pulses. The spectrum of this compound (upper trace) was acquired with only 80 transients and hence the shoulders are not resolved. Despite the lower signal-to-noise ratio, the ^2H quadrupolar parameters may be determined from the "horns" of the Pake doublet. The ^2H relaxation time for Zeise's salt also is long, but the line shape is clearly resolved (lower trace). The ^2H quadrupolar parameters derived from the simulations are summarized in Table 4.2. The parameters for the platinum-ethylene complexes are similar to those reported for ethane-$^2H_6$[270] and ethylene-$^2H_1$[271] also listed in Table 4.2. The latter ^2H quadrupolar parameters are those expected in the absence of motional averaging. *Ab initio* calculation of the EFG tensors for ethylene and Zeise's salt suggest that the quadrupolar parameters for the two compounds, summarized in Table 4.2, are virtually identical.

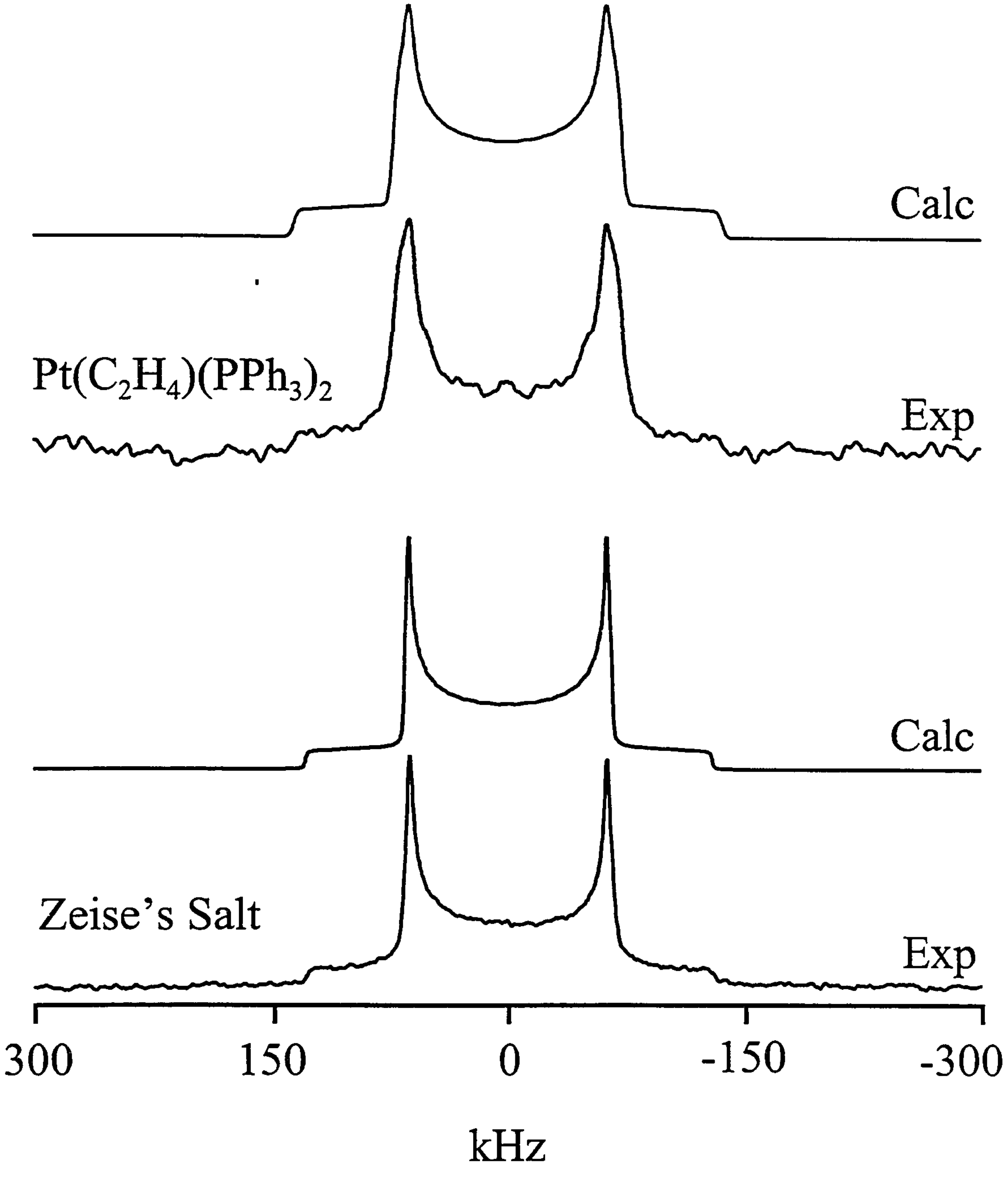

Figure 4.11 Calculated and experimental ^2H NMR spectra of stationary samples of $Pt(C_2{}^2H_4)(PPh_3)_2$ and Zeise's salt-$^2H_4$, acquired at 9.4 T; 80 and 49 transients, respectively, were added.

Table 4.2 Deuterium NMR Parameters for Ethane, Ethylene, $Pt(C_2H_4)(PPh_3)_2$ and Zeise's Salt.[a]

	C_Q/kHz	η	Reference
Ethane	163(3)	0	270
Ethylene (Exp)	175.3(13)	0.039(1)	271
Ethylene (Calc)	196.2	0.051	This work
$Pt(C_2H_4)(PPh_3)_2$	181(4)	0.075(20)	This work
Zeise's salt (Exp)	172(2)	0.025(20)	This work
Zeise's salt (Calc)[b]	205.3	0.021	This work

a. Measured at room temperature. Uncertainties in the last digits are given in parentheses.

b. Calculations were performed on the anion of Zeise's salt.

The ^2H NMR parameters for the platinum-ethylene complexes are similar to those expected for the ligand in the absence of motion, demonstrating that the ethylene ligands in these complexes are not undergoing large-amplitude motion. The observed ^2H NMR spectra (Figure 4.11) do not preclude small amplitude motions of the ethylene ligand;[160] the long recycle delays required for these experiments indicate long ^2H T_1s. Hence, if there is small amplitude motion of the ethylene ligand, it is ineffective in causing relaxation.[272] It would have been instructive to measure T_1 via the inversion recovery experiment: this is impractical given the very long recycle delays.

A Computational Study of the Internal Dynamics. Figure 4.12 illustrates the barrier to internal rotation for the ethylene ligand in Zeise's salt, calculated at the MP2/6-31G* level. The large barrier, 93 kJ mol^{-1}, suggests that the ethylene ligand does not

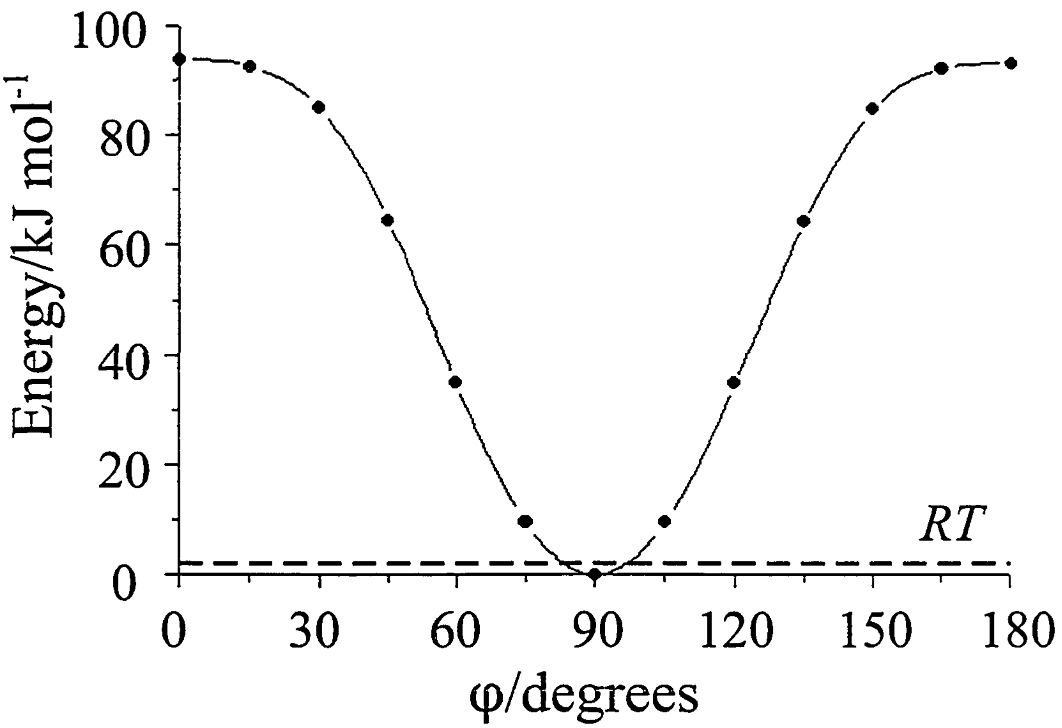

Figure 4.12 Calculated barrier to internal rotation for the ethylene ligand of Zeise's salt. The angle formed by the C,C bond with the $PtCl_3$ plane is defined by φ. The dashed line corresponds to *RT* at 300 K; the solid curve is a fit to the calculated points.

rotate, in agreement with experimental results. If a Boltzmann distribution of orientations for the ethylene ligand is assumed, there is a low probability that the ethylene ligand will deviate from its most stable conformation by more than an energy difference of *RT*, where *R* is the gas constant and *T* is the temperature. The dashed line in Figure 4.12 indicates this value for 300 K; the ethylene may be expected to fluctuate about the minimum, but not to orientations that place the energy of the compound significantly above the dashed line. Clearly, large amplitude motion is not expected, although motion of ± 10° is allowed with this model. These results must be considered in light of the necessary approximations of this model. In particular, these calculations are for an isolated molecule and hence do not consider intermolecular effects, which might further restrict the motion of the ethylene. Single-point RHF/6-31G* calculations on $Pt(C_2H_4)(PPh_3)_2$, with the ethylene oriented in or perpendicular to the plane defined by the platinum and the two phosphorus atoms, accurately predict that the planar conformation of the ethylene is favored, with an 85 kJ mol^{-1} difference between the two conformers. In an early computational study on isolated molecules using the extended Hückel method, Hoffman and coworkers predicted a barrier to internal rotation of approximately 80 kJ mol^{-1} for the ethylene ligand in Zeise's salt, a value only slightly lower than that predicted for $Pt(C_2H_4)(PPh_3)_2$.[273] A recent study of $Pt(C_2H_4)(PPh_3)_2$ using DFT predicted a large barrier to internal motion for the ethylene ligand, 149 kJ mol^{-1}; the favored conformation places the ethylene in the plane defined by the platinum and phosphorus atoms.[274] Calculations by Ziegler and coworkers have shown that relativistic effects are an important factor in the Pt-ethylene bonding of this complex.[70]

If motion of the ethylene ligand is assumed to be about a cone as illustrated in Figure 4.13, the angle φ defining the magnitude of the motion can be estimated using a model proposed by Zilm and Grant:[55]

$$r_{\mathrm{eff}}^3 = \frac{1}{2}(3\cos^2 - 1)r_{\mathrm{diffrac}}^3 \qquad 4.1$$

where r_{diffrac} is the value of r_{CC} determined by diffraction techniques and r_{eff} is that predicted from R_{eff} according to eq 2.15. From the experimental values of R_{eff} and r_{diffrac} discussed above, and ignoring any other motion, φ can have values ranging from 0 to 17°. However, in light of the ^{2}H NMR and computational study, discussed above, the amplitude of the motion is thought to be small. For $Pt(C_2H_4)(PPh_3)_2$, the measured value of $R(^{13}C,^{13}C)$ is close to that expected from the value of r_{CC} determined by X-ray crystallography,[24] consistent with the conclusion that the ethylene ligand is rigid in this complex.

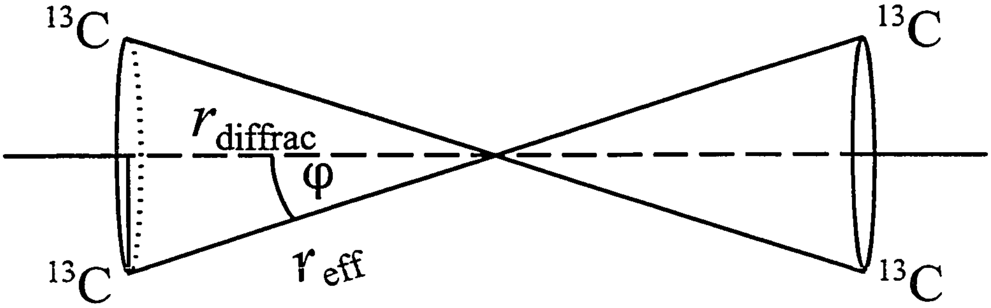

Figure 4.13 Possible librational motion of the ethylene ligand of Zeise's salt.

The investigation of the internal dynamics of the ethylene ligand of $Pt(C_2H_4)(PPh_3)_2$ confirms previous observations that this ligand is not subject to significant motion at 300 K. The ^{2}H NMR study indicates that the ethylene ligand for Zeise's salt does not undergo large amplitude motion, a conclusion that is supported by *ab initio* calculations.

4.4 Summary

The carbon chemical shift tensors for $Pt(C_2H_4)(PPh_3)_2$ and Zeise's salt have been characterized by solid-state NMR. The magnitudes of the δ_{11} and δ_{22} components of the carbon CS tensors for ethylene are very sensitive to coordination with platinum, decreasing significantly, but the δ_{33} components are virtually unaffected. The CS tensors are particularly sensitive to coordination of ethylene with Pt(0), but coordination with Pt(II) also leads to significant changes in the CS tensors. These observations have been rationalized in terms of Ramsey's theory of nuclear magnetic shielding and the structural modifications that occur upon coordination with Pt(0) and Pt(II). Agreement between theoretical and experimental carbon chemical shift tensors is generally good. Hence, orientations for the CS tensors in the molecular framework have been proposed on the basis of the experimental/theoretical results.

A ^{2}H NMR study of the ethylene-$^2H_4$ derivatives of $Pt(C_2H_4)(PPh_3)_2$ and Zeise's salt demonstrates that the ethylene ligands in these complexes are not subject to significant motion in the solid state at 300 K. This conclusion is supported by *ab initio* calculations of the barrier to internal rotation of the ethylene. Hence, the carbon chemical shift tensors reported herein are those expected in the absence of motional averaging.

Chapter 5

An Experimental and Theoretical Solid-State Carbon-13 NMR Investigation of *trans*-Stilbene and Pt(η^2-*trans*-stilbene)(PPh$_3$)$_2$

5.1 Introduction

The characterization of the alkenyl carbon chemical shift tensors for a substituted-alkene coordinated with a metal can offer valuable insights into magnetic shielding properties. Since the alkenyl carbon CS tensor for the Pt(0)-ethylene complex has been characterized as part of this thesis (Chapter 4), a substituted-ethylene complex, Pt(η^2-*trans*-stilbene)(PPh$_3$)$_2$, PtTSB, was investigated. The structure of PtTSB is illustrated in Figure 5.1. By preparing samples in which the alkenyl carbon atoms are $^{13}C_2$-labelled, it was possible to determine the principal components of the alkenyl carbon CS tensors as well as their orientations relative to the alkenyl C,C bond. Orientations for the CS tensors in the molecular framework are proposed, based on the results of calculations from first principles. To complement this study, the alkenyl carbon CS tensors for *trans*-stilbene (TSB) were also investigated. The structure of TSB is also illustrated in Figure 5.1.

5.2 Experimental

Trans-stilbene-α,β-$^{13}C_2$ (99.5% ^{13}C) was obtained from MSD Isotopes (Montreal) and used without further purification. Pt(η^2-*trans*-stilbene-α,β-$^{13}C_2$)(PPh$_3$)$_2$ was prepared from *trans*-stilbene-α,β-$^{13}C_2$ by Devon Latimer according to a procedure described in the literature.[275] The product is a fine, dull grey, crystalline powder. Preliminary work on this

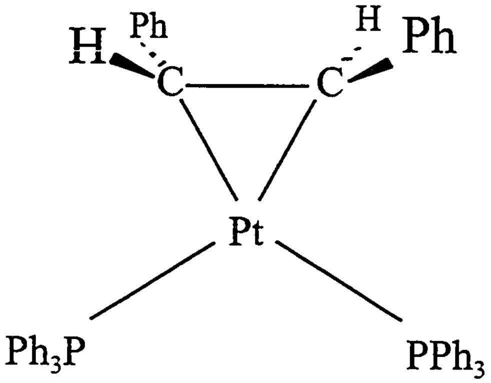

PtTSB

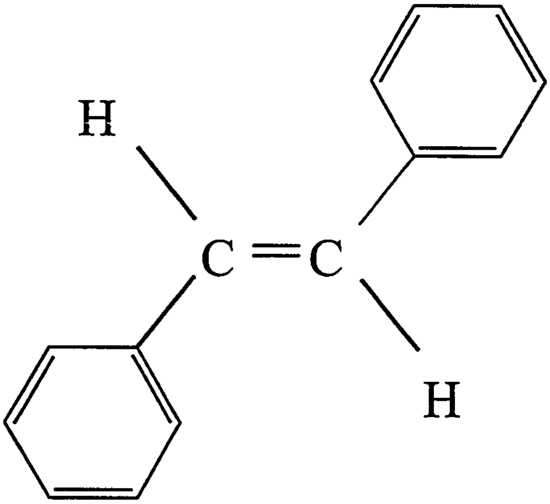

TSB

Figure 5.1 Structures of Pt(η^2-*trans*-stilbene)(PPh$_3$)$_2$ (PtTSB) and *trans*-stilbene (TSB). The former is based on the reported structure for Pt(η^2-4,4'-dinitro-*trans*-stilbene)(PPh$_3$)$_2$.[245]

project was done by Dr. Gang Wu.

The acquisition of solid-state ^{13}C NMR spectra has been described in Section 2.7. Spectra were obtained on Bruker MSL-200 (B_0 = 4.7 T) and AMX-400 (B_0 = 9.4 T) NMR spectrometers. Cross polarization under the Hartmann-Hahn match condition, with contact times of 5 ms, high-power proton decoupling, with ^{1}H 90° pulses of 2.8 - 3.8 μs, and recycle times of 100 - 120 s were used in acquiring all ^{13}C NMR spectra. Carbon-13 NMR spectra of MAS samples were calculated using the program NMRLAB.[142] This program, mounted on an SGI Indy workstation, performed a powder averaging by sampling 10000 crystal orientations according to the Monte Carlo method. Calculation of chemical shift tensors from first principles has been summarized in Chapter 3.

5.3 Results and Discussion

5.3.1 Solid-State Carbon-13 NMR Spectra of *trans*-Stilbene

Carbon-13 NMR spectra of $^{13}C_2$-labelled MAS samples of TSB are shown in Fig. 5.2. The isotropic chemical shift, 128.0 ± 0.5 ppm, is typical of alkenyl carbon nuclei[34,53] and is in agreement with the results observed for this compound in solution.[45] The structure of TSB shows that the monoclinic crystals (space group $P2_1/c$, $Z = 4$, density = 1.160 g cm^{-3}) consist of two crystallographically distinct molecules lying at approximate inversion centres of the unit cell, one of which exhibits orientational disorder.[33,276,277] The molecules at the disordered site are related by an approximate 2-fold rotation about an axis joining the *para* carbon atoms of the phenyl groups (Figure 5.3). Hoekstra and coworkers found almost no indication of disorder in their diffraction study of TSB at 113 K.[278] Crystallographically distinct nuclei are

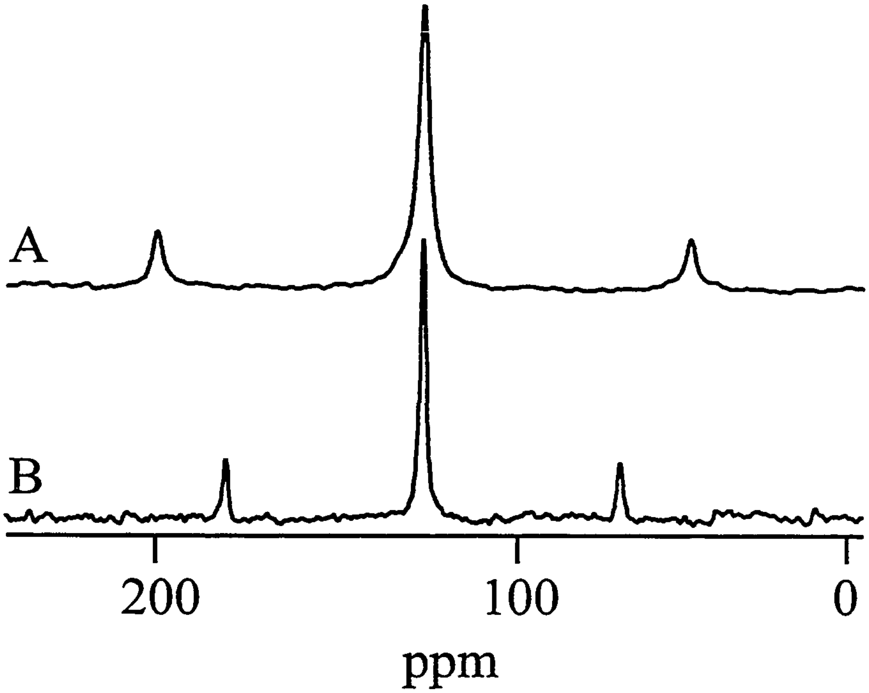

Figure 5.2 Carbon-13 NMR spectra of MAS samples of *trans*-stilbene-α,β-$^{13}C_2$ at (A) ν_{rot} = 4 kHz and B_0 = 4.7 T and (B) ν_{rot} = 6 kHz and B_0 = 9.4 T; 64 transients for (A) and 1 transient for (B) were added.

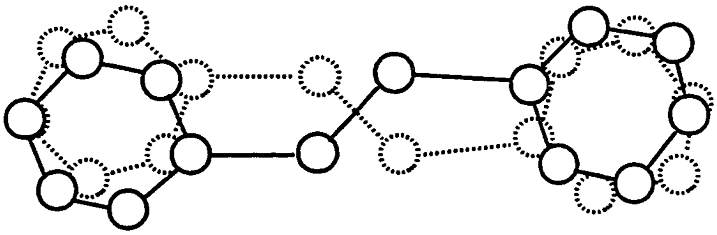

Figure 5.3 Orientational disorder at one of the sites in the reported crystal structure of *trans*-stilbene. One of the molecules is shown with complete lines, the other with dotted lines. For clarity, the hydrogen atoms have been omitted. From reference 33.

not resolved in the ^{13}C NMR spectra of MAS samples of TSB acquired at 9.4 and 4.7 T.

Simulated and experimental ^{13}C NMR spectra of stationary samples of TSB are shown in Figure 5.4. The data derived from the simulation are summarized in Table 5.1. The alkenyl ^{13}C nuclei in each of the two molecules of the unit cell of *trans*-stilbene are related by a centre of inversion,[33] constituting A_2 spin systems. Since the two crystallographically distinct molecules have, within error, identical isotropic carbon chemical shifts, the spectra consist of two subspectra, as expected for an A_2 spin-system (see Appendix A.1 for a detailed discussion of the solid-state NMR spectra of A_2 spin systems).

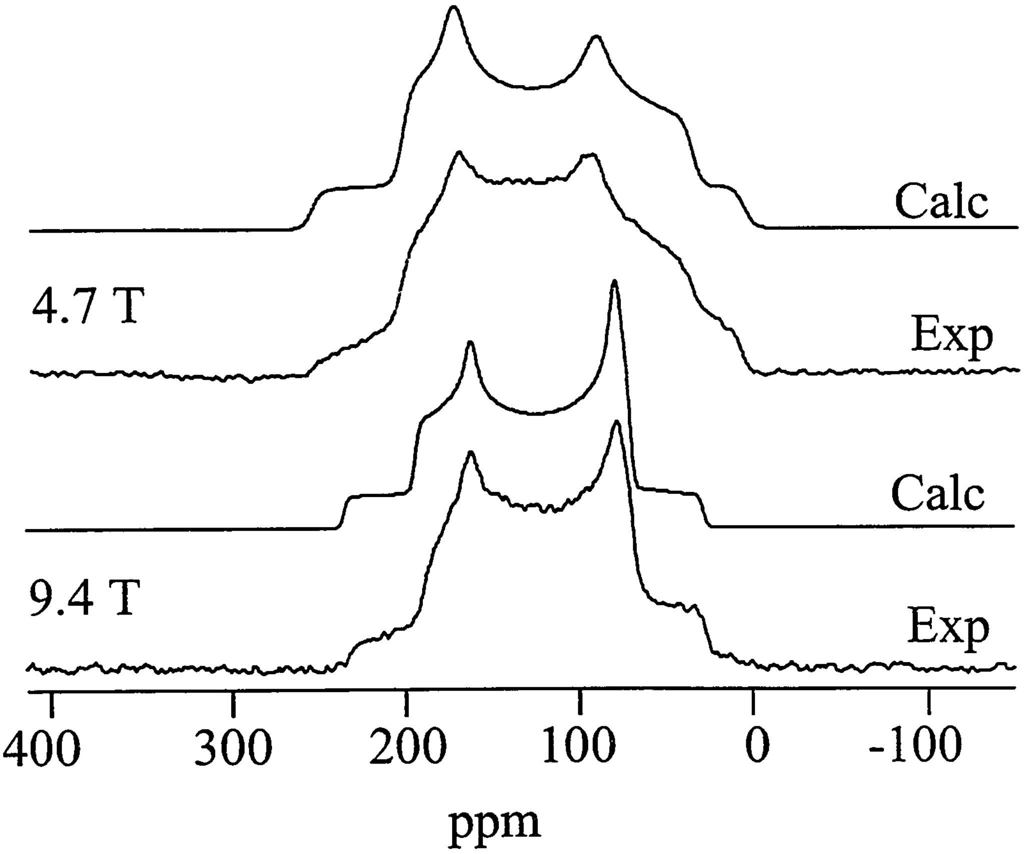

Figure 5.4 Calculated and experimental ^{13}C NMR spectra of a stationary sample of *trans*-stilbene-α,β-$^{13}C_2$ at B_0 = 4.7 and 9.4 T; 566 and 802 transients, respectively, were added for the spectra acquired at 4.7 and 9.4 T.

Table 5.1 Calculated and Experimental Alkenyl Carbon Chemical Shift Tensor Principal Components for *trans*-Stilbene and Pt(η^2-*trans*-Stilbene)(PPh$_3$)$_2$.[a,b]

	δ_{11}	δ_{22}	δ_{33}	δ_{iso}	Ω	κ	θ_{11}	θ_{22}	θ_{33}	α
					***trans*-stilbene**					
Exp[c]	215	120	49	128	166	-0.14	85	5	90	0
Calc[d]	235	104	36	125	199	-0.32	88	3	88	0
					Pt(η^2-*trans*-stilbene)(PPh$_3$)$_2$					
Exp[c]	92	71	41	68	51	0.18	33	67	68	0
Calc[d]	58	39	31	42.7	27	-0.41	48	56	60	46

a. Chemical shifts, relative to δ_{iso}(TMS) = 0, and the span, Ω, are in ppm.

b. See section 2.1 for an explanation of the symbols used herein.

c. Uncertainties are estimated to be ± 2 ppm for the principal components of the CS tensor, ± 0.5 ppm for δ_{iso} and ± 5° for θ_{ii} and α.

d. Calculated at the RHF/cc-pVTZ level of theory. See Chapter 3 for a detailed discussion of the *ab initio* calculations.

A single set of CS parameters was assumed for the two sites of TSB; the agreement between observed and calculated ^{13}C NMR spectra (Fig. 5.4) indicates that this is a reasonable assumption. The parameters derived from the simulation of the experimental spectra are summarized in Table 5.1. For comparison, the parameters calculated from first principles at the RHF/cc-pVTZ level of theory are included in this table. The alkenyl carbon CS tensor orientation, assigned on the basis of the experimental/theoretical results as discussed in Chapter 4, is illustrated in Figure 5.5. The orientation is similar to that reported for other alkenes, such as ethylene[55] and *trans*-2-butene:[54] δ_{11} is approximately in the molecular plane perpendicular to the alkenyl C,C bond, δ_{22} is along the C,C bond and δ_{33} is perpendicular to

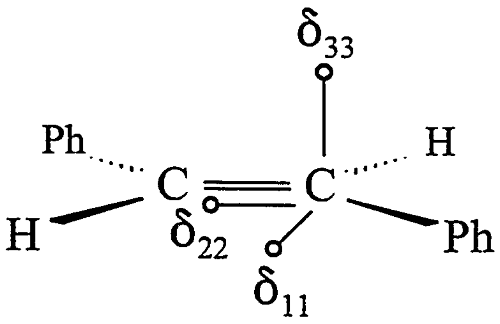

Figure 5.5 Orientations of the alkenyl carbon CS tensors for *trans*-stilbene.

the molecular plane.

The accepted alkenyl C,C bond length for TSB, as determined by X-ray diffraction, is 1.326 ± 0.006 Å,[33] less than the value of 1.35 - 1.36 Å calculated by an *ab initio* geometry optimization.[279,280] The unusually short experimental bond length has been attributed to large amplitude motion of the phenyl groups,[281,282] or to motion of the phenyl group combined with rotation of the molecule.[283,284] It has also been suggested that the experimental bond length may be misleading,[280] due to the disorder in the crystal.[33] The alkenyl C,C bond length for TSB may be estimated from $R_{\mathrm{eff}}(^{13}\mathrm{C},^{13}\mathrm{C})$ according to eq 2.15 if $\Delta^1J(^{13}\mathrm{C},^{13}\mathrm{C})$ is assumed to be negligible (Section 2.1.4). The ^{13}C,^{13}C dipolar coupling constant used to calculate the spectra shown in Fig. 5.4, 2.8 ± 0.2 kHz, corresponds to $r_{\mathrm{CC}} = 1.39 \pm 0.03$ Å; significantly greater than the value determined from X-ray diffraction.[33] While vibrational motion generally results in a reduced ^{13}C,^{13}C dipolar coupling[107] and hence a greater value of r_{CC}, the large difference between the value reported by Bouwstra and coworkers[33] and that expected from the value of R_{eff} implies that the accepted value of r_{CC} may indeed be too low, as suggested by Choi and Kertesz.[280] However, since the motion of the alkenyl C,C bond suggested by Saito and Ikemoto[283,284] will also lead to a reduced ^{13}C,^{13}C dipolar coupling,[55] definite conclusions about r_{CC} are not possible at this time. The alkenyl C,C bond lengths for the two types of molecules present in the unit cell differ by 0.004 Å, which corresponds to a difference of only 30 Hz in their respective dipolar coupling values, negligible compared to the uncertainty in R_{eff}. Hence, only one value of the ^{13}C,^{13}C dipolar coupling constant was used in the line shape calculations described above.

5.3.2 Carbon-13 NMR Spectra of MAS Samples of Pt(η^2-*trans*-Stilbene)(PPh$_3$)$_2$

The ^{13}C NMR spectra of MAS samples of ^{13}C$_2$-labelled samples of PtTSB are shown in Figs. 5.6 A and B. Comparison with the NMR spectra of TSB (Fig. 5.2) shows that the isotropic alkenyl carbon nuclei are shielded by 60 ppm upon coordination with Pt(0). This compares to the increased shielding of approximately 87 ppm observed for coordination of ethylene with Pt(0); similar values have been reported for Pt-alkene complexes measured in solution (Section 1.3). The ^{13}C NMR spectra of MAS samples of PtTSB exhibit broad isotropic peaks, with widths at half height of 350 Hz at 4.7 T and 500 Hz at 9.4 T, much broader than the approximately 200 Hz line widths observed at both 4.7 and 9.4 T for the corresponding isotropic peaks of TSB. Indirect (J) and direct dipolar coupling interactions with the protons should be removed by decoupling. However, Chaloner and coworkers have reported values of 20.5 and 26.7 Hz for $^2J(^{31}\text{P},^{13}\text{C})_{trans}$ for coupling to the two ^{31}P nuclei of PtTSB,[46] measured in solution. These values "are suspicious"[285] since the phosphorus and alkenyl carbon nuclei are chemically equivalent in solution. Nevertheless, similar values have

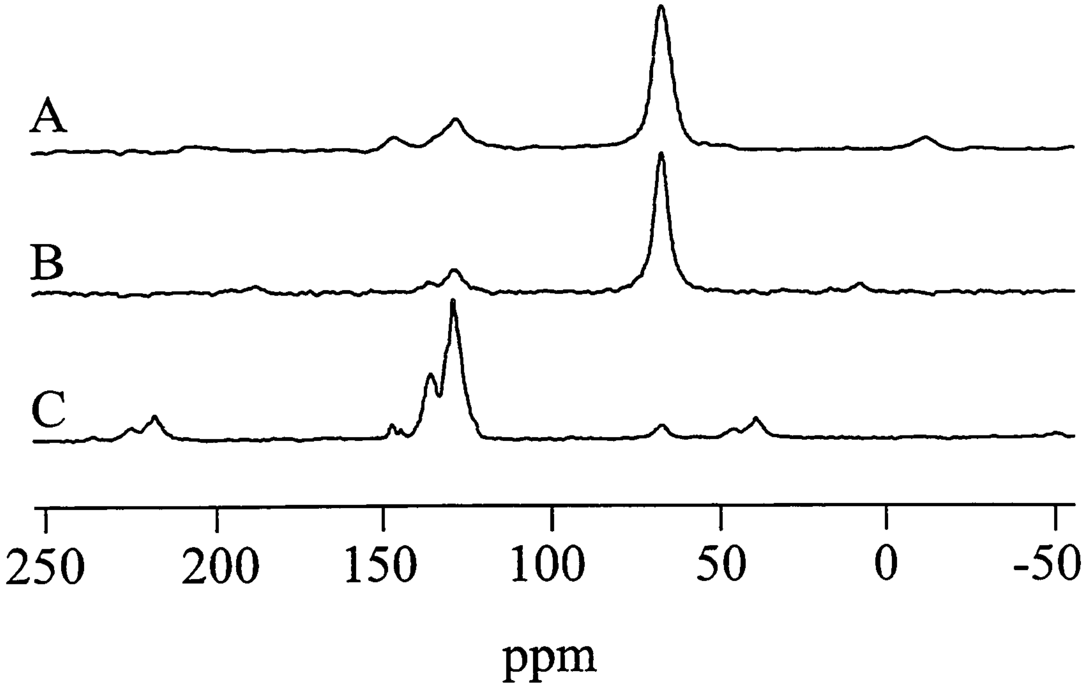

Figure 5.6 Carbon-13 NMR spectra of MAS samples of Pt(η^2-*trans*-stilbene)($PPh_3)_2$. Traces (A) and (B) are those of the $^{13}C_2$-labelled samples, acquired at 4.7 T with ν_{rot} = 4 kHz and at 9.4 T with ν_{rot} = 6 kHz, respectively; 64 and 16 transients were added. Trace (C) is that of a natural abundance carbon sample, acquired at 9.4 T with ν_{rot} = 8 kHz; 1879 transients were added.

been reported for $^2J(^{31}P,^{13}C)$ in $Pt(C_2H_4)(PPh_3)_2$.[42] Likewise, $^1J(^{195}Pt,^{13}C)$ has not been reported for PtTSB but is expected to be comparable to that reported for $Pt(C_2H_4)(PPh_3)_2$, 196 Hz;[42] this is expected to broaden the bases of the ^{13}C NMR peaks, a consequence of the 33.8 % natural abundance of ^{195}Pt. Hence, the observed line broadening is ascribed primarily to spin-spin coupling interactions with ^{195}Pt and ^{31}P. Mechanisms for line-broadening in solid-state NMR spectra of MAS samples have been discussed in detail.[286-288] There is no indication of a significant isotropic chemical shift difference for the two ^{13}C nuclei.

The ^{13}C NMR spectra of MAS samples of the $^{13}C_2$-labelled samples of PtTSB contain a weak peak at approximately 128 ppm (Fig. 5.6 A and B). Since the ^{13}C NMR spectrum of PtTSB at natural abundance (Fig. 5.6 C) contains a relatively intense peak at this frequency, the peaks at 128 ppm in Figs. 5.6 A and B are attributed to the natural abundance aromatic ^{13}C nuclei of PtTSB—not surprising for a molecule containing a total of 8 phenyl groups.

Figure 5.7 illustrates the experimental and calculated spectra of MAS samples of the $^{13}C_2$-labelled samples of PtTSB obtained at various spinning frequencies. Parameters used in the calculation of the spectra are those obtained from an analysis of the stationary sample (*vide infra*). The high-frequency portions of the experimental spectra are complicated by peaks arising from aromatic ^{13}C nuclei at natural abundance, but the spinning sidebands of the alkenyl carbon nuclei are well-resolved at lower frequencies. The asymmetry in the first-order spinning sidebands of the spectrum obtained with ν_{rot} = 2 kHz (Fig 5.7 C) support the conclusion that the spin pair are crystallographically equivalent but magnetically nonequivalent (*i.e.*, the alkenyl carbon CS tensors are not related by a centre of inversion) since a single transition is expected for the sidebands of an A_2 spin system (Section 2.4.2). The splitting calculated for the isotropic peak (Fig. 5.7 C) is also a consequence of the magnetically nonequivalent nuclei. This effect is not resolved in the experimental spectrum, probably because of broadening due to $^1J(^{195}\text{Pt},^{13}\text{C})$ and $^2J(^{31}\text{P},^{13}\text{C})$, discussed above, which are not included in the calculation of the simulated spectrum. The isotropic peaks of the experimental spectra are not affected significantly by ν_{rot}, supporting the contention that the line broadening arises from unresolved $^1J(^{195}\text{Pt},^{13}\text{C})$ and $^2J(^{31}\text{P},^{13}\text{C})$.

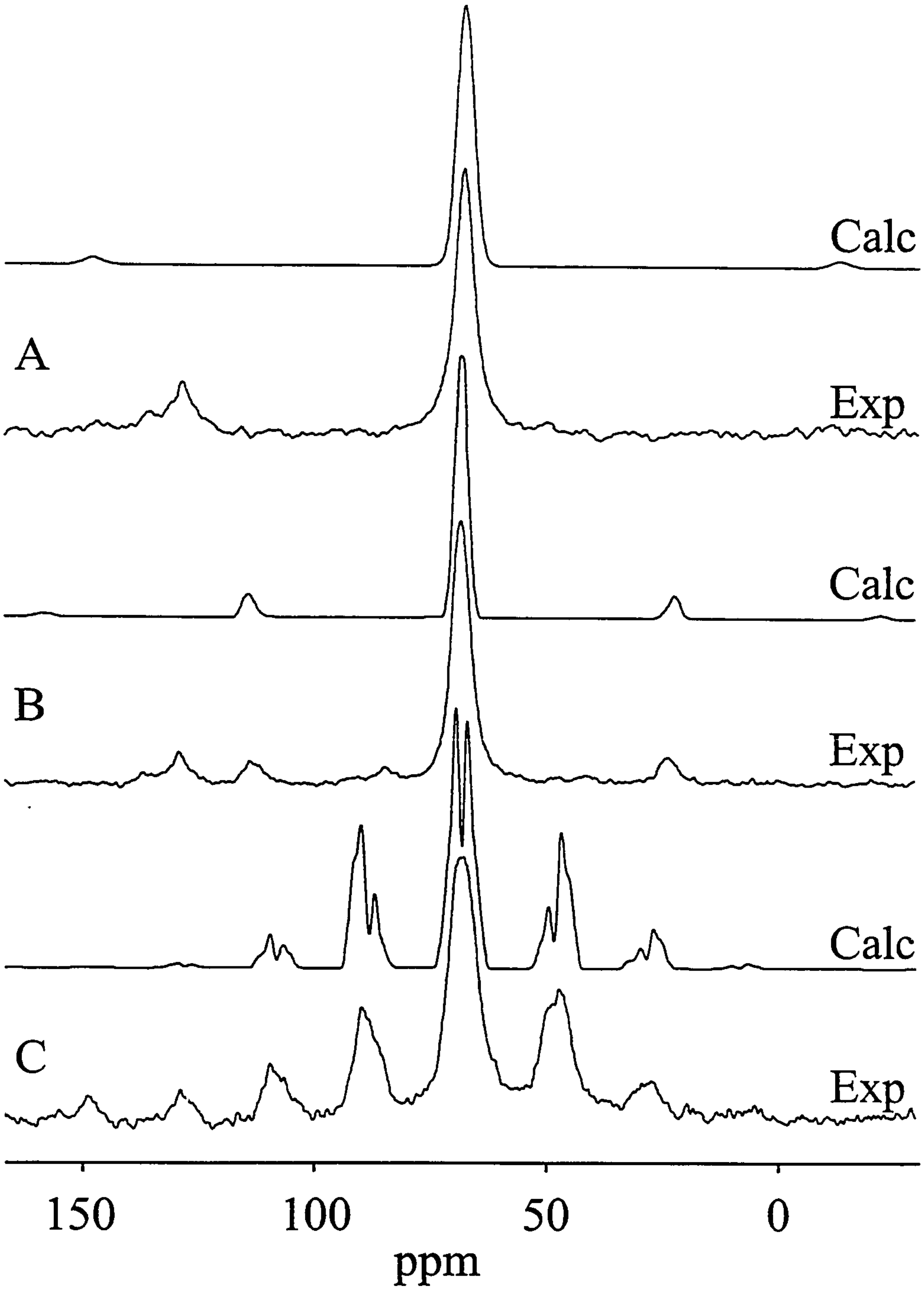

Figure 5.7 Calculated and experimental spectra of MAS samples of Pt(η^2-*trans*-stilbene)(PPh_3)$_2$. All spectra were acquired at 9.4 T, with ν_{rot} = 8 kHz (A), 4.5 kHz (B) and 2 kHz (C). 36, 128 and 129 transients were added for traces (A), (B) and (C), respectively.

5.3.3 Carbon-13 NMR Spectra of Stationary Samples of Pt(η^2-*trans*-stilbene)(PPh$_3$)$_2$

Carbon-13 NMR spectra of stationary $^{13}C_2$-labelled samples of PtTSB are shown in Fig. 5.8 with the corresponding simulated spectra. The latter were calculated on the assumption that the CS tensors for the two alkenyl carbon nuclei are related by a C_2-symmetry axis. The parameters derived from this fit are summarized in Table 5.1.

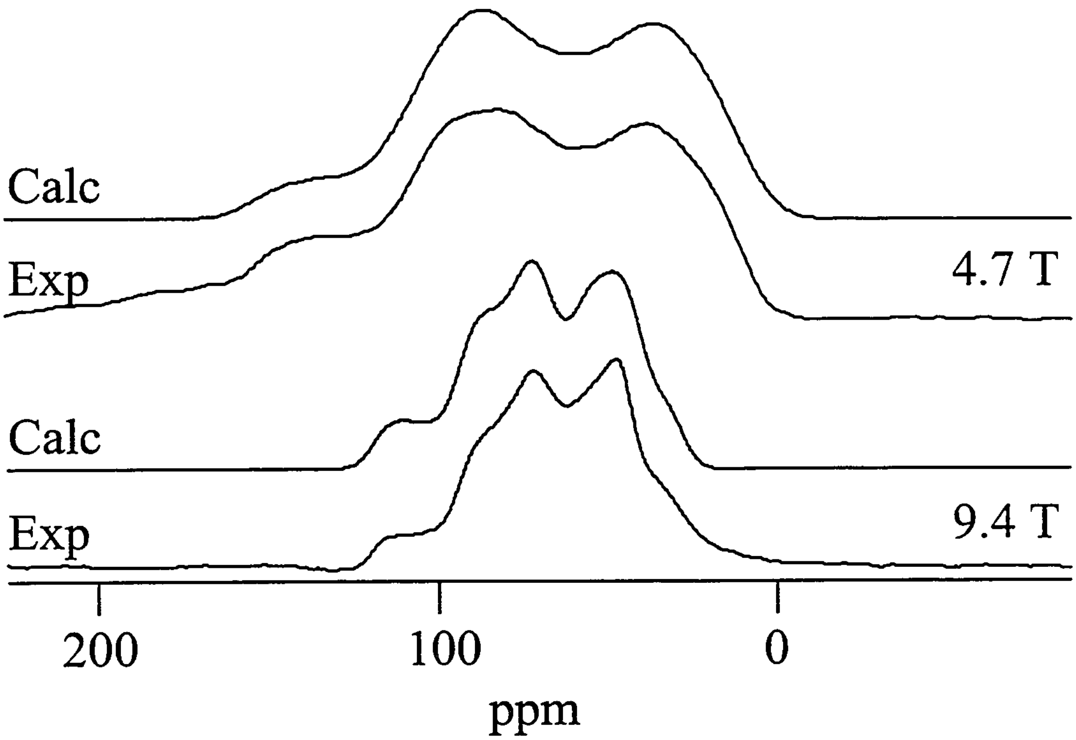

Figure 5.8 Calculated and experimental ^{13}C NMR spectra of stationary samples of Pt(*trans*-stilbene-α,β-$^{13}C_2$)(PPh$_3$)$_2$ at B_0 = 4.7 and 9.4 T. 880 and 6000 transients, respectively, were added.

The ^{13}C NMR spectra of stationary $^{13}C_2$-labelled samples of PtTSB were calculated with a dipolar coupling of 2.5 ± 0.2 kHz. Neglecting the contribution from ΔJ, this corresponds to a C,C bond length of 1.45 ± 0.03 Å. Although PtTSB has not been investigated by diffraction techniques, the alkenyl C,C bond is not expected to be very different from that for 4,4'-dinitro-*trans*-stilbene*bis*(triphenylphosphine)platinum (space group $P\bar{1}$, $Z = 2$),[245] 1.416 ± 0.045 Å. Hence, the bond length suggested from the experimental value for $R_{\text{eff}}(^{13}\text{C},^{13}\text{C})$ is reasonable. Factors affecting measured dipolar couplings have been discussed above. The agreement between r_{CC} predicted from R_{eff} and that expected from the diffraction study cited above suggests that motion is not significant for the *trans*-stilbene moiety of PtTSB.

To fix the alkenyl carbon CS tensor orientations in the molecular axis system, CS tensors calculated from first principles are considered; these are listed in Table 5.1. Agreement between calculated and experimental orientations is reasonable, particularly in view of the small span for PtTSB. CS tensor orientations are also very sensitive to the geometry about the alkenyl carbon atoms; unfortunately, the exact structure of PtTSB is not known. A high-level *ab initio* geometry optimization of PtTSB is impractical and would not necessarily yield the geometry prevailing in the solid state. Attempts to grow single crystals of PtTSB suitable for X-ray diffraction measurements have been unsuccessful.

The calculated orientation of the δ_{33} components for the alkenyl carbon nuclei of PtTSB suggests that δ_{33} lies 23° out of the C,Pt,C plane, as illustrated in Fig. 5.9 A. With δ_{33} oriented as shown, the experimental value of θ_{22}, 67°, places δ_{22} either approximately along the bond to the *ipso*-carbon of the stilbene phenyl ring (Fig. 5.9 B) or towards the alkenyl hydrogen; the former is in agreement with calculations on the model compound. Hence, on the basis of the experimental/theoretical results, the orientation of the alkenyl carbon CS

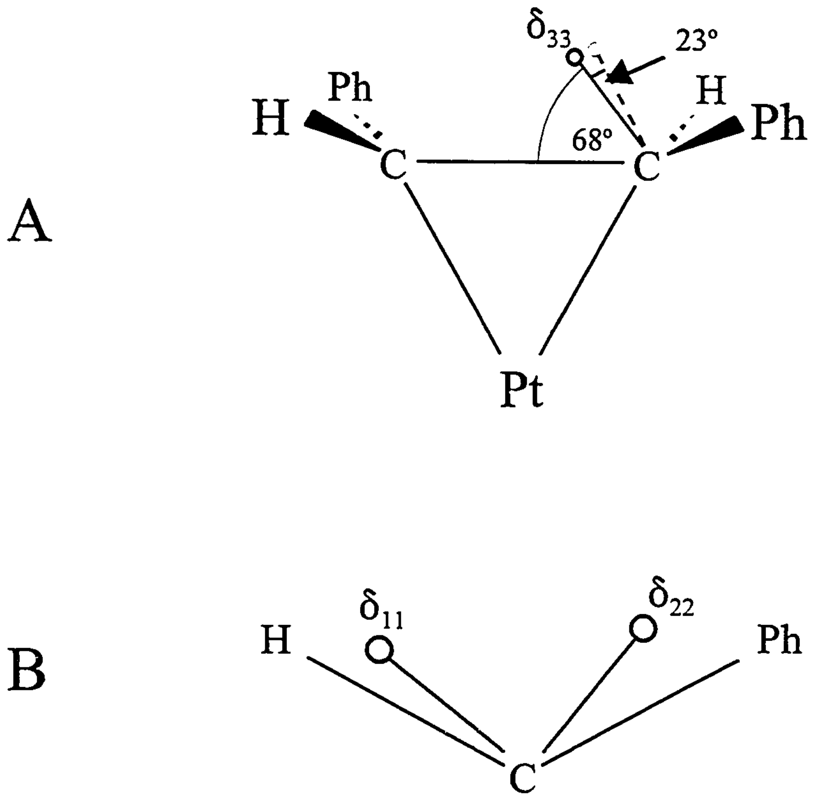

Figure 5.9 Orientation of the alkenyl carbon CS tensor for Pt(*trans*-stilbene)$(PPh_3)_2$. That for the other alkenyl carbon nucleus is related to the one illustrated here by the C_2 symmetry of the molecule. The orientation of the δ_{33} component is shown in (A); this component is 23° out of the plane defined by the platinum and alkenyl carbon atoms. In (B), the orientation of the δ_{11} and δ_{22} components, approximately in the H,C,C_{ipso} plane, are shown. Note that δ_{11} is slightly in and δ_{22} is slightly out of the plane of the page.

tensors for PtTSB are assigned as illustrated in Figure 5.9 A and B.

A possible orientation for δ_{33} based on the experimental value of θ_{33}, 68°, has the component lying in the general direction of the platinum nucleus, while the orientation suggested here places this component roughly perpendicular to the plane defined by the alkenyl phenyl and hydrogen substituents. It is noted that the δ_{33} component for the carbon nuclei of ferrocene also is oriented in this general direction relative to the iron nucleus[74] (Fig. 1.11); the calculated orientation for the alkenyl carbon nuclei of $Pt(C_2H_4)(PPh_3)_2$ have a similar orientation (Fig. 4.4).

5.3.4 Comparison of the Chemical Shift Tensors for *trans*-Stilbene and Pt(*trans*-Stilbene)$(PPh_3)_2$

Comparison of the alkenyl carbon CS tensors for TSB and PtTSB (Table 5.1) reveals significant differences in the magnitudes of their corresponding principal components. Upon coordination with Pt(0), the span of the alkenyl carbon CS tensors are reduced from 166 ppm to 51 ppm, primarily due to changes in δ_{11} and δ_{22}. The different geometry about the alkenyl carbon atoms for TSB and PtTSB make a comparison of the shielding in specific directions difficult. It is noted that the orientations of the alkenyl carbon CS tensors for PtTSB reflect the geometry about the alkenyl carbons: δ_{11} and δ_{22} are approximately in the plane defined by the alkenyl carbon and its two substituents, with δ_{33} approximately perpendicular to this plane.

The model proposed by Dewar, Chatt and Duncanson[28] offers a qualitative explanation for the changes in the magnitudes of the CS tensor components upon coordination with Pt(0). The deshielding in the directions of δ_{11} and δ_{22} for TSB is thought to be primarily a consequence of the mixing of σ and π^* as well as π and σ^* orbitals, as for ethylene (Section 3.2). Hence, donation of electron density to the π^* orbitals of the alkenyl carbon nuclei of the complex reduces this mixing, resulting in the observed increased shielding. Alkenes coordinated with metals are thought to have properties intermediate between those of alkenes and those of alkanes.[1] The span of the CS tensor for PtTSB, 51 ppm, is indeed intermediate between that for TSB, 166 ppm, and those for ethane, 7 ppm,[192] and other methylene groups.[53]

The effect of coordination of ethylene or TSB with Pt(0) is comparable. The isotropic shielding increases significantly in both cases; δ_{11} is very sensitive to coordination. The orientations of the CS tensors for PtTSB are not significantly different from those reported for $Pt(C_2H_4)(PPh_3)_2$ (Chapter 4). More examples would be instructive but it is expected that the trends discussed in Chapters 4 and 5 are in general true for alkenes coordinated with Pt(0).

5.4 Summary

It has been shown that the alkenyl carbon chemical shift tensors for *trans*-stilbene change dramatically upon coordination with platinum(0). In particular, the span of the alkenyl carbon chemical shift tensor is reduced significantly for PtTSB, primarily because of changes in the shielding in the directions of δ_{11} and δ_{22}. The orientations of the alkenyl carbon CS tensors for PtTSB are sensitive to the orientation of the substituents about the alkenyl carbons. Orientations for the carbon CS tensors, based on the combined experimental/theoretical results, are reported. The alkenyl carbon CS tensors for PtTSB are similar to those for $Pt(C_2H_4)(PPh_3)_2$ discussed in Chapter 4.

Chapter 6

An Investigation of the Alkynyl Carbon Chemical Shift Tensors for Diphenylacetylene and Pt(η^2-Diphenylacetylene)(PPh_3)$_2$

6.1 Introduction

The ^{13}C NMR literature on metal-alkyne complexes is very limited. There are not many reports of samples examined in isotropic liquids;[12] the NMR studies of solid metal-alkyne complexes[59] were discussed in Section 1.5.4. To investigate a typical platinum-alkyne complex, Pt(η^2-diphenylacetylene-1,2-$^{13}C_2$)(PPh_3)$_2$ (PtDPA, see Fig. 6.1) was prepared. This sample was chosen because of the similarities between this complex and its *trans*-stilbene analogue, and because the $^{13}C_2$-labelled ligand could readily be prepared from samples available in the lab (*vide infra*). The alkynyl carbon chemical shift tensors have been characterized by the dipolar-chemical shift method (Section 2.4.1). Orientations for the CS tensors in the molecular framework are proposed based on a combination of experimental results and *ab initio* calculations.

To complement the investigation of PtDPA, the alkynyl carbon CS tensors for diphenylacetylene (DPA) have also been characterized using the dipolar-chemical shift method. There have been few ^{13}C NMR studies of solid alkynes. The carbon CS tensor for acetylene was reported by Zilm and Grant,[55] that of 2-butyne was reported by Pines and coworkers,[65] as well as by Beeler *et al.*,[73] who also reported the alkynyl carbon CS tensors for propyne. These studies found axially-symmetric alkynyl carbon CS tensors with the direction of greatest shielding along the C,C bond. Comparable values were also reported

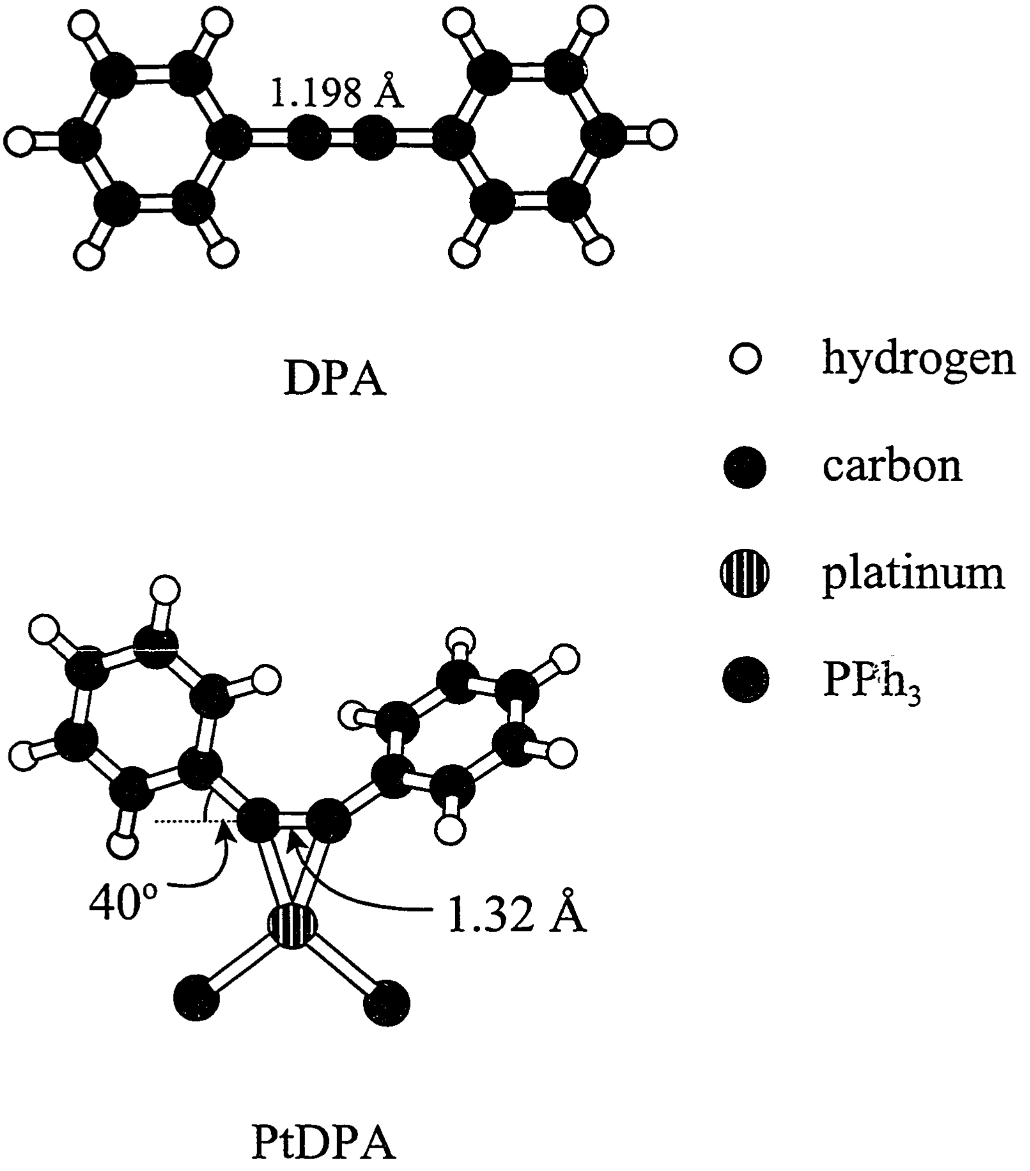
1.198 Å
DPA
○ hydrogen
● carbon
◍ platinum
● PPh$_3$
40°
1.32 Å
PtDPA

Figure 6.1 Structures of diphenylacetylene[32] (DPA) and Pt(η^2-diphenylacetylene)(PPh$_3$)$_2$[291] (PtDPA). The orientations of the phenyl rings of PtDPA are from reference 31.

for diacetylene.[289] In addition to these studies, the principal components of the terminal carbon CS tensor for phenylacetylene were reported by Farrar and coworkers, based on the results of a ^{13}C NMR relaxation study of samples in several isotropic fluids.[252]

The structure of DPA has been reported by Mavridis and Moustakali-Mavridis[32] and by Espiritu and White.[290] The molecule (space group $P2_1/a$, $Z = 4$, density = 1.129 g cm^{-3}) is planar with an alkynyl C,C bond length of 1.198 ± 0.009 Å (Figure 6.1).[32] A complete structure for PtDPA has not been reported, but in a preliminary report, Glanville and coworkers[291] reported that the alkynyl carbon atoms are in the plane defined by the platinum and phosphorus atoms, with a C,C bond length of 1.32 ± 0.09 Å. The alkynyl C,C bond forms an angle of approximately 140° with the bond to the *ipso* carbon atom. The orientation of the alkynyl phenyl rings relative to the plane defined by the platinum and phosphorus atoms was not reported, but is not expected to be very different from that for the same ligand of the trimethylphosphine analogue of PtDPA. In their investigation of Pt(η^2-diphenylacetylene)(PMe$_3$)$_2$, (space group $P2_12_12_1$, $Z = 4$, density = 1.783 g cm^{-3}) Packett *et al.* reported that the phenyl groups are approximately in the plane defined by the platinum and phosphorus atoms,[31] as illustrated in Figure 6.1. The bond to the *ipso* carbon is oriented approximately as for the PtDPA. The bonding of metal-alkyne complexes has been discussed in Section 1.2.

6.2 Experimental

Sample Preparation. A sample of DPA at natural abundance was acquired commercially (Aldrich) and used without further purification. Diphenylacetylene-1,2-$^{13}C_2$

was prepared from *trans*-stilbene-α,β-$^{13}C_2$ (MSD Isotopes, 99 % ^{13}C) according to standard techniques.[292] 0.510 g *trans*-stilbene was dissolved in 10 ml of acetic acid and 1.093 g pyridinium hydrobromide perbromide was added to the solution, which was heated (approximately 80° C) for about 5 minutes. After cooling, 0.862 g of *meso*-stilbene dibromide was collected. This product was dissolved in 3.5 ml triethylene glycol in a test tube to which approximately 0.25 g (5 pellets) of KOH was added. A thermometer placed in triethylene glycol in a smaller test tube was immersed in the test tube containing the *meso*-stilbene. The sample was heated to 160° C for about 5 minutes. The solution was allowed to cool, then 10 ml H_2O was added. The white powder, diphenylacetylene, was characterized by its melting point (59 - 60° C) and by ^{13}C NMR spectroscopy. The yield was 0.421 g (83.5 %).

Pt(η^2-diphenylacetylene)(PPh_3)$_2$ was prepared under a nitrogen atmosphere from DPA according to procedures suggested in the literature.[259] 0.495 g $PtCl_2(PPh_3)_2$ was dissolved in 25 ml of N_2-purged ethanol; 0.4 ml 85 % hydrazine was added. After stirring for several minutes, 0.209 g diphenylacetylene dissolved in 10 ml of ethanol was added and the mixture was heated to boiling, then allowed to cool slowly. The product, a dull white powder, was collected by filtration; 0.434 g of Pt(η^2-diphenylacetylene)(PPh_3)$_2$, corresponding to a yield of 87 %, was recovered. The product was characterized by its melting point (160 - 164° C), IR spectra, as well as by solution ^{13}C and ^{31}P NMR spectra. These samples were prepared with the assistance of Chris McDonald.

NMR. Carbon-13 and ^{31}P NMR spectra of solid samples were obtained on Chemagnetics CMX Infinity 200 and Bruker AMX-400 NMR spectrometers. Contact times of 2 ms with ^{1}H 90° pulses of 3.0 to 4.0 μs and recycle delays of 20 s (^{13}C) or 10 s (^{31}P) were used to acquire all NMR spectra. Variable-amplitude cross polarization[293] (VACP) was used to acquire the ^{13}C NMR spectra. Peaks in the ^{13}C NMR spectra were referenced to TMS by setting the high-frequency isotropic peak of adamantane to 38.56 ppm;[180] those of the ^{31}P NMR spectra were referenced to 85% H_3PO_4(aq) by setting the isotropic peak of solid $NH_4H_2PO_4$ to +0.81 ppm. The isotropic peaks of the ^{13}C NMR spectrum of a $^{13}C_2$-labelled MAS sample of PtDPA was simulated using the program XSim[294] which is based on the program NUMARit.[295] Since these programs calculate isotropic peaks, spinning sidebands from the experimental spectra were summed into the isotropic peak before simulation of the spectra. Contributions to the spectra from the aromatic ^{13}C at natural abundance were removed by subtraction of a spectrum of the natural abundance spectrum (4.7 T) or by the use of a dipolar-dephasing experiment (9.4 T),[296] which removes the contribution of all but the quaternary carbon nuclei.

Proton-decoupled ^{13}C and ^{31}P NMR spectra of DPA and PtDPA dissolved in CD_2Cl_2 (approximately 0.1 M) were acquired on the Bruker AMX-400 NMR spectrometer. Peaks in the ^{13}C NMR spectra were referenced to TMS by setting the solvent ^{13}C peak to 54.0 ppm; those for the ^{31}P NMR spectra were referenced to an external 85 % H_3PO_4(aq) sample. The FIDs were zero-filled from 16 K to 64 K points before processing without applying a line broadening function. Recycle delays were 2 s. The contributions to the ^{13}C NMR spectrum of the labelled sample from the aromatic ^{13}C nuclei at natural abundance were subtracted as described previously. Carbon-13 and ^{31}P NMR spectra of the $^{13}C_2$-labelled samples were simulated using the program XSim.[294] Calculation of the carbon CS tensors for DPA and

PtDPA from first principles have been discussed in Section 3.5.3.

6.3 Results and Discussion

6.3.1 Carbon-13 NMR Spectra of Diphenylacetylene

The ^{13}C NMR spectra of diphenylacetylene-1,2-$^{13}C_2$ are shown in Figure 6.2; Table 6.1 summarizes the data derived from the NMR line shape simulations. The isotropic

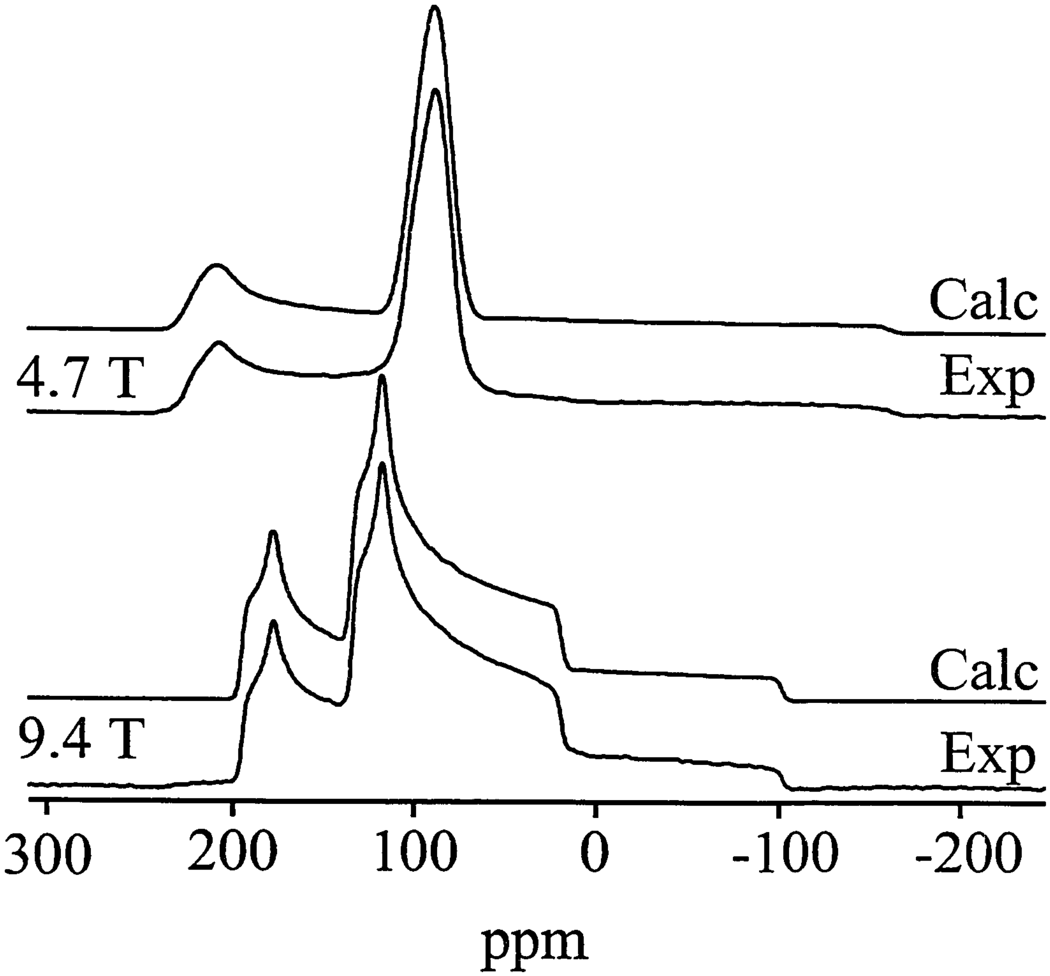

Figure 6.2 Carbon-13 NMR spectra of stationary samples of diphenylacetylene-1,2-$^{13}C_2$.

Table 6.1 Experimental and Calculated Carbon Chemical Shift Tensors for Diphenylacetylene and Pt(Diphenylacetylene)$(PPh_3)_2$.[a]

	δ_{11}	δ_{22}	δ_{33}	δ_{iso}	Ω	κ	θ_{11}	θ_{22}	θ_{33}	α
Diphenylacetylene										
Exp[b]	165	147	-42	89.8	207	0.83	90	90	0	0
Calc[c]	170	147	-69	82.7	239	0.81	90	90	0	0
Pt(diphenylacetylene)$(PPh_3)_2$										
Exp[d]	207	141	32	127	175	0.24	75	15	90	0
	216	140	26	128	190	0.19	80	10	90	0
	232	141	27	133	205	0.12	82	9	85	0
	230	145	30	135	200	0.15	69	22	83	0
Calc[c]	238	84	0	107	238	-0.29	79	11	89	0
	246	105	1	117	245	-0.15	74	18	83	9

a. Chemical shifts, relative to δ_{iso}(TMS) = 0, and the span, Ω, are in ppm.

b. Uncertainties are estimated to be: ± 0.2 ppm for δ_{iso}; ± 2 ppm for the principal components of the CS tensors and ± 3° for the θ_{ii} and α.

c. Calculated at the RHF/cc-pVTZ level of theory. See Section 3.5.3 for a detailed discussion of the *ab initio* calculations.

d. Uncertainties are estimated to be: ± 1 ppm for δ_{iso}; ± 5 ppm for the principal components of the CS tensors; ± 5° for the θ_{ii} and ± 10° for α.

chemical shift, δ_{iso} = 89.8 ppm, is comparable to that measured in solution.[297] The alkynyl carbon nuclei are deshielded compared to those of acetylene,[55] but are similar to those for the alkynyl nuclei of 2-butyne.[73] The difference is primarily due to the deshielding in the direction of the C,C bond, reflecting the importance of molecular symmetry in magnetic shielding. As discussed in Section 2.2, $\sigma^p_\parallel = 0$ for acetylene, but in the absence of a C_∞ axis, σ^p is significant, leading to deshielding in the direction of the C,C bond for DPA. Previous reported alkynyl CS tensors are all axially symmetric; this is not required by the symmetry of DPA, D_{2h}.

In the absence of significant intermolecular interactions, the symmetry of DPA requires that the CS tensor be oriented such that one component is along the C,C bond, one is perpendicular to the molecular plane and the other component is perpendicular to the C,C bond, in the molecular plane. Since $\theta_{33} = 0°$ (Table 6.1), δ_{33} is the component along the C,C bond, as for other alkynyl carbon CS tensors. Further information about the CS tensor orientation is not available from the experimental data, since $\theta_{ii} = 90°$ for both δ_{11} and δ_{22}. Hence, the results of *ab initio* calculations are considered; for comparison, the data for the alkynyl carbon CS tensors calculated with the cc-pVTZ basis set are included in Table 6.1. These calculations have been discussed in Section 3.5.3; it is noted here that calculations accurately predict that δ_{33} is along the C,C bond. The experimental/calculated results suggest that δ_{11} is perpendicular to the molecular plane and that δ_{22} is in the molecular plane, perpendicular to the alkynyl C,C bond, as illustrated in Figure 6.3. In view of the small difference between δ_{11} and δ_{22}, the assignment of the CS tensor orientations based on the *ab initio* calculations must be regarded as tentative. This does not affect the underlying conclusion: a non-axially symmetric CS tensor with δ_{33} along the alkynyl C,C bond is determined.

Carbon-13 NMR spectra of DPA (Fig. 6.2) were simulated with $R_{\mathrm{eff}} = 4025 \pm 50$ Hz, corresponding to $r_{\mathrm{CC}} = 1.236 \pm 0.003$ Å, compared to an R_{eff} of 4420 ± 100 Hz predicted from the experimental value of r_{CC}, 1.198 ± 0.009 Å.[32] Factors affecting the observed ^{13}C,^{13}C dipolar coupling have been discussed in Chapter 4. The ^{13}C NMR spectra of stationary

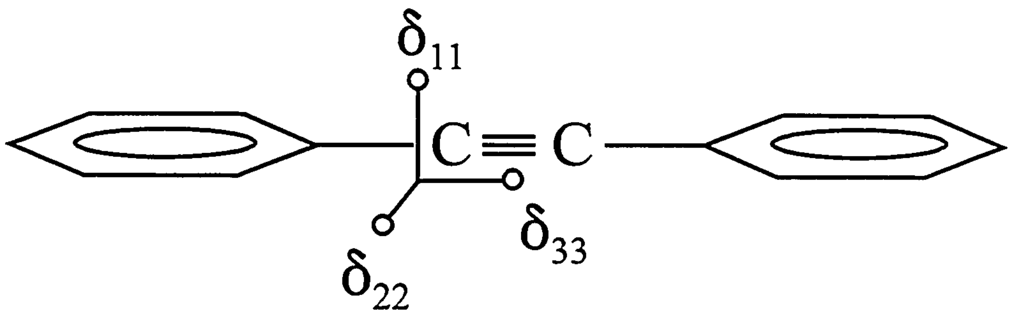

Figure 6.3 Orientation of the alkynyl carbon CS tensors for diphenylacetylene.

samples of diphenylacetylene-1,2-$^{13}C_2$ exhibit some unusual, field-dependent line shapes (Figure 6.2), which result from the combined effect of the anisotropic magnetic shielding and $R_{eff}(^{13}C,^{13}C)$. A detailed discussion of these line shapes is given in Appendix A.1.

6.3.2 Solid-State ^{31}P and Solution ^{13}C NMR of Pt(η^2-diphenylacetylene)(PPh$_3$)$_2$

Before discussing the ^{13}C NMR spectra of solid PtDPA, it is useful to consider the insight gained from the analysis of the ^{13}C and ^{31}P NMR spectra of this compound in solution, as well as from ^{31}P NMR spectra of solid samples.

Figure 6.4 illustrates the proton-decoupled ^{13}C NMR spectrum of the $^{13}C_2$-labelled sample of PtDPA dissolved in CD_2Cl_2. The complex pattern is that of an AA'XX' spin system,[298] with satellite peaks arising from $^1J(^{195}Pt,^{13}C)$. The parameters derived from the simulation of this spectrum are summarized in Table 6.2. The value for $^1J(^{13}C,^{13}C)$, 85.8 ± 0.4 Hz, is significantly less than that expected for an alkyne. For example, $^1J(^{13}C,^{13}C) = 171.5$

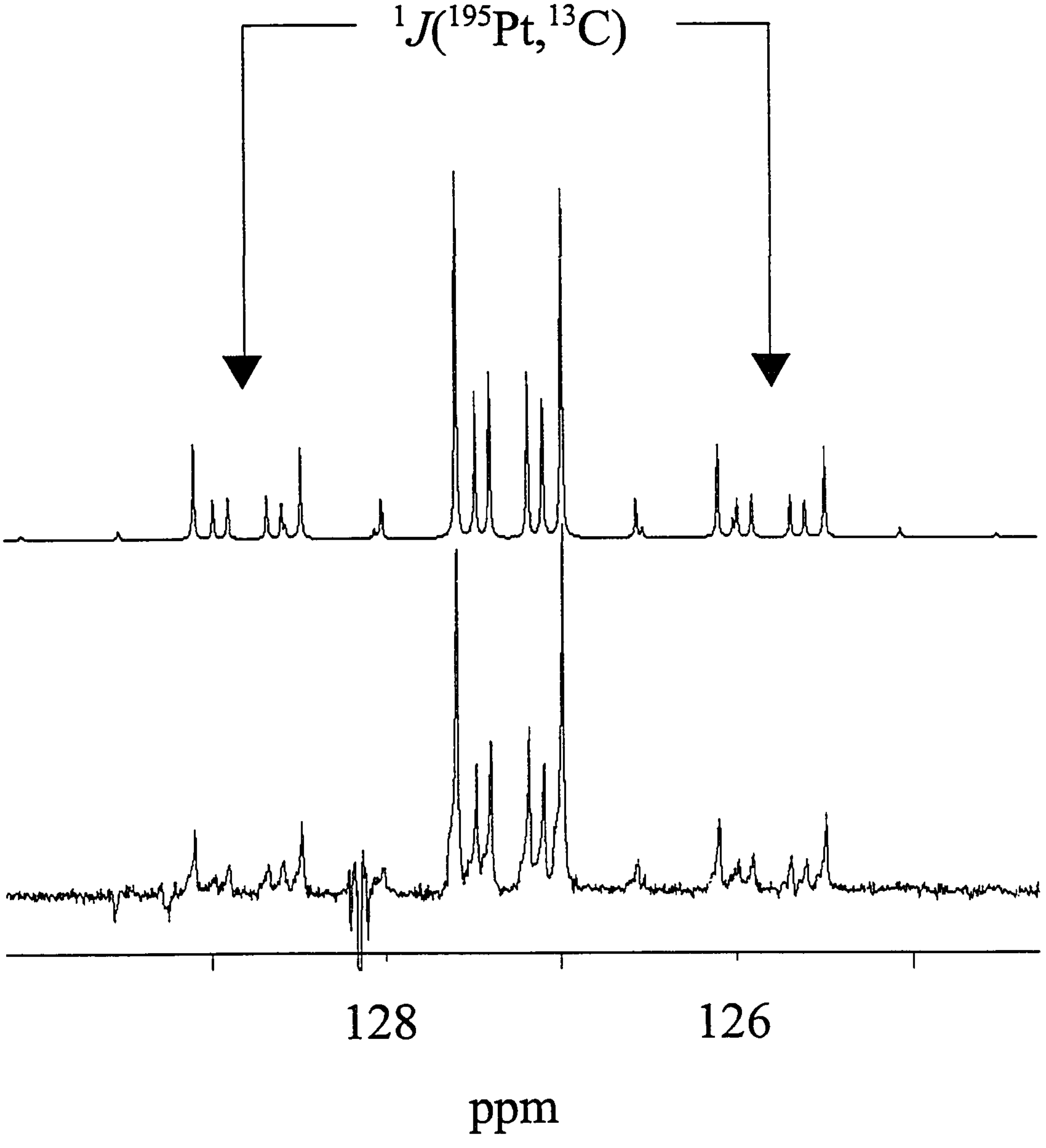

Figure 6.4 Calculated (upper trace) and experimental ^{13}C NMR spectra for a 0.1 M sample of Pt(η^2-diphenylacetylene-1,2-$^{13}C_2$)(PPh_3)$_2$ in CD_2Cl_2. 280 transients were added. The distortion at approximately 128 ppm is a consequence of imperfect subtraction of the signal from the aromatic ^{13}C nuclei at natural abundance.

Table 6.2 Parameters Derived From the ^{13}C and ^{31}P NMR Spectra of Pt(η^2-Diphenylacetylene)(PPh_3)$_2$ in CD_2Cl_2.[a]

Parameter	Value	Parameter	Value
$\delta(^{13}C)$/ppm	127.895(4)	$^2J(^{31}P,^{13}C)_{trans}$/Hz[b]	±68.6(4)
$\delta(^{31}P)$/ppm[c]	27.5(4)	$^2J(^{31}P,^{13}C)_{cis}$ /Hz[b]	∓7.2(4)
$^1J(^{13}C,^{13}C)$/Hz	85.8(4)	$^2J(^{31}P,^{31}P)$/Hz	31.8(4)
$^1J(^{195}Pt,^{13}C)$/Hz	301.4(4)	$^1J(^{195}Pt,^{31}P)$/Hz[c]	3450(5)

a. Unless otherwise noted, the parameters are from the analysis of the ^{13}C NMR spectrum. Uncertainties are the larger of the RMS deviation of the data or the digital resolution of the spectra, 0.4 Hz/point.

b. Only the relative signs of these parameters are determined from the analysis.

c. Determined from the ^{31}P NMR spectra of PtDPA in CD_2Cl_2.

Hz for acetylene.[299] The value for $^2J(^{31}P,^{31}P)$, 31.8 ± 0.4 Hz, is similar to that reported by Chaloner *et al.*[46] for Pt(H-CC-CH_2OH)(PPh_3)$_2$, 35 Hz. Chisholm and coworkers reported a value of 27 ± 3 Hz for the sum of the *J* coupling to the *cis* and *trans* phosphorus nuclei of Pt(η^2-2-butyne)(PPh_3)$_2$,[38] significantly less than the 61.4 ± 0.4 Hz reported here. Carbon-13 NMR studies of platinum complexes coordinated with unsymmetric alkenes have shown that the larger *J*-coupling involves carbon nuclei *trans* to the phosphorus nuclei (Section 1.3). It is expected that this is the case here, but this has not been determined experimentally. Likewise, only the relative signs of $^2J(^{31}P,^{13}C)$ are determined. Wrackmeyer has shown that the sum $^2J(^{31}P,^{13}C)_{cis} + {}^2J(^{31}P,^{13}C)_{trans}$ for Pt(C_2H_4)(PPh_3)$_2$, is positive;[42] since $|^2J(^{31}P,^{13}C)_{trans}| > |^2J(^{31}P,^{13}C)_{cis}|$, it follows that the former is positive.

Finally, it is noted that a peak at 89.8 ppm in the ^{13}C NMR spectrum of the $^{13}C_2$-

labelled sample of PtDPA in CD_2Cl_2 (not shown) suggests that DPA is dissociating from platinum in this solvent. This peak increased in intensity over time such that the peaks at 127 to 128 ppm were not detectable after 24 hours. The observation of $^1J(^{195}Pt,^{13}C)$ and $^2J(^{31}P,^{13}C)$ indicates that exchange is not significant here.

Phosphorus-31 NMR spectra of MAS samples of solid PtDPA are illustrated in Figure 6.5. The satellite peaks are due to $^1J(^{195}Pt,^{31}P) = 3420 \pm 50$ Hz, similar to that observed in solution. The four peaks between 25 and 35 ppm are invariant to B_0 and hence represent separate ^{31}P sites. The two ^{31}P nuclei of the PtDPA molecule are known to be non-equivalent;[291] the four peaks observed here suggest that the asymmetric unit of the crystal structure contains at least two molecules, each with distinct phosphorus atoms. These peaks do not show any splitting due to $^2J(^{31}P,^{13}C)$ or $^2J(^{31}P,^{31}P)$, although comparison of the isotropic peaks for the $^{13}C_2$-labelled and natural-abundance carbon samples (Fig. 6.5, inset) demonstrates that $^2J(^{31}P,^{13}C)$ leads to a line broadening of 50 to 60 Hz. This is similar to the sum of the *cis* and *trans* coupling observed for the sample in solution.

6.3.3 Carbon-13 NMR of MAS Samples of Pt(η^2-Diphenylacetylene-1,2-$^{13}C_2$)(PPh_3)$_2$

Two broad peaks are observed in the isotropic region of a ^{13}C NMR spectrum of the $^{13}C_2$-labelled MAS sample of PtDPA acquired at 9.4 T, illustrated in Figure 6.6. Since *i*) the alkynyl carbon atoms are in significantly different environments;[291] *ii*) there are four non-equivalent phosphorus sites in the ^{31}P NMR spectra (Section 6.3.2); *iii*) the total intensity of the two peaks are approximately equal; and *iv*) the centre of mass of the broad peaks are invariant to B_0, it is concluded that the spectrum is that arising from four separate carbon

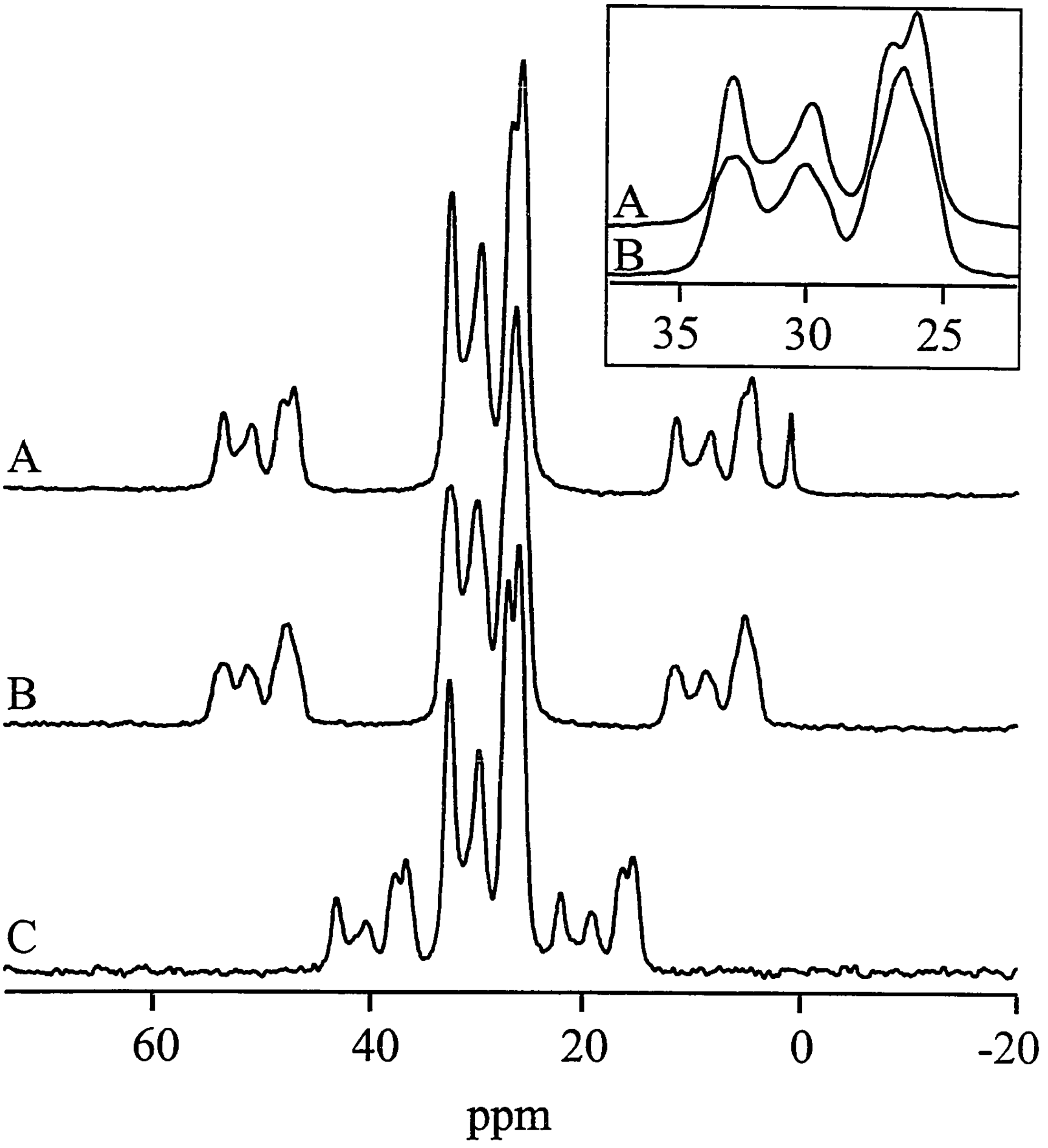

Figure 6.5 Phosphorus-31 NMR spectra of MAS samples of Pt(η^2-diphenylacetylene)(PPh_3)$_2$. Trace (A) is that for a natural-abundance carbon sample acquired at 4.7 T with ν_{rot} = 6 kHz. The sharp peak at approximately 1 ppm is thought to be an experimental artifact. Trace (B) is the spectrum of the $^{13}C_2$-labelled sample acquired as for (A) and trace (C) is the ^{31}P NMR spectrum of the $^{13}C_2$-sample acquired at 9.4 T with ν_{rot} = 12.5 kHz. 2000 and 600 transients, respectively, were added for the spectra acquired at 4.7 and 9.4 T. The inset is an expansion of the isotropic region of the spectra acquired at 4.7 T.

sites, two in each peak. These are referred to, from low to high frequencies, as C_A, C_B, C_C and C_D.

The fine structure observed in the high-frequency peak of the spectrum acquired at 9.4 T is much greater than the signal-to-noise ratio and has been observed in spectra of MAS samples acquired on separate occasions. Suspecting that the fine structure arises from *J*-coupling interactions, the spectra were simulated with the *J*-coupling parameters listed in Table 6.2. There are three possible combinations of spin pairs from the four carbon sites: *i*) C_A,C_B and C_C,C_D; *ii*) C_A,C_C and C_B,C_D; or *iii*) C_A,C_D and C_B,C_C. The chemical shift difference between the centre of the two peaks is approximately 750 Hz at 9.4 T, significantly greater than the value of $^1J(^{13}C,^{13}C)$ from NMR spectra of the sample in solution (Section 6.3.2). Hence combinations *ii* and *iii* yield similar, essentially *AX* spectra, while combination *i* yields isotropic peaks corresponding to a tightly *J*-coupled *AB* spin pair (*i.e.*, the *J*-coupling is significant compared to the isotropic chemical shift difference between the coupled nuclei). Using the *J*-coupling data in Table 6.2 and the appropriate chemical shifts, either of the three possible spin-pair combinations will yield a simulated spectrum that has peaks at the frequencies observed in the spectrum acquired at 9.4 T. However, only by assuming that the spin pairs are tightly *J*-coupled (combination *i*) is it possible to obtain a calculated spectrum with intensities that are similar to those of the experimental spectrum, as illustrated in Figure 6.6. The isotropic chemical shifts obtained from this simulation are summarized in Table 6.1. The combination of *J*-coupling and chemical shift differences leads to a fortuitous overlap of the multiplet peaks from C_C and C_D for the spectrum acquired at 9.4 T. The smaller chemical shift difference (in frequency units) for the spectrum acquired at 4.7 T yields a spectrum for

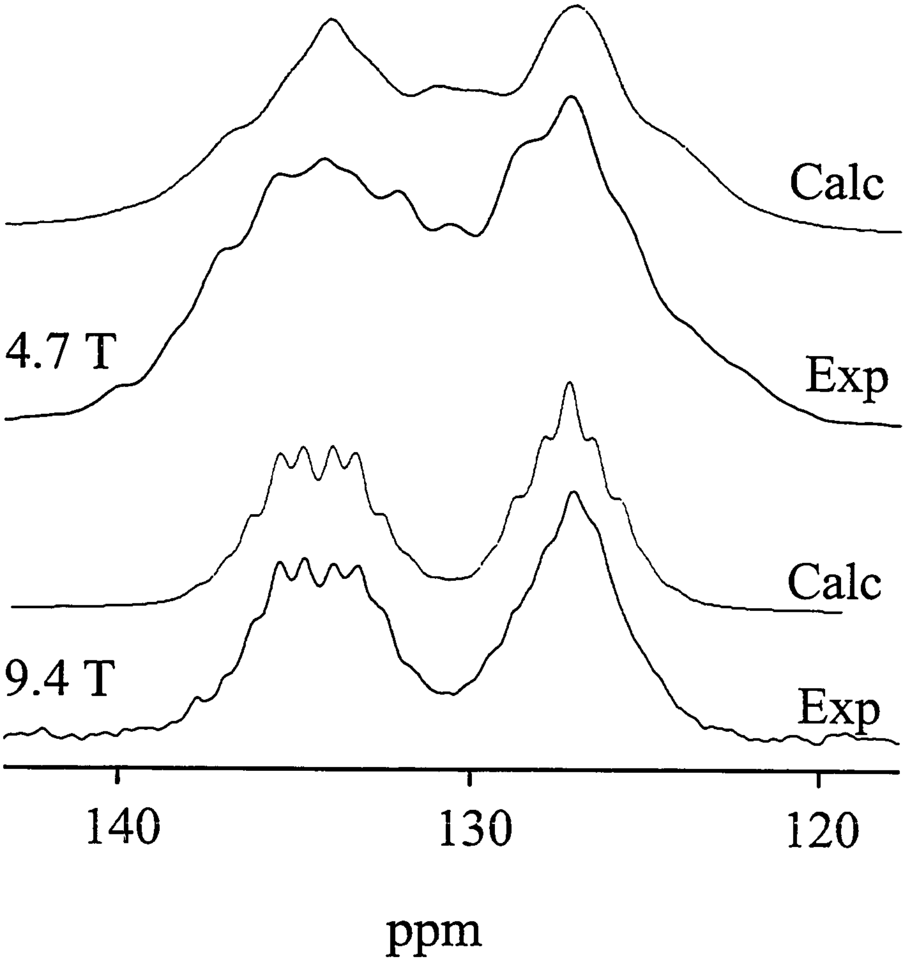

Figure 6.6 Experimental and calculated isotropic region of the ^{13}C NMR spectra of MAS samples of Pt(η^2-diphenylacetylene-1,2-$^{13}C_2$)(PPh$_3$)$_2$, at 4.7 T with ν_{rot} = 5 kHz or at 9.4 T with ν_{rot} = 8 kHz. 16 and 108 transients, respectively, were added for spectra acquired at 4.7 and 9.4 T.

which specific transitions are not resolved; the calculated spectrum shown here is that obtained using the parameters from the fit to the spectrum obtained at 9.4 T.

The spectra of MAS samples do not exhibit significant spinning-frequency dependence. This is consistent with the assignment of spin pairs cited above: these are approaching A_2 spin systems, for which a single transition, and hence no spinning-frequency dependence, is expected (Section 2.4.2).

Comparison of δ_{iso} for DPA with those for PtDPA (Table 6.1) shows that the isotropic shielding of the alkynyl carbon nuclei decreases significantly upon coordination of DPA with platinum, consistent with trends observed from solution NMR studies of metal-acetylene complexes.[12] A comparison of the individual tensor components follows the discussion of the CS tensor orientation below.

Two-dimensional NMR experiments (COSY[300] and SECSY[301]) were attempted to confirm the assignment of the chemical shifts as discussed above, but were inconclusive. In view of the discrepancies in the spectrum acquired at 4.7 T, the assignment of the chemical shifts for the spin pairs as discussed above must be regarded as tentative. Nevertheless, the chemical shifts for the four alkynyl carbon sites are certain to within 1 ppm. In general, the effects of $^{1}J(^{13}C,^{13}C)$ are not resolved in spectra of stationary samples. Hence, tentative conclusions about the magnitudes of the indirect coupling interactions do not affect analysis of the stationary spectra, discussed below. It is possible to simulate the spectra of a stationary sample of PtDPA with any of the three possible spin pair combinations discussed above; the principal components and their orientations relative to the $^{13}C,^{13}C$ dipolar vector are similar in all cases. In the ensuing discussion, it will be assumed that case (*i*) prevails.

6.3.4 Carbon-13 NMR Spectra of Stationary Samples of Pt(η^2-diphenylacetylene-1,2-$^{13}C_2$)(PPh_3)$_2$

The calculated and experimental ^{13}C NMR spectra of stationary samples of $^{13}C_2$-labelled samples of PtDPA are shown in Figure 6.7. Since the program used for the simulation can only calculate spectra for dipolar-coupled spin pairs, separate simulations were done for the two spin pairs (C_A,C_B and C_C,C_D) using the isotropic chemical shifts listed in Table 6.1; the two spectra were added to yield the calculated spectra shown in Figure 6.7. The data derived from the simulation of the experimental spectra are summarized in Table 6.1. The simulation of the experimental spectra was undertaken with the assumption that the four carbon nuclei are in similar environments; hence the CS tensors are not expected to be significantly different.

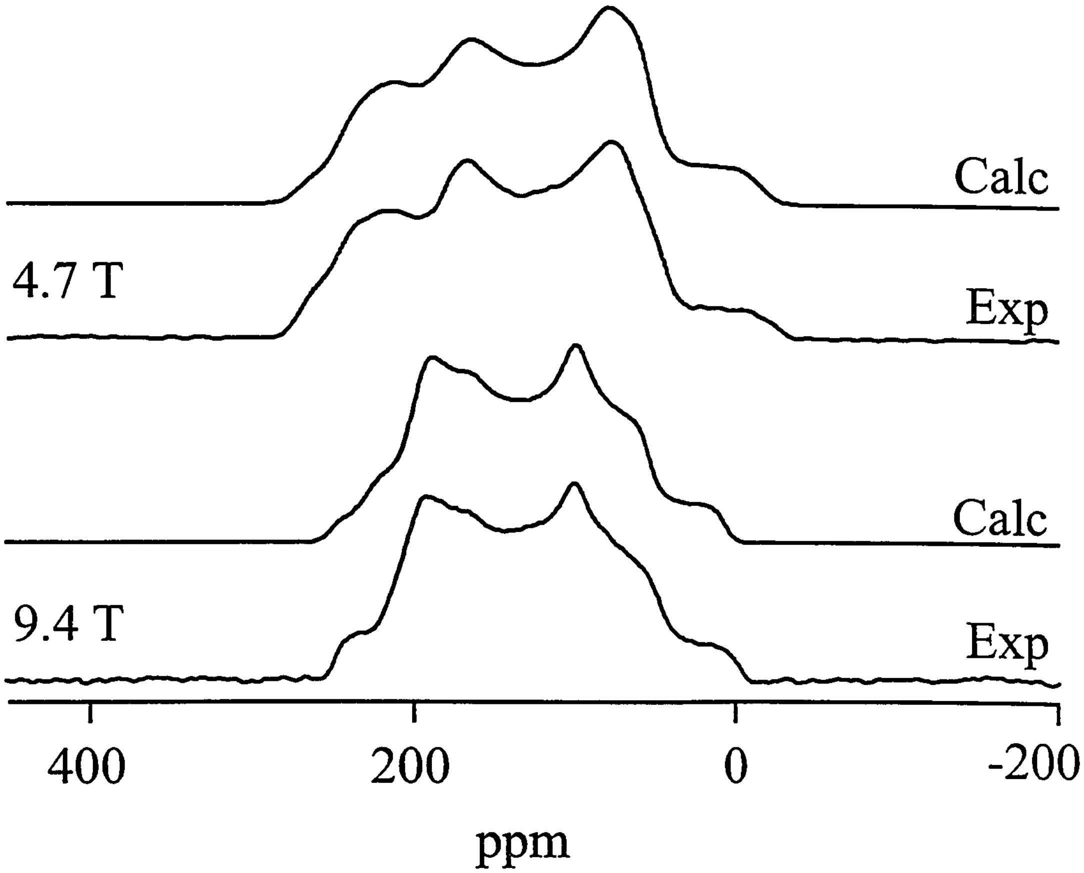

Figure 6.7 Calculated and experimental ^{13}C NMR spectra of stationary samples of Pt(η^2-diphenylacetylene-1,2-$^{13}C_2$)(PPh_3)$_2$. 1076 and 1176 transients were added for spectra acquired at 4.7 and 9.4 T, respectively.

Spectra of stationary powder samples were simulated with $R_{\text{eff}} = 3100 \pm 50$ Hz, which, assuming ΔJ is negligible (Section 2.1.4), corresponds to $r_{\text{CC}} = 1.35 \pm 0.01$ Å. This is within error of the value reported by Glanville and coworkers,[291] $r_{\text{CC}} = 1.32 \pm 0.09$ Å. In comparing the value of r_{CC} obtained from this study with that reported by Glanville and coworkers, it must be acknowledged that the data reported by the latter are preliminary with a large uncertainty, and that the authors reported only one molecule in the asymmetric unit, contrary to indications from solid-state NMR. Unfortunately, it has not been possible to obtain diffraction data for this complex. Comparable values for r_{CC}, 1.29 ± 0.06 Å, have been reported by Packett and coworkers for the trimethylphosphine derivative of this complex.[31] As discussed previously (Chapter 4), agreement between r_{CC} obtained from diffraction data and from R_{eff} suggest that motion of the ^{13}C,^{13}C dipolar vector is not significant.

Calculation from first principles of the CS tensors for PtDPA have been discussed in Section 3.5.3; for comparison, the data calculated with the cc-pVTZ basis set are included in Table 6.1. Only two carbon sites are predicted since calculations were performed on a single molecule. These calculations are qualitatively in agreement with experiment. In particular, the orientations of the principal components relative to the alkynyl C,C bond are generally in agreement, within error, with experimental values. Hence, orientations for the alkynyl carbon CS tensors are proposed, based on the experimental θ_{ii} and the results of the *ab initio* calculations, as illustrated in Figure 6.8. Since calculations and experiment suggest that the orientations of the CS tensors for all alkynyl carbon sites are similar, a representative alkynyl carbon CS tensor is discussed in the ensuing discussion. The combined experimental/theoretical results show that the direction of greatest shielding is approximately

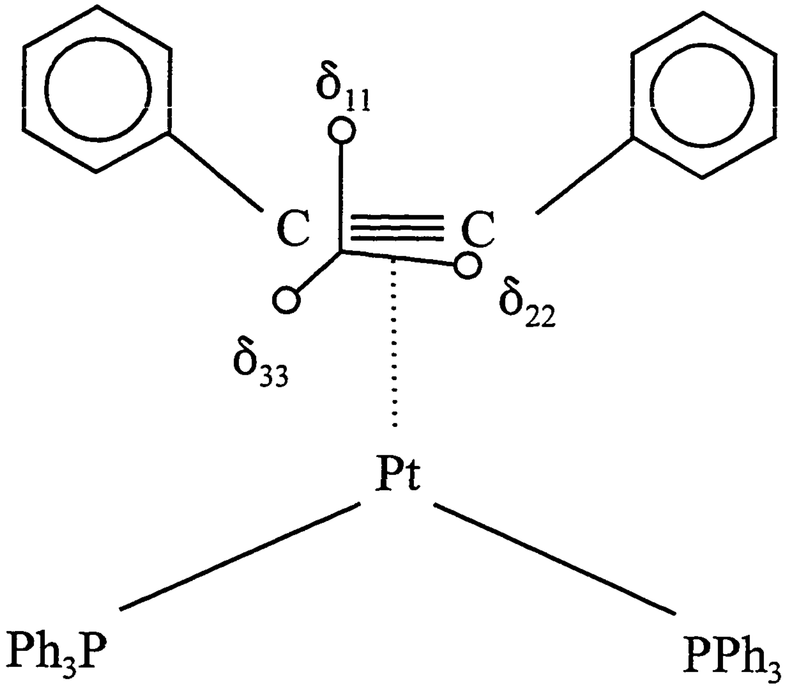

Figure 6.8 Orientations of the alkynyl carbon CS tensors for Pt(η^2-diphenylacetylene)(PPh_3)$_2$. The δ_{33} component is approximately perpendicular to the Pt,C,C plane.

perpendicular to the plane defined by the platinum and alkynyl carbon atoms, δ_{22} is approximately along the alkynyl C,C bond and δ_{33} is approximately perpendicular to this bond, in the plane defined by the alkynyl carbon and platinum atoms.

6.3.5 A Comparison of the Chemical Shift Tensors for Diphenylacetylene and Pt(η^2-Diphenylacetylene)(PPh_3)$_2$.

To compare the alkynyl carbon CS tensors for DPA and PtDPA, the orientations of the tensors must be considered. Since the δ_{11} and δ_{22} components of the alkynyl carbon CS tensor for DPA have similar values, 165 and 147 ppm, they will be considered as equal in the ensuing discussion to facilitate comparison of the magnetic shielding in specific directions. The magnetic shielding in the direction of the C,C bond decreases greatly upon coordination:

δ_{33}(DPA) - δ_{22}(PtDPA) = -184 ppm. The magnetic shielding perpendicular to the plane defined by the platinum and alkynyl carbon atoms increases by approximately 120 ppm, and that in the Pt,C,C plane, perpendicular to the C,C bond, decreases by about 65 ppm. These results again demonstrate the importance of considering orientations when comparing CS tensors; the δ_{22} components for DPA and PtDPA have similar magnitudes but very different orientations relative to the alkynyl C,C bond. The factors thought to give rise to the observed CS tensor for PtDPA are discussed in the following section.

6.3.6 A Comparison of the Chemical Shift Tensors for *trans*-Stilbene and Pt(η^2-Diphenylacetylene)(PPh_3)$_2$.

The orientation of the alkynyl phenyl groups for the DPA ligand of PtDPA are such that the structure approaches that of *cis*-stilbene; the phenyl groups are almost coplanar (Fig. 6.1). Although the alkenyl carbon CS tensors for *cis*-stilbene are not known, they are not expected to be very different from those for *trans*-stilbene (TSB) (Section 5.3.1). For example, the principal components of the carbon CS tensors for *cis* and *trans*-2-butene do not differ by more than 15 ppm and they have the same orientation.[54] Hence, a comparison of the alkenyl carbon CS tensors for TSB and the alkynyl carbon CS tensors for PtDPA is very instructive. The average values for the principal components of the alkynyl carbon CS tensors for PtDPA, δ_{11} = 221 ppm, δ_{22} = 142 ppm and δ_{33} = 29 ppm, are similar to those measured for uncoordinated TSB: δ_{11} = 215 ppm, δ_{22} = 120 ppm and δ_{33} = 39 ppm. The alkynyl carbon CS tensor orientation for PtDPA (Fig. 6.8) is also similar to that for the alkenyl carbon CS tensor for TSB (Fig. 5.5): δ_{11} is approximately in the plane defined by the phenyl groups and the alkenyl or alkynyl carbon atoms, δ_{22} is approximately along the C,C bond and δ_{33} is approximately perpendicular to the aforementioned plane.

Although there is some uncertainly about the structure of PtDPA, the alkynyl carbon CS tensors are consistent with the suggestion that the structure of an alkynyl ligand coordinated with a metal is affected to a greater extent than is that of an alkenyl ligand.[2] It is also noted that the value of $^{1}J(^{13}C,^{13}C)$ for PtDPA in solution, 85.7 Hz, is not much greater than the corresponding value for TSB, 72.9 Hz.[302]

The effect on the carbon CS tensors of coordination with platinum has been discussed in terms of Ramsey's theory (Section 3.2).[184] The deshielding in the direction of the C,C bond of DPA following coordination with Pt(0) reflects the less symmetrical environment about the alkynyl carbon nuclei of PtDPA. For *trans*-stilbene, the deshielding in this direction has been attributed to low-lying σ^* and π^* MOs mixing with occupied π and σ MOs, respectively (Section 5.3.4). In light of the similar carbon CS tensors and the similar geometry about the unsaturated carbon nuclei of the two compounds, it is tempting to attribute the observed carbon CS tensor for PtDPA to a similar mixing of MOs, but it is acknowledged that the electronic structure of PtDPA is more complicated. A detailed computational study of the MOs giving rise to the observed shielding would be instructive, but is not practical at this time (see Section 7.3).

6.4 Summary

The alkynyl carbon chemical shift tensors for diphenylacetylene and Pt(η^2-diphenylacetylene)$(PPh_3)_2$ have been characterized by ^{13}C and ^{31}P NMR spectroscopy of samples in the solid state and dissolved in CD_2Cl_2 as well as by *ab initio* calculations. The alkynyl carbon CS tensors for DPA are similar to those for 2-butyne, but the phenyl groups break the degeneracy in the components perpendicular to the C,C bond. Fine structure in the spectra of MAS samples of PtDPA are attributed to a fortuitous overlap of peaks from four non-equivalent carbon sites. Orientations for the carbon CS tensors have been proposed, based on a combined experimental/theoretical approach. The magnitudes and orientations of the alkynyl carbon CS tensors for PtDPA are similar to those for *trans*-stilbene.

Chapter 7

Proposed Future Studies

7.1 Further Studies of Platinum Complexes.

The investigation of alkenyl carbon chemical shift tensors reported in this thesis, combined with those of Gay and Young,[57] and of Oldfield *et al.*,[58] represent a significant body of solid-state NMR data on platinum-alkene complexes. Extensions of this work might be considered if unique systems can be studied (*vide infra*) or if the carbon CS tensors can be characterized more fully with a single-crystal NMR experiment. Growing single crystals of these complexes suitable for NMR studies is difficult. In fact, despite requiring much smaller crystals for diffraction studies, the structures of some of the complexes investigated in this thesis have not been fully characterized, probably because of difficulties in growing even small single crystals. Analyzing single crystals with NMR of a dilute spin such as ^{13}C is particularly difficult; labelling enhances the signal intensity greatly, but introduces complications because of inter- and intramolecular dipolar coupling.

Coordination of Pt(0) with fullerenes, $Pt(\eta^2\text{-}C_{60})(PPh_3)_2$, (Figure 7.1) has been described.[303,304] The synthesis is straightforward: C_{60} exchanges with the ethylene ligand of $Pt(C_2H_4)(PPh_3)_2$.[304] An alternate synthesis entails the displacement of HCl from $HPtCl(PPh_3)_2$.[305] The preparation of a sample that is ^{13}C-labelled at the sites of platinum coordination is impractical, precluding a study of the carbon CS tensor by the dipolar-chemical shift method. However, our lab has acquired a sample of $^{13}C_{60}$. Analysis of $Pt(\eta^2\text{-}^{13}C_{60})(PPh_3)_2$ by MAS NMR can offer some valuable insight into the nature of the magnetic shielding of the directly bonded and more distant carbon nuclei in this unique platinum complex.

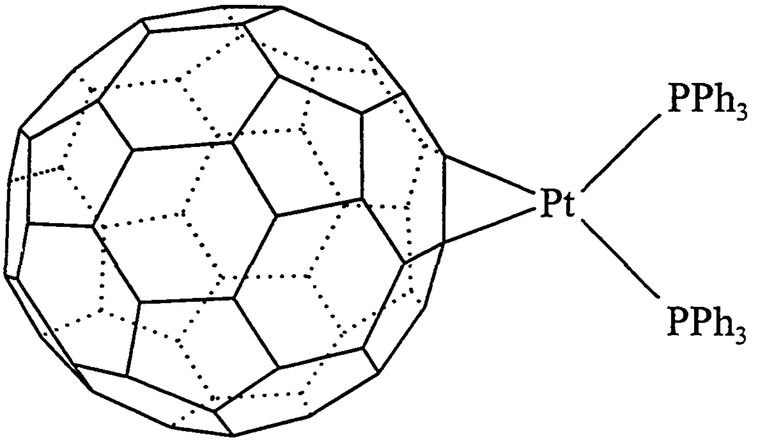

Figure 7.1 Molecular structure of Pt(η^2-C_{60})(PPh_3)$_2$. From reference 303.

7.2 Solid-State NMR Studies of Other Metal-Alkene and Metal-Alkyne Complexes

Since the principal components of several platinum-alkene complexes have been characterized, an extension of this work is the investigation of unsaturated carbon ligands coordinated with related metal centres. It is not practical to summarize the numerous possible syntheses of η^2-coordinated alkenes and alkynes; a few examples are given below. The synthesis of nickel complexes of alkenes[306,307] and alkynes[308] have been reviewed. Likewise, the preparation of palladium-alkene[307] and alkyne[308] complexes have been described. The preparation of group 9 alkene complexes has been reviewed by Komiya and Fukuoka.[309]

The calculation from first principles of the magnetic shielding tensor for Ni(C_2H_4)(PPh_3)$_2$, discussed in Section 3.5.2, suggests a unique orientation for the alkenyl carbon magnetic shielding tensor. Unfortunately, the dipolar-chemical shift method will not confirm whether the δ_{11} and δ_{33} components are interchanged, since the predicted orientation has both components perpendicular to the C,C bond. Nevertheless, the characterization of the principal components for this complex would be a valuable complement to the data for the platinum-ethylene complexes, since the structures of the complexes are comparable, and the metals both formally have d^{10} electronic configurations. Preparation of the $^{13}C_2$-labelled sample of $Ni(C_2H_4)(PPh_3)_2$ entails the preparation of $Ni(^{13}C_2H_4)_3$ from Ni(cyclododecatriene).[306] The latter, if not commercially available, may be prepared by reduction of nickel acetylacetonate with diethylaluminum ethoxide.[306] A benefit of this synthesis is that it may be possible to investigate the intermediate product, $Ni(^{13}C_2H_4)_3$, before the synthesis of $Ni(^{13}C_2H_4)(PPh_3)_2$, although the $^{13}C,^{13}C$ dipolar interaction from other ethylene ligands on the molecule may complicate the spectra. The preparation of $Pd(\eta^2\text{-}C_2H_4)(PPh_3)_2$ has also been described. The procedure entails the reduction of $Pd(acac)_2$ with $AlEt_2(OEt)$ in the presence of ethylene.[310]

A related series of compounds which have not been investigated by solid-state NMR are η^3-allyl metal complexes. The preparation of $Ni(\eta^3\text{-}C_3H_5)_2$ has been described.[311] Because of the absence of other carbon atoms in this molecule, it may be possible to obtain spectra of MAS samples suitable for analysis using the method of Herzfeld and Berger.[118] However, because of the low melting point, 0° C, acquisition of NMR spectra would have to be undertaken at low temperatures. The preparation of a similar palladium complex has also been described.[312]

7.3 Further Computational Studies

Calculation of magnetic shielding tensors from first principles for large organometallic complexes is a fairly recent application of computational NMR. Hence, numerous extensions of the work summarized in Chapter 3 are suggested. Higher-level calculations should be undertaken when feasible to establish whether the basis set limit is approached by the data presented here. The options currently available to the computational chemist are extensive. A detailed investigation of the most effective and efficient technique for the calculation of magnetic shielding tensors for large molecules was not practical at the onset of this project but would be very useful. For example, is the CSGT method more efficient than GIAO, and if so, does it yield more accurate results? Likewise, the choice of functionals for DFT calculations warrants a careful investigation.

In general, only qualitative discussions about the factors responsible for the observed magnetic shielding properties are possible at this time. A quantitative description of the MOs involved in magnetic shielding is in principle available from the calculations. Wiberg and coworkers have presented calculated data on several small molecules, including acetylene, in which the contributions to the calculated magnetic shielding tensor components are assessed on an MO by MO basis.[195] Unfortunately, calculations were performed with a development version of Gaussian which is not yet commercially available. Calculations performed using the IGLO method also provides a breakdown of orbital contributions to magnetic shielding;[196] calculations using IGLO are not currently possible with the programs available in the lab.

Chapter 8

Concluding Remarks

The principal components of the alkenyl and alkynyl carbon chemical shift tensors for some platinum complexes have been characterized by solid-state ^{13}C NMR spectroscopy. Orientations for these components relative to the $^{13}C,^{13}C$ dipolar vector have been determined. Orientations for the chemical shift tensors in the molecular framework have been proposed, based on a combination of experimental results and calculations of the carbon CS tensors from first principles. The internal dynamics for the ethylene moiety in Zeise's salt and $Pt(C_2H_4)(PPh_3)_2$ have been investigated by ^2H NMR; the results indicate that motion of the ethylene ligand is not significant in the solid state, a conclusion that is supported by *ab initio* calculations.

The numerous interactions that must be considered when examining solid samples, discussed in Chapter 2, complicate NMR spectra greatly. For this reason, solid samples are not examined routinely by NMR. The work presented in this thesis demonstrates that, rather than being a hindrance, the interactions that are manifested in the NMR spectra of solid samples contain a wealth of information about fundamental molecular properties. By determining chemical shift tensors and their orientations in the molecular framework, it was possible to assess the effect on the carbon magnetic shielding of coordination with platinum. The importance of determining the tensor orientations to properly interpret magnetic shielding has been demonstrated.

Despite the difficulties inherent in the calculation of CS tensors for large molecules, the combination of experimental and theoretical methods presented in this thesis provides valuable insight into carbon CS tensors for transition metal-alkene or alkyne complexes. Since the analysis of single crystals usually is not practical for organometallic complexes, computational techniques, along with the constraints imposed by the experimental results, offer the most information about the carbon CS tensors. The work presented in this thesis spans approximately three years. In that time, the capacity of computers has grown such that calculations that were very challenging at the start of this project are now performed routinely in this and many other labs. Hence, it is felt that the elucidation of CS tensors using the combined experimental/theoretical approach outlined in this thesis is a viable method of characterizing CS tensors as fully as possible.

Appendix

A.1 Stationary Powder NMR Line Shapes For an A_2 Spin System: Diphenylacetylene-1,2-$^{13}C_2$

The powder NMR line shape for diphenylacetylene-1,2-$^{13}C_2$ (DPA) exhibits some unusual features (Figure 6.2). To understand these line shapes, it is useful to consider the data in frequency units with an isotropic frequency $\nu_{iso} = 0$. Since the alkynyl ^{13}C nuclei of DPA are related to each other by a centre of inversion, they comprise an A_2 spin system and hence $\nu_A = \nu_B$ for all orientations of the crystallites in the applied magnetic field. For an A_2 spin system, J_{iso} does not contribute to the line shape and $d = \pm b$ (eq 2.33). For $d = +b$, $P_1 = P_4 = 0$ (eqs 2.27 and 2.30) and the spectrum is described by two transitions, ν_2 and ν_3; the same result obtains for $d = -b$ since in that case $\nu_1 = \nu_3$ and $\nu_4 = \nu_2$. The spectrum may thus be described by ν_2 and ν_3 (eqs 2.28 and 2.29), which may be simplified:

$$\nu_2 = \nu_A + \frac{3}{4}R_{eff}(3\cos^2\zeta - 1) \qquad \text{A.1}$$

and

$$\nu_3 = \nu_A - \frac{3}{4}R_{eff}(3\cos^2\zeta - 1) \qquad \text{A.2}$$

Recalling that $R_{eff} = 4.025$ kHz and that $\zeta = 90°$ for ν_{11} and ν_{22}, and 0° for ν_{33}, the transition frequencies for crystallites oriented such that the principal components of the CS tensor are parallel to $\mathbf{B}_0$ may be calculated with eqs A.1 and A.2. Table A.1 summarizes the transition frequencies in the directions of the principal components for the spectra acquired at 4.7 and 9.4 T. Figure A.1 illustrates the calculated transitions for the ^{13}C NMR spectrum of DPA acquired at 4.7 T. Since $P_2 = P_3$, the transitions have equal intensities, but the much smaller span of ν_2 compared to ν_3 results in an almost isotropic peak for the former. The sum of these subspectra (Figure A.1, upper trace) represents the total spectrum, shown here without line broadening. Table A.1 also includes the transition frequencies expected for diphenylacetylene-1,2-$^{13}C_2$ acquired at 2.35 T to demonstrate an interesting property of dipolar coupled NMR spectra. Because $R_{eff}(^{13}C,^{13}C)$ is independent of the applied field strength, at 2.35 T this interaction would dominate the spectrum and the sense of ν_2 would be reversed so that the transition frequency in the most shielded direction actually appears at the highest frequency. Of course the magnetic shielding properties are unchanged: the positive value for ν_2 in the direction of the C,C bond is offset by the relatively large negative value for ν_3. A similar analysis for an *AX* spin system has been reported by Harris and coworkers.[313]

Table A.1 Transition Frequencies in the Directions of the Principal Components of the Alkynyl Carbon CS Tensor for Diphenylacetylene.

	2.35 T		4.7 T		9.4 T	
	ν_2/kHz	ν_3/kHz	ν_2/kHz	ν_3/kHz	ν_2/kHz	ν_2/kHz
ν_{iso}	0	0	0	0	0	0
ν_{11}	-1.1	4.9	0.7	6.8	4.5	10.5
ν_{22}	-1.6	4.4	-0.2	5.9	2.7	8.7
ν_{33}	2.7	-9.3	-0.5	-12.7	-7.2	-19.2

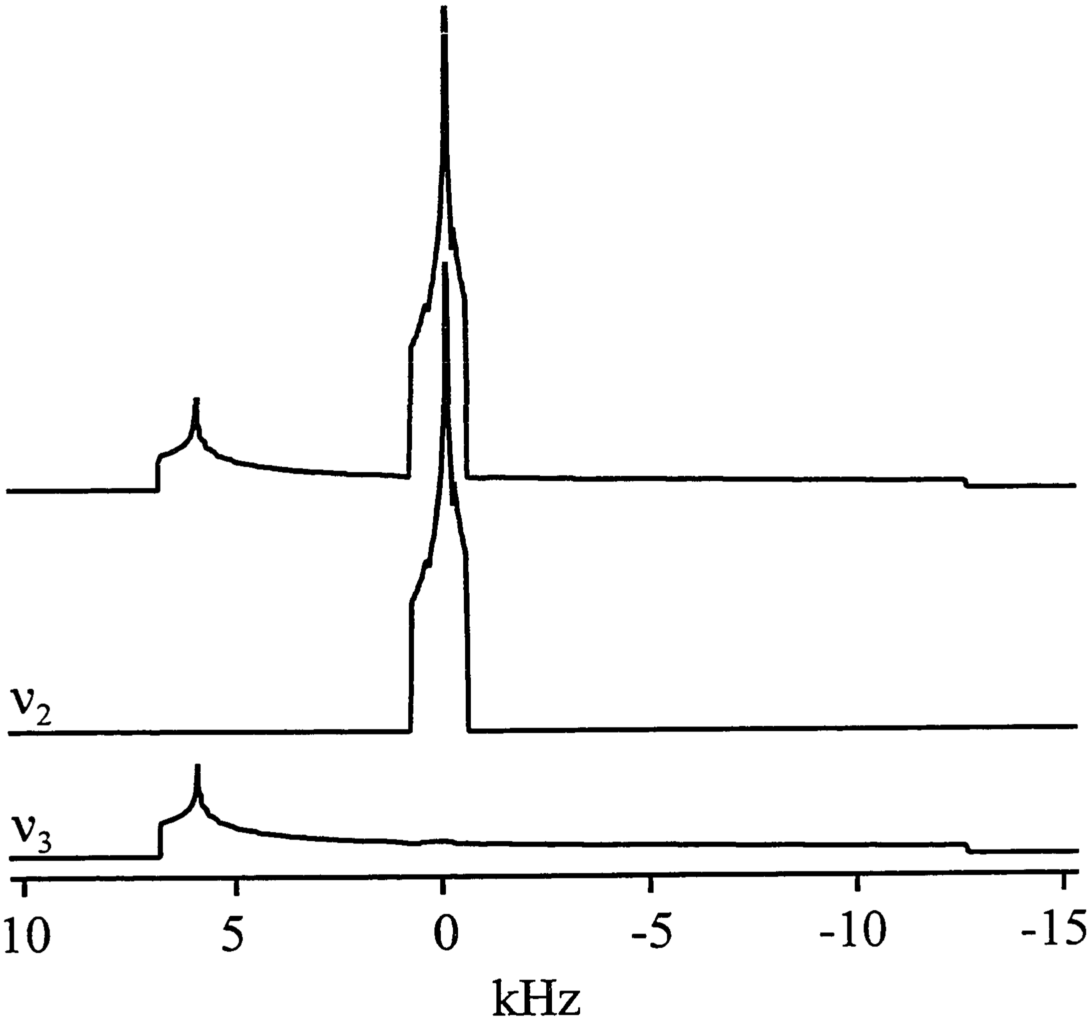

Figure A.1 Calculated transitions for the ^{13}C NMR spectrum of solid diphenylacetylene at 4.7 T. The upper trace is the sum of transitions ν_2 and ν_3.

References

1. F. R. Hartley, in *Comprehensive Organometallic Chemistry.* Edited by G. Wilkinson, Pergamon Press: Oxford, 1982, Vol. 6, p. 471.

2. F. A. Cotton and G. Wilkinson, *Advanced Inorganic Chemistry*, 5th Ed. John Wiley and Sons: New York, 1988.

3. J. E. Huheey, E. A. Keiter and R. L. Keiter, *Inorganic Chemistry*, 4th Ed. HarperCollins College Publishers: New York, 1993, p. 662.

4. G. B. Young, in *Comprehensive Organometallic Chemistry II.* Edited by E. W. Abel, F. G. A. Stone, G. Wilkinson and R. J. Puddephatt, Pergamon Press: New York, 1995, Vol. 9, p. 533.

5. *NMR and the Periodic Table.* Edited by R. K. Harris and B. E. Mann, Academic Press: London, 1978.

6. *The Multinuclear Approach to NMR Spectroscopy.* Edited by J. B. Lambert and F. G. Riddell, D. Reidel Publishing: Dordrecht, 1983.

7. *NMR of Newly Accessible Nuclei.* Edited by P. Laszlo, Academic Press: New York, 1983, Vols 1 and 2.

8. *Multinuclear NMR.* Edited by J. Mason, Plenum Press: New York, 1987.

9. *Transition Metal Nuclear Magnetic Resonance.* Edited by P. S. Pregosin, Elsevier: Amsterdam, 1991.

10. *Advanced Applications of NMR to Organometallic Chemistry.* Edited by M. Gielen, R. Willem and B. Wrackmeyer, John Wiley and Sons: Chichester, 1996.

11. D. A. Ganson and W. D. Vernon, in *Topics in Carbon-13 NMR Spectroscopy.* Edited by G. C. Levy, John Wiley and Sons: New York, 1976, Vol. 2, p. 270.

12. B. E. Mann and B. F. Taylor, *^{13}C NMR Data for Organometallic Compounds.* Academic Press: London, 1981.

13. P. W. Jolly and R. Mynott, *Adv. Organomet. Chem.* **19**, 257 (1981).

14. M. Mehring, *Principles of High Resolution NMR in Solids*, 2nd Ed. Springer-Verlag: Berlin, 1983.

15. B. C. Gerstein and C. R. Dybowski, *Transient Techniques in NMR of Solids.* Academic Press: Orlando, 1985.

16. C. A. Fyfe, *Solid State NMR for Chemists*. C.F.C. Press: Guelph, 1983.

17. E. O. Stejskal and J. D. Memory, *High Resolution NMR in the Solid State*. Oxford University Press: New York, 1994.

18. For continuity, the terms alkenyl and alkynyl are used to describe both coordinated and uncoordinated ligands, although in the former case this does not correspond to a strict definition of the terms.

19. (a) W. C. Zeise, *Pogg. Ann. Phys.* **9**, 632 (1827). (b) W. C. Zeise, *Pogg. Ann. Phys.* **21**, 497 (1831). (c) For a discussion of the work of W.C. Zeise, including an English-language translation of ref. (b), see: G. B. Kaufman, *Classics in Coordination Chemistry*, Part 2: Selected Papers. Dover Publications: New York, 1976, p. 17. References (a) and (b) are cited from this text.

20. W. C. Zeise, *Pogg. Ann. Phys.* **40**, 250 (1837), *c.f.* reference 19c.

21. A. Dedieu, *Chem. Rev.* **100**, 543 (2000).

22. G. Frenking and N. Fröhlich, *Chem. Rev.* **100**, 717 (2000).

23. See references 1 and 4 for a compilation of structural data and references to the original literature.

24. P.-T. Cheng and S. C. Nyburg, *Can. J. Chem.* **50**, 912 (1972).

25. J. L. Duncan, *Mol. Phys.* **28**, 1177 (1974).

26. E. Hirota, Y. Endo, S. Saito and J. L. Duncan, *J. Mol. Spectrosc.* **89**, 285 (1981).

27. R. A. Love, T. F. Koetzle, G. J. B. Williams, L. C. Andrews and R. Bau, *Inorg. Chem.* **14**, 2653 (1975).

28. (a) M. J. S. Dewar, *Bull. Soc. Chim. Fr.* **18**, C71 (1951). (b) J. Chatt and L. A. Duncanson, *J. Chem. Soc.* 2939 (1953).

29. S. Strömberg, M. Svensson and K. Zetterberg, *Organometallics*, **16**, 3165 (1997).

30. N. Rösch and R. Hoffmann, *Inorg. Chem.* **13**, 2656 (1974).

31. D. L. Packettt, A. Syed and W. C. Trogler, *Organometallics*, **7**, 159 (1988).

32. A. Mavridis and I. Moustakali-Mavridis, *Acta Crystallogr.* **B33**, 3612 (1977).

33. J. A. Bouwstra, A. Schouten and J. Kroon, *Acta Crystallogr.* **C40**, 428 (1984).

34. J. B. Stothers, *Carbon-13 NMR Spectroscopy*. Academic Press: New York, 1972.

35. E. Breitmaier and W. Voelter, *Carbon-13 NMR Spectroscopy*, 3rd Ed. VCH: Weinheim, 1987, p. 293.

36. H.-O. Kalinowski, S. Berger and S. Braun, *Carbon-13 NMR Spectroscopy*. John Wiley and Sons: Chichester, 1988, p. 250.

37. K. Pihlaja and E. Kleinpeter, *Carbon-13 NMR Chemical Shifts in Structural and Steroechemical Analysis*. VCH Publishers: New York, 1994, p. 327.

38. M. H. Chisholm, H. C. Clark, L. E. Manzer and J. B. Stothers, *J. Am. Chem. Soc.* **94**, 5087 (1972).

39. See reference 35, p. 192.

40. M. Green, J. A. K. Howard, J. L. Spencer and F. G. A. Stone, *J. Chem. Soc., Dalton Trans.* 271 (1977).

41. N. C. Harrison, M. Murray, J. L. Spencer and F. G. A. Stone, *J. Chem. Soc., Dalton Trans.* 1337 (1978).

42. B. Wrackmeyer, *Z. Naturforsch.* **52b**, 1019 (1997).

43. M. A. M. Meester, D. J. Stufkens and K. Vrieze, *Inorg. Chim. Acta*, **21**, 251 (1977).

44. (a) L. F. Farnell, E. W. Randall and E. Rosenberg, *Chem. Commun.* 1078 (1971). (b) D. G. Cooper and J. Powell, *Inorg. Chem.* **15**, 1959 (1976). (c) M. A. M. Meester, D. J. Stufkens and K. Vrieze, *Inorg. Chim. Acta*, **16**, 191 (1976).

45. P. E. Hansen, O. K. Poulsen and A. Berg, *Org. Magn. Reson.* **8**, 632 (1976).

46. P. A. Chaloner, S. E. Davies and P. B. Hitchcock, *Polyhedron*, **16**, 765 (1997).

47. A. Kumar, J. D. Lichtenhan, S. C. Critchlow, B. E. Eichinger and W. T. Borden, *J. Am. Chem. Soc.* **112**, 5633 (1990).

48. E. Breitmaier and W. Voelter, *^{13}C NMR Spectroscopy*. Verlag Chemie: Weinheim, 1974, p. 129.

49. A. Bax and R. Freeman, *J. Magn. Reson.* **45**, 177 (1981).

50. J. Kaski, P. Lantto, J. Vaara and J. Jokisaari, *J. Am. Chem. Soc.* **120**, 3993 (1998).

51. G. Pellizer, M. Graziani, M. Lenarda and B. T. Heaton, *Polyhedron*, **2**, 657 (1983).

52. A. Olsson and P. Kofod, *Inorg. Chem.* **31**, 183 (1992).

53. T. M. Duncan, *A Compilation of Chemical Shift Anisotropies*. Farragut Press: Chicago, 1994, p. C-1.

54. K. W. Zilm, R. T. Conlin, D. M. Grant and J. Michl, *J. Am. Chem. Soc.* **102**, 6672 (1980).

55. K. W. Zilm and D. M. Grant, *J. Am. Chem. Soc.* **103**, 2913 (1981).

56. A. M. Orendt, J. C. Facelli, A. J. Beeler, K. Reuter, W. J. Horton, P. Cutts, D. M. Grant and J. Michl, *J. Am. Chem. Soc.* **110**, 3386 (1988).

57. I. D. Gay and G. B. Young, *Organometallics* **15**, 2264 (1996).

58. R. Havlin, M. McMahon, R. Srinivasan, H. Le and E. Oldfield, *J. Phys. Chem. A*, **101**, 8908 (1997).

59. G. M. Wallraff, Ph.D. Thesis, University of Utah, 1985.

60. Y. Huang, D. F. R. Gilson and I. S. Butler, *J. Chem. Soc., Dalton Trans.* 2881 (1992).

61. S. Ding and C. A. McDowell, *Chem. Phys. Lett.* **268**, 194 (1997).

62. P. J. J. A. Timmermans, A. Mackor, A. L. Spek and B. Kojić-Prodić, *J. Organomet. Chem.* **276**, 287 (1984).

63. J. H. van den Hende and W. C. Baird, Jr. *J. Am. Chem. Soc.* **85**, 1009 (1963).

64. A. Albinati, S. V. Meille and G. Carturan, *J. Organomet. Chem.* **182**, 269 (1979).

65. A. Pines, M. G. Gibby and J. S. Waugh, *Chem. Phys. Lett.* **15**, 373 (1972).

66. K. W. Zilm, A. J. Beeler, D. M. Grant, J. Michl, T.-C. Chou and E. L. Allred, *J. Am. Chem. Soc.* **103**, 2119 (1981).

67. D. B. Chesnut and D. W. Wright, *J. Comp. Chem.* **12**, 546 (1991).

68. P. Pyykkö and J.-P. Desclaux, *Acc. Chem. Res.* **12**, 276 (1979).

69. P. Pyykkö, *Chem. Rev.* **88**, 563 (1988).

70. J. Li, G. Schreckenbach and T. Ziegler, *Inorg. Chem.* **34**, 3245 (1995).

71. M. Kaupp, V. G. Malkin, O. L. Malkina and D. R. Salahub, *J. Am. Chem. Soc.* **117**, 1851 (1995).

72. M. Kaupp, O. L. Malkina and V. G. Malkin, *J. Chem. Phys.* **106**, 9201 (1997).

73. A. J. Beeler, A. M. Orendt, D. M. Grant, P. W. Cutts, J. Michl, K. W. Zilm, J. W. Downing, J. C. Facelli, M. S. Schindler and W. Kutzelnigg, *J. Am. Chem. Soc.* **106**, 7672 (1984).

74. A. M. Orendt, J. C. Facelli, Y. J. Jiang and D. M. Grant, *J. Phys. Chem. A*, **102**, 7692 (1998).

75. H. Strub, A. J. Beeler, D. M. Grant, J. Michl, P. W. Cutts and K. W. Zilm, *J. Am. Chem. Soc.* **105**, 3333 (1983).

76. D. E. Wemmer and A. Pines, *J. Am. Chem. Soc.* **103**, 34 (1981).

77. C. D. Hughes, M. H. Sherwood, D. W. Alderman and D. M. Grant, *J. Magn. Reson. A*, **102**, 58 (1993).

78. K. J. Hallock, D. K. Lee and A. Ramamoorthy, *Chem. Phys. Lett.* **302**, 175 (1999).

79. M. Linder, A. Höhener and R. R. Ernst, *J. Magn. Reson.* **35**, 379 (1979).

80. M. M. Maricq, J. S. Waugh, J. L. Fletcher and M. J. McGlinchey, *J. Am. Chem. Soc.* **100**, 6902 (1978).

81. S. Pausak, J. Tegenfeldt and J. S. Waugh, *J. Chem. Phys.* **61**, 1338 (1974).

82. D.E. Wemmer, D. J. Ruben and A. Pines, *J. Am. Chem. Soc.* **103**, 28 (1981).

83. M. M. Maricq and J. S. Waugh, *J. Chem. Phys.* **70**, 3300 (1979).

84. T.C. Farrar and E. D. Becker, *Pulse Fourier Transform NMR*. Academic Press: New York, 1971.

85. R. K. Harris, *Nuclear Magnetic Resonance Spectroscopy*. John Wiley and Sons: New York, 1986.

86. S. W. Homans, *A Dictionary of Concepts in NMR*. Clarendon Press: Oxford, 1993.

87. H. Günther, *NMR Spectroscopy*, 2nd Ed. John Wiley and Sons: Chichester (1995).

88. K. Schmidt-Rohr and H. W. Spiess, *Multidimensional Solid-State NMR and Polymers*. Academic Press: London, 1994.

89. T. D. W. Claridge, *High-Resolution NMR Techniques in Organic Chemistry.* Pergamon: Amsterdam, 1999.

90. J. W. Akitt and B. E. Mann, *NMR and Chemistry*, 4th Ed. Stanley Thornes Ltd.: Cheltenham, UK, 2000.

91. A. Abragam, *The Principles of Nuclear Magnetism.* Oxford University Press: Glasgow, 1961.

92. C. P. Slichter, *Principles of Magnetic Resonance*, 3rd Ed. Springer-Verlag: Berlin, 1990.

93. J. A. Ripmeester and C. I. Ratcliffe, in *Comprehensive Supramolecular Chemistry.* Edited by J. L. Atwood, J. E. D. Davies, D. D. MacNicol, F. Vögtle, J.-M. Lehn and J. A. Ripmeester, Elsevier: Oxford, 1996, Vol. 8, p. 323.

94. F. A. L. Anet and D. J. O'Leary, *Concepts Magn. Reson.* **3**, 193 (1991).

95. U. Haeberlen, in *Advances in Magnetic Resonance.* Edited by J. S. Waugh, Academic Press: New York, 1976, Supplement 1.

96. F. A. L. Anet and D. J. O'Leary, *Concepts Magn. Reson.* **4**, 35 (1992).

97. M. Mehring, *NMR Basic Princ. Prog.* **11**, 1 (1976).

98. M. A. Kennedy and P. D. Ellis, *Concepts Magn. Reson.* **1**, 35 (1989).

99. M. A. Kennedy and P. D. Ellis, *Concepts Magn. Reson.* **1**, 109 (1989).

100. R. J. Iuliucci, C. G. Phung, J. C. Facelli and D. M. Grant, *J. Am. Chem. Soc.* **118**, 4880 (1996).

101. R. J. Iuliucci, C. G. Phung, J. C. Facelli and D. M. Grant, *J. Am. Chem. Soc.* **120**, 9305 (1998).

102. K. Eichele, G. C. Ossenkamp, R. E. Wasylishen and T. S. Cameron, *Inorg. Chem.* **38**, 639 (1999).

103. M. Gee, R. E. Wasylishen, K. Eichele and J. F. Britten, *J. Phys Chem. A*, **104**, 4598 (2000).

104. R. E. Wasylishen, R. D. Curtis, K. Eichele, M. D. Lumsden, G. H. Penner, W. P. Power and G. Wu, in *Nuclear Magnetic Shieldings and Molecular Structure.* Edited by J. A. Tossell, Kluwer Academic Publishers: Dordrecht, 1993, p. 297.

105. D. L. Bryce and R. E. Wasylishen, *J. Am. Chem. Soc.* Submitted (2000).

106. R. E. Wasylishen, in *Encyclopedia of Nuclear Magnetic Resonance*. Edited by D. M. Grant and R. K. Harris, John Wiley and Sons: Chichester, 1996, p. 1685.

107. Y. Ishii, T. Terao and S. Hayashi, *J. Chem. Phys.* **107**, 2760 (1997).

108. J. Kaski, J. Vaara and J. Jokisaari, *J. Am. Chem. Soc.* **118**, 8879 (1996).

109. G. E. Pake, *J. Chem. Phys.* **16**, 327 (1948).

110. M. E. Stoll, R. W. Vaughan, R. B. Saillant and T. Cole, *J. Chem. Phys.* **61**, 2896 (1974).

111. W. P. Power and R. E. Wasylishen, *Ann Rep. NMR Spectrosc.* **23**, 1 (1991).

112. M. H. Cohen and F. Reif, *Solid State Phys.* **5**, 321 (1957).

113. E. A. C. Lucken, *Nuclear Quadrupole Coupling Constants*. Academic Press: London, 1969.

114. C. J. Jameson, in *Encyclopedia of Nuclear Magnetic Resonance*. Edited by D. M. Grant and R. K. Harris, John Wiley and Sons: Chichester, 1996, p. 1273.

115. A. K. Jameson and C. J. Jameson, *Chem. Phys. Lett.* **134**, 461 (1987).

116. For a recent example of the debate over notation, see (a) R. K. Harris, *Solid State Nucl. Magn. Reson.* **10**, 177 (1998); and (b) C. J. Jameson, *Solid State Nucl. Magn. Reson.* **11**, 265 (1998).

117. J. Mason, *Solid State Nucl. Magn. Reson.* **2**, 285 (1993).

118. J. Herzfeld and A. E. Berger, *J. Chem. Phys.* **73**, 6021 (1980).

119. N. J. Clayden, C. M. Dobson, L.-Y. Lian and D. J. Smith, *J. Magn. Reson.* **69**, 476 (1986).

120. G. M. Bernard, G. Wu, M. D. Lumsden, R. E. Wasylishen, N. Maigrot, C. Charrier and F. Mathey, *J. Phys. Chem. A*, **103**, 1029 (1999).

121. M. Gee, R. E. Wasylishen, K. Eichele, G. Wu, T. S. Cameron, F. Mathey and F. Laporte, *Can. J. Chem.* **78**, 118 (2000).

122. K. Eichele and R. E. Wasylishen, *J. Magn. Reson.* **106A**, 46 (1994).

123. H. van Willigen, R. G. Griffin and R. A. Haberkorn, *J. Chem. Phys.* **67**, 5855 (1977).

124. R. D. Curtis, J. W. Hilborn, G. Wu, M. D. Lumsden, R. E. Wasylishen and J. A. Pincock, *J. Phys. Chem.* **97**, 1856 (1993).

125. M. D. Lumsden, G. Wu, R. E. Wasylishen and R. D. Curtis, *J. Am. Chem. Soc.* **115**, 2825 (1993).

126. G. A. Webb, in *Nuclear Magnetic Shieldings and Molecular Structure.* Edited by J. A. Tossell, Kluwer Academic Publishers: Dordrecht, 1993, p. 1.

127. D. B. Chesnut, *Ann. Rep. NMR Spectrosc.* **29**, 71 (1994).

128. J. Gauss, *Ber. Bunsenges. Phys. Chem.* **99**, 1001 (1995).

129. A. C. de Dios, *Prog. NMR Spectrosc.* **29**, 229 (1996).

130. J. C. Facelli, in *Encyclopedia of Nuclear Magnetic Resonance.* Edited by D. M. Grant and R. K. Harris, John Wiley and Sons: Chichester, 1996, p. 4327.

131. C. J. Jameson and A. C. de Dios in *Nuclear Magnetic Resonance—A Specialist Periodical Report.* Edited by G. Webb, Royal Society of Chemistry, Cambridge, 1999, Vol. 28 and previous volumes in this annual series.

132. A. C. de Dios, J. L. Roach and A. E. Walling, in *Modeling NMR Chemical Shifts.* Edited by J. C. Facelli and A. C. de Dios, American Chemical Society: Washington, DC, 1999, Chapter 16.

133. G. Wu and R. E. Wasylishen, *J. Magn. Reson.* **102A**, 183 (1993).

134. G. Wu and R. E. Wasylishen, *J. Chem. Phys.* **99**, 6321 (1993).

135. G. Wu, B. Sun, R. E. Wasylishen and R. G. Griffin, *J. Magn. Reson.* **124**, 366 (1997).

136. S. Dusold, E. Klaus, A. Sebald, M. Bak, and N. C. Nielsen, *J. Am. Chem. Soc.* **119**, 7121 (1997).

137. R. G. Griffin, In *Encyclopedia of Nuclear Magnetic Resonance*, D. M. Grant and R. K. Harris, Eds., John Wiley and Sons: Chichester, 1996, p. 4174.

138. G. Wu, K. Eichele and R. E. Wasylishen, in *Phosphorus-31 NMR Spectral Properties in Compound Characterization and Structural Analysis.* Edited by L. D. Quin and J. G. Verkade, VCH Publishers: New York, 1994, p. 441.

139. A. Schmidt and S. Vega, *J. Chem. Phys.* **96**, 2655 (1992).

140. T. Nakai and C. A. McDowell, *J. Chem. Phys.* **96**, 3452 (1992).

141. G. Wu and R. E. Wasylishen, *J. Chem. Phys.* **98**, 6138 (1993).

142. B. Sun and R. G. Griffin, unpublished.

143. M. Bak and J. T. Rasmussen, University of Aarhus, 1999.

144. R. R. Ernst, in *Encyclopedia of Nuclear Magnetic Resonance*. Edited by D. M. Grant and R. K. Harris, John Wiley and Sons: Chichester, 1996, p. 3122.

145. B. C. Gerstein, in *Encyclopedia of Nuclear Magnetic Resonance*. Edited by D. M. Grant and R. K. Harris, John Wiley and Sons: Chichester, 1996, p. 1835.

146. L. Müller, A. Kumar and R. R. Ernst, *J. Magn. Reson.* **25**, 383 (1977).

147. K. W. Zilm, G. G. Webb, A. H. Cowley, M. Pakulski and A. Orendt, *J. Am. Chem. Soc.* **110**, 2032 (1988).

148. T. Nakai and C. A. McDowell, *J. Am. Chem. Soc.* **116**, 6373 (1994).

149. T. Nakai and C. A. McDowell, *Solid State Nucl. Magn. Reson.* **4**, 163 (1995).

150. K. Eichele, R. E. Wasylishen, R. W. Schurko, N. Burford and W. A. Whitla, *Can. J. Chem.* **74**, 2372 (1996).

151. J. Senker, H. Jacobs, M. Müller, W. Press and G. Neue, *J. Phys. Chem. B*, **103**, 4497 (1999).

152. M. de Langen and K. O. Prins, *Chem. Phys. Lett.* **299**, 195 (1999).

153. S.-I. Nishikiori, *J. Incl. Phen. Macro. Chem.* **34**, 331 (1999).

154. X. Xie and S. Hayashi, *J. Phys. Chem. B*, **103**, 5956 (1999).

155. J. H. Davis in *Isotopes in the Physical and Biomedical Sciences*, Vol. 2. Edited by E. Buncel and J. R. Jones, Elsevier: Amsterdam, 1991, Chapt. 3.

156. R. R. Vold, in *Understanding Chemical Reactivity*. Edited by R. Tycko, Kluwer Academic Publishers: Dordrecht, 1994, Vol. 8, p. 27.

157. L. S. Batchelder in *Encyclopedia of Nuclear Magnetic Resonance*. Edited by D. M. Grant and R. K. Harris, John Wiley and Sons: Chichester, 1996, p. 1574.

158. N. Chandrakumar, *NMR Basic Princ. Prog.* **34**, 1 (1996).

159. G. L. Hoatson and R.L. Vold, *NMR Basic Princ. Prog.* **32**, 1 (1994).

160. R. R. Vold and R. L. Vold, *Adv. Magn. Opt. Reson.* **16**, 85 (1991).

161. A. Müller and U. Haeberlen, *Chem. Phys. Lett.* **248**, 249 (1996).

162. P. Speier, H. Zimmermann, U. Haeberlen and Z. Luz, *Mol. Phys.* **95**, 1153 (1998).

163. H. W. Spiess, *NMR Basic Princ. Prog.* **15**, 55 (1978).

164. C. M. Gall, J. A. DiVerdi and S. J. Opella, *J. Am. Chem. Soc.* **103**, 5039 (1981).

165. A. F. Thomas, *Deuterium Labeling in Organic Chemistry*. Appleton-Century-Crofts: New York, 1971.

166. *Isotopes in the Physical and Biomedical Sciences*; Vol. 1 Labelled Compounds (Part A). Edited by E. Buncel and J. R. Jones, Elsevier, Amsterdam, 1987.

167. L. S. Batchelder, C. H. Niu and D. A. Torchia, *J. Am. Chem. Soc.* **105**, 2228 (1983).

168. J. Hirschinger and A. D. English, *J. Magn. Reson.* **85**, 542 (1989).

169. D. A. Torchia and A. Szabo, *J. Magn. Reson.* **49**, 107 (1982).

170. P. M. Henrichs, J. M. Hewitt and M. Linder, *J. Magn. Reson.* **60**, 280 (1984).

171. M. Bloom, J. H. Davis and M. I. Valic, *Can. J. Phys.* **58**, 1510 (1980).

172. H. W. Spiess and H. Sillescu, *J. Magn. Reson.* **42**, 381 (1981).

173. J. H. Davis, K. R. Jeffrey, M. Bloom, M. I. Valic and T. P. Higgs, *Chem. Phys. Lett.* **42**, 390 (1976).

174. A. D. Ronemus, R. L. Vold and R. R. Vold, *J. Magn. Reson.* **70**, 416 (1986).

175. M. S. Greenfield, A. D. Ronemus, R. L. Vold, R. R. Vold, P. D. Ellis and T. R. Raidy, *J. Magn. Reson.* **72**, 89 (1987).

176. R. R. Vold and R. L. Vold, *J. Magn. Reson.* **70**, 144 (1986).

177. A. Pines, M. G. Gibby and J. S. Waugh, *J. Chem. Phys.* **56**, 1776 (1972).

178. A. Pines, M. G. Gibby and J. S. Waugh, *J. Chem. Phys.* **59**, 569 (1973).

179. A. E. Bennett, C. M. Rienstra, M. Auger, K. V. Lakshmi and R. G. Griffin, *J. Chem. Phys.* **103**, 6951 (1995).

180. W. L. Earl and D. L. VanderHart, *J. Magn. Reson.* **48**, 35 (1982).

181. D. W. Alderman, M. S. Solum and D. M. Grant, *J. Chem. Phys.* **84**, 3717 (1986).

182. K. B. Wiberg, J. D. Hammer, K. W. Zilm, J. R. Cheeseman and T. A. Keith, *J. Phys. Chem. A*, **102**, 8766 (1998).

183. W. Robien, in *Encyclopedia of Computational Chemistry*. Edited by P. v. R. Schleyer, John Wiley and Sons: New York, 1998, p. 1845.

184. N. F. Ramsey, *Phys. Rev.* **78**, 699 (1950).

185. C. J. Jameson and J. Mason, in *Multinuclear NMR*. Edited by J. Mason, Plenum Press: New York, 1987, Chapter 3.

186. W. H. Flygare, *Molecular Structure and Dynamics*. Prentice-Hall: Englewood Cliffs, New Jersey, 1978, Chapter 6.

187. J. B. Grutzner, in *Recent Advances in Organic NMR Spectroscopy*. Edited by J. B. Lambert and R. Rittner, Norell Press: Landisville, New Jersey, 1987, p. 17.

188. G. A. Webb, in *Encyclopedia of Nuclear Magnetic Resonance*. Edited by D. M. Grant and R. K. Harris, John Wiley and Sons: Chichester, 1996, p. 4307.

189. T. D. Gierke and W. H. Flygare, *J. Am. Chem. Soc.* **94**, 7277 (1972).

190. G. Malli and C. Froese, *Int. J. Quantum Chem.* **IS** 95 (1967).

191. C. J. Jameson and H. S. Gutowsky, *J. Chem. Phys.* **40**, 1714 (1964).

192. M. S. Solum, J. C. Facelli, J. Michl and D. M. Grant, *J. Am. Chem. Soc.* **108**, 6464 (1986).

193. K. W. Zilm and J. C. Duchamp, in *Nuclear Magnetic Shieldings and Molecular Structure*. Edited by J. A. Tossell, Kluwer Academic Publishers: Dordrecht, 1993, p. 315.

194. G. M. Bernard, K. Eichele, G. Wu, C. W. Kirby and R. E. Wasylishen, *Can. J. Chem.* **78**, 614 (2000).

195. K. B. Wiberg, J. D. Hammer, K. W. Zilm and J. R. Cheeseman, *J. Org. Chem.* **64**, 6394 (1999).

196. W. Kutzelnigg, U. Fleischer and M. Schindler, *NMR Basic Princ. Prog.* **23**, 165 (1991).

197. U. Fleischer, C. v. Wüllen and W. Kutzelnigg, in *Encyclopedia of Computational Chemistry*. Edited by P. v. R. Schleyer, John Wiley and Sons: New York, 1998, p.

1827.

198. R. Höller and H. Lischka, *Mol. Phys.* **41**, 1017 (1980).

199. R. Höller and H. Lischka, *Mol. Phys.* **41**, 1041 (1980).

200. R. Ditchfield, *Mol Phys.* **27**, 789 (1974).

201. K. Wolinski, J. F. Hinton, and P. Pulay, *J. Am. Chem. Soc.* **112**, 8251 (1990).

202. G. Rauhut, S. Puyear, K. Wolinski and P. Pulay, *J. Phys. Chem.* **100**, 6310 (1996).

203. P. Pulay, J. F. Hinton and K. Wolinski, in *Nuclear Magnetic Shieldings and Molecular Structure*. Edited by J. A. Tossell, Kluwer Academic Publishers: Dordrecht, 1993, p. 243.

204. W. Kutzelnigg, *Isr. J. Chem.* **19**, 193 (1980).

205. M. Schindler and W. Kutzelnigg, *J. Chem. Phys.* **76**, 1919 (1982).

206. M. Schindler and W. Kutzelnigg, *J. Am. Chem. Soc.* **105**, 1360 (1983).

207. M. Schindler and W. Kutzelnigg, *Mol. Phys.* **48**, 781 (1983).

208. W. Kutzelnigg, Ch. v. Wüllen, U. Fleischer, R. Franke and T. v. Mourik, in *Nuclear Magnetic Shieldings and Molecular Structure*. Edited by J. A. Tossell, Kluwer Academic Publishers: Dordrecht, 1993, p. 141.

209. T. A. Keith and R. F. W. Bader, *Chem. Phys. Lett.* **210**, 223 (1993).

210. B. B. Laird, R. B. Ross and T. Ziegler, in *Chemical Applications of Density-Functional Theory*. Edited by B. B. Laird, R. B. Ross and T. Ziegler, American Chemical Society: Washington, DC, 1996, p. 1.

211. M. Kaupp, V. G. Malkin and O. L. Malkina, in *Encyclopedia of Computational Chemistry*. Edited by P. v. R. Schleyer, John Wiley and Sons: New York, 1998, p. 1857.

212. For a recent review, see M. Bühl, M. Kaupp, O. L. Malkina and V. G. Malkin, *J. Comput. Chem.* **20**, 91 (1999).

213. G. Schreckenbach and T. Ziegler, *J. Phys. Chem.* **99**, 606 (1995).

214. A. M. Lee, N. C. Handy and S. M. Colwell, *J. Chem. Phys.* **103**, 10095 (1995).

215. G. Schreckenbach, R. M. Dickson, Y. Ruiz-Morales and T. Ziegler, in *Chemical Applications of Density-Functional Theory*. Edited by B. B. Laird, R. B. Ross and T. Ziegler, American Chemical Society: Washington, DC, 1996, p. 328.

216. M. Bühl, *Chem. Phys. Lett.* **267**, 251 (1997).

217. G. Frenking and U. Pidun, *J. Chem. Soc., Dalton Trans.* 1653 (1997).

218. M. Kaupp, V. G. Malkin, O. L. Malkina and D. R. Salahub, *Chem. Phys. Lett.* **235**, 382 (1995).

219. M. Kaupp, V. G. Malkin, O. L. Malkina, and D. R. Salahub, *Chem. Eur. J.* **2**, 24 (1996).

220. M. Kaupp, *Chem. Ber.* **129**, 527 (1996).

221. M. Kaupp, *Chem. Ber.* **129**, 535 (1996).

222. G. Schreckenbach, Ph.D. Thesis, University of Calgary, 1996.

223. M. Kaupp, O. L. Malkina and V. G. Malkin, *Chem. Phys. Lett.* **265**, 55 (1997).

224. J. Gauss, *J. Chem. Phys.* **99**, 3629 (1993).

225. Y. Ruiz-Morales, G. Schreckenbach and T. Ziegler, *J. Phys. Chem.* **100**, 3359 (1996).

226. R. Salzmann, M. Kaupp, M. T. McMahon and E. Oldfield, *J. Am. Chem. Soc.*, **120**, 4771 (1998).

227. D. B. Chesnut and K. D. Moore, *J. Comp. Chem.* **10**, 648 (1989).

228. D. B. Chesnut, B. E. Rusiloski, K. D. Moore and D. A. Egolf, *J. Comp. Chem.* **14**, 1364 (1993).

229. Gaussian 94, Revision B.2. M. J. Frisch, G. W. Trucks, H. B. Schlegel, P. M. W. Gill, B. G. Johnson, M. A. Robb, J. R. Cheeseman, T. Keith, G. A. Petersson, J. A. Montgomery, K. Raghavachari, M. A. Al-Laham, V. G. Zakrzewski, J. V. Ortiz, J. B. Foresman, J. Cioslowski, B. B. Stefanov, A. Nanayakkara, M. Challacombe, C. Y. Peng, P. Y. Ayala, W. Chen, M. W. Wong, J. L. Andres, E. S. Replogle, R. Gomperts, R. L. Martin, D. J. Fox, J. S. Binkley, D. J. Defrees, J. Baker, J. P. Stewart, M. Head-Gordon, C. Gonzalez and J. A. Pople, Gaussian, Inc., Pittsburgh PA, 1995.

230. Gaussian 98, Revision A.4. M. J. Frisch, G. W. Trucks, H. B. Schlegel, G. E. Scuseria, M. A. Robb, J. R. Cheeseman, V. G. Zakrzewski, J. A. Montgomery, Jr., R. E. Stratmann, J. C. Burant, S. Dapprich, J. M. Millam, A. D. Daniels, K. N. Kudin,

M. C. Strain, O. Farkas, J. Tomasi, V. Barone, M. Cossi, R. Cammi, B. Mennucci, C. Pomelli, C. Adamo, S. Clifford, J. Ochterski, G. A. Petersson, P. Y. Ayala, Q. Cui, K. Morokuma, D. K. Malick, A. D. Rabuck, K. Raghavachari, J. B. Foresman, J. Ciolowski, J. V. Ortiz, B. B. Stefanov, G. Liu, A. Liashenko, P. Piskorz, I. Komaromi, R. Gomperts, R. L. Martin, D. J. Fox, T. Keith, M. A. Al-Laham, C. Y. Peng, A. Nanayakkara, C. Gonzalez, M. Challacombe, P. M. W. Gill, B. Johnson, W. Chen, M. W. Wong, J. L. Andres, C. Gonzalez, M. Head-Gordon, E. S. Replogle and J. A. Pople. Gaussian, Inc. Pittsburgh, PA. 1998.

231. P. J. Hay and W. R. Wadt, *J. Chem. Phys.* **82**, 270 (1985).

232. Basis sets were obtained from the Extensible Computational Chemistry Environment Basis Set Database, Version 1.0, as developed and distributed by Molecular Science Computing Facility, Environmental and Molecular Sciences Laboratory which is part of the Pacific Northwest Laboratory, P.O. Box 999, Richland, Washington 99352, USA, and funded by the U.S. Department of Energy. The Pacific Northwest Laboratory is a multi-program laboratory operated by the Batelle Memorial Institute for the U.S. Department of Energy under contract DE-AC06-76RLO 1830. Contact David Feller or Karen Schuchardt for further information. These basis sets may be downloaded from the internet at: http://www.emsl.pnl.gov:2080/forms/basisform.html.

233. M. J. Frisch, M. Head-Gordon and J. A. Pople, *Chem. Phys. Lett.* **166**, 281 (1990).

234. Gaussian 98 Online Users Reference: http://www.gaussian.com/g98.htm

235. A. D. Becke, *J. Chem Phys.* **98**, 5648 (1993).

236. C. Lee, W. Yang and R. G. Parr, *Phys. Rev.* **B37**, 785 (1988).

237. J. S. Binkley, J. A. Pople and W. J. Hehre, *J. Am. Chem. Soc.* **102**, 939 (1980).

238. P. C. Harihanan and J. A. Pople, *Theoret. Chim. Acta*, **28**, 213 (1973).

239. R. Krishnan, J. S. Binkley, R. Seeger and J. A. Pople, *J. Chem. Phys.* **72**, 650 (1980).

240. T. H. Dunning, Jr. *J. Chem. Phys.* **90**, 1007 (1989).

241. D. Woon and K. Peterson, unpublished results. Cited from reference 232.

242. P. G. Eller, R. R. Ryan and R. O. Schaeffer, *Cryst. Struct. Commun.* **6**, 163 (1977).

243. W. Dreissig and H. Dietrich, *Acta Crystallogr.* **B37**, 931 (1981).

244. M. Hodgson, D. Parker, R. J. Taylor and G. Ferguson, *J. Chem. Soc., Chem. Commun.* 1309 (1987).

245. J. M. Baraban and J. A. McGinnety, *Inorg. Chem.* **13**, 2864 (1974).

246. K. R. Pörschke, R. Mynott, K. Angermund and C. Krüger, *Z. Naturforsch.* **40b**, 199 (1985).

247. H.-C. Weiss, D. Bläser, R. Boese, B. M. Doughan and M. M. Haley, *Chem. Commun.* 1703, 1997.

248. M. Gerisch, F. W. Heinemann, H. Bögel and D. Steinborn, *J. Organomet. Chem.* **548**, 247 (1997).

249. T. A. Keith and R. F. W. Bader, *Chem. Phys. Lett.* **194**, 1 (1992).

250. J. R. Cheeseman, G. W. Trucks, T. A. Keith and M. J. Frisch, *J. Chem. Phys.* **104**, 5497 (1996).

251. W. Mendenhall and R. J. Beaver, *Introduction to Probability and Statistics*, 8th Ed. PWS-Kent Publishing: Boston, 1990.

252. T. C. Farrar, M. J. Jablonsky and J. L. Schwartz, *J. Phys. Chem.* **98**, 4780 (1994).

253. R. Challoner and A. Sebald, *Solid State Nucl Magn. Reson.* **4**, 39 (1995).

254. B. E. Mann, in *Comprehensive Organometallic Chemistry*. Edited by G. Wilkinson, Pergamon: Oxford, 1982, Vol. 3, p 89.

255. S. A. Vierkötter and C. E. Barnes, *J. Am. Chem. Soc.* **116**, 7445 (1994).

256. M. A. Gallop, B. F. G. Johnson, J. Keeler, J. Lewis, S. J. Heyes and C. M. Dobson, *J. Am. Chem. Soc.* **114**, 2510 (1992).

257. L. W. Reeves, *Can. J. Chem.* **38**, 736 (1960).

258. S. Maričić, C. R. Redpath and J. A. S. Smith, *J Chem. Soc.* 4905 (1963).

259. D. M. Blake and D. M. Roundhill, *Inorg. Synth.* **18**, 120 (1978).

260. P. B. Chock, J. Halpern and F. E. Paulik, *Inorg. Synth.* **28**, 349 (1990).

261. K. Eichele, G. Wu, R. E. Wasylishen and J. F. Britten, *J. Phys. Chem.* **99**, 1030 (1995).

262. M. Rance and R. A. Byrd, *J. Magn. Reson.* **52**, 221 (1983).

263. M. D. Lumsden, R. E. Wasylishen and J. F. Britten, *J. Phys. Chem.* **99**, 16602 (1995).

264. E. K. Wolff, R. G. Griffin and J. S. Waugh, *J. Chem. Phys.* **67**, 2387 (1977).

265. W. S. Veeman, *Prog. NMR Spectrosc.* **16**, 193 (1984).

266. See reference 14, Chapter 7.

267. S. H. Alarcón, A. C. Olivieri and R. K. Harris, *Solid State Nucl. Magn. Reson.* **2**, 325 (1993).

268. K. Eichele, R. E. Wasylishen, J. S. Grossert and A. Olivieri, *J. Phys. Chem.* **99**, 10110 (1995).

269. J. A. J. Jarvis, B. T. Kilbourn and P. G. Owston, *Acta Crystallogr.* **B27**, 366 (1971).

270. L. J. Burnett and B. H. Muller *J. Chem. Phys.* **55**, 5829 (1971).

271. J. Kowalewski, T. Lindblom, R. Vestin and T. Drakenberg, *Mol. Phys.* **31**, 1669 (1976).

272. M. Alla, R. Eckman and A. Pines, *Chem. Phys. Lett.* **71**, 148 (1980).

273. T. A. Albright, R. Hoffman, J. C. Thibeault and D. L. Thorn, *J. Am. Chem. Soc.* **101**, 3801 (1979).

274. F. Nunzi, A. Sgamellottti, N. Re and C. Floriani, *J. Chem. Soc., Dalton Trans.* 3487 (1999).

275. J. Chatt, B. L. Shaw and A. A. Williams, *J. Chem. Soc.* 3269 (1962).

276. C. J. Finder, M. G. Newton and N. L. Allinger, *Acta Crystallogr.* **B30**, 411 (1974).

277. J. Bernstein, *Acta Crystallogr.* **B31**, 1268 (1975).

278. A. Hoekstra, P. Meertens and A. Vos, *Acta Crystallogr.* **B31**, 2813 (1975).

279. V. Molina, M. Merchán and B. O. Roos, *J. Phys. Chem. A*, **101**, 3478 (1997).

280. C. H. Choi and M. Kertesz, *J. Phys. Chem. A*, **101**, 3823 (1997).

281. K. Ogawa, T. Sano, S. Yoshimura, Y. Takeuchi and K. Toriumi, *J. Am. Chem. Soc.* **114**, 1041 (1992).

282. K. Ogawa, J. Harada and S. Tomoda, *Acta Crystallogr.* **B51**, 240 (1995).

283. K. Saito and I. Ikemoto, *Bull. Chem. Soc. Jpn.* **69**, 909 (1996).

284. K. Saito and I. Ikemoto, *Physica B*, **219 & 220**, 417 (1996).

285. P. A. Chaloner, private communication.

286. D. L. VanderHart, W. L. Earl and A. N. Garroway, *J. Magn. Reson.* **44**, 361 (1981).

287. M. Alla and E. Lippmaa, *Chem. Phys. Lett.* **87**, 30 (1982).

288. M. A. Hemminga, P. A. De Jager, J. Krüse and R. M. J. N. Lamerichs, *J. Magn. Reson.* **71**, 446 (1987).

289. V. R. Cross and J. S. Waugh, *J. Magn. Reson.* **25**, 225 (1977).

290. A. A. Espiritu and J. G. White, *Zeit. Krist.* **147**, 177 (1978).

291. J. O. Glanville, J. M. Stewart and S. O. Grim, *J. Organomet. Chem.* **7**, P9 (1967).

292. L. F. Fieser and K. L. Williamson, *Organic Experiments*, 5th Ed. D.C. Heath: Lexington, Massachusetts, 1983, p. 321.

293. O. B. Peersen, X. Wu, I. Kustanovich and S. O. Smith, *J. Magn. Reson.* **A104**, 334 (1993).

294. K. Marat, University of Manitoba, 1997.

295. J. S. Martin, A. R. Quirt and K. E. Worvill, The NMR Program Library, Daresville Laboratory: Daresville, UK.

296. S. J. Opella and M. H. Frey, *J. Am. Chem. Soc.* **101**, 5854 (1979).

297. See reference 36, p. 162.

298. H. Günther, *Angew. Chem. Int. Ed. Eng.* **11**, 861 (1972).

299. R. M. Lynden-Bell and N. Sheppard, *Proc. Roy. Soc. (London), Ser. A*, **269**, 385 (1962).

300. W. P. Aue, E. Bartholdi and R. R. Ernst, *J. Chem. Phys.* **64**, 2229 (1976).

301. K. Nagayama, A. Kumar, K. Wüthrich and R. R. Ernst, *J. Magn. Reson.* **40**, 321 (1980).

302. P. E. Hansen, O. K. Poulsen and A. Berg, *Org. Magn. Reson.* **12**, 43 (1979).

303. P. J. Fagan, J. C. Calabrese and B. Malone, *Science*, **252**, 1160 (1991).

304. P. J. Fagan, J. C. Calabrese and B. Malone, *Acc. Chem. Res.* **25**, 134 (1992).

305. S. Schreiner, T. Gallaher and H. K. Parsons, *Inorg. Chem.* **33**, 3021 (1994).

306. P. W. Jolly, in *Comprehensive Organometallic Chemistry*. Edited by G. Wilkinson, Pergamon Press: Oxford, 1982, Vol. 6, p. 101.

307. F. Ozawa, in *Synthesis of Organometallic Compounds*. Edited by S. Komiya, John Wiley and Sons, Chichester, 1997, p. 249.

308. E. O. Greaves, C. J. L. Lock and P. M. Maitlis, *Can. J. Chem.* **46**, 3879 (1968).

309. S. Komiya and A. Fukuoka, in *Synthesis of Organometallic Compounds*. Edited by S. Komiya, John Wiley and Sons, Chichester, 1997, p. 219.

310. R. S. Paonessa, A. L. Prignano and W. C. Trogler, *Organometallics*, **4**, 647 (1985).

311. S. O'Brien, M. Fishwick, B. McDermott, M. G. H. Wallbridge and G. A. Wright, *Inorg. Synth.* **13**, 73 (1972).

312. Y. Tatsuno, T. Yoshida and S. Otsuka, *Inorg. Synth.* **28**, 342 (1990).

313. R. K. Harris, K. J. Packer and A. M. Thayer, *J. Magn. Reson.* **62**, 284 (1985).